Universidade de São Paulo
Instituto de Física

Explorando correlações iniciais: correlações internas de um ambiente e a estatística do calor entre sistemas correlacionados

Versão original

Naim Elias Comar

Orientador: Prof. Dr. Gabriel Teixeira Landi

Tese de doutorado apresentada ao Instituto de Física como requisito parcial para a obtenção do título de Doutor em Ciências.

Banca Examinadora:
Prof. Dr. Gabriel Teixeira Landi - Orientador (Instituto de Física da USP)
Prof. Dr. Barbara Lopes Amaral (Instituto de Física da USP)
Prof. Dr. Fernando Antonio Nazareth Nicacio (Instituto de Física da UFRJ)
Prof. Dr. Frederico Borges de Brito (Instituto de Física de São Carlos/USP)
Prof. Dr. Nadja Kolb Bernardes (Departamento de Física da UFPE)

São Paulo
2023

FICHA CATALOGRÁFICA
Preparada pelo Serviço de Biblioteca e Informação
do Instituto de Física da Universidade de São Paulo

Comar, Naim Elias

Explorando correlações iniciais: correlações internas de um ambiente e a estatística do calor entre sistemas correlacionados. São Paulo, 2023.

Tese (Doutorado) - Universidade de São Paulo. Instituto de Física. Depto. de Física dos Materiais e Mecânica.

Orientador: Prof. Dr. Gabriel Teixeira Landi.

Área de Concentração: Física.

Unitermos: 1. Informação quântica.

USP/IF/SBI-035/2023

University of São Paulo
Physics Institute

Exploring initial correlations: internal environment correlations and the heat statistics between correlated systems

Original version

Naim Elias Comar

Supervisor: Prof. Dr. Gabriel Teixeira Landi

Thesis submitted to the Physics Institute of the University of São Paulo in partial fulfillment of the requirements for the degree of Doctor of Science.

Examining Committee:
Prof. Dr. Gabriel Teixeira Landi - Supervisor (Institute of Physics at USP)
Prof. Dr. Bárbara Lopes Amaral (Institute of Physics at USP)
Prof. Dr. Fernando Antonio Nazareth Nicacio (UFRJ Institute of Physics)
Prof. Dr. Frederico Borges de Brito (Physics Institute of São Carlos/USP)
Prof. Dr. Nadja Kolb Bernardes (Department of Physics at UFPE)

São Paulo
2023

“The best that most of us can hope to achieve in physics is simply to misunderstand at a deeper level.”

— Wolfgang Pauli

Aos meus avós Cecília Sousa de Oliveira, Matilde Lizzul Comar, Kalil Abrahão Elias e Alcibiade Valerio Comar, *in memoriam*.

Agradecimentos

Eu gostaria de dar os meus principais agradecimentos à minha mãe Sônia de Sousa Elias e ao meu pai Mário Vito Comar, pelo enorme suporte, amor e por terem feito possível tudo o que alcancei na vida. Um agradecimento muito especial também ao meu orientador, Gabriel Teixeira Landi, por ter me aceitado como seu orientando e ter sido um orientador extremamente atencioso, competente, compreensivo e principalmente muito entusiasmante pelo seu exemplo como cientista, estes quatro anos trabalhando juntos realmente me ensinaram muito sobre a Física em si e sobre a diversão e dificuldades em tentar expandir sua construção.

Quero agradecer às minhas irmãs Suyane Elias Comar e Temily Elias Comar por toda ajuda em momentos difíceis e também pelo companheirismo em todos os momentos. Muitos agradecimentos à Simone França Costa, por ser a melhor companheira que eu poderia imaginar e por ter me dado muito apoio, amor e paciência, principalmente no período de escrita. Obrigado às minhas tias Soila Elias, Solange Elias e Regina Martins pelo carinho de sempre e às minhas primas Simone, Jacqueline e Alexia, assim como suas famílias queridas que tenho no coração.

Quero agradecer muito também aos meus amigos, sem o apoio, alegria, descontração e companhia essencial deles, este trabalho não seria possível. Portanto, queria agradecer a Alexandre Santos, Ana Carolina Rainho, Ana Paula Sachelaride, André Santana de Araújo, Anielton Camargo, Arthur Cazon Vincoleto, Austin Ramsés Nascimento Silva, Bárbara Malheiros, Beatriz Nemezio Rainho, Bonifácio Lima, Brenda Bertotto Malabarba, Bruna Shinohara de Mendonça, Caio Medonça Pimentel, Carla Estfani Lopes dos Santos, Catarina Pasta Aydar, Daniel Beltrão, Diego Spiering, Douglas Gomes, Ester Schulz, Fábio Chagas da Silva, Felipe Godoy, Felipe Sampaio, Fernando Augusto Joaquim, Fernando Freire, Flora Collins Benjamim, Francisca Crislane Vieira de Brito, Gabriel Petian, Gabriela de Oliveira, Gizelly Ayumi Yamamoto, Guilhereme Coelho, Guilherme Nunes, Hanna Martins Morilhas, Henrique Berquó, Jader Rodrigues, João Carlos Juliano, José Augusto Padovese, José Eduardo Peres y Peres, Kian Shaikhzadeh Santos, Lavínia Helena Aune Ferreira, Léo Bindilatti, Lívia Lopes, Lucas Magno, Lucas Palhano, Lucas Pimenta, Luciano Barcelos, Macus Saad, Marcus Lemes, Moisés Medeiros, Nadia Soraya Linares Zepeda, Navid Portela Salehi, Níkolas Shildberg, Rafaela Geising, Riis Rhavia Assis Bachega, Roberto Baldijão, Roberto Parra, Rodrigo Frausino, Rodrigo Ramos, Rogério Camargo, Romulo Oliveira dos Santos, Rudá Pereira, Silvio Jonas da Silva Junior, Thandryus Augusto, Uric Bonatti Cardoso, Victor, William Santos, Williams Ribeiro, Xavier Júnior e a muitos outros amigos que não escrevi aqui por falta de memória no momento, mas que com certeza também me ajudaram muito neste caminho. Agradeço também às pessoas muito queridas que moraram comigo neste período, Ana Camila Costa Esteves, Ana Flávia de Freitas Gutierres, Aryella Faé Ra-

bello, Brenda Bertotto Malabarba, Ewerton Igor de França Barros, Lucas Aguiar, Lucas Cagnotto de Moraes, Matheus Henry Przygocki, Melissa de Oliveira Guirelli e Rafael Patrick Marcelino Rodrigues, numa convivência muito amigável e cheia de carinho que me faz me sentir muito em casa. Agradeço à grande professora Néia Barbosa do Grupo de Teatro da Poli e aos amigos que fiz lá: Andrey Luis Barbosa Gomes, Isabela Mosna Esteves, Júlio Barbosa de Moura, Lucas Yohan Salles, Mariana Mendes Lima, Pedro Leite Godinho e muitos outros. Obrigado à professora Bárbara Amaral e aos amigos que fiz em seu grupo de pesquisa, entre eles a Amanda Maria Fonseca, Giulio Camilo e o Gustavo B. Pimentel. E finalmente, os grandes colegas e amigos que fiz no muito simpático e entusiasmante grupo de pesquisa do Gabriel Landi: André Timpanaro, Adalberto Varizi, Alberto Jonatas Bezerra da Silva, Artur Machado Lacerda, Bruno Ortega Goes, Franklin Luis dos Santos Rodrigues, Heitor Peres Casagrande, Lui Zuccherelli de Paula, Marcelo Janovitch B. Pereira, Mariana Afeche Cipolla, Otavio Molitor, Pedro Vinicius Portugal, Rodolfo Reis Soldati e Rodrigo Pereira Silva, pelo apoio que vieram desde a companhia muito amigável e discussões interessantes a assuntos técnicos na pesquisa. Dentre esses amigos do grupo de pesquisa, agradeço também a profunda amizade feita com Gabriel Oliveira Alves, Luis Felipe Santos da Silva e Rolando Ramirez Camasca. Muitos agradecimentos ao professor Manoel Roberto Robilotta pelas profundas e instigantes conversas sobre Física e sobre a vida na carreira acadêmica.

Queria também agradecer às funcionárias Rosana Batista Gimenes e Sandra Regina Rodrigues Ribeiro pela constante ajuda no nosso dia-a-dia no DFMT. E à Andrea Wirkus, Cláudia Conde Barioni, Éber de Patto Lima e Marlon Rezende Faria por sempre esclarecer minhas dúvidas na CPG.

Finalmente, eu gostaria de agradecer muito ao Conselho Nacional de Desenvolvimento Científico e Tecnológico (CNPq), pois este trabalho não seria possível sem o seu auxílio financeiro.

Abstract

This thesis has the objective of exploring new effects caused by initial correlations in quantum systems, with extensive use of continuous-variables methods. Two main projects are highlighted. The first project aims to understand how the presence of initial correlations in an environment affects the dynamics of a system interacting with it. We analyze this problem from the point of view of Collisional Models of qubits and bosonic Gaussian states, in which we show how initial correlations between the environment parts steer the system's evolution. As a consequence, the standard Homogenization procedure can be disrupted. In the second project, we make use of Bayesian Networks to obtain the statistics of general thermodynamic quantities for two initially correlated systems and we explore the role of the initial density matrix ambiguity of mixture in this statistics. As an important application, we compute the effects of correlations in the statistics of the heat exchanged. Results for the statistics of the heat are obtained numerically for qubits and analytically for bosonic Gaussian states.

Keywords: Quantum correlations; Open quantum systems; Quantum Information; Continuous-Variables; Collisional models; Homogenization; Bayesian Networks; Heat distribution; Quantum Thermodynamics.

Resumo

Esta tese tem como objetivo explorar novos efeitos causados por correlações iniciais em sistemas quânticos, com grande uso de métodos de variáveis-contínuas. Dois projetos principais são destacados. O primeiro projeto visa entender como a presença de correlações iniciais em um ambiente afeta a dinâmica de um sistema que interage com ele. Analisamos este problema do ponto de vista dos Modelos Collisionais de qubits e estados Gaussianos bosônicos, nos quais mostramos como as correlações iniciais entre as partes do ambiente direcionam a evolução do sistema. Como consequência, o procedimento conhecido de Homogeneização pode ser corrompido. No segundo projeto, fazemos uso de Redes Bayesianas para obter as estatísticas de grandezas termodinâmicas gerais para dois sistemas inicialmente correlacionados e exploramos o papel da ambigüidade de mistuda da matriz densidade inicial nesta estatística. Adicionalmente, fizemos uma aplicação importante, a de calcular efeitos das correlações nas estatísticas do calor trocado entre dois sistemas. Os resultados para as estatísticas do calor são obtidos numericamente para qubits e analiticamente para estados Gaussianos bosônicos.

Palavras-chave: Correlações quânticas; Sistemas quânticos abertos; Informação Quântica; Variáveis-Contínuas; Modelos colisionais; Homogeneização; Redes Bayesianas; Distribuição do calor; Termodinâmica Quântica.

Contents

1 Introduction **1**
- 1.1 Collisional model with initially correlated ancillae . . . 2
- 1.2 Statistics of thermodynamic quantities using Bayesian Networks . . . 3
- 1.3 Structure of the thesis . . . 5

I Background **7**

2 Open Quantum Systems and Collisional Models **8**
- 2.1 The density matrix . . . 9
- 2.2 Dynamics . . . 11
  - 2.2.1 Closed systems - Unitary operators . . . 11
  - 2.2.2 Open systems - Kraus matrices . . . 12
- 2.3 Collisional Models . . . 14
  - 2.3.1 General case (correlated ancillae) . . . 14
  - 2.3.2 Markovian case . . . 17
  - 2.3.3 Qubit example, thermalizing machines . . . 18
  - 2.3.4 Steady-states . . . 20
  - 2.3.5 SWAP and Partial SWAP . . . 21
  - 2.3.6 Homogenization . . . 22
  - 2.3.7 Physical implementations of CMs . . . 25

3 Quantum Information and Bayesian Networks **29**
- 3.1 Generalized measurements . . . 29
- 3.2 Entropy . . . 30
  - 3.2.1 The Shannon Entropy . . . 30
  - 3.2.2 The von Neummann Entropy . . . 32
- 3.3 Mutual Information and Correlations . . . 34
  - 3.3.1 Relative Entropy . . . 34
  - 3.3.2 Mutual Information . . . 34
  - 3.3.3 Entanglement . . . 36
  - 3.3.4 Quantum discord . . . 37
- 3.4 Bayesian Networks . . . 40
  - 3.4.1 Definition and examples . . . 40
  - 3.4.2 Dynamical BNs for quantum systems (QBNs) . . . 42

4 Continuous Variables Framework **45**
4.1 Bosonic modes . . . 45
4.1.1 Canonical vectors . . . 46
4.1.2 CCRs and the symplectic form . . . 47
4.2 Second quantization and the Fock space . . . 48
4.3 Displacement operator and coherent states . . . 49
4.4 Characteristic function . . . 53
4.5 Quasi-probability distributions . . . 54
4.5.1 Wigner fucntion . . . 55
4.5.2 The s-ordered quasi-probability distribution . . . 55
4.5.3 Glauber-Sudarshan P-function . . . 56
4.5.4 Husimi Q-function . . . 56
4.6 Gaussian states . . . 57
4.6.1 Definitions . . . 57
4.6.2 Bona-fide conditions for covariance matrices . . . 59
4.6.3 Dynamics of canonical operators and statistical moments . . . 59
4.6.4 Symplectic operators . . . 62
4.6.5 Covariance matrix parametrization . . . 63
4.6.6 Characteristic function and quasi-probability distributions of Gaussian states . . . 65
4.7 Gaussian operations . . . 66
4.7.1 Tensor product . . . 67
4.7.2 Unitary operations . . . 67
4.7.3 Partial trace . . . 69
4.7.4 Gaussian CPTP-maps . . . 71
4.7.5 Applying a channel in only one partition . . . 73
4.7.6 One-mode Gaussian channels . . . 73
4.8 Entropic quantities for Gaussian states . . . 75
4.8.1 Diagonalization of Gaussian states to thermal states of free modes 75
4.8.2 Entropy of a Gaussian state . . . 76
4.8.3 Quantum discord between two Gaussian bosonic modes . . . 77

II Main projects **86**

5 Initially Correlated Ancillae - Minimal Qubit Model CM **87**
5.1 Preparing the correlated ancillae environment . . . 88
5.1.1 Hamiltonian graph states . . . 88
5.1.2 Properties of the initial ancillae and their correlations . . . 90
5.2 Homogenization procedure with initial correlations between ancillae: Breaking Homogenization . . . 95

6 Initially Correlated Ancillae - Gaussian States CM **100**
6.1 Preliminaries . . . 101
6.1.1 The Stinespring dilation procedure . . . 101
6.1.2 The Beam Splitter interaction . . . 103
6.1.3 Correlations block-matrices . . . 104

6.2 Main results . . . 105
6.2.1 Correlated nearest-neighbors . . . 105
6.2.2 General case . . . 110
6.2.3 Distance dependent correlations . . . 111
6.2.4 Ancillae evolution . . . 113
6.3 Constructing initially correlated ancillae from H-Graphs . . . 116
6.3.1 Constructing covariance matrix elements . . . 117
6.3.2 Constructing desired correlations from choosing the cyclic graph . 119
6.3.3 Application to the Algebraically decaying correlations case . . . 121
6.3.4 Analysing $\xi_d^{(p)}$ . . . 124

7 Obtaining Observables Shifts Using QBNs 126
7.1 General results . . . 127
7.1.1 Statement of the problem . . . 127
7.1.2 Characteristic function of the change probability distribution . . . 129
7.1.3 Statistical moments of the change probability distribution . . . 130
7.1.4 Comparison with TPM . . . 131
7.2 Application to qubits . . . 132
7.2.1 Setup and statistical moments . . . 133
7.2.2 Obtaining the probability distribution . . . 136
7.3 Dependence on the ambiguity of mixtures . . . 137
7.3.1 The variance for the qubits case . . . 138

8 Heat Exchanged Between Bosonic Modes 141
8.1 Probability distribution for the heat exchanged . . . 142
8.1.1 Statement of the problem . . . 142
8.1.2 Choosing the ensemble and the seed probability . . . 143
8.1.3 The characteristic function . . . 145
8.2 Heat statistical moments . . . 146
8.2.1 Average of heat . . . 146
8.2.2 Heat variance . . . 149
8.3 The variance for different QBN choices . . . 151
8.3.1 The ambiguity of mixing . . . 151
8.3.2 Different seed probability choices . . . 154
8.4 Investigations on correlations . . . 155
8.4.1 Profile of correlations in the initial state . . . 155
8.4.2 Correlations behaviour during evolution . . . 157

9 Conclusions and further perspectives 160

A Some proofs and definitions in Open Quantum Systems and Collisional Models 165
A.1 Some properties of purity . . . 165
A.2 The partial trace . . . 166
A.3 Interaction Picture . . . 167
A.4 Thermal states . . . 169
A.5 Proof of $\rho^n_{S,\text{rest}} \to 0$ and $\rho^n_{A,\text{rest}} \to 0$ . . . 170

B Some proofs and definitions in Quantum Information **174**
B.1 Some useful equations . . . 174
B.2 Proof of Eq. (3.10) . . . 175

C Some proofs and definitions in Continuous Variables **176**
C.1 Notation for vectors and matrices of operators . . . 176
C.2 The direct sum . . . 177
C.3 General Gaussian integral . . . 177
C.4 Proof of Eq. (4.23) . . . 177
C.5 Proof of Eq. (4.31) . . . 178
C.6 Proof of the formula of coherent state expanded in the Fock basis (Eq. (4.32)) . . . 179
C.7 Completeness relation for coherent states . . . 180
C.8 Proof of the Fourier-Weyl relation . . . 180
C.9 Proof of Eq. (4.47) . . . 182
C.10 Proof of Eq. (4.52) . . . 182
C.11 Proof of Eq. (4.54) . . . 183
C.12 Proof of the Robertson-Schrödinger relation (Eq. (4.63)) . . . 184
C.13 Density matrix and covariance matrix of free Gaussian bosonic modes . . . 185
C.14 Obtaining symplectic eigenvalues . . . 187
C.15 Justifying the existence of a Hamiltonian matrix corresponding to any symplectic matrix . . . 189
C.16 Proof for the parametrization of Eq. (4.82) . . . 190
C.17 Computation of quasi-probability distributions for Gaussian states . . . 192
C.18 Proof that the commutator between any second order operators is a second order operator . . . 193
C.19 Proof of Eq. (4.124) . . . 194
C.20 Proof of Simon normal form statement . . . 195
C.21 Proof that $S(\mathcal{E}(|\alpha\rangle\langle\alpha|)) = S(\mathcal{E}(|0\rangle\langle 0|))$ for any Gaussian channel $\mathcal{E}$ . . . 195
C.22 Computations to obtain Eq. (4.139) . . . 196
C.23 Two-mode squeezed thermal state, EPR state and friends . . . 196
C.23.1 Two-mode squeezed thermal state . . . 197
C.23.2 EPR state . . . 198

D Some proofs and definitions in Obtaining Observables Shifts Using QBNs **199**
D.1 Proof of Eq. (7.20) . . . 199
D.2 Matrices for generating ensembles in Subsection 7.3.1 . . . 201

E Some proofs and definitions in Heat Exchanged Between Bosonic Modes **202**
E.1 The QBN generated by post-measurements . . . 202
E.2 Computations of Eqs. (8.16) and (8.17) . . . 203
E.3 Isserlis' Theorem and $\langle Q_A^2 \rangle$ . . . 205
E.4 Locally thermal states D-plus and D-minus . . . 206

List of Figures

2.1 Schematic of collisions, where the system S is interacting individually with the k-th ancilla during a time τ going to interact with the next ancilla also during a time τ. 15

2.2 Schematic of homogenization. From left to right, the system S interacts with the ancillae at time $0 < t < \tau$, $\tau < t < 2\tau$, $2\tau < t < 3\tau$ and $(n-1)\tau < t < n\tau$, respectively. The color changes on the system represents the different states it passes trough until it gets very similar to the ancillae and the whole system becomes homogeneous. 24

2.3 Micromaser setup: An atomic beam oven emits Rydberg atoms which pass trough a velocity selector tuning the flux of atoms so that each atom passes one at a time through the cavity containing electromagnetic fields. (This figure was taken from Ref. [21].) 27

3.1 Three random variables A, B and C disposed in a causal order. 40

3.2 Example of directed graph representing relations of causality between random variables. 41

3.3 A directed graph with in internal cycle, provoking a causal loop between the random variables A, B, C and D. 43

3.4 BN for the dynamical evolution of a quantum system. The upper line describes the global state evolution (which we often call *hidden layer*) and the dashed arrows indicates the causal dependence of the reduced states on the global states at each instant t_k. 44

4.1 *State decomposition*: Depicted in black lines, the state ρ_{AB} can be decomposed as an initial state ρ_{aB} in which the first mode (in part A) passes trough a quantum channel $\mathcal{E}$. *Remote preparation* : Depicted in red symbols, the effect of the generalized measurement $\mathcal{M}_B$ in ρ_{aB} creates the ensemble $\mathcal{P} = \{p_k, \rho_{a|k}\}_k$ of states in A which, passing through the quantum channel, becomes the ensemble $\mathcal{A} = \{p_k, \rho_{a'|k}\}_k$. The ensemble $\mathcal{A}$ is also generated by the backaction, in A, of the generalized measurement $\mathcal{M}_B$ in ρ_{AB}. (This figure was taken from Ref. [128] with modifications.) . 80

4.2 *State decomposition*: Depicted in black lines, the state ρ_{AB} can be decomposed as an initial state ρ_{aB} in which the first mode (in part A) passes trough an inverse squeezing operator $\hat{S}^{-1}(r)$, a quantum channel $\mathcal{E}$ and a sequeezing operator $\hat{S}(\xi)$. *Remote preparation* : Depicted in red symbols, the effect of the generalized measurement $\mathcal{M}_B$ in ρ_{aB} creates the ensemble $\mathcal{P} = \{p_k, \rho_{a|k}\}_k$ of states in A which, passing through the quantum channel and squeezing operators, becomes the ensemble $\mathcal{A} = \{p_k, \rho_{a'|k}\}_k$. The ensemble $\mathcal{A}$ is also generated by the backaction, in A, of the generalized measurement $\mathcal{M}_B$ in ρ_{AB}. (This figure was taken from Ref. [128] with modifications.) 82
4.3 Plot of c_+ and c_- points, for different fixed a and b of states in the Simon normal form generated 2×10^5 times by random choices of r and τ, according to the parametrization of Eqs. (4.141), (4.142), (4.143) and (4.144). The pink curves delimit the bona-fide region of states. 85

5.1 Cyclic graph with 9 ancillae (at the vertices), each interacting only with the first and second neighbors (interactions represented by the edges). . . 90
5.2 Population of the excited state of $\rho_A \times$ total number of ancillae N_A, for different values of k. 92
5.3 Population of $\rho_A \times$ values of k, for different values of N_A. 93
5.4 Mutual information between neighbors $\times$ distance between neighbors, for $N_A = 7$ and different values of k. 94
5.5 Mutual information between first neighbors $\times$ k, for different values of N_A. For larger values of N_A, the plots loose resolution since they are computationally more demanding. 95
5.6 Plots of population of $\rho_S \times$ number of steps for ancillae prepared with the NN1 cyclic graph with $N_A = 17$, for different values of k. Each line correspond to a different value of g strength of the partial SWAP interaction, from top to bottom $g = 0.5$, $g = 1.0$ and $g = 1.5$. The red dashed lines indicate the value of the population of the respective ρ_A, which is the value in which the system's population converges if homogenizaton happens. 97
5.7 Plots of population of $\rho_S \times$ number of steps for ancillae prepared with the NN2 cyclic graph with $N_A = 17$, for different values of k. Each line correspond to a different value of g strength of the partial SWAP interaction, from top to bottom $g = 0.5$, $g = 1.0$ and $g = 1.5$. The red dashed lines indicate the value of the population of the respective ρ_A, which is the value in which the system's population converges if homogenizaton happens. 98
5.8 Plots of population of $\rho_S \times$ number of steps for ancillae prepared with the NN3 cyclic graph with $N_A = 17$, for different values of k. Each line correspond to a different value of g strength of the partial SWAP interaction, from top to bottom $g = 0.5$, $g = 1.0$ and $g = 1.5$. The red dashed lines indicate the value of the population of the respective ρ_A, which is the value in which the system's population converges if homogenizaton happens. 99

6.1 Values of $\frac{\cos(g\tau)K}{K-\cos(g\tau)} \times g\tau$ for different values of K in the interval $g\tau \in [0, 2\pi]$. 113
6.2 $\Gamma_n(K, gt) \times n$ for different values of K, for $g = 0.8$ and $t = 1$ fixed. . . . 116
6.3 $\Gamma_n(K, gt) \times n$ for different values of g, for $K = 2$ and $t = 1$ fixed. 116
6.4 Example of a graph with ancillae in the vertices and the thickness of the edges between them represent the strength of the correlations (in this case the correlations are weaker for more distant ancillae), given by the adjacency matrix. 117
6.5 Correlations $(\xi_d^{(q)}) \times d$: distance of the neighbor ancilla from the first ancilla. The blue line is the correlation given by Eq. (6.66) mirrored from $n/2$, while the red line is the correlation of the graph state generated by our method. The parameters are $k = 1.0$, $\xi_0^{(q)} = 1.0$ and $K = 1.05$, with n indicated above the plots. 122
6.6 Correlations $(\xi_d^{(q)}) \times d$: distance of the neighbor ancilla from the first ancilla. The blue line is the correlation given by Eq. (6.66) mirrored from $n/2$, while the red line is the correlation of the graph state generated by our method. The parameters are $k = 1.0$, $\xi_0^{(q)} = 1.0$ and $K = 2.0$, with n indicated above the plots. 123
6.7 Correlations $(\xi_d^{(q)}) \times d$: distance of the neighbor ancilla from the first ancilla. The blue line is the correlation given by Eq. (6.66) mirrored from $n/2$, while the red line is the correlation of the graph state generated by our method. The parameters are $k = 1.0$, $\xi_0^{(q)} = 1.0$ and $K = 5.0$, with n indicated above the plots. 123
6.8 Correlations $(\xi_d^{(q)}) \times d$: distance of the neighbor ancilla from the first ancilla. The blue line is the correlation given by Eq. (6.66) mirrored from $n/2$, while the red line is the correlation of the graph state generated by our method. The parameters are $k = 1.0$, $\xi_0^{(q)} = 1.0$ and $n = 100$, with K indicated above the plots. 124

7.1 Heat (in unites of ω_0)/ Variance of the heat (in unites of ω_0^2) $\times\, t$. The blue lines represent the heat received by A and the blue dashed lines represent the variance of the heat when the the qubits are initially correlated. The red lines represent the heat received by A and the red dashed lines represent the variance of the heat when the the qubits are initially uncorrelated. The parameters are $g = 1$, $\beta_A = 2/\omega_0$ and $\beta_B = 1/\omega_0$. Each plot has a different value of α. In the first line we have, from left to right, $\mathrm{Im}(\alpha) = -\frac{e^{-\omega_0(\beta_A+\beta_B)/2}}{(1+e^{-\omega_0\beta_A})(1+e^{-\omega_0\beta_B})}$ and $\mathrm{Im}(\alpha) = +\frac{e^{-\omega_0(\beta_A+\beta_B)/2}}{(1+e^{-\omega_0\beta_A})(1+e^{-\omega_0\beta_B})}$, and in the second line $\mathrm{Im}(\alpha) = -1/20$ and $\mathrm{Im}(\alpha) = +1/20$. 135
7.2 $P(\mathcal{Q}_A) \times t$, for different values of $\mathcal{Q}_A$, computed numerically with the inverse Fourier transform of the characteristic function of Eq. (7.27). The initial joint state is prepared at $\rho_{AB}(0)$ of Eq. (7.22) with $\beta_A = 2/\omega_0$, $\beta_B = 1/\omega_0$, $\alpha = -i\frac{e^{-\omega_0(\beta_A+\beta_B)/2}}{(1+e^{-\omega_0\beta_A})(1+e^{-\omega_0\beta_B})}$ and we have $g = 1$. 137

7.3 Variance of $\mathcal{Q}_A$ (in units of ω_0^2) $\times$ t. The green curves represent the variance computed with the ensembles generated by the respective matrix M (see Appendix D) with the use of Eq. (7.30) while the gray curves represent the variance computed in an eigen-ensemble. The initial state $\rho_{AB}(0)$ is given by Eq. (7.22) with $\beta_A = 2/\omega_0$, $\beta_B = 1/\omega_0$ and $\alpha = -i \exp\left[-\omega_0(\beta_A + \beta_B)\right] / \left((1 + e^{-\omega\beta_A})(1 + e^{-\omega\beta_B})\right)$. For the unitary $U(g,t)$ we have $g = 1$. 140

8.1 $\langle \mathcal{Q}_A \rangle$ in units of ω (solid lines) and var$(\mathcal{Q}_A)$ in units of $\omega^2/3$ (dashed lines) $\times$ interaction time. For the blue curves in the plot on the left we have an initial state in the Simon form with $\mathbf{a} = 1.3$, $\mathbf{b} = 2.0$ and $c_+ = c_- = -1.0$, this state is correspondent to a D-minus thermal state. For the blue curves in the plot on the right we have an initial state in the Simon form with $\mathbf{a} = 2.0$, $\mathbf{b} = 1.3$ and $c_+ = c_- = 1.0$, this state is correspondent to a D-plus thermal state. The red curves correspond to initial locally thermal states but with no correlations ($c_+ = c_- = 0$) with $\mathbf{a} = \mathbf{1.3}$ and $\mathbf{a} = \mathbf{2.0}$ on the left and $\mathbf{a} = 2.0$ and $\mathbf{b} = 1.3$ on the right. The interaction strength is $g = 1.0$. 149

8.2 $\langle \mathcal{Q}_A \rangle$ in units of ω (solid lines) and var$(\mathcal{Q}_A)$ in units of $\omega^2/3$ (dashed lines) $\times$ interaction time. For all the curves in the plots we have initial states in the Simon form with $\mathbf{a} = 1.3$ and $\mathbf{b} = 2.0$. For the blue curves we have the respective values of $c_- = -c_+$ indicated above each plot, these initial states correspond to two-mode squeezed thermal states (see Appendix C, Section C.72). The red curves correspond to the same initial locally thermal states but with no correlations ($c_+ = c_- = 0$). The interaction strength is $g = 1.0$. 151

8.3 $\langle \mathcal{Q}_A \rangle$ in units of $\omega \times$ interaction time. The states are initially in the Simon form with $\mathbf{a} = 1.3$, $\mathbf{b} = 2.0$ and the values of the correlation parameters are indicated above the plots. For the blue curves we have the numerical calculation of the average by computing the trace in the finite Fock basis and for the red curves we have the plot of the average computed using the result of Eq. (8.24). The interaction strength is $g = 1.0$. 152

8.4 var$(\mathcal{Q}_A)$ in units of $\omega^2 \times$ interaction time. For the two plots in the left, the states are initially in the Simon form with $\mathbf{a} = 1.3$, $\mathbf{b} = 2.0$ and the values of the correlation parameters are indicated above the plots. For the plot in the right, the state is initially in the Simon form with $\mathbf{a} = 2.0 > \mathbf{b} = 1.3$ and $c_+ = c_- = 1.0$. For the blue curves we have the numerical computations using the eigen-ensemble choice while in the red curves we use our analytical results in the coherent states ensemble choice. The interaction strength is $g = 1.0$. 153

8.5 var$(\mathcal{Q}_A)$ in units of $\omega^2 \times$ interaction time. For all the plots the states are initially in the Simon form with $\mathbf{a} = 1.3$, $\mathbf{b} = 2.0$ and the values of the correlation parameters are indicated above the plots. For the blue curves we have the numerical computations using the eigen-ensemble choice while in the red curves we use our analytical results in the coherent states ensemble choice. The interaction strength is $g = 1.0$. 154

8.6 var($\mathcal{Q}_A$) in units of $\omega^2 \times$ interaction time. For all the plots, the states are initially in the Simon form with $\mathbf{a} = 1.3$, $\mathbf{b} = 2.0$ and the values of the correlation parameters are indicated above the plots. For the blue curves we have the numerical computations using the eigen-ensemble choice while in the red, gray and purple curves we use our analytical results in the coherent states ensemble choice for the P-function, W-function and Q-function chosen as seed probabilities. The interaction strength is $g = 1.0$. 156
8.7 From left to right: mutual information, quantum discord and classical information content in function of c_+ (horizontal axis) and c_- (vertical axis), for Simon states prepared with $a = 2$ and $b = 10$. 157
8.8 Heat average in units of ω (red), mutual information (black), quantum discord (blue) and classical correlations content (yellow) $\times$ time of interaction. Each plot represents a different initial state, all the initial states are in the Simon form with $a = 1.3$, $b = 2.0$ and with the correlation terms are described above each plot. 158
8.9 Heat variance in units of ω^2 (purple), mutual information (black), quantum discord (blue) and classical correlations content (yellow) $\times$ time of interaction. Each plot represents a different initial state, all the initial states are in the Simon form with $a = 1.3$, $b = 2.0$ and with the correlation terms are described above each plot. 158
8.10 Heat average (red), heat variance in units of ω^2 (blue) and mutual information (black) $\times$ time of interaction. Each plot represent a different initial state, all the initial states are in the Simon form with $a = 1.3$, $b = 2.0$ and with the correlation terms are described above each plot. 159

Chapter 1

Introduction

By the end of the 20th century, the merging of two important fields of knowledge, namely, Information Theory and Quantum Theory, set the formulation of the Quantum Information Theory [1–4]. This formulation was the result to the effort of enlightening questionings concerning to the foundations of Quantum Theory as well to the use of these clarifications for the flowering of ideas to new technologies. This movement is often called the *Second Quantum Revolution* [5, 6], and the technologies developed include Quantum Computing [1, 7], Quantum Cryptography [1], Quantum Simulation, Quantum Sensing and Quantum Metrology [8] which caused enormous attention to technology companies and hence even more research interest.

In the heart of such revolution is the concept of *quantum correlations* whose primordial researches can be traced to 1935 with the work of Einstein, Podolsky and Rosen (EPR) [9], Erwin Schrödinger [10] and debates with Niels Bohr [11]. The controversy was mainly about if the predictions of correlations pointed by EPR in Quantum Theory could cause it to be an incomplete theory, in the sense to be a theory with the necessity of additional *hidden variables* locally generated in a common past and without further nonlocal "spooky" interactions to explain such correlations. This was solved by John Bell in 1964 [12] by proving that, *only if* a certain average of observable respect a set of inequalities (now called Bell inequalities), then the correlations described by EPR could be caused by local hidden variables. It happens that Quantum Theory predicts such violation and this gave rise to the concept of a new kind of fully quantum (in the sense of without classical analogue) correlations, now called *entanglement*, which could not be explained by local

hidden variables. These events marked the beginning of what more recently caused the Second Quantum Revolution. Due to the importance of these discoveries nowadays, the most recent Nobel Prize in Physics was awarded to Alain Aspect, John F. Clauser and Anton Zeilinger due to their pioneering work on violating experimentally Bell's inequalities [13]. Therefore, quantum correlations are recently between the most prominent subjects in pure and applied physics and exploring new effects concerning them can blossom into new ideas and applications.

Inside this broader context, this thesis has the objective of searching for new effects caused by quantum correlations in cases where systems start their interactions already correlated. We use mainly the tools of quantum continuous-variables [14–16] to investigate the effects of initial correlations between quantum systems in their dynamical evolution and thermodynamic quantities. Our work can be stated in two main projects, the first one is concerned about a system evolution interacting with an initially correlated environment, being more concerned with the dynamics of the system. The second project has the main goal of obtaining the statistics of thermodynamic quantities of two initially correlated systems, specially of their heat distribution, using the framework of Beyesian Networks. The two projects can be described as follows.

1.1 Collisional model with initially correlated ancillae

This first project aims to explore an almost uncharted question of relaxation towards equilibrium: how do initial correlations between the environment parts affect the system equilibration? The analysis towards the answer in general can easily become intractable as the size of the environment becomes large, also general and standard bath models can present additional features that can obscure the effects caused by the initial correlations. For these reasons, we chose to focus on the so-called collisional models [17–21], in which we assume total control over environment features since here we suppose that the bath is composed of large number of smaller subunits (the ancillae) that interact individually with the system one at a time, each of these interactions is called a *collision*. This way, we are able to obtain manageable answers to the problem by extending methods already explored.

The effect of initial correlations between parts of the environment on the system evolution is, as already said, the main inquiry of this project, and it can be understood as the following analogy suggests. Suppose a group of workers (ancillae) want to convince a boss (system) that he/she must buy them new tools, but each of them enters and argues to the boss alone at his office (interact individually and one at a time). If the workers talked to each other before going to the boss' office and have some plan or information shared (correlations), then the result of the boss' mind (final state of the system) will be different than if they had not talked to each other.

Our results reveal an unfamiliar phenomenon of steering caused by the initial correlations between the environmental parts. We obtain these results numerically for the case where system and ancillae are qubits and analytically, which a more complete description, for the case where the system and ancillae are bosonic modes. These last more detailed results were possible due to the use of continuous-variables methods. As a comparison to well-known results, we make a contrast with the results of [19], where for a certain kind of interaction and initially identical ancillae, the whole system and ancillae become a set of identical parts, this is the so-called *homogenization*. We show that homogenization can become impossible if the ancillae are initially correlated.

1.2 Statistics of thermodynamic quantities using Bayesian Networks

With the Second Quantum Revolution, increasing attention has been brought to the growing field of Quantum Thermodynamics [22–25] from reasons that range from extending the Thermodynamic laws to the quantum domain, understanding fundamental relations between thermodynamics and information [26–28] to studies of the enhancement of the efficiency of quantum thermal machines using quantum features [29–32]. However, the description of the statistics of thermodynamic quantities, such as heat and work is often made with the use of Two-Point Measurement (TPM) procedure [33–35] which spoils the coherence of the initial state and consequently the effect of quantum correlations due to the supposition of measurements. Alternatives without this undesired feature involve work operator definitions [36, 37], which cannot hold fluctuation relations [34, 35, 38–

40], and quasi-probabilities [41, 42] which cannot be described by a quantum measurement. The objective of this second project is to fulfill this gap of constructing a statistics of thermodynamic quantities which fully accounts for initial quantum correlations and coherence, focusing primarily in the specific case of obtaining the probability distribution for the heat exchanged between two initially correlated systems interacting as a closed system.

By making use of the concept of Bayesian Networks (BNs) [43–47] in the context of quantum theory, Ref. [48] successfully described fluctuation relations fully considering the effect of initial correlations and coherence. Additionally, this framework can be described by quantum measurements protocols [49]. Therefore, we chose the BN framework to obtain our statistics for thermodynamic quantities. The BN concept has wide application in statistics, engineering and mainly in artificial intelligence. It consists in a method which infers the probabilities of the evolution of the system from conditional distributions of the previous state of the system, supposing a causal relation from this past.

We follow the construction initiated in Ref. [48], focusing in deepening our understanding on the statistics of thermodynamic quantities. We obtain general formulae for the characteristic function (and consequently, the statistical moments) for the probability distribution of the *change* (or variation) of an observable during an evolution of the system, such changes of observable can represent thermodynamic quantities, such as heat and work. Our results reveal a dependence of the probability distribution on the initial density matrix choice of ensemble to represent it. The consequence of the different choice of ensembles turns to be one of our main attentions due to the different interpretations it can result.

As our main goal and application, we apply this framework to understand deeply the statistics of heat exchanged between two systems and the consequences of initial correlations in this exchange. As a well-known effect caused by initial correlations, we recover the heat flow inversion [50–53], which was obtained experimentally for the interaction of two qubits [54]. And we propose conditions for such inversion to happen for the case of two bosonic modes interacting. Due to the unexplored character of the subject, we study the variance of the heat probability distribution and how it behaves with the presence of correlations. This is done numerically for the case of two qubits, and analytically for

the case of two bosonic modes. Interesting features are raised due to the different choice of ensembles to be made in continuous-variables for bosonic modes, such as the use of quasi-probabilities.

1.3 Structure of the thesis

This thesis will be organized as follows. It is divided in two parts, Part I (chapters 2 to 4) resumes the background used to obtain our results, there is no original result among the chapters of this part. In Part II (chapters 5 to 8) we have our main projects and the results contained in these chapters are original. Chapters 5 and 6 refer to the first project of the thesis while chapters 7 and 8 refer to the second project.

Chapter 2 contain a brief resume of Open Quantum Systems paradigm with the essential parts needed to construct our work and we introduce and define the concept of collisional models as well as the notion of homogenization. In Chapter 3 we present a resume of the parts concerning to Quantum Information that we shall use. We also define in this chapter precisely what we denominate as correlations and quantum correlations, introducing the concept of *Quantum Discord*, for further use, being a broader concept of quantum correlations than the aforementioned entanglement. The last section of this chapter will make a brief presentation of BNs and how it is applied to describe the evolution of quantum systems.

In Chapter 4 we present the framework of continuous-variables. This is an extensive chapter since it permit us to obtain analytical results specially when dealing with Gaussian states, so a considerable part of the text will be restrained to a careful construction and explanation of such methods. This makes a large part of our results to be possibly applicable in the realm of bosonic states and Quantum Optics [55, 56].

In Chapter 5 we present the structure and results for the simulations of our qubit minimal collisional model with initially correlated ancillae. Chapter 6 is devoted to the structure and analytical results of our collisional model with initially correlated ancillae, where the state and ancillae are bosonic modes. The last section of this chapter will expose our construction of correlated environments made of bosonic Gaussian states with the use of graph states.

Chapter 7 will develop briefly the concept of BN, then apply it to find the statistics for the changes of observable for bipartite initially correlated systems in very general terms. Here we expose general results about the statistics of such changes as well as applications to the case of two qubits initially correlated. Finally, in Chapter 8 we apply Chapter 7 results to obtain conclusions for the heat probability distribution between two bosonic modes and the relation between this distribution and the quantum correlations between the modes.

Finally, Chapter 9 is devoted to the final remarks and possible future works concerning to the thesis results.

Part I

Background

Chapter 2

Open Quantum Systems and Collisional Models

In first two sections of this chapter we shall give a short introduction to the paradigm of Open Quantum Systems [57–59] which deals successfully with quantum phenomena, maintaining untouched all Quantum Mechanics postulates, but adding the concept of open evolution in a similar way to the Stochastic Physics [60–62]. This framework had its foundations constructed by von Neumann, Kraus, Lindblad and many others, generally obtaining the system's evolution by considering finite time steps, given by Kraus operations, or solving Lindblad Master Equations (analogously as the classical Master Equations case) to obtain continuum time evolution. We shall focus here in the first approach which are the methods used in the present work.

In this paradigm, commonly a bath is decomposed in a continuum of quantum harmonic modes, these modes interact with the system via a coupling which is appropriate to the physical phenomenon in description. Finding the dynamics of the system under this interaction with these baths is normally a daunting problem and most solutions involve Markovian (past independent) approximations. As a less orthodox approach, Collisional Models (CMs) [20, 21, 63] (also dubbed as "Collision Models" and "repeated interaction schemes") suppose that the bath is composed of large number of smaller subunits (the ancillae) that interact individually with the system one at a time. In the present quantum formulation, these models were first proposed by Jayaseetha Rau in 1963 [17], which was inspired in Boltzman's *Stosszahlansatz* molecular chaos hypothesis [62, 64].

Since then, CMs have became very attractive for a vast range of applications, ranging from weak measurements to a very satisfactory description of the micromaser [65–70]. At the beginning of the 21st century, the interest in quantum computation brought attention to the implementation of collisional models with interactions involving two qubits, which resulted in the concept of *homogenization* [18, 19], a well explored concept in this thesis, as well as studies of using CMs to describe the decoherence of qubits [71]. In the past decade, CMs have a major role in studies of non-Markovian dynamics and Quantum Thermodynamics [63, 72–88]. In the last section of this chapter, we shall introduce the framework of CMs, a few examples of models and physical implementations in order to prepare for the description of the first project of this thesis.

2.1 The density matrix

Open quantum systems, as the name suggests, deals with systems that interact with an environment capable to exchange energy and information. Although the closed quantum systems formalism could encompass systems that exchange energy (with a time dependent hamiltonian), it would never be capable of describing systems that dissipate information. The reason is because all the closed quantum system formalism only deals with the hypothesis that we know in which quantum state the system is and its evolution will be deterministic according to Schrödinger's Equation. We must have a formalism that takes into account the lack of information about which quantum state the system is and obtain an equation where the evolution is not necessarily deterministic.

In classical stochastic processes or statistical mechanics, when we don't know the state of the system, we can associate to each classical state (for instance a point (x, p) on the phase space) a probability $P(x, p)$ that the system is in this state. In the quantum case, the same can be done for a set of quantum states $\{|\psi_k\rangle\}$ in a Hilbert space $\mathcal{H}$, assigning a probability P_k for each $|\psi_k\rangle$. The difference exists when we compute the average of an observable A. To accomplish this we must to take into consideration the quantum and classical uncertainties ("classical uncertainties" here refers to the lack of information) and

we have to make a classical average over quantum averages

$$\langle A \rangle = \sum_k P_k \langle \psi_k | A | \psi_k \rangle . \tag{2.1}$$

In order to compress quantum and classical information into a single object describing the state, von Neumann introduced [89] the **density matrix**

$$\boxed{\rho = \sum_k P_k |\psi_k\rangle \langle \psi_k| ,} \tag{2.2}$$

and with this definition we may write averages like Eq. (2.1) as

$$\boxed{\langle A \rangle = \sum_k P_k \langle \psi_k | A | \psi_k \rangle = \mathrm{Tr}(A\rho).} \tag{2.3}$$

There are some requirements that a generic operator must satisfy if we want to consider it as a physical density matrix. First we must notice that, due to the normalization of the kets $|\psi_k\rangle$ and probabilities $\sum_k P_k = 1$, we must have a density matrix normalization $\mathrm{Tr}(\rho) = 1$. And second, for any generic ket $|\phi\rangle$, we must have $\langle \phi | \rho | \phi \rangle = \sum_k P_k |\langle \phi | \psi \rangle|^2 \geq 0$, which states that ρ must be a *positive semi-definite* matrix (in symbols $\rho \geq 0$). So, for an operator to be able to describe a physical density matrix, it *must* satisfy

$$\text{Positive semi-definite:} \quad \boxed{\rho \geq 0,} \text{ and} \tag{2.4}$$

$$\text{Normalization:} \quad \boxed{\mathrm{Tr}(\rho) = 1.} \tag{2.5}$$

Also, it is important to remember that ρ *must be a hermitian operator*, and this is covered by the positive semi-definite condition (all positive semi-definite operators are hermitian).

We shall often refer to the density matrix ρ as "the state" of a given system. The reason for this is similar to describing a classical state by a probability distribution: the distribution is the best description one can have, given the information accessible (even though it is not the full description given by a phase space point), and the same is true for the density matrix, serving as a "distribution" of quantum states. The non-diagonal terms of the density matrix are often called *coherence* terms. These terms are dependent on the

basis we choose to represent the density matrix and represent the superposition terms in the respective basis.

When one has certainty about the state of the system, then we say that the state is *pure*. This happens if for some j, $P_j = 1$ and $P_k = 0,\ \forall k \neq j$ in Eq. (2.2), which implies that $\rho = |\psi\rangle\langle\psi|$, for some state $|\psi\rangle$ (we omit the j here just for convenience). In this case the density matrix is equivalent to the ket $|\psi\rangle$, and there is no lack of information about the system. But it is really important to remember that, in general terms, Eq. (2.2) cannot be factorized as a pure state, i.e., we really have lack of information about which quantum state the system is, and for this case we say that the state is *mixed*.

To show if a density matrix can be parametrized as a pure state or not is, in general not an easy task. To this end, one may define the *purity* of the state ρ as

$$\mathcal{P}(\rho) = \mathrm{Tr}\left(\rho^2\right). \tag{2.6}$$

It can be shown (see appendix A) that the purity of a state ρ is 1 *if and only if* ρ is a pure state and also that $1/d \leq \mathcal{P}(\rho) \leq 1$ for any ρ. Consequently, purity is the decisive witness which points out if a state is pure or not.

2.2 Dynamics

2.2.1 Closed systems - Unitary operators

As we are used to, the dynamics for a closed pure system $|\psi(t)\rangle$ with a hamiltonan H in Quantum Mechanics is given by the Schrödinger Equation (setting $\hbar \to 1$ throughout)

$$\boxed{i\frac{\partial\,|\psi(t)\rangle}{\partial t} = H\,|\psi(t)\rangle\,,} \tag{2.7}$$

which has the following solution

$$|\psi(t)\rangle = U(t-t_0)\,|\psi(t_0)\rangle\,, \tag{2.8}$$

where, for time independent hamiltonians, we have the unitary operator

$$U(t-t_0) = e^{-iH(t-t_0)}, \tag{2.9}$$

and $|\psi(t_0)\rangle$ is the initial system state.

We may notice that the evolution of any system initially in $|\psi_k(t_0)\rangle$ also evolves as $|\psi_k(t)\rangle = U(t-t_0)\,|\psi_k(t_0)\rangle$. So for a density matrix like in Eq. (2.2), the evolution is

$$\rho(t) = U(t-t_0)\rho(t_0)U^\dagger(t-t_0), \tag{2.10}$$

for an initial density matrix $\rho(t_0) = \sum_k P_k\,|\psi_k(t_0)\rangle\,\langle\psi_k(t_0)|$ in a closed system.

Eq. (2.10) sets the evolution for any time step $t - t_0$ of a density matrix, and is the solution of the equation that plays the same role as Schrödinger's Equation, but for density matrices, the so-called *von Neumann Equation*

$$\boxed{\frac{d\rho(t)}{dt} = -i[H, \rho(t)].} \tag{2.11}$$

2.2.2 Open systems - Kraus matrices

One of the standard approaches to deal with open quantum systems is to consider the system state $\rho_S(t_0)$ (acting on a Hilbert space $\mathcal{H}_S$) and environment state $\rho_E(t_0)$ (acting on a Hilbert space $\mathcal{H}_E$) together as an initially uncorrelated joint system $\rho_{SE}(t_0) = \rho_S(t_0) \otimes \rho_E(t_0)$ and make an unitary evolution of this joint system $\rho_{SE}(t) = U(t-t_0)\rho_{SE}(t_0)U^\dagger(t-t_0)$. The system resulted from tracing out the environment (see Appendix A for the definition of partial trace) will be our evolved system $\rho_S(t) = \mathrm{Tr}_E[\rho_{SE}(t)]$ and the map from $\rho_S(t_0)$ to $\rho_S(t)$, in general, will not be unitary. The procedure of evolving unitarily the joint system and tracing out the environment is called *Stinespring representation* and can be made to describe an open quantum system, as the following discussion shows.

Writing the above procedure explicitly, we obtain

$$\boxed{\rho_S(t) = \mathrm{Tr}_E\{U\rho_S(t_0) \otimes \rho_E(t_0)U^\dagger\},} \tag{2.12}$$

where we are omitting the $(t - t_0)$ in U just for practicality. Now if we make a spectral decomposition of the initial environment density matrix

$$\rho_E(t_0) = \sum_m q_m \left|m\right\rangle_E \left\langle m\right|_E ,$$

(where the sub index E in $\left|m\right\rangle_E$ just makes it explicit that $\left|m\right\rangle$ belongs to the basis of $\mathcal{H}_E$ that diagonalizes ρ_E) and apply it in Eq. (2.12), we obtain

$$\rho_S(t) = \mathrm{Tr}_E \left\{ \sum_m q_m U \left|m\right\rangle_E \rho_S(t_0) \left\langle m\right|_E U^\dagger \right\} = \sum_{m,k} q_m \left\langle k\right|_E U \left|m\right\rangle_E \rho_S(t_0) \left\langle m\right|_E U^\dagger \left|k\right\rangle_E , \tag{2.13}$$

where in the last equality we computed the partial trace in the same basis as $\left|m\right\rangle_E$. Finally, if we define (putting $(t - t_0)$ back to U)

$$M_{k,m}(t - t_0) = \sqrt{q_m} \left\langle k\right|_E U(t - t_0) \left|m\right\rangle_E , \tag{2.14}$$

and rename the collective index (k, m) to α, we obtain

$$\rho_S(t) = \sum_\alpha M_\alpha(t - t_0)\rho(t_0)M_\alpha^\dagger(t - t_0). \tag{2.15}$$

This equation has the form of the *Kraus representation* [90]

$$\boxed{\mathcal{E}(\rho) = \sum_\alpha M_\alpha \rho M_\alpha^\dagger.} \tag{2.16}$$

of a *quantum channel* $\mathcal{E}$, where M_α are called *Kraus matrices* and must satisfy

$$\boxed{\sum_\alpha M_\alpha^\dagger M_\alpha = 1.} \tag{2.17}$$

Quantum channels are the linear operations that transform density matrices onto density matrices, maintaining all their properties (Eq. (2.4) and Eq. (2.5)) and hence are appropriate operations for the general description of open quantum systems dynamics (such as unitary operators are for closed systems). They are called linear completely

positive trace preserving (CPTP) maps[1]. It can be shown (see, for instance, [1, 57, 91]) that every linear CPTP map can be described in the form of a Kraus representation (Eq. (2.16)) and vice-versa for a set of Kraus matrices, thus it sets a necessary and sufficient condition to describe an open system dynamics. Its intuition can be founded in making a parallel to Markov chains for discrete time evolution. We shall follow this scheme in our work, considering interactions that last finite time between part of the environment (the ancillae) and making the partial trace in order to obtain the desired dynamics of our collisional model.

2.3 Collisional Models

2.3.1 General case (correlated ancillae)

Suppose we have a system S that starts interacting, at a time $t = 0$, with an environment E, which is separated in n sub systems A_j ($1 \geq j \geq n$) named *ancillae*. We say that we have a Collisional Model (CM) whenever the system interacts individually, one at a time and only once with each ancilla and we call each of these interactions a *collision* (see Fig. 2.1). There are studies on CMs in which the ancillae interact with themselves after the instant $t = 0$ (see, for instance, [80]), but in our case we assume that this is not the case.[2]

Given those demands, the depiction of the system's interaction with the j-th ancilla, during a time τ (we suppose all ancilla-system interactions last the same time), is given by a unitary operator

$$U_j = e^{-iH_j\tau}, \tag{2.18}$$

in which

$$H_j = H_S + H_{A_j} + V_j, \tag{2.19}$$

where H_S is the system's internal Hamiltonian, H_{A_j} is the internal Hamiltonian of the

[1] Actually, the term *completely positive* means a stronger assumption: that given a density matrix ρ, then the matrix $(\mathcal{I} \otimes \mathcal{E})(\rho)$ must also be positive, where $\mathcal{I}$ is the identity operator acting on an extra system R of arbitrary dimensionality.

[2] We do consider that the ancillae may interact with themselves before starting the dynamics with the system, in order for them to be initially correlated. In fact, the study of the effects of such initial correlations in the system is one of the main themes of this thesis.

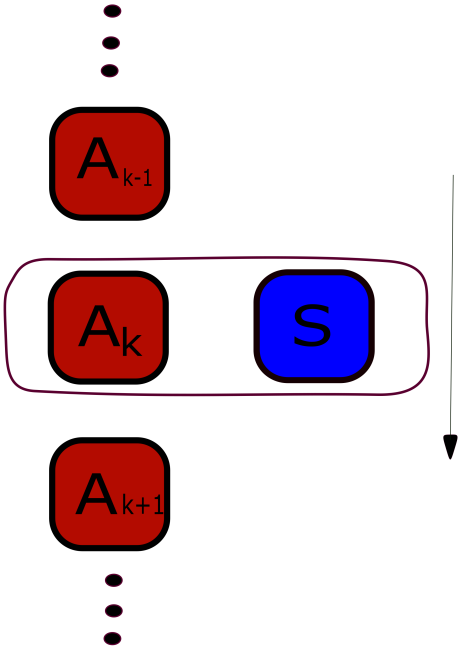

Figure 2.1: Schematic of collisions, where the system S is interacting individually with the k-th ancilla during a time τ going to interact with the next ancilla also during a time τ.

j-th ancilla and V_j describes the interaction between the system and the j-th ancilla. Then the joint state of system plus all ancillae after the n-th collision is given by

$$\rho_{SE}^{n} = U_n U_{n-1} \cdots U_2 U_1 \rho_S^0 \otimes \rho_E^0 U_1^\dagger U_2^\dagger \cdots U_{n-1}^\dagger U_n^\dagger, \tag{2.20}$$

where we supposed that the initial joint state ρ_{SE}^0 is the tensor product between the initial system ρ_S^0 and the environment ρ_E^0 (remembering, inside this environment state are all the ancillae and possible correlations among them) since their interaction only starts at $t = 0$. Furthermore, we trace out all the environment in order to obtain the system's *stroboscopic*[3] evolution after the n-th collision

$$\begin{aligned} \rho_S^n &= \mathrm{Tr}_E \left\{ \rho_{SE}^n \right\} \\ &= \mathrm{Tr}_E \left\{ U_n U_{n-1} \cdots U_2 U_1 \rho_S^0 \otimes \rho_E^0 U_1^\dagger U_2^\dagger \cdots U_{n-1}^\dagger U_n^\dagger \right\}. \end{aligned} \tag{2.21}$$

[3] "Stroboscopic" means that our interest is only in the evolution steps multiples of τ, no attention is given for the intermediate time evolution.

Suppose we wish to analyse the evolution of the system after the second collision ($n = 2$), Eq. (2.21) will result in

$$\begin{aligned}\rho_S^2 &= \mathrm{Tr}_E \left\{ U_2 U_1 \rho_S^0 \otimes \rho_E^0 U_1^\dagger U_2^\dagger \right\} \\ &= \mathrm{Tr}_{A_2} \left\{ U_2 \, \mathrm{Tr}_{A_1} \left\{ U_1 \rho_S^0 \otimes \rho_E^0 U_1^\dagger \right\} U_2^\dagger \right\} \\ &= \mathrm{Tr}_{A_2} \left\{ U_2 \rho_{SA_2} U_2^\dagger \right\} \\ &\neq \mathrm{Tr}_{A_2} \left\{ U_2 \rho_S^1 \otimes \rho_{A_2} U_2^\dagger, \right\} \end{aligned} \tag{2.22}$$

where we defined $\rho_{SA_2} = \mathrm{Tr}_{A_1} \left\{ U_1 \rho_S \otimes \rho_E U_1^\dagger \right\}$ as a density matrix that acts on $\mathcal{H}_S \otimes \mathcal{H}_{A_2}$, where $\mathcal{H}_{S(A_2)}$ is the Hilbert space of $S(A_2)$. The last line of Eq.(2.22) above happens because ρ_{SA_2} cannot in general be parametrized as a tensor product $\rho_S^1 \otimes \rho_{A_2}$ (where ρ_S^1 is the density matrix of the evolved system after the first collision) due to the initial correlation between the ancillae. This way the ρ_S^2 in Eq. (2.22) cannot result in a map between ρ_S^1 and ρ_S^2, and the evolution of the system from the first collision into the second will not be a CPTP map. The reason for this is that the initial correlations causes the system evolution to be non-Markovian, since after the first collision the second ancilla already obtain information about the system. The information about the initial system affects the system itself at the second collision, clearly this narrative also happens for all further collisions.

As the case above suggests, non-Markovianity preclude intermediate maps to be CPTP, i.e., if we have a CPTP map $\mathcal{E}_{t_2-t_0}$ that evolves a state from t_0 to t_2, we cannot break it in two CPTP maps $\mathcal{E}_{t_2-t_1}$ and $\mathcal{E}_{t_1-t_0}$ such that $\mathcal{E}_{t_2-t_0} = \mathcal{E}_{t_2-t_1}\mathcal{E}_{t_1-t_0}$ for some intermediate time t_1. This aspect of Non-Markovianity is studied in CMs (see, for instance, Refs. [72–86]) and is a caveat for obtaining the evolution of the system, since it makes impossible to gradually describe the system's evolution by a cumulative sequence of simpler steps. Chapters 5 and 6, which are intended for the results of the first project of the thesis, focus on obtaining non-Markovian dynamics caused by the initial correlations between the ancillae. In the rest of this chapter we shall present the standard Markovian CMs framework, as well as special cases, such as homogenization, that will contrast with the results of the following chapters.

2.3.2 Markovian case

For standard CMs we suppose, in addition to the assumptions above, that initially all ancillae are uncorrelated, so that the environment is factorized as

$$\rho_E^0 = \rho_{A_1} \otimes \rho_{A_2} \otimes \cdots \otimes \rho_{A_n}, \tag{2.23}$$

where each ρ_{A_j} acts on its respective ancilla Hilbert space $\mathcal{H}_j$. Using this at Eq. (2.21) we obtain a major simplification in our strobocopic evolution

$$\rho_S^n = \mathrm{Tr}_{A_n}\left\{U_n \cdots \mathrm{Tr}_{A_2}\left\{U_2\,\mathrm{Tr}_{A_1}\left\{U_1\rho_S^0 \otimes \rho_{A_1}U_1^\dagger\right\} \otimes \rho_{A_2}U_2^\dagger\right\}\cdots \otimes \rho_{A_n}U_n^\dagger\right\}, \tag{2.24}$$

where we just used that the partial trace over A_m does not affect operators that don't act on $\mathcal{H}_{A_m}$. Now, if we define a map $\mathcal{E}^{(n)}$, called *collision map* or *stroboscopic map*, acting on a state ρ_S as

$$\boxed{\mathcal{E}^{(n)}(\rho_S) = \mathrm{Tr}_{A_n}\left\{U_n\rho \otimes \rho_{A_n}U_n^\dagger\right\},} \tag{2.25}$$

then Eq. (2.24) can be rewritten as

$$\rho_S^n = \mathcal{E}^{(n)}(\mathcal{E}^{(n-1)}(\cdots\mathcal{E}^{(1)}(\rho_S^0))), \tag{2.26}$$

which represents the successive application of CPTP maps, since the map in Eq. (2.25) is CPTP as consequence of having the form of a Stinespring reprentation (see Eq. (2.12)). This successive application of CPTP maps forming a CPTP map indicate that all the stroboscopic dynamics is Markovian. This is a direct consequence of the absence of initial correlations between the ancillae.

As done in most of studies in CMs and will be often done in this work, we consider that all the ancillae are isomorfic and start at exactly the same state, thus $\rho_{A_j} = \rho_A$ for every j. The internal Hamiltonian of the system and ancillae will be set to 0 (unless specified),[4] and the interaction between the ancillae and the system are equal, i.e., $V_j = V$[5] for all j in Eq. (2.19) and consequently all unitary operators are the same ($U_j = U$ for all j). In

[4] Actually, this condition of setting H_S and H_{A_j} to 0 is equivalent of demanding that $H_S = H_{A_j}$, $[H_S, V_j] = 0$, and going to the interaction picture (see Appendix A).

[5] Of course, the operators V_n are identical but each act only on the system and their respective ancillae A_n.

this case the stroboscopic map will be independent of n, $\mathcal{E}^{(n)} = \mathcal{E},\ \forall n$, and hence

$$\rho_S^n = \mathcal{E}^n(\rho_S^0), \tag{2.27}$$

which means that it will be sufficient to find the map $\mathcal{E}$ and apply it n times in the initial state in order to obtain the full evolution. Similarly we can obtain the state of the n-th ancilla after its collision with the system, it will be the result of tracing out the system from the evolution of $\rho_S^n \otimes \rho_A$, explicitly

$$\rho_A^n = \mathrm{Tr}_S \left\{ U \rho_S^n \otimes \rho_A U^\dagger \right\} = \mathrm{Tr}_S \left\{ U(\mathcal{E}^n(\rho_S^0) \otimes \rho_A) U^\dagger \right\}. \tag{2.28}$$

2.3.3 Qubit example, thermalizing machines

Proceeding with the restrictions above, we assume that the system and ancillae are qubits (all-qubit model) and that all the ancillae are initially in a *thermal state* (see Appendix A, in particular Eq. A.22)

$$\rho_{\text{th}} = (1 - p_{\text{th}}) P_0 + p_{\text{th}} P_1, \tag{2.29}$$

when $0 \leq p_{\text{th}} \leq 1/2$, $P_0 = |0\rangle\langle 0|$, $P_1 = |1\rangle\langle 1|$, are the projectors of the eigenstates of σ_z ($|0\rangle$ and $|1\rangle$) with eigenvalues -1 and 1 respectively. If we set the Hamiltonian of each ancilla qubit to $H_0 = E\sigma_z$ (with $E > 0$), then $|0\rangle$ is the ground state qubit and $|1\rangle$ is the excited state and hence p_{th} is the probability that the qubit is in the ground state. If we now ask which are the unitaries U that could construct a collision map $\mathcal{E}$ such that

$$U(\rho_{\text{th}} \otimes \rho_{\text{th}}) = \rho_{\text{th}} \otimes \rho_{\text{th}} \ \text{ and} \tag{2.30}$$

$$\rho_S^n = \mathcal{E}^n(\rho_S^0) \xrightarrow{n\to\infty} \rho_{\text{th}},\ \forall \rho_S^0. \tag{2.31}$$

The most general answer is that the unitaries must have the form of Eq. (2.18) (remembering that in this case they are all identical, independent of j) with the Hamiltonian

$$H(g, g_z) = g(\sigma_+ \otimes \sigma_- + \sigma_- \otimes \sigma_+) + g_z \sigma_z \otimes \sigma_z, \tag{2.32}$$

where g and g_z are real numbers and

$$\sigma_- = \sigma_+^\dagger = \frac{1}{2}(\sigma_x - i\sigma_y) = |0\rangle\langle 1|\,. \tag{2.33}$$

This result was obtained in Ref. [18], which also brands that any setup responsible for the quantum operation respecting Eqs. (2.30) and (2.31) is called a *thermalizing machine* and the process of the system relaxing towards ρ_{th} is called *thermalization*. These terms are easily justified since Eq. (2.30) affirms that if the system is at the same state as the thermal ancillae, then the evolution stagnate, while Eq. (2.31) means that the quantum operation is such that system's state will converge to the thermal ancillae independent of the system's initial state, i.e., this CM setup will make the system eventually thermalize.

As an example of thermalization made with simple computations, we suppose that all the ancillae start with the state $\rho_A = |0\rangle\langle 0|$ (this is the ground state, which is the thermal state at the limit $T \to 0$, so we are supposing a very cold environment) and the initial system state is an arbitrary qubit which can be always parametrized as

$$\rho_S^0 = \begin{pmatrix} \langle 0|\rho_S^0|0\rangle & \langle 0|\rho_S^0|1\rangle \\ \langle 1|\rho_S^0|0\rangle & \langle 1|\rho_S^0|1\rangle \end{pmatrix} = \begin{pmatrix} 1-p & C \\ C^* & p \end{pmatrix}, \tag{2.34}$$

where $0 \leq p \leq 1/2$ and $(1-2p)^2 + 4|C|^2 \leq 1$ which are conditions that come from of positivity and unit trace. Here p is the *population* of the excited state $|1\rangle$ and C is the *coherence*. Now if we explicitly compute the unitary with the Hamiltonian given by Eq. (2.32), we obtain

$$\begin{aligned} U(g,g_z) &= e^{-iH(g,g_z)\tau} \\ &= e^{-i2g_z\tau}(|00\rangle\langle 00| + |11\rangle\langle 11|) + \cos(g\tau)(|10\rangle\langle 10| + |01\rangle\langle 01|) - i\sin(g\tau)(\sigma_+\sigma_- + \sigma_-\sigma_+), \end{aligned} \tag{2.35}$$

where we just used that $|00\rangle, |11\rangle$ and $\frac{1}{\sqrt{2}}(|10\rangle \pm |01\rangle)$ are the eigenvectors of $H(g,g_z)$ with eigenvalues g_z, g_z and $\pm g - g_z$, respectively and use it to expand the exponential operator in the eigenvector basis (also we omitted the tensor product sign $|a\rangle \otimes |b\rangle = |ab\rangle$ for convenience). We can now use the unitary above to obtain the collision map, according

to Eq. (2.25)

$$\begin{aligned}\mathcal{E}(\rho_S^0) &= \mathrm{Tr}_A\left\{U(g,g_z)\rho_S^0\otimes|0\rangle\langle 0|U^\dagger(g,g_z)\right\}\\ &= \begin{pmatrix}(1-p)+\sin^2(g\tau)p & e^{2ig_z\tau}\cos(g\tau)C\\ e^{-2ig_z\tau}\cos(g\tau)C^* & \cos^2(g\tau)p\end{pmatrix}.\end{aligned} \tag{2.36}$$

By iterating this map[6] n times in order to obtain the system's evolution after the n-th collision (according to Eq. (2.27)), we obtain

$$\rho_S^n = \begin{pmatrix}1-p_n & C_n\\ C_n^* & p_n\end{pmatrix}, \tag{2.37}$$

where $C_n = e^{2ig_z n\tau}\cos^n(g\tau)C$ and $p_n = \cos^{2n}(g\tau)p$. As we can see, C_n and p_n go to 0 as n gets large (of course, if $g\tau$ isn't an integer multiplied by π). This highlights two effects of dissipation due the bath: the *decoherence* (the vanishing of the off-diagonal terms), as usually happens when a quantum system is interacting with a thermal bath (in this case, even with the bath at a very low temperature), and the decay of the population of the excited state $|1\rangle$, pushing the system to the steady-state $|0\rangle\langle 0|$. This steady-state is nothing but the thermalization of the system towards the initial 0 temperature ancillae state.

2.3.4 Steady-states

We already tacitly used the concept of *steady-state* as the state in which the system converge after a long time interacting with the environment. For making this definition more concrete, we say that a state ρ^* is a steady-state of a map $\mathcal{E}$, if and only if

$$\boxed{\mathcal{E}(\rho^*) = \rho^*.} \tag{2.38}$$

ρ^* is also called a fixed point of the map.

Notice that the steady-state needs not to be unique. A map that has a unique stateady-

[6] For the case of $g_z = 0$ this map is the same as the well-known *amplitude damping* [1, 91].

state is called *ergotic*, and if

$$\mathcal{E}^n(\rho) \to \rho^*, \tag{2.39}$$

for large n and any density matrix ρ, then this map is said to be *mixing*. Consequently, any mixing map is ergotic, and thus if one proves the mixing of a map which leads the initial state to ρ^*, it will be the unique steady-state (this will be our procedure in bosonic CMs in Chapter 5).

The process of thermalization in Eqs. (2.30) and (2.31) is a mixing map which has ρ_{th} as fixed point. A slightly more general concept is that of *thermal operations*, in which the ancillae need not be isomorphic to the state but the state thermalize to a thermal state in the same temperature as the ancillae. This is an important concept in the context of *Resource Theories* and it can be proved that any energy conseving unitary generating a CM map like in Eq. (2.25) (with ancillae in thermal states) is a thermal operation [92]. This kind of unitary will describe the main interactions studied in this thesis, including the *Partial SWAP*.

2.3.5 SWAP and Partial SWAP

Another important case of a thermalizing machine which will be important in this thesis is when the interaction is given by $g_z = g/2$ in Eq. (2.32), here the Hamiltonian will have the form

$$H(g, g/2) = \frac{g}{2}\vec{\sigma}\cdot\vec{\sigma}, \tag{2.40}$$

where $\vec{\sigma}\cdot\vec{\sigma} = \sigma_x^1\otimes\sigma_x^2 + \sigma_y^1\otimes\sigma_y^2 + \sigma_z^1\otimes\sigma_z^2$, we used that $\sigma_+^1\sigma_-^2 + \sigma_-^1\sigma_+^2 = \frac{1}{2}(\sigma_x^1\sigma_x^2 + \sigma_y^1\sigma_y^2)$ and here $\sigma_i^{1(2)}$ means the i Pauli matrix acting in the first(second) qubit. This Hamiltonian is, except for a constant term, equivalent to the *SWAP Operation*

$$S = \frac{1}{2}\left(\mathbf{I} + \vec{\sigma}\cdot\vec{\sigma}\right), \tag{2.41}$$

where $\mathbf{I}$ is the identity operator. The SWAP operation is a very important quantum channel having applications from Open Quantum Systems to Quantum Computation. Its main

property is that, given two states $|\psi\rangle$ and $|\phi\rangle$, then

$$\boxed{S(|\psi\rangle \otimes |\phi\rangle) = |\phi\rangle \otimes |\psi\rangle\,.} \tag{2.42}$$

Actually, Eq. (2.42) is a more general definition of the SWAP, being valid for any set of two vectors in a Hilbert space. Conversely, Eq. (2.41) is equivalent to Eq. (2.42) only for the case of two cubits.

A direct consequence of Eq. (2.42) is

$$SS = S^2 = \mathbf{I}, \tag{2.43}$$

which can be used to directly show that the SWAP generates the *Partial SWAP Operation*

$$\boxed{U_P(g\tau) = e^{-ig\tau S} = \cos(g\tau)\mathbf{I} + i\sin(g\tau)S.} \tag{2.44}$$

It can be shown (see Ref. [19]) that the Partial SWAP of Eq. (2.44) is, except for an irrelevant phase term, the only unitary U that satisfies the following two properties

$$\mathrm{Tr}_1\{U\rho \otimes \rho U^\dagger\} = \rho \quad \text{and} \tag{2.45}$$

$$\mathrm{Tr}_2\{U\rho \otimes \rho U^\dagger\} = \rho, \tag{2.46}$$

for qubits (the subscripts 1 and 2 indicate that the partial trace is realized in the subspace of the first and second two level Hilbert space, respectively). In Chapter 4, in the continuous-variables context, we shall present the *Beam Splitter* as the Partial SWAP, with the same properties, for the bosonic modes case.

2.3.6 Homogenization

We shall focus on the procedure proposed in [19], where the so-called *homogenization* was defined for qubits systems. This procedure consists of a CM where all ancillae have the same structure as the system (like qubits, in the case of [19]), are initially identical and *uncorrelated* and the unitary responsible for the interactions between system and ancillae acts in such a way that, after the system collides with all the ancillae, the system and

ancillae will be all approximately identical.

The homogenization procedure is very similar to the procedure of thermalizing, but in this case, as we shall see, we are free to involve any kind of ancillae state in the process, not only thermal states. The process is outlined as follows. Suppose we have a CM with identical ancilae initially in a *generic* state ρ_A^0 and a system initially at state ρ_S^0 and they interact in each collision via the same unitary U (the condition here are just like in the thermalizing machine, but notice that the ancillae states ρ_A don't need to be at a thermal state). Hence the system after the n-th collision will evolve according to the stroboscopic map in Eq. (2.27) and the n-th ancilla after its collision with the system will be given by (2.28). We say that *homogenization happens when for all* $\delta > 0$ *there is a finite number of collisions* N_δ *such that*

$$D(\rho_S^N, \rho_A) \leq \delta, \quad \forall N \geq N_\delta, \tag{2.47}$$

$$D(\rho_A^n, \rho_A) \leq \delta, \quad \forall n, \ 1 \leq n \leq N, \tag{2.48}$$

where $D(\bullet, \bullet)$ means any distance between operators and in this work we shall use the trace distance.[7]

These two conditions means that not only the system must get as close as we want to the initial ancillae state ρ_A, independent of the initial system state ρ_S^0, but also the ancillae must never get too distant from its initial state after their collision with the system. The result is that the final states must all be similar, and the ancillae turn the system to look like one of them, transforming the system and environment in an homogeneous set of very similar parts (see Fig. 2.2).

It can be shown, for the all-qubit case, that homogenization is achieved if the unitary U that rules the interaction in the collisions is the Partial SWAP given in Eq. (2.44). This can be seen by direct application of our Stinespring representation to CMs using this

[7] Suppose we have two densisty matrices ρ and σ, then the **trace distance** between them will be

$$D(\rho, \sigma) = \frac{1}{2} \operatorname{Tr} |\rho - \sigma|, \tag{2.49}$$

where $|A| = \sqrt{A^\dagger A}$ is the positive square root of $A^\dagger A$.

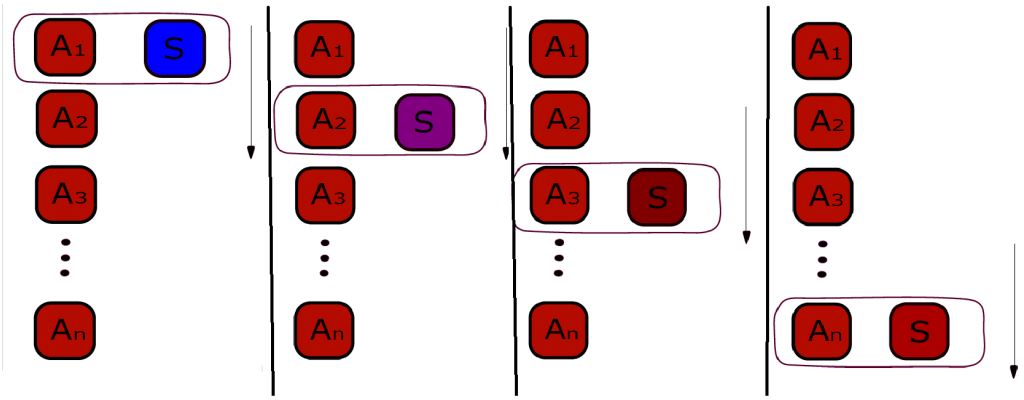

Figure 2.2: Schematic of homogenization. From left to right, the system S interacts with the ancillae at time $0 < t < \tau$, $\tau < t < 2\tau$, $2\tau < t < 3\tau$ and $(n-1)\tau < t < n\tau$, respectively. The color changes on the system represents the different states it passes trough until it gets very similar to the ancillae and the whole system becomes homogeneous.

particular unitary. Starting with Eq. (2.25), we obtain

$$\rho_S^1 = c^2\rho_S^0 + s^2\rho_A + ics[\rho_A, \rho_S^0], \tag{2.50}$$

when c and s are $\cos(g\tau)$ and $\sin(g\tau)$, respectively. Following the interaction of the same channel n times, as Eq. (2.27) suggests, we obtain the system's state after the n-th collision

$$\begin{aligned}\rho_S^n &= c^2\rho_S^{n-1} + s^2\rho_A + ics[\rho_A, \rho_S^{n-1}] \\ &= s^2\sum_{j=0}^{n-1} c^2\rho_A + \rho_{\text{rest}}^n \\ &= (1-c^{2n})\rho_A + \rho_{S,\text{rest}}^n\end{aligned} \tag{2.51}$$

where ρ_{rest}^n is a ρ_S^0 dependent part that will go to 0 as $n \to \infty$ (see Appendix A). Similarly, we can use Eq. (2.28) and the equation above to obtain the state of the n-th ancilla after its collision

$$\begin{aligned}\rho_A^n &= s^2\rho_S^{n-1} + c^2\rho_A + ics[\rho_S^{n-1}, \rho_A] \\ &= s^2(1-c^{2(n-1)})\rho_A + \rho_{A,\text{rest}}^n,\end{aligned} \tag{2.52}$$

where $\rho^n_{A,\text{rest}}$ is also a ρ^0_S dependent part that goes to 0 as $n \to \infty$ (see Appendix A), meaning that $\rho^n_S \to \rho_A$ and $\rho^n_A \to \rho_A$ for large n. Therefore, both system and ancillae converge to ρ_A for sufficient large n.

There is one more restriction needed so that homogenization can be correctly achieved. Notice that in the first line of Eq. (2.52) the term $[\rho^{n-1}_S, \rho_A]$ is the one responsible for $\rho^n_{A,\text{rest}}$ and it gets smaller at each collision since ρ^{n-1}_S gets closer to ρ_A. From this observation we can conclude that

$$D(\rho^n_A, \rho_A) \leq D(\rho^{n-1}_A, \rho_A), \tag{2.53}$$

which means that the first collision pushes the ancilla further away while the next collisions pushes lesser and lesser (which makes sense since the system gets closer and closer to ρ_A). Thus the condition from Eq. (2.48) actually bounds $D(\rho^1_A, \rho_A)$ for each δ, putting a bound in the Partial SWAP parameter $g\tau$. This restriction turns to be (see Appendix A for the proof)

$$\sin(g\tau) \leq \sqrt{\delta/2}. \tag{2.54}$$

Finally, this sets the sufficient conditions for homogenization, which can be used for quantum cloning protocols and quantum-safe cryptography with a classical communication [19]. We can also prove, as will be done in Chapter **??**, that homogenization can also happen when system and ancillae are bosonic states. This proof will be done analytically obtaining the stroboscopic evolution for all time steps. Importantly, in both cases homogenization demands that the steady-state of this kind of CM must be the initial state of the ancillae itself. The main original result of the first project of this thesis is to show that the presence of initial correlations between the ancillae in CMs tends to steer the steady-states far from its original steady-states and, in the special case of homogenization, steering the steady-state away from the ancillae state [93].

2.3.7 Physical implementations of CMs

In this subsection we present a few examples about how CMs can describe important open quantum systems dynamics, going beyond a set of theoretical insightful models.

A very intuitive dynamic that can be associated with CMs are the ones concerning a dilute gas of particles, following Boltzman's *Stosszahlansatz* molecular chaos hypothesis

[64]. However, these models need to consider the time interval τ during the interaction between the system and each ancilla to be a random variable in order to obtain a reliable description of gases [62]. This set of CMs, which are frequently called *stochastic CMs*, have not the same structure and dynamics of the models described in this chapter, which are sometimes called of *periodic CMs*. Recently, an insightful manner to mimic any stochastic CM using periodic CMs was proposed [94].

Perhaps the most natural physical setup that can fit to a CM description is the *micromaser* [69, 70]. In general terms, a *maser* is a device similar to a laser, producing coherent photons around the microwave spectrum by stimulated emission, as opposed to a laser, which produces coherent photons around the visible light spectrum. The micromaser is a specific case where a filtered stream of Rydberg atoms (heavy atoms with valence electrons behaving approximately as electrons of a hydrogen atom, see Ref. [95]) are sent trough a cavity so that each atom flies alone inside the cavity and interacts *individually* with the electromagnetic fields inside the cavity (see Fig. 2.3). This way, the CM described above for the Markovian case is almost perfectly suitable since we can treat each atom as an individual ancilla (uncorrelated with the other atoms) which interacts one at a time with the electromagnetic field of the cavity, which plays the role of the system.

The micromaser setup is also the most adequate apparatus for the application of the *Janyes-Cummings* (JC) model,[8] since both consider the presence of only one atom at a time interacting with the cavity field, being different from most lasers and masers where the cavity field actually interacts collectively with many atoms. Therefore, the CM describing the micromaser has the JC interaction Hamiltonian

$$V = g(a\sigma_+ + a^\dagger\sigma_-), \tag{2.55}$$

where g is the interaction strength, a ($a^\dagger$) are the annihilation (creation) operators of the field mode[9] and σ_- (σ_+) are the qubits operators given by Eq. (2.33).

The setup can then be modeled by the Markovian CM with identical ancillae and interactions, as described in Susbsec. 2.3.2, with the interaction Hamiltonian of Eq. (2.19)

[8] The JC model is a largely applicable model of *light-matter* interaction [55, 57, 91], where the matter is described by a qubit (in this case, the atom) and the light is an electromagnetic mode.

[9] Importantly, the atom qubit interacts only with *one mode* of the electromagnetic spectrum in the cavity. This is justified by the *rotating wave approximation* (RWA) [55, 91].

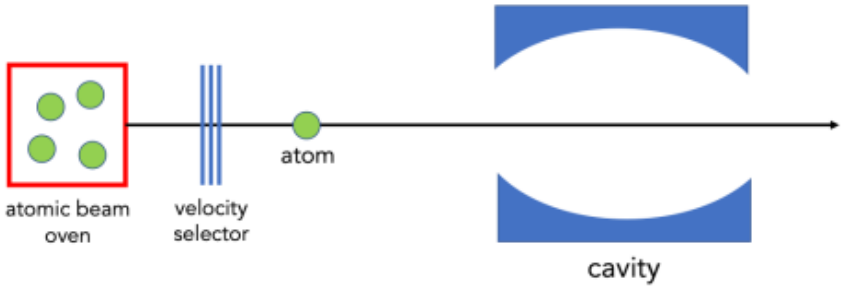

Figure 2.3: Micromaser setup: An atomic beam oven emits Rydberg atoms which pass trough a velocity selector tuning the flux of atoms so that each atom passes one at a time through the cavity containing electromagnetic fields. (This figure was taken from Ref. [21].)

given by Eq. (2.55) in the interaction picture (see Appendix A). Such CM is an approximation of the real micromaser setup, but can reproduce the main important features of the real phenomena [95, 96]. A more complete description of the micromaser can be found in Refs. [95, 97].

Beyond the micromaser example, which is a direct application of CMs in a physical setup, CMs are extremely useful to create effective models of realistic open quantum systems situations. Important examples include the full simulation of Markovian dynamics from single qubits [81, 98] and the reproduction of any Markovian dynamics with the *multipartite collision model* (a generalization of the CM described in this chapter with multipartite system) [99].

Finally, another major example is the fact that a CM description can also emerge very naturally from one of the most common microscopic system-bath model, namely the interaction with the one-dimensional waveguide. In this model, the system is described by a generic system with frequency ω_0 and annihilation (creation) operator $A(A^\dagger)$, and the environment is represented by a continuum of bosonic modes, with annihilation (creation) operators $b_\omega(b_\omega^\dagger)$ and frequencies that range from $-\infty$ to ∞. The Hamiltonian of the full joint system is given by

$$H = H_S + H_E + V, \tag{2.56}$$

where

$$H_S = \omega_0 A^\dagger A, \quad H_E = \int_{-\infty}^{\infty} d\omega(\omega_0+\omega) b_\omega^\dagger b_\omega \quad \text{and} \quad V = \sqrt{\frac{\gamma}{2\pi}} \int_{-\infty}^{\infty} d\omega (A^\dagger b_\omega + A b_\omega^\dagger), \tag{2.57}$$

where γ is a constant coupling strength. This is the so-called *white noise* coupling [55]. The above Hamiltonian is justified by the RWA (which explains the presence of non-physical negative frequencies) together with the *weak coupling approximation*, which is very often used in quantum optics [55, 57, 100].

By making a Fourier transform we can define *time modes*, for any real t,

$$b_t = \frac{1}{\sqrt{2\pi}} \int_{-\infty}^{\infty} d\omega b_\omega e^{-i\omega t}. \tag{2.58}$$

These time modes can represent quantum harmonic modes since they satisfy $[b_t, b_{t'}^\dagger] = \delta(t - t')$ and $[b_t, b_{t'}], = [b_t^\dagger, b_{t'}^\dagger] = 0$. In order to make a discrete time step evolution, we can discretize the real line in intervals with equal lengths so that $t_n - t_{n-1} = \Delta t$ for finite Δt and any integer n. This way, we may redefine the time modes for discrete steps

$$b_n = \frac{1}{\sqrt{\Delta t}} \int_{t_{n-1}}^{t_n} dt b_t, \tag{2.59}$$

which also satisfy the commutation relations for any n. Going to the interaction picture (see Appendix A), the Hamiltonian of Eqs. (2.56) and (2.57) reduces to

$$V_n = \sqrt{\frac{\gamma}{\Delta t}} (A^\dagger b_n + A b_n^\dagger), \tag{2.60}$$

which is time dependent, since the interaction will affect only each mode n when $t \in [t_n, t_{n-1}]$. Consequently, this model is exactly a CM where the ancillae are described by the time discrete modes represented by the operators $b_n(b_n^\dagger)$. This CM picture of open systems under white noise is explained and applied in the context of waveguide-QED in Refs. [100, 101]. In this thesis, such CM in which all the ancillae are bosonic modes will be explored in detail, since its formalism makes it possible to obtain analytical solutions to the effects of initial correlations between the ancillae in the system's dynamics.

Chapter 3

Quantum Information and Bayesian Networks

Quantum Information (QI) is a largely growing field in the past decades, specially with the advent of promising new quantum technologies [102]. The rich history of the creation and development of this field is well narrated in Ref. [1] and excellent introductory and detailed texts approaching general themes about QI are found in Refs. [1, 2, 15]. In this Chapter we mainly focus in the aspects of quantum information used to quantify correlations between quantum states and how to identify which correlations have intrinsic quantum aspects. These subjects are going to be essential for the analysis and interpretations of the main projects of this thesis.

As a second subject of this Chapter, we present the concept of *Bayesian Networks*. The exposition will be brief and primarily focused in the application needed for our second project (Chapters 7 and 8).

3.1 Generalized measurements

Quantum measurements are among the most controversial subjects of quantum mechanics, hence the discussion of its postulates can render extensive texts. Here we only expose the postulates which are useful to the present thesis. More complete discussions explaining and motivating the postulates are given in Refs. [1, 2, 15, 57, 103] and examples for the exposition of interpretations are given in Refs. [103, 104]. The postulates are the

following:

- Any measurement can be described in terms of a set of Kraus matrices $\{M_k\}_k$, satisfying Eq. (2.17), given the measurement setup. Each of this choices define a *Positive Operator Value Measure* (POVM).[1] The result of each measurement is labeled by a index k of the the corresponding Kraus matrix M_k;

- The probability of obtaining the outcome k is

$$\boxed{p_k = \mathrm{Tr}\left(M_k \rho M_k^\dagger\right);} \tag{3.1}$$

- After the measurement is done, if the result of k is recorded, the effect of the measurement in the state ρ, called *backaction*, will be to evolve

$$\boxed{\rho \to \frac{M_k \rho M_k^\dagger}{p_k}.} \tag{3.2}$$

The items above are sufficient to describe any generalized quantum measurement. An important class of quantum measurements are the *projective measurements*, where the Kraus matrices M_k are simply the projectors $|k\rangle\langle k|$ in some basis $\{|k\rangle\}_k$. This results in the familiar "wave function collapse" rule $p_k = |\langle\psi|k\rangle|^2$ and $|\psi\rangle \to |k\rangle$ for measuring a pure state $|\psi\rangle$.

3.2 Entropy

3.2.1 The Shannon Entropy

Entropy is a central concept not only in QI but also in Classical Information Theory [105]. Since Shannon's revolutionary paper in 1948 [106], the quantity now known as *Shannon entropy* can be undoubtedly interpreted as a measure of the average information carried by a random variable *after* we learn its value. At the same time, at is often done in physics, we interpret it as the lack of information we have about a random variable *before* we learn its value.

[1] The POVM is a set of operators $\{E_k\}_k$ such that $E_k = M_k^\dagger M_K$.

If we have a random variable X with a probability distribution $p(X)$, then the Shannon entropy associated with this distribution is[2]

$$H(p(X)) = -\sum_x p(x) \log p(x), \tag{3.3}$$

where we consider the limit $\lim_{y\to 0} y \log y = 0$, for the case where $p(x) = 0$. As already mentioned, this quantity measures the average information carried by a random variable, given its probability distribution. A heuristic justification for this statement can be given as follows.

Let X be a random variable with the corresponding probability distribution $p(X)$ and suppose that we want to construct a "surprise" function (say $\mathcal{S}$) which measures the amount of unexpected learning that would be obtained if it is revealed to us the value of this random variable. For instance, if we learn that x is the value of the random variable and $p(x)$ is close to 1, it means that the learning was not unexpected resulting in $\mathcal{S}(x)$ small. Conversely, if $p(x) \ll 1$, then $\mathcal{S}(x)$ should be a large number. Hence, intuitively we expect $\mathcal{S}(x)$ to be inversely proportional to $p(x)$, but it is also desirable that it respects the additive property, i.e. having the surprise of learning x *and* of learning y (in symbols $\mathcal{S}(x, y)$) should give $\mathcal{S}(x)+\mathcal{S}(y)$. The only function of $p(X)$ that satisfies both properties (except by a multiplicative constant) is

$$\mathcal{S}(x) = \log\left(\frac{1}{p(x)}\right). \tag{3.4}$$

Intuitively, this unexpected learning can be identified as information since unexpected results tend to be more relevant and give us more information. Hence, the average of this value can be interpreted as the average of information obtained if we learn a random variable

$$\langle \mathcal{S} \rangle = \sum_x p(x)\mathcal{S}(x) = -\sum_x p(x) \log(p(x)), \tag{3.5}$$

which is exactly the Shannon entropy.

This intuitive, although not formal, argument was taken from Ref. [27]. More formal

[2]Here the log is taken as the natural logarithm. This differs from many QI and information theory books which define the log with base 2.

arguments for the Shannon entropy interpretation can be found in Refs. [1, 2, 105] and in Shannon's original paper [106].

3.2.2 The von Neummann Entropy

We also need a quantity which encompass the information content of a quantum state. For defining this quantity, we assume it depends on the density matrix ρ of a quantum state, since it has the informational content of the probability distribution of each possible pure quantum state (see Sec. 2.1). But naively one could guess that, given a density matrix

$$\rho = \sum_i p_i \left|\psi_i\right\rangle \left\langle\psi_i\right|, \tag{3.6}$$

the appropriate entropy that represents the quantum state should be just the Shannon entropy of the probability distribution of the states $\{|\psi_i\rangle\}_i$

$$H(p_i) = -\sum_i p_i \log(p_i). \tag{3.7}$$

It turns out that this is not a good choice since the probability distribution $\{p_i\}_i$ is dependent on the ensemble $\{|\psi_i\rangle\}_i$ and in general, the states $\{|\psi_i\rangle\}_i$ are not necessarily orthogonal, hence indistinguishable. The interpretation of Shannon entropy as being the average measure of information only makes sense if we can distinguish the outcomes of the random variables.

A more accurate attempt would be to make the spectral decomposition

$$\rho = \sum_i \lambda_i \left|\lambda_i\right\rangle \left\langle\lambda_i\right|, \tag{3.8}$$

where $\{\lambda_i\}_i$ and $\{|\lambda_i\rangle\}_i$ are the eigenvalues and eigenvectors or ρ, respectively, and compute the Shannon entropy of the eigenvalues[3]

$$H(\lambda_i) = -\sum_i \lambda_i \log(\lambda_i). \tag{3.9}$$

[3]The eigenvalues of ρ are also a valid probability distribution (see Appendix A).

This equation can be rewritten as

$$-\sum_i \lambda_i \log(\lambda_i) = -\operatorname{Tr}(\rho \log \rho), \tag{3.10}$$

its proof is simple and can be found in Appendix B. The quantity above is invariant under a change of basis, since the eigenvalues are basis independent. Importantly, the eigenstates $\{|\lambda_i\rangle\}_i$ are orthogonal and thus are distinguishable, hence it represents a more suitable entropy for quantum states. This quantity is the *von Neumann entropy*

$$\boxed{S(\rho) = -\operatorname{Tr}(\rho \log \rho),} \tag{3.11}$$

and is the correct candidate to represent the information contained in a quantum state [1, 2, 15].

From Eq. (3.10) it is immediate to see that the von Neumann entropy is always a positive quantity. Another important aspect is that the von Neumann entropy vanishes for pure states and assumes its maximal value at the maximally mixed state $\rho = \mathbf{I}/d$, for finite-dimensional Hilbert states with dimension d. Thus

$$0 \leq S(\rho) \leq \log d. \tag{3.12}$$

Indeed, the von Neumann entropy has a similar interpretation as the purity (see Eq. (2.6)). If we have a pure state, then we have no ignorance about the system since we know the state it is in, and if we have a maximally mixed state, then we have the most ignorant case, since we have equal probability of being in any quantum state.

The von Neumann entropy has an enormous set of properties [1, 2, 15]. But in this thesis it will be sufficient to use the fact that it is a quantity invariant under a unitary transformation[4] and to work with its conceptual role of representing the amount of ignorance we have about a quantum system. We shall use this concept to the construction of quantities representing *correlations*. From now on, we refer to the von Neumann entropy of a quantum state simply as the *entropy*.

[4]Suppose that U is a unitary transformation and that $\rho' = U\rho U^\dagger$. Then $S(\rho') = \operatorname{Tr}\left(U\rho U^\dagger \log\left(U\rho U^\dagger\right)\right) = \operatorname{Tr}\left(U\rho U^\dagger U \log(\rho) U^\dagger\right) = \operatorname{Tr}\left(\rho \log \rho\right) = S(\rho)$, where in the second equality we used that a unitary U infiltrates in any well-defined function of operators.

3.3 Mutual Information and Correlations

3.3.1 Relative Entropy

As an entropic-like distance, we shall define the *Relative Entropy*[5] or *Kullback-Leibler divergence*

$$\boxed{S(\rho||\sigma) = \mathrm{Tr}(\rho \log \rho) - \mathrm{Tr}(\rho \log \sigma),} \tag{3.13}$$

where ρ and σ are density matrices. This quantity is always non-negative

$$S(\rho||\sigma) \geq 0, \tag{3.14}$$

and vanishes for the case where $\rho = \sigma$. The proof of such inequality is non-trivial and can be found in Refs. [1, 15].

From the non-negativity of the relative entropy we can have an intuitive idea of entropic distance. Although it is important to underline that this is not an actual distance, since it is not symmetric, i.e., in general $S(\rho||\sigma) \neq S(\sigma||\rho)$, and does not satisfy the triangle inequality.

3.3.2 Mutual Information

We are interpreting entropy as the measure of ignorance over a quantum system. A useful quantity would be the *information* of a quantum system described by a quantum state ρ. It is intuitively defined as the entropic distance between the state ρ and the state in which the ignorance is maximum. In other words, it is the relative entropy between the state ρ and the maximally mixed state $\pi = \mathbf{I}/d$ (assuming a d-dimensional Hilbert space)

$$\begin{aligned} \mathcal{I}(\rho) &= S(\rho||\pi) \\ &= \log(d) - S(\rho). \end{aligned} \tag{3.15}$$

[5] This Relative Entropy is often called *Quantum Relative Entropy* since it is the quantum counterpart of the classical Relative Entropy defined as $H(p(x)||q(x)) = \sum_x p(x) \log\left(\frac{p(x)}{q(x)}\right)$, given two probability distributions $p(x)$ and $q(x)$.

From Eq. (3.12) we obtain that

$$0 \leq \mathcal{I}(\rho) \leq \log(d), \tag{3.16}$$

with its minimum at $\rho = \pi$ and maximum where ρ is a pure state.

With this concept in hand, it is straightforward to have an intuitive idea of the quantity called *mutual information*. Given a system divided in two parties A and B, in which the global state is ρ_{AB}, the mutual information between the two parties is defined as

$$\boxed{\mathcal{I}_{\rho_{AB}}(A:B) = S(\rho_{AB}||\rho_A \otimes \rho_B),} \tag{3.17}$$

where $\rho_A = \mathrm{Tr}_B(\rho_{AB})$ and $\rho_B = \mathrm{Tr}_A(\rho_{AB})$.

The mutual information embrace all the content of the *correlations* between the parties A and B. In general, $\rho_A \otimes \rho_B \neq \rho_{AB}$ since the partial trace which generates the local state ρ_A vanishes with all the B dependence, i.e., their correlations. Thus the product $\rho_A \otimes \rho_B$ represents completely uncorrelated states and consequently its distance to the global state ρ_{AB} measures their correlations.

A more explicit representation of the aforementioned ideas can be seen in the following formulas. From the definition of relative entropy (Eq. (3.13)), we have

$$S(\rho_{AB}||\rho_A \otimes \rho_B) = -S(\rho_{AB}) - \mathrm{Tr}(\rho_{AB} \ln \rho_A) - \mathrm{Tr}(\rho_{AB} \ln \rho_B). \tag{3.18}$$

Now, noticing that

$$\begin{aligned} &- \mathrm{Tr}(\rho_{AB} \log \rho_A) = - \mathrm{Tr}_A(\mathrm{Tr}_B(\rho_{AB}) \log \rho_A) \\ &= - \mathrm{Tr}_A(\rho_A \log \rho_A) \\ &= S(\rho_A), \end{aligned} \tag{3.19}$$

with a similar result for $- \mathrm{Tr}(\rho_{AB} \log \rho_B)$ and applying it in Eq. (3.18), we obtain

$$\boxed{\mathcal{I}_{\rho_{AB}}(A:B) = S(\rho_A) + S(\rho_B) - S(\rho_{AB}),} \tag{3.20}$$

which is a simpler way to compute the mutual information in various applications.

Finally, using the definition of information (Eq. (3.15)) in Eq. (3.20) and the fact that $\log(d_A d_B) = \log d_A + \log d_B$, we conclude that

$$\boxed{\mathcal{I}_{\rho_{AB}}(A:B) = \mathcal{I}(\rho_{AB}) - \mathcal{I}(\rho_A) - \mathcal{I}(\rho_B),} \tag{3.21}$$

where $d_A(d_B)$ is the dimension of the Hilbert space of $A(B)$. The equation above simply states that "the mutual information between A and B is the information contained in ρ_{AB} minus the information contained locally in ρ_A and ρ_B", that is, the mutual information represent the correlations between the parties.

3.3.3 Entanglement

We gave justifications to the fact that the mutual information represents the total correlations between two parties. However, to conclude which of these correlations have quantum origins without classical counterpart is a hard task and still a very fruitful research field nowadays [107]. Here, we briefly introduce concept of *entanglement*, which is the most known type of quantum correlations, due to its applications as an important resource in quantum technologies and conceptual problems [108].

Suppose a system is divided in two parties A and B. A pure state $|\psi\rangle$ representing this system is called a *product state* if it can be parametrized as tensor product

$$|\psi\rangle = |\psi_A\rangle \otimes |\psi_B\rangle\,, \tag{3.22}$$

where $|\psi_A\rangle$ ($|\psi_B\rangle$) belong to the Hilbert space of $A(B)$. Any pure state which is not a product state is called an *entangled state*.

Notice that for the case of pure states it is not hard to have a decisive witness of entanglemet. If a state $|\psi\rangle$ is a product state just like in Eq. (3.22), then clearly the partial trace of its density matrix over A or B will result in a pure state, i.e.

$$\mathrm{Tr}_A(|\psi\rangle\langle\psi|) = |\psi_B\rangle\langle\psi_B|\,. \tag{3.23}$$

Otherwise, if a state $|\psi\rangle$ is a entangled state, then the partial trace of its density matrix

over A or B will result in a mixed state. Consequently, the entropy of the reduced state will be non-zero. So, if

$$S\left(\mathrm{Tr}_{A(B)}(|\psi\rangle\langle\psi|)\right) > 0, \tag{3.24}$$

the state will be entangled. Otherwise, it will be a product state.

With the use of the *Schmidt decomposition* [1, 2, 91], it can be shown that for any pure state $S\left(\mathrm{Tr}_A(|\psi\rangle\langle\psi|)\right) = S\left(\mathrm{Tr}_B(|\psi\rangle\langle\psi|)\right)$ and this quantity can also represent a quantifier of entanglement.

Unfortunately, for the case of mixed states, the problem of quantifying entanglement is much more challenging. For a system divided in parties A and B, a state ρ is said to be *separable* when

$$\rho = \sum_i p_i \rho_A^i \otimes \rho_B^i, \tag{3.25}$$

where $\{p_i\}_i$ is a probability distribution, ρ_A^i are density matrices in A and ρ_B^i are density matrices in B. A mixed state is said to be entangled when it is not a separable state.

The meaning of Eq. (3.25) is that a separable state is a classical mixture of quantum states ρ_A^i and ρ_B^i which are only locally quantum. It can be shown that such states can always be prepared by the so-called *Local Operations and Classical Communications* (LOCCs) [108]. To distinguish if a mixed state is separable or not is, in general, a very arduous task.

3.3.4 Quantum discord

Due to the difficulties mentioned above in characterizing entanglement for mixed states, we focus in another quantifier of quantum correlations, the so-called *quantum discord*.

The concept of quantum discord was first proposed in Refs. [109–111]. It is a discrepancy between the mutual information among two parties and the maximum amount of information we can get form one party by measuring the other party. Intuitively, one may think that the maximum information we can get by one party looking at the other party is equal to their total correlations, but we shall see that this statement is true only for classical systems. For quantum systems we get a mismatch due to quantum backactions.

This can be seen in the following discussion. Given a system divided in two parties A and B, suppose that their states can be represented by classical probability distributions

$p(X)^A$ and $p(Y)^B$, respectively. We can define the *conditional entropy*

$$H(A|B) = -\sum_y p(y)^B \sum_x p(x|y)^A \log\big(p(x|y)^A\big), \tag{3.26}$$

which is the average of the Shannon entropy of the conditional probability of A given we obtain an outcome from B, this conditional probability distribution is given by *Bayes' Theorem* [105]

$$\boxed{p(x|y)^A = \frac{p(x,y)^{AB}}{p(y)^B},} \tag{3.27}$$

where $p(x,y)^{AB}$ is the joint probability distribution of A and B.

The conditional entropy in Eq. (3.26) is interpreted as the lack of information we have about A given we know the outcomes of B. It can be shown (see Appendix B) that the mutual information between A and B is given by[6]

$$\boxed{\mathcal{I}(A:B) = H(A) - H(A|B),} \tag{3.28}$$

where $H(A)$ is the Shannon entropy of A given its probability distribution $p(X)^A$. The equation above simply states that the mutual information between A and B is the ignorance of A less the ignorance of A given that we know the outcomes of B.

We can try to define a similar conditional entropy for the quantum case. In this case, obtaining the outcome of the subsystem B cannot be done without taking into consideration the effects of the measurement on it. Hence we suppose that, if choose a generalized measurement described by the Kraus matrices $\{M_k^B\}_k$ in B, the joint system ρ_{AB} will suffer a backaction

$$\rho_{AB|k} = \frac{(\mathbf{I}_A \otimes M_k^B)\rho_{AB}(\mathbf{I}_A \otimes M_k^B)^\dagger}{p_k}, \tag{3.29}$$

if the outcome is k, with probability

$$p_k = \mathrm{Tr}\left((\mathbf{I}_A \otimes M_k^B)\rho_{AB}(\mathbf{I}_A \otimes M_k^B)^\dagger\right). \tag{3.30}$$

With the reduced state $\rho_{A|k} = \mathrm{Tr}_B\left(\rho_{AB|k}\right)$ we can define the *quantum-classical condi-*

[6] This mutual information, defined for classical systems, has exactly the form of Eq. (3.20), but switching von Neumann entropies for Shannon entropies and density matrices for probability distributions.

tional entropy

$$S_M(A|B) = \sum_k p_k^B S(\rho_{A|k}), \tag{3.31}$$

which follows exactly the same idea of the conditional entropy of Eq. (3.26), but with the influence of the backaction in the quantum state and the dependence on the choice of measurement $\{M_k^B\}_k$. Its interpretation is also similar, it represents the ignorance of the system A given we know the outcomes of the generalized measurements $\{M_k^B\}_k$.

It is useful to define the quantity

$$\mathcal{J}_M(A|B) = S(\rho_A) - S_M(A|B), \tag{3.32}$$

which means the information obtained by A with the outcomes of the quantum measurement $\{M_k^B\}_k$ of B, very similar to the mutual information in Eq. (3.28). For the classical case, the quantity equivalent to Eq. (3.32) must be the mutual information, but for the quantum case this is not always true. For this reason one defines the *quantum discord*

$$\boxed{\mathcal{D}_M(A|B) = \mathcal{I}(A:B) - \mathcal{J}_M(A|B),} \tag{3.33}$$

meaning the mismatch between the total correlations and the information obtained by A after the outcomes of $\{M_k^B\}_k$ in B.

A more compelling quantity is the *measurement independent discord*

$$\boxed{\mathcal{D}(A|B) = \min_{\{M_k^B\}_k} \mathcal{D}_M(A|B)}, \tag{3.34}$$

which is the minimum discord obtained over all possible measurements. It is the case where we obtain the maximum information about A with measurements in B, i.e., maximizing $\mathcal{J}_M(A|B)$. A non-zero value of this quantity means that there is no measurement that can give us full information about the correlations, as it is possible in classical systems. From now on we shall refer to the measurement independent discord simply as the *quantum discord* (and to the quantum discord of Eq. (3.33) as the *measurement dependent discord*).

This correlation quantifier, without classical counterparts, has several applications in

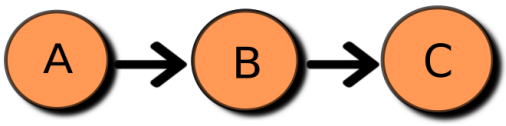

Figure 3.1: Three random variables A, B and C disposed in a causal order.

quantum information, quantum thermodynamics, open quantum systems, and many-body physics [107]. In this thesis it will be useful to indicate genuine quantum correlations between Gaussian systems in Chapter 8.

3.4 Bayesian Networks

Bayesian Networks (BNs) was first introduced in its modern terms by Judea Pearl in 1985 [47]. In Judea's words, his study was "motivated by attempts to devise a computational model for humans' inferential reasoning", from which he obtained a graph-type model for inferring probabilities from conditional distributions disposed in a causal order. This concept is used in a large range of applications, mainly in Artificial Intelligence, which was its initial proposal application.

This concise presentation will focus only on the necessary concepts for the second project of the thesis, which took a large inspiration from [48] in introducing the BN concept to quantum systems. For a complete introduction to the subject of BNs, see Refs. [43–46].

3.4.1 Definition and examples

Suppose we have three random variables A, B and C disposed in a causal order where A causes B and B causes C (see Fig. 3.1). The approach to relate these quantities is to assign to each arrow a conditional probability according to the causal order . For instance, for the case of Fig. 3.1, the joint probability distribution $P(A, B, C)$ is

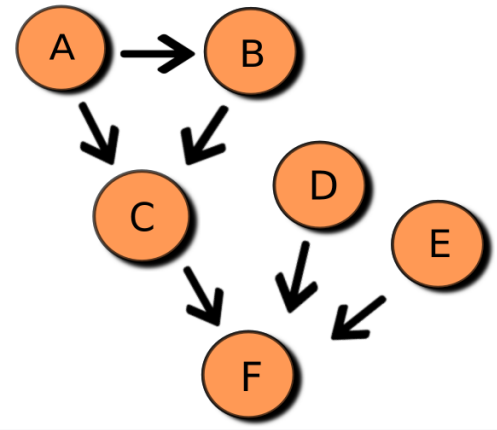

Figure 3.2: Example of directed graph representing relations of causality between random variables.

$$\begin{aligned} P(A,B,C) &= P(C|B,A)P(B,A) \\ &= P(C|B,A)P(B|A)P(A) \\ &= P(C|B)P(B|A)P(A), \end{aligned} \tag{3.35}$$

where the last equation holds since the random variable C depends only on B.[7]

For more complex relations of causality, instead of an ordered string (as in Fig. 3.1) the causal orders can be described by directed graphs where the directed edges means causal relations and each vertex represents a random variable. Fig. 3.2 gives an example of a directed graph describing more complex relations of causality. For this case, the joint probability $P(A,B,C,D,E,F)$ is

$$\begin{aligned} P(A,B,C,D,E,F) =& P(F|A,B,C,D,E)P(A,B,C,D,E) \\ =& P(F|C)P(A,B,C)P(F|D)P(D)P(F|E)P(E), \end{aligned} \tag{3.36}$$

where in the last equality we used that the random variable F only depends on C, D and E and these three variables are independent of each other. The joint probability $P(A,B,C)$ can be computed separately

[7] Of course, the random variable C has a causal relation with A. But, once the random variable B ins known ($B = b$), the random variable C will be fully specified by $P(C|B = b)$, thus A and C become independent. This property is known as a *d-separation* between A and C [44, 45].

$$\begin{aligned} P(A,B,C) &= P(C|A,B)P(A,B) \\ &= P(C|A)P(C|B)P(B|A)P(A) \\ &= P(C|A)P(C|B)P(B|A)P(A). \end{aligned} \tag{3.37}$$

Combining the two equations above, we obtain

$$P(A,B,C,D,E,F) = P(C|A)P(F|C)P(C|B)P(B|A)P(A)P(F|D)P(D)P(F|E)P(E). \tag{3.38}$$

If in a directed graph there is a link from A to B, we say that A is a *parent* of B. In the directed graph of Fig. 3.2 F has parents C, D and E; C has parents A and B, and B has only the parent A. Notice that in Eq. (3.38), the joint probability distribution is just the chain product of the conditional probabilities between the random variables and its parents times the probability distributions of the random variables without parents. This is a general property of *Baysean Networks*, the BNs *are sets of random variables with their causal relations described in acyclic directed graphs*[8]. For similar reasons as the examples above, we have the following theorem [44, 45].

Theorem (Chain rule for Bayesian Networks): For the set $\{A_1, \cdots, A_n\}$ of all random variables in a BN, the joint probability distribution will be

$$\boxed{P(A_1, \cdots, A_n) = \prod_{i=1}^{n} P(A_i|\text{pa}(A_i)),} \tag{3.39}$$

where $\text{pa}(A_i)$ is the set of all parents of A_i.

For these reasons, BNs yields a compact representation for joint probability distributions of sets of random variables with causal relations.

3.4.2 Dynamical BNs for quantum systems (QBNs)

In this Subsection we make an application of BNs for estimating the probability of reduced quantum systems to be in a particular conditional trajectory as the system evolves,

[8] Acyclic directed graphs are directed graphs which have no cycles in their inner structure, or directed loops. This avoids causal loops causing feedback cycles (see Fig. 3.3), which makes the modeling too difficult.[44]

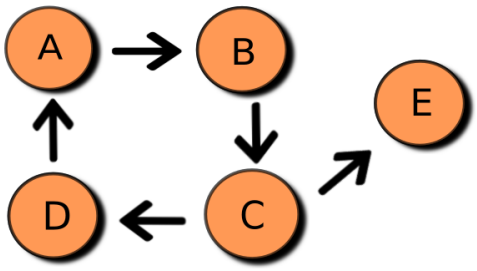

Figure 3.3: A directed graph with in internal cycle, provoking a causal loop between the random variables $A,\ B,\ C$ and D.

these are called *Quantum Bayesian Networks (QBNs)*. This structure will be the basis of the second main project of this thesis and has great influence from [48, 112, 113].

The setup is the following. Consider a state divided in two parties A and B and with the initial joint state

$$\rho_{AB}(0) = \sum_s P_s \left|\psi_s(0)\right\rangle \left\langle\psi_s(0)\right|, \tag{3.40}$$

where $\{P_s, |\psi_s(0)\rangle\}_s$ is an ensemble of quantum states which are not necessarily orthogonal. If we have a global unitary evolution $U(t)$ of the joint system, then each state of the ensemble $\{|\psi_s(0)\rangle\}_s$ will evolve deterministically as

$$\left|\psi_s(t)\right\rangle = U(t) \left|\psi_s(0)\right\rangle. \tag{3.41}$$

Looking now at the reduced local systems, suppose we have observable $\mathcal{O}_A$ in A and $\mathcal{O}_B$ in B with eigenvectors $\{|a_i\rangle\}_i$ and $\{|b_j\rangle\}_j$, respectively. We know that, if the global state is $|\psi_s(t)\rangle$, then the conditional probability of the reduced states being in the eigenkets $|a_k\rangle$ in A and $|b_k\rangle$ in B is[9]

$$\boxed{P(a_k, b_k|\psi_s(t)) = |\left\langle a_k, b_k|\psi_s(t)\right\rangle|^2.} \tag{3.42}$$

With this conditional probability in hand, we can create a BN (see Fig 3.4) for finding the probability of the joint system passing trough the states $|a_0, b_0\rangle, |a_1, b_1\rangle, |a_2, b_2\rangle, \cdots, |a_n, b_n\rangle$ for time instants $(0, t_1, t_2, \cdots, t_n)$, respectively. From the Theorem given in Eq. (3.39),

[9] We will denote $|a_k, b_k\rangle$ as the tensor product of vectors in A and B, $|a_k, b_k\rangle = |a_k\rangle_A \otimes |b_k\rangle_B$.

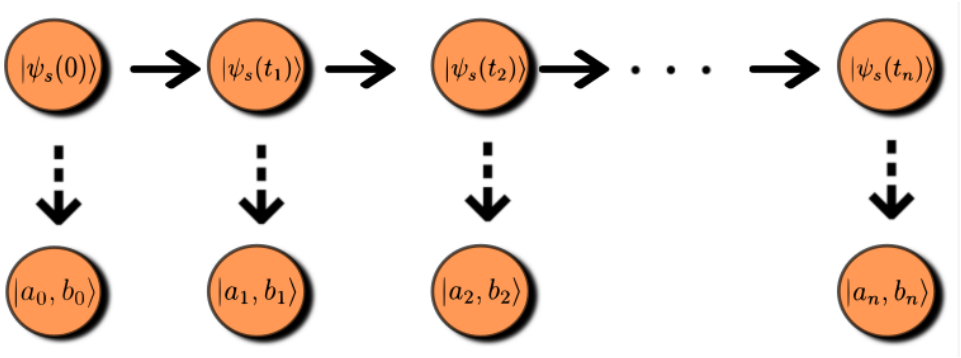

Figure 3.4: BN for the dynamical evolution of a quantum system. The upper line describes the global state evolution (which we often call *hidden layer*) and the dashed arrows indicates the causal dependence of the reduced states on the global states at each instant t_k.

the probability of realising such states is

$$\boxed{\mathcal{P}(\psi_s(0), a_0, b_0, a_1, b_1, \cdots, a_n, b_n) = P_s P(a_0, b_0|\psi_s(0)) P(a_1, b_1|\psi_s(t_1)) \cdots P(a_n, b_n|\psi_s(t_n)),} \tag{3.43}$$

where we omitted the conditional probabilities from $\psi_s(t_k)$ to $\psi_s(t_{k+1})$ since these transitions are deterministic and thus the conditional probabilities are 1. Consequently, the only global probability in which this joint distribution depends is on the initial ensemble $\{\psi_s(0)\}_s$.

Finally, for obtaining a conditional trajectory $(a_0, b_0, a_1, b_1, \cdots, a_n, b_n)$ of the reduced states, we must only marginalize over all s from the initial density matrix ensemble

$$\boxed{\mathcal{P}(a_0, b_0, a_1, b_1, \cdots, a_n, b_n) = \sum_s P_s P(a_0, b_0|\psi_s(0)) P(a_1, b_1|\psi_s(t_1)) \cdots P(a_n, b_n|\psi_s(t_n)).} \tag{3.44}$$

These results will be essential for obtaining the average shifts of observable in the second project of the thesis, shown in Chapter 7.

Chapter 4

Continuous Variables Framework

4.1 Bosonic modes

In this chapter we shall describe the framework of quantum continuous-variables. This exposition is based mostly on Serafini pedagogical compendium [14], also well-marked references can be founded in [15, 16]. The subject consists in the set of tools needed to describe the degrees of freedom that satisfy canonical commutation relations (CCR)

$$\boxed{[\hat{q}_j, \hat{p}_j] = i,} \tag{4.1}$$

where $\hat{q}_j$ and $\hat{p}_j$ are, respectively, the position and momentum operators[1] of the degree of freedom j. The degrees of freedom that satisfy Eq. (4.1) are called *bosonic modes* (in contrast to *fermionic modes* that satisfy anti-commutation relations).

This structure is widely used in quantum optics [55, 56], quantum information and quantum computation [1, 2, 15, 114], for instance in continuous-variables clusters [115], many-body and condensed matter physics [116, 117]. In our case we shall use it in our first project to describe a CM in which the system and ancillae are bosonic modes as a realization of the bosonic case described in the subsection 2.3.7 and in the second project as an application of the heat distribution obtained with QBNs.

We will focus on the use of *Gaussian states* and *Gaussian operations*. This enable

[1] In this chapter, as well as in the chapters involving continuum variables, we identify all operators acting on some Hilbert space with a hat. The reason for such terminology will make itself clear in the following sections.

us to describe the effects of the environment in the system with the same approach as the Stinespring dilation (Eq. (2.12), but with a much smaller number of variables. This will simplify dramatically the complexity of our computations.

4.1.1 Canonical vectors

We now define some objects concerning bosonic modes that will simplify our treatment and notation. We start with the vector of operators

$$\hat{\mathbf{r}} = (\hat{q}_1, \hat{p}_1, \hat{q}_2, \hat{p}_2, \cdots, \hat{q}_n, \hat{p}_n)^\top, \tag{4.2}$$

where n is the total number of modes of the system in question. As we can see, $\hat{\mathbf{r}}$ is nothing but the vector of all canonical operators (or quadratures) of a system, and can be rearranged to

$$\hat{\mathbf{z}} = (\hat{q}_1, \hat{q}_2, \cdots, \hat{q}_n, \hat{p}_1, \hat{p}_2, \cdots, \hat{p}_n)^\top, \tag{4.3}$$

and the relation between both vectors is given by

$$\hat{\mathbf{r}}_j = \sum_{k=1}^{2n} L_{jk} \hat{\mathbf{z}}_k, \tag{4.4}$$

where $\hat{\mathbf{r}}_j$, $\hat{\mathbf{z}}_j$ are respectively the j^{th} element of $\hat{\mathbf{r}}$ and $\hat{\mathbf{z}}$, and L_{jk} is the permutation matrix

$$L_{jk} = \begin{cases} \delta_{\frac{j+1}{2},k}, & \text{for } j \text{ odd} \\ \delta_{N+\frac{j}{2},k}, & \text{for } j \text{ even} \end{cases}. \tag{4.5}$$

Moreover, we have the creation and annihilation operators $\hat{a}_j^\dagger$ and $\hat{a}_j$, related to the quadrature variables by

$$\hat{a}_j = \frac{\hat{q}_j + i\hat{p}_j}{\sqrt{2}}, \tag{4.6}$$

the main importance of these last operators become clear in the *second quantization* context, as will be detailed later in this Chapter, in Section 4.2. For arranging these operators we define the vector

$$\hat{\mathbf{a}} = (\hat{a}_1, \hat{a}_1^\dagger, \hat{a}_2, \hat{a}_2^\dagger, \cdots, \hat{a}_n, \hat{a}_n^\dagger)^\top. \tag{4.7}$$

The elements of $\hat{\mathbf{a}}$ can be related to the elements of $\hat{\mathbf{r}}$ by means of Eq. (4.6), resulting in

$$\hat{\mathbf{a}} = \bar{U}\hat{\mathbf{r}}, \tag{4.8}$$

where[2]

$$\bar{U} = \bigoplus_{j=1}^{n} \bar{u}, \quad \text{with} \quad \bar{u} = \frac{1}{\sqrt{2}} \begin{pmatrix} 1 & i \\ 1 & -i \end{pmatrix}. \tag{4.9}$$

4.1.2 CCRs and the symplectic form

Given a system of n bosonic modes ordered according to Eq. (4.2), we define a $2n \times 2n$ matrix Ω as

$$\begin{aligned} \Omega &= \bigoplus_{j=1}^{n} \Omega_1 \\ &= \mathbb{I}_n \otimes \Omega_1, \\ \text{where } \Omega_1 &= \begin{pmatrix} 0 & 1 \\ -1 & 0 \end{pmatrix}, \end{aligned} \tag{4.10}$$

called *symplectic form*. It has the following properties that shall be useful to us

$$\Omega = -\Omega^\top \text{ (anti-symmetric)}, \tag{4.11}$$

$$\Omega = -\Omega^{-1} \Leftrightarrow \Omega^2 = -\mathbb{I}_{2n}, \tag{4.12}$$

$$\Omega\Omega^\top = \Omega^\top\Omega = -\Omega^2 = \mathbb{I}_{2n}, \tag{4.13}$$

where $\mathbb{I}_k$ is the $k \times k$ identity matrix.

The importance of the symplectic form makes itself clear when we write the CCR (Eq. (4.1)) in terms of $\hat{\mathbf{r}}$, resulting in

$$\boxed{[\hat{\mathbf{r}}, \hat{\mathbf{r}}^\top] = i\Omega,} \tag{4.14}$$

where we used the notation given in Appendix C, specially Eqs. (C.3) and (C.6). This will be the cornerstone to define the symplectic group during this chapter.

[2]The symbol $\oplus$ means the *direct sum* operation, see Appendix C, Section C.2, for the definition.

For completeness and further use, we present the corresponding relation for $\hat{z}$

$$[\hat{z}, \hat{z}^\top] = i\mathcal{J}, \text{ where } \mathcal{J} = \begin{pmatrix} 0_n & \mathbb{I}_n \\ -\mathbb{I}_n & 0_n \end{pmatrix}, \tag{4.15}$$

where 0_n is the $n \times n$ null matrix. Finally, the CCR for $\hat{\mathbf{a}}$ is

$$[\hat{\mathbf{a}}, \hat{\mathbf{a}}^\dagger] = \bigoplus_{j=1}^{n} \sigma_z \equiv \Sigma, \tag{4.16}$$

where σ_z is the z Pauli matrix.

4.2 Second quantization and the Fock space

The second quantization formalism is based on the idea of counting how many particles or "field excitations" each bosonic mode has. It is based on the structure existent from the creation and annihilation operators (Eq. (4.6)). If a mode j has its local Hamiltonian $H_j = \omega_j \left(a_j^\dagger a_j + \frac{1}{2}\right)$, then the eigenvectors of such Hamiltonian are discretized as $|m\rangle_j$, where m is a natural number. This way, the spectrum will be

$$H_j |m\rangle_j = \omega_j \left(m + \frac{1}{2}\right) |m\rangle_j , \tag{4.17}$$

having a lower bound when $m = 0$ such that $\hat{a}_j |0\rangle_j = 0$. The eigenvectors $|m\rangle_j$ relate to themselves and with the operators as

$$\hat{a}_j |m\rangle_j = \sqrt{m}\, |m-1\rangle_j , \tag{4.18}$$

$$\hat{a}_j^\dagger |m\rangle_j = \sqrt{m+1}\, |m+1\rangle_j . \tag{4.19}$$

The results above are just the standard Simple Quantum Harmonic Oscillator solution that can be found in any Quantum Mechanics textbook. But now this structure is used to interpret the excitations as the number of particles in a mode. For instance $|3\rangle_j$ represents a state with 3 particles in the mode j, $|8\rangle_k$ a state with 8 particles in the mode k and so on. The space to accommodate this scheme is called *Fock space*, which is the tensor

product of the Hilbert spaces corresponding to each number of particles.[3] For a mode j, the corresponding Fock space is

$$\mathcal{F}_j = \mathcal{H}_0^j \otimes \mathcal{H}_1^j \otimes \mathcal{H}_2^j \otimes \mathcal{H}_3^j \otimes \cdots = \bigotimes_{m=0}^{\infty} \mathcal{H}_m^j, \tag{4.20}$$

where $\mathcal{H}_m^j$ is the Hilbert space with m particles of the mode j. A tensor product of all the eigenvectors of the free mode Hamiltonian (like in Eq. (4.17)) is called a *Fock basis*, and is a basis of the Fock space. Finally, if we are working with a system of n modes, the full Hilbert space will be

$$\mathcal{H} = \bigotimes_{j=1}^{n} \mathcal{F}_j. \tag{4.21}$$

In this work, we shall always be acting in a Hilbert space like in Eq. (4.21) whenever we have a system of n bosonic modes.

4.3 Displacement operator and coherent states

Of major importance in continuous varible quantum mechanics is the unitary *displacement operator* (or *Weyl operator*) defined as

$$\hat{D}_{\mathbf{r}} = e^{i\mathbf{r}^\top \Omega \hat{\mathbf{r}}}, \tag{4.22}$$

where $\mathbf{r}$ is an arbitrary $2n$ vector with real components, and notice that $\hat{D}_{\mathbf{r}}^\dagger = \hat{D}_{-\mathbf{r}}$. The name "displacement" turns to be intuitive if we look at the following property

$$\boxed{\hat{D}_{\mathbf{r}}^\dagger \hat{\mathbf{r}} \hat{D}_{\mathbf{r}} = \hat{\mathbf{r}} - \mathbf{r},} \tag{4.23}$$

i.e., the action of this unitary on the vector of canonical operators is just its displacement (this equation is proved in Appendix C, Section C.4).

Another relation frequently used is the *composition* property

$$\boxed{\hat{D}_{\mathbf{r}_1+\mathbf{r}_2} = \hat{D}_{\mathbf{r}_1} \hat{D}_{\mathbf{r}_2} e^{i\mathbf{r}_1^\top \Omega \mathbf{r}_2/2},} \tag{4.24}$$

[3] It is important to remember that the tensor product of Hilbert spaces is also a Hilbert space, thus Fock spaces are Hilbert spaces.

where $\mathbf{r}_1$ and $\mathbf{r}_2$ are generic $2n$ vectors with real components. The composition property can be proved by direct application of the *Baker-Campbell-Hausdorff* (BCH) or *Zassenhaus* formula,[4] and it can be an alternative way of defining the non commutative properties of the canonical quantum operators.

Displacement operators are also used to define *coherent states*, which may be seen as a cornerstone to phase space methods in continuum variables. First, define α as a vector of length n with complex components

$$\alpha_j = (q_j + ip_j)/\sqrt{2}, \tag{4.26}$$

with q_j and p_j being real numbers. And define the $2n$ real vector $\mathbf{r}$ related to q_j and p_j as

$$\mathbf{r} = (q_1, p_1, q_2, p_2, \cdots, q_n, p_n)^\top. \tag{4.27}$$

Then we can rewrite Eq. (4.22) as

$$\hat{D}_\alpha = \hat{D}_{-\mathbf{r}} = e^{\sum_{j=1}^{n}\left(\alpha_j \hat{a}_j^\dagger - \alpha_j^* \hat{a}_j\right)}. \tag{4.28}$$

It can be shown, using the BCH formula, that

$$\boxed{\hat{D}_\alpha^\dagger \hat{a}_j \hat{D}_\alpha = \hat{a}_j + \alpha_j.} \tag{4.29}$$

We are now in the position to define the coherent state $|\alpha\rangle$ as

$$\boxed{|\alpha\rangle = \hat{D}_\alpha |0\rangle,} \tag{4.30}$$

where $|0\rangle = \bigotimes_{j=1}^{n} |0\rangle_j$ is the vacuum of the whole Hilbert space of Eq. (4.21). Consequently, $|\alpha\rangle$ is the eigenvector of the $\hat{a}_j$ operators (see the proof of the following equation

[4] This formula can be formulated as follows, let $\hat{A}$ and $\hat{B}$ be operators, then

$$e^{\hat{A}+\hat{B}} = e^{\hat{A}} e^{\hat{B}} e^{-\frac{1}{2!}[\hat{A},\hat{B}]} e^{\frac{1}{3!}(2[\hat{B},[\hat{A},\hat{B}]]+[\hat{A},[\hat{A},\hat{B}]])} \cdots. \tag{4.25}$$

in Appendix C, Section C.5)

$$\hat{a}_j \left|\alpha\right\rangle = \alpha_j \left|\alpha\right\rangle . \tag{4.31}$$

It is often useful to describe a coherent state $\left|\alpha\right\rangle$[5] in the Fock basis. This is given by the following equation (see Appendix C, Section C.6, for the proof)

$$\boxed{\left|\alpha\right\rangle = \sum_{m=0}^{\infty} e^{-|\alpha|^2/2} \frac{\alpha^m}{\sqrt{m!}} \left|m\right\rangle .} \tag{4.32}$$

Other important properties for further use are

$$\boxed{\hat{D}_\alpha \hat{D}_\beta = e^{\frac{1}{2}(\alpha\beta^* - \alpha^*\beta)} \hat{D}_{\alpha+\beta},} \tag{4.33}$$

this is equivalent to the composition property of Eq. (4.24), and the overlap between two coherent states $\left|\alpha\right\rangle$ and $\left|\beta\right\rangle$

$$\begin{aligned}
\left\langle\beta|\alpha\right\rangle &= \left\langle 0\right| \hat{D}_{-\beta} \hat{D}_\alpha \left|0\right\rangle \\
&= \left\langle 0\right| \hat{D}_{\alpha-\beta} \left|0\right\rangle e^{\frac{1}{2}(\alpha\beta^* - \alpha^*\beta)} \\
&= \left\langle 0|\alpha-\beta\right\rangle e^{\frac{1}{2}(\alpha\beta^* - \alpha^*\beta)} \\
&= e^{-\frac{1}{2}|\alpha-\beta|^2} e^{\frac{1}{2}(\alpha\beta^* - \alpha^*\beta)},
\end{aligned} \tag{4.34}$$

where in the second equality we used Eq. (4.33) and in the last equality we applied $\left\langle 0\right|$ in Eq. (4.32) to obtain the overlap between $\left|0\right\rangle$ and a coherent state. This overlap results in

$$\begin{aligned}
\left\langle 0|\alpha\right\rangle &= \sum_{m=0}^{\infty} e^{-|\alpha|^2/2} \frac{\alpha^m}{\sqrt{m!}} \left\langle 0|m\right\rangle \\
&= \sum_{m=0}^{\infty} e^{-|\alpha|^2/2} \frac{\alpha^m}{\sqrt{m!}} \delta_{0,m} \\
&= e^{-|\alpha|^2/2}.
\end{aligned}$$

[5] In this case, as in all the following results and demonstrations, we will assume all coherent states as being of only one mode (say, mode k), i.e., $\left|\alpha_k\right\rangle = \hat{D}_{\alpha_k} \left|0\right\rangle$, where $\hat{D}_{\alpha_k} = e^{\alpha_k \hat{a}_k^\dagger - \alpha_k^* \hat{a}_k}$ but we shall omit the k for simplicity of notation. The generalization to a number n of modes is straightforward since $\left|\alpha\right\rangle = \bigotimes_{j=1}^{n} \left|\alpha_j\right\rangle$ and $\hat{D}_\alpha = \prod_{j=1}^{n} \hat{D}_{\alpha_j}$.

Moreover, the set of all the coherent states $\{|\alpha\rangle, \alpha \in \mathbb{C}\}$ form an "overcomplete" basis for the Hilbert space of the corresponding mode. This means that, although it is not an orthogonal set, as we can see in Eq. (4.34), the set can span all the Hilbert space. Indeed, a completeness relation can be shown (see Appendix C, Section C.7) involving the coherent basis

$$\boxed{\frac{1}{\pi}\int_{\mathbb{C}} d^2\alpha\, |\alpha\rangle\langle\alpha| = \hat{\mathbb{I}},} \tag{4.35}$$

where $\hat{\mathbb{I}}$ is the identity operator of the Hilbert space and $\int_{\mathbb{C}} d^2\alpha$ means an integration over the entire complex plane. This provides an alternative way of computing the trace of an operator by using continuous-variables

$$\begin{aligned}
\mathrm{Tr}\left\{\hat{A}\right\} &= \sum_{m=0}^{\infty} \langle m|\hat{A}|m\rangle \\
&= \frac{1}{\pi}\int_{\mathbb{C}} d^2\alpha \sum_{m=0}^{\infty} \langle m|\alpha\rangle\langle\alpha|\hat{A}|m\rangle \\
&= \frac{1}{\pi}\int_{\mathbb{C}} d^2\alpha \langle\alpha|\hat{A}\sum_{m=0}^{\infty}|m\rangle\langle m|\alpha\rangle \\
&= \frac{1}{\pi}\int_{\mathbb{C}} d^2\alpha \langle\alpha|\hat{A}|\alpha\rangle\,.
\end{aligned} \tag{4.36}$$

To end our presentation about coherent states and displacement operators, we shall present the *Fourier-Weyl relation*. This is the statement that any bounded operator $\hat{A}$ acting on the Hilbert space of a mode can be constructed by an integral of displacement operators weighted by $\mathrm{Tr}\left\{\hat{D}_\alpha\hat{A}\right\}$ (see the proof in Appendix C, Section C.8). More precisely

$$\boxed{\hat{A} = \frac{1}{\pi}\int_{\mathbb{C}} d^2\alpha\, \mathrm{Tr}\left\{\hat{D}_\alpha\hat{A}\right\}\hat{D}_{-\alpha}.} \tag{4.37}$$

This relation follows an idea similar to a Fourier expansion. When we have a function of a real variable x expanded as $f(x) = \frac{1}{2\pi}\int dp\mathcal{F}(p)e^{-ixp}$, the weight here is the Fourier transform $\mathcal{F}(p)$ and the function e^{-ixp} has the same role as the displacement operator in Eq. (4.37). This parallel will be useful to gain some intuition on the concept of *characteristic function* of a density matrix, which will be discussed below in Sec. 4.4.

A direct consequence of the Fourier-Weyl relation is the orthogonality relation[6] for

[6]This orthogonality is defined in terms of the *Hilbert-Schmidt inner product* between two operators.

displacement operators. If we put the displacement operator itself as $\hat{A}$ in Eq. (4.37), we obtain

$$\hat{D}_\beta = \frac{1}{\pi}\int_{\mathbb{C}} d^2\alpha \,\mathrm{Tr}\Big\{\hat{D}_\alpha \hat{D}_\beta\Big\}\hat{D}_{-\alpha},$$

which means that we can treat the trace term as a Dirac delta function

$$\boxed{\mathrm{Tr}\Big\{\hat{D}_{-\alpha}\hat{D}_\beta\Big\} = \pi\delta^2(\beta-\alpha),} \tag{4.38}$$

which is the desired orthogonality relation. Moreover, the orthogonality relation of can be rewritten for n modes in the real plane as

$$\boxed{\mathrm{Tr}\Big\{\hat{D}_{\mathbf{r}}\hat{D}_{-\mathbf{s}}\Big\} = (2\pi)^n\delta^{2n}(\mathbf{r}-\mathbf{s}).} \tag{4.39}$$

4.4 Characteristic function

The *characteristic function* of a density matrix ρ is the weight function of the Fourier-Weil relation (Eq. (4.37)) if we expand the density matrix itself. More precisely, if

$$\rho = \frac{1}{\pi}\int_{\mathbb{C}} d^2\alpha\chi(\alpha)\hat{D}_{-\alpha}, \tag{4.40}$$

then, from the Fourier-Weyl relation (Eq. (4.37))

$$\chi(\alpha) = \mathrm{Tr}\Big\{\hat{D}_\alpha\rho\Big\} \tag{4.41}$$

is the characteristic function. The existence of this function for every ρ is guaranteed by the validity of the Fourier-Weyl relation.

From making the straightforward generalization to n modes and the change of variables from α to $\mathbf{r}$ (given by Eq. (4.26)), Eq. (4.40) results in

$$\rho = \frac{1}{(2\pi)^n}\int_{\mathbb{R}^{2n}} d\mathbf{r}\chi(\mathbf{r})\hat{D}_{\mathbf{r}}, \tag{4.42}$$

Given two operators $\hat{A}$ and $\hat{B}$ in a Hilbert space, their Hilbert-Schmidt inner product will be $\mathrm{Tr}\Big\{\hat{A}^\dagger\hat{B}\Big\}$.

where $d\mathbf{r} = dq_1 dp_1 dq_2 dp_2 \cdots dq_n dp_n$ similar to a phase space integral, and

$$\chi(\mathbf{r}) = \mathrm{Tr}\Big\{\hat{D}_{-\mathbf{r}}\rho\Big\}. \tag{4.43}$$

Again, this follows the same reasoning as the characteristic function $\varphi(y)$ of a probability density function $p(x)$, which are related by $p(x) = \frac{1}{2\pi}\int dy\varphi(y)e^{-ixy}$. Here the characteristic function is the Fourier transform of the probability density and has the role of a weight function in the integral, similarly $\chi(\mathbf{r})$ has the role of the weight and $\hat{D}_{\mathbf{r}}$ has the role of e^{-ixy} in Eq. (4.42).

Since a physical density matrix ρ must satisfy a set of properties, there is also a set of properties that $\chi(\mathbf{r})$ must satisfy in order to describe a physical state. First of all, from the definition we can conclude that the characteristic function must be a continuous function. Now, from the normalization condition of Eq. (2.5), we must have

$$\begin{aligned}\chi(0) &= \mathrm{Tr}\Big\{\hat{D}_0\rho\Big\} \\ &= \mathrm{Tr}\{\rho\} \\ &= 1,\end{aligned} \tag{4.44}$$

where 0 here means the $2n$ vector of entries 0 and we used that $\hat{D}_0 = \mathbb{I}$, where $\mathbb{I}$ is the $2n$ identity matrix. Furthermore, the positive semi-definite condition (Eq. (2.4)) is equivalent to (see Ref. [14] for an heuristic justification)

$$X \geq 0 \;\text{ where }\; X_{jk} = \chi(\mathbf{r}_j - \mathbf{r}_k)e^{i\mathbf{r}_k^\top \Omega \mathbf{r}_j}/2. \tag{4.45}$$

Also, from the fact that ρ is hermitian, we must have $\chi(\mathbf{r})^* = \chi(-\mathbf{r})$ and it can be shown that this is also a consequence of $X \geq 0$ (as it should be, since $\rho \geq 0$ implies ρ hermitian).

4.5 Quasi-probability distributions

Given a quantum state described in a phase space by the eigenvalues of canonical operators, it is possible to define weight functions in this phase space which are used to

compute the average of obseravables. These weight functions are called *quasi-probability distributions* since they don't satisfy necessary probability distribution properties but can have similar interpretations.

4.5.1 Wigner fucntion

We can define *Wigner function* (or *W-function*) as the Fourier transform of the characteristic function

$$W(\alpha) = \frac{1}{\pi^2}\int_{\mathbb{C}} d\beta^2 \chi(\alpha) e^{(\alpha\beta^* - \alpha^*\beta)}. \tag{4.46}$$

Going to the phase space with the eigenvalues of the quadrature operators, via Eq. (4.26), we obtain (see Appendix C, Section C.9)

$$W(q,p) = \frac{2}{\pi}\int_{\mathbb{R}} dq' e^{i2pq'} \langle q - q'| \rho |q + q'\rangle . \tag{4.47}$$

Now, if we integrate $W(q,p)$ over all p, we have

$$\boxed{\frac{1}{2}\int_{-\infty}^{\infty} dp W(q,p) = \langle q| \rho |q\rangle ,} \tag{4.48}$$

so the integral of the Wigner function over the quadrature eigenvalues of p is twice the probability distribution of the projective measuring of the conjugate quadrature q. Analogous results are easily obtained for any pair of quadrature operators.

4.5.2 The s-ordered quasi-probability distribution

For $s \in [-1, 1]$, we can define the *s-ordered characteristic function* as

$$\chi_s(\alpha) = \mathrm{Tr}\Big(\hat{D}_\alpha \rho\Big) e^{\frac{s}{2}|\alpha|^2}, \tag{4.49}$$

reducing to the characteristic function $\chi_s(\alpha)$ when $s = 0$ ($\chi_0(\alpha) = \chi(\alpha)$).

Further, we can define the *s-ordered quasi-probability distribution* $W_s(\alpha)$ as the Fourier transform of the s-ordered characteristic function

$$W_s(\alpha) = \frac{1}{\pi^2}\int_{\mathbb{C}} d^2\beta \; e^{(\alpha\beta^* - \alpha^*\beta)} \chi_s(\beta), \tag{4.50}$$

which reduces to the Wigner function for the case of $s = 0$.

This is a normalized function, since

$$\begin{aligned}\int_{\mathbb{C}} d^2\alpha W_s(\alpha) &= \int_{\mathbb{C}} d^2\beta\ \delta^2(\beta)\chi_s(\beta) \\ &= \chi(0) \\ &= 1. \end{aligned} \tag{4.51}$$

We shall expose in the following that others important quasi-probabilities results from the s-ordered quasi-probabilities for $s = 1$ and $s = -1$.

4.5.3 Glauber-Sudarshan P-function

For the case of $s = 1$, the s-ordered quasi-probability satisfies an exceptional property. It will be the function responsible for the diagonal decomposition of the density matrix described by the modes of α, i.e., if we define $P(\alpha) = W_1(\alpha)$, then

$$\boxed{\rho = \int_{\mathbb{C}} d^2\alpha P(\alpha) \left|\alpha\right\rangle \left\langle\alpha\right| .} \tag{4.52}$$

The equation above is proved in Appendix C, Section C.10, and $P(\alpha)$ is called the *Glauber-Sudarshan P-representation* (or *P-function*).

4.5.4 Husimi Q-function

One can define the *Husimi Q-function* as

$$Q(\alpha) = W_{-1}(\alpha). \tag{4.53}$$

The function $Q(\alpha)$ receives the interpretation of being the probability of an *heterodyne measurement*[7] to yield the outcome α, since one can prove (see Appendix C, Section C.11,

[7] An heterodyne measurement is a generalized measurement with Kraus matrices $M_\alpha = \frac{1}{\sqrt{\pi}} \left|\alpha\right\rangle \left\langle\alpha\right|$, where $\left|\alpha\right\rangle$ is a coherent state. Heterodyne measurements are of major importance in Quantum Optics [55, 118, 119]

for the proof) that

$$\boxed{Q(\alpha) = \frac{1}{\pi} \langle \alpha | \rho | \alpha \rangle .} \tag{4.54}$$

Finally, it is worth to mention that the quasi-probability distributions are extremely useful to computations of averages of creation and annihilation operators in normal, anti-normal and symmetric ordering [14, 55, 120]. In this thesis we shall not use such properties directly.

4.6 Gaussian states

4.6.1 Definitions

We start by defining the *second order Hamiltionian* as a Hamiltonian that is constructed with the canonical operators at maximum order 2, its more general form is

$$\hat{H} = \frac{1}{2} \hat{\mathbf{r}}^\top H \hat{\mathbf{r}} + \hat{\mathbf{r}}^\top \mu, \tag{4.55}$$

where H is a $2n \times 2n$ real matrix and a positive definite operator ($H > 0$)[8] called the *Hamiltonian matrix* (notice that this is not the Hamiltonian *operator*) and μ is a real vector with dimension $2n$. A more suitable way of representing general second order Hamiltonians is given as follows. If we assign

$$\tilde{\mathbf{r}} = -H^{-1} \mu, \tag{4.56}$$

then, except from a constant term, we can write

$$\begin{aligned} \hat{H} &= \frac{1}{2} \hat{D}_{-\tilde{\mathbf{r}}} \hat{\mathbf{r}}^\top H \hat{\mathbf{r}} \hat{D}_{\tilde{\mathbf{r}}} \\ &= \frac{1}{2} (\hat{\mathbf{r}} - \tilde{\mathbf{r}})^\top H (\hat{\mathbf{r}} - \tilde{\mathbf{r}}). \end{aligned} \tag{4.57}$$

Equipped with these definitions, we define Gaussian states as *thermal states with a second order Hamiltonian $\hat{H}$ in which its Hamiltonian matrix is positive definite $H > 0$*

[8] H must be symmetric (since $\hat{H}$ must be hermitian). But, additionally, the positive definite restriction is there to ensure the thermodynamic stability of the Hamiltonian operator (i.e., their eigenvalues must be bounded from below).

(the necessity of $H > 0$ is a direct consequence of the thermal state being thermally stable)

$$\boxed{\rho_G = \frac{e^{-\beta\hat{H}}}{Z},} \tag{4.58}$$

where $Z = \mathrm{Tr}\left\{e^{-\beta\hat{H}}\right\}$ is the partition function and $\beta > 0$ is the inverse of the temperature (here we also always set the Boltzmann constant to 1). This definition includes pure states, which can be taken as the limit of the above equation with $\beta \to \infty$

$$\rho_{\text{pure}} = \lim_{\beta\to\infty} \frac{e^{-\beta\hat{H}}}{Z}. \tag{4.59}$$

Another important concept in the context of Gaussian states are the statistical moments, i.e., the averages of different orders of canonical operators. The *first moments* are the average of the canonical operators

$$\boxed{\langle\hat{\mathbf{r}}\rangle = \mathrm{Tr}\{\rho_G\hat{\mathbf{r}}\}.} \tag{4.60}$$

As for the second moments, it is convenient to combine them in terms of the *covariance matrix*

$$\boxed{\begin{aligned}\sigma &= \frac{1}{2}\,\mathrm{Tr}\left[\rho_G\{(\hat{\mathbf{r}}-\bar{\mathbf{r}}),(\hat{\mathbf{r}}-\bar{\mathbf{r}})^\top\}\right]\\ &= \frac{1}{2}\left\langle\{(\hat{\mathbf{r}}-\bar{\mathbf{r}}),(\hat{\mathbf{r}}-\bar{\mathbf{r}})^\top\}\right\rangle,\end{aligned}} \tag{4.61}$$

where the anti-commutator inside the trace is defined just like in Appendix C, Section C.1 and we defined $\bar{\mathbf{r}} = \langle\hat{\mathbf{r}}\rangle$. If we execute the anti-commutator, use the distributive property of averages and use Eq. (4.14) in the equation above, we obtain

$$\boxed{\sigma = \langle\hat{\mathbf{r}}\hat{\mathbf{r}}^\top\rangle - \langle\hat{\mathbf{r}}\rangle\langle\hat{\mathbf{r}}\rangle^\top - \frac{i}{2}\Omega,} \tag{4.62}$$

which can be a much more suitable way of computing the covariance matrix.

4.6.2 Bona-fide conditions for covariance matrices

Given that covariance matrices represent the second moments of canonical operators, they must have restrictions on their components due to the uncertainty-relations. The restriction is given by the following inequality (see Appendix C, Section C.12, for the proof of this condition)

$$\boxed{\sigma + \frac{i\Omega}{2} \geq 0.} \tag{4.63}$$

This is the restriction that a covariance matrix must obey to represent a valid quantum state and is called *Roberson-Schrödinger relation*, or also referred as *bona-fide* condition.

4.6.3 Dynamics of canonical operators and statistical moments

We start our development for the dynamics of Gaussian states from analysing the evolution of the vector of canonical operators $\hat{\mathbf{r}}$ in the Heisenberg picture for closed systems under the action of a second order Hamiltonian from Eqs. (4.55) and (4.57). Additionally, we analyse the evolution of the statistical moments for closed systems under the same Hamiltonian.

For the vector of canonical operators, the Heisenberg Equation implies

$$\frac{d\hat{\mathbf{r}}_j}{dt} = (\Omega H \hat{\mathbf{r}})_j + (\Omega\mu)_j \,. \tag{4.64}$$

The equation above is equivalent to stating that

$$\begin{aligned} \frac{d\hat{\mathbf{r}}}{dt} &= \Omega(H\hat{\mathbf{r}} + \mu) \\ &= \Omega H(\hat{\mathbf{r}} + H^{-1}\mu). \end{aligned} \tag{4.65}$$

So, if we define $\hat{\mathbf{r}}'$ such that

$$\hat{\mathbf{r}} = \hat{\mathbf{r}}' - H^{-1}\mu, \tag{4.66}$$

then

$$\frac{d\hat{\mathbf{r}}'}{dt} = \Omega H \hat{\mathbf{r}}', \tag{4.67}$$

which has the solution

$$\hat{\mathbf{r}}'(t) = e^{\Omega H(t-t_0)}\hat{\mathbf{r}}'(t_0).$$

Now using that $\hat{\mathbf{r}}'(t_0) = \hat{\mathbf{r}}(t_0) + H^{-1}\mu$ and $\hat{\mathbf{r}}'(t) = \hat{\mathbf{r}}(t) + H^{-1}\mu$ in the equation above, we obtain

$$\hat{\mathbf{r}}(t) = e^{\Omega H(t-t_0)}\hat{\mathbf{r}}(t_0) + \left(e^{\Omega H(t-t_0)} - \mathbb{I}\right) H^{-1}\mu, \tag{4.68}$$

where $\mathbb{I}$ is the $2n \times 2n$ identity operator. This is the general solution for the Heisenberg vector of canonical operators that we intended to find. The solution above can be rewritten in terms of $\tilde{\mathbf{r}}$ from Eq. (4.56) as

$$\boxed{\hat{\mathbf{r}}(t) = \hat{D}_{\tilde{\mathbf{r}}}\left(e^{\Omega H(t-t_0)}\hat{D}_{-\tilde{\mathbf{r}}}\hat{\mathbf{r}}(t_0)\hat{D}_{\tilde{\mathbf{r}}}\right)\hat{D}_{-\tilde{\mathbf{r}}}.} \tag{4.69}$$

Notice that the general solution above reduces to the simple form

$$\boxed{\hat{\mathbf{r}}(t) = e^{\Omega H(t-t_0)}\hat{\mathbf{r}}(t_0),} \tag{4.70}$$

if $\mu = 0$. The general solution of Eq. (4.69) can be understood as translating $\hat{\mathbf{r}}(t_0)$, so that the Hamiltonian is quadratic in this new frame (see Eq. (4.57)); making the quadratic Hamiltonian evolution, and then translating back the vector to its initial frame.

Focusing now in the dynamics of statistical moments, we start by studying the first moments evolution. The time derivative for the vector of the first moments given in Eq. (4.60) can be obtained by applying the density matrix ρ in both sides of Eq. (4.65) and taking the trace, arriving at

$$\frac{d\langle\hat{\mathbf{r}}\rangle}{dt} = \Omega(H\langle\hat{\mathbf{r}}\rangle + \mu). \tag{4.71}$$

The equation above has the exact same structure as Eq. (4.65), thus its solution is analogous

$$\boxed{\langle\hat{\mathbf{r}}(t)\rangle = \left\langle\hat{D}_{\tilde{\mathbf{r}}}\left(e^{\Omega H(t-t_0)}\hat{D}_{-\tilde{\mathbf{r}}}\hat{\mathbf{r}}(t_0)\hat{D}_{\tilde{\mathbf{r}}}\right)\hat{D}_{-\tilde{\mathbf{r}}}\right\rangle.} \tag{4.72}$$

Again, if the Hamiltonian has no linear term ($\mu = 0$), we have

$$\boxed{\langle\hat{\mathbf{r}}(t)\rangle = e^{\Omega H(t-t_0)}\langle\hat{\mathbf{r}}(t_0)\rangle.} \tag{4.73}$$

For the second moments, we study the evolution of the covariance matrix. From taking the derivative of Eq. (4.62) with respect to time, we obtain

$$\frac{d\sigma}{dt} = \frac{d}{dt}\langle \hat{\mathbf{r}}\hat{\mathbf{r}}^\top \rangle - \frac{d\langle \hat{\mathbf{r}} \rangle}{dt}\langle \hat{\mathbf{r}} \rangle^\top - \langle \hat{\mathbf{r}} \rangle \frac{d\langle \hat{\mathbf{r}} \rangle^\top}{dt}, \tag{4.74}$$

for computing the term with $\frac{d}{dt}\langle \hat{\mathbf{r}}\hat{\mathbf{r}}^\top \rangle$ we observe that, in the Heisenberg picture,

$$\begin{aligned}\frac{d}{dt}(\hat{\mathbf{r}}\hat{\mathbf{r}}^\top) &= \frac{d\hat{\mathbf{r}}}{dt}\hat{\mathbf{r}}^\top + \hat{\mathbf{r}}\frac{d\hat{\mathbf{r}}^\top}{dt} \\ &= \Omega H \hat{\mathbf{r}}\hat{\mathbf{r}}^\top + \Omega\mu\hat{\mathbf{r}}^\top + \hat{\mathbf{r}}\hat{\mathbf{r}}^\top(\Omega H)^\top + \hat{\mathbf{r}}(\Omega\mu)^\top,\end{aligned}$$

where in the second equality we used Eq. (4.65) and the transpose of it. We can now apply the density matrix in the equation above and take the trace of it, obtaining

$$\frac{d}{dt}\langle \hat{\mathbf{r}}\hat{\mathbf{r}}^\top \rangle = \Omega H \langle \hat{\mathbf{r}}\hat{\mathbf{r}}^\top \rangle + \Omega\mu\langle \hat{\mathbf{r}}^\top \rangle + \hat{\mathbf{r}}\hat{\mathbf{r}}^\top(\Omega H)^\top + \hat{\mathbf{r}}(\Omega\mu)^\top. \tag{4.75}$$

Lastly, using Eq. (4.75), the transpose of it, Eq. (4.65) and the transpose of it in Eq. (4.74), we obtain

$$\boxed{\frac{d\sigma}{dt} = \Omega H \sigma + \sigma(\Omega H)^\top,} \tag{4.76}$$

which is our differential equation for a general second order Hamiltonian evolution of the covariance matrix. Its solution is simple and is given by

$$\boxed{\sigma(t) = e^{\Omega H(t-t_0)}\sigma(t_0)\left(e^{\Omega H(t-t_0)}\right)^\top.} \tag{4.77}$$

There are three things that must be observed in the solution above. First, the evolution of $\sigma(t)$ does not depend on the first moment $\langle \hat{\mathbf{r}}(t) \rangle$, both of them evolve in a *decoupled* way. Second, the solution of $\sigma(t)$ does not depend at all on the linear terms of the Hamiltonian, it only depends on the Hamiltonian matrix H of the quadratic part. Third, the matrix $e^{\Omega H(t-t_0)}$ clearly plays a major role in both $\sigma(t)$ and $\langle \hat{\mathbf{r}}(t) \rangle$ solutions; for this reason, and further simplifications in the following of the thesis, we shall refer to it as $S_H = e^{\Omega H t}$ (from now on we set $t_0 = 0$ just for convenience).

4.6.4 Symplectic operators

As already anticipated above, the matrix S_H has a major role in the evolution of statistical moments. We shall point the condition that these operators must satisfy in order to describe valid a physical evolution for vectors of operators. These conditions are analogous to the condition of unitarity for evolution operators acting on Hilbert space states.

Since in our applications we shall deal only with quadratic Hamiltonians without linear terms, and the extension to Hamiltonians with linear terms can be simply accounted with applications of displacement operators in Eqs. (4.57), (4.69) and (4.72), we shall from now on only consider quadratic Hamiltonians. Hence the evolution will be fully described by the Hamiltonian matrix H.

In this context (where $\tilde{\mathbf{r}} = 0$) we obtain, by Eq. (4.70),

$$\hat{\mathbf{r}}(t) = \hat{S}_{\hat{H}}^{\dagger} \hat{\mathbf{r}}(0) \hat{S}_{\hat{H}} = S_H \hat{\mathbf{r}}(0), \tag{4.78}$$

where $\hat{S}_{\hat{H}} = e^{-i\hat{H}t}$ is the time evolution unitary operator. This implies, for any vector of canonical operators $\hat{\mathbf{r}}$, that

$$\hat{S}_{\hat{H}}^{\dagger} \hat{\mathbf{r}} \hat{S}_{\hat{H}} = S_H \hat{\mathbf{r}}, \tag{4.79}$$

this equation makes explicit part of the enormous simplification that the continuous-variables framework can offer to us. The left hand side sets the evolution to the canonical operators given by the unitary operators acting at each one of the vector elements, remembering that these unitaries act on a infinite dimensional Hilbert space. This evolution is equally obtained, on the right hand side, by the action of a much simpler $2n \times 2n$ matrix (with real components) on the canonical vector, simplifying manifestly our computations.

Notice that the evolution operator $\hat{S}_{\hat{H}}$ is unitary and thus represents a physical transformation between states. Therefore, it must maintain the CCR for the vectors of canonical operators $\hat{\mathbf{r}}$, i.e., if we call $\hat{\mathbf{r}}' = \hat{S}_{\hat{H}}^{\dagger} \hat{\mathbf{r}} \hat{S}_{\hat{H}}$, then we must also have $[\hat{\mathbf{r}}', \hat{\mathbf{r}}'^{\top}] = i\Omega$. This must

imply, from Eq. (4.79) that

$$\begin{aligned}[\hat{\mathbf{r}'}, \hat{\mathbf{r}'}^{\top}] &= [S_H\hat{\mathbf{r}}, (S_H\hat{\mathbf{r}})^{\top}] \\ &= S_H[\hat{\mathbf{r}}, \hat{\mathbf{r}}]S_H^{\top} \\ &= iS_H\Omega S_H^{\top} \\ &= i\Omega. \end{aligned} \tag{4.80}$$

The equation above implies that

$$S_H\Omega S_H^{\top} = \Omega,$$

is the necessary and sufficient condition for a real $2n \times 2n$ matrix to be considered a transformation capable of substituting the unitary evolution as in Eq. (4.79). Stating properly, any $2n \times 2n$ real matrix S that satisfies

$$\boxed{S\Omega S^{\top} = \Omega,} \tag{4.81}$$

is called a *symplectic transformation* and forms a *symplectic group* with the others transformations satisfying this property,[9] in symbols $S \in S_{p_{2n,\mathbb{R}}}$. This is the group in which all the elements can possibly describe a physical unitary transformation acting in $2n$ vectors of operators.

4.6.5 Covariance matrix parametrization

It can be shown that for Gaussian states we have a one to one parametrization of the density matrix in terms of the first moments and the covariance matrix of the state. More precisely, if we know the covariance matrix σ (Eq. (4.61)) and the first moments $\bar{\mathbf{r}} = \langle\hat{\mathbf{r}}\rangle$ (Eq. (4.60)) of a Gaussian state, than we can obtain its density matrix by the relation

[9] We call an application of a transformation A on a transformation $\mathcal{O}$ as *application by congruence* when we have $A\mathcal{O}A^{\top}$. For instance, in Eq. (4.81) at the left hand side S acts by congruence in Ω.

$$\boxed{\begin{aligned}\rho_G &= \frac{e^{-\frac{1}{2}(\hat{\mathbf{r}}-\bar{\mathbf{r}})^\top M(\hat{\mathbf{r}}-\bar{\mathbf{r}})}}{Z},\\ \text{where}\quad M &= 2\text{arccoth}(2i\Omega\sigma)i\Omega,\end{aligned}} \tag{4.82}$$

and $Z = \text{Tr}\left(e^{-\frac{1}{2}(\hat{\mathbf{r}}-\bar{\mathbf{r}})^\top M(\hat{\mathbf{r}}-\bar{\mathbf{r}})}\right)$ is just a normalization constant.

The proof for the parametrization of Eq. (4.82) can be found in Appendix C, Section C.16, and is made with the use of the *Normal Mode Decomposition* or *Williamson's theorem*. This theorem can be stated as follows. Suppose M is a $2n \times 2n$ positive definite real matrix, then there is a symplectic transformation $S \in S_{p_{2n,\mathbb{R}}}$, such that

$$\boxed{M = SDS^\top,} \tag{4.83}$$

where

$$D = \text{diag}(d_1, d_1, \cdots, d_n, d_n), \tag{4.84}$$

with $d_j > 0,\ \forall j \in [1, \cdots, n]$ called *symplectic eigenvalues*.[10] In Appendix C, Section C.14, we present a method of obtaining the symplectic eigenvalues given a positive definite matrix M.

Conversely, if we have the density matrix of a Gaussian operator ρ_G, we can obtain its first moments and covariance matrix by Eqs. (4.60) and (4.61), thus completing the one to one correspondence.

This correspondence is another critical advantage of dealing with Gaussian states. A density matrix description of a bosonic Gaussian state requires infinite elements, while the description of a $2n$ vector of averages and a $2n \times 2n$ covariance matrix require a finite number of parameters. This parametrization of quantum states in first and second moments is analogous to the intuitive parametrization of Gaussian probability distributions in terms of their first and second moments.

[10] The proof of this theorem can be found in Refs. [14, 121–125].

4.6.6 Characteristic function and quasi-probability distributions of Gaussian states

Another important aspect of Gaussian states is that their characteristic function have a particularly simple form. Using Eq. (4.82) in the definition of Eq. (4.43), one can show[11] that the characteristic function of a Gaussian state with first moments vector $\bar{\mathbf{r}} = \langle \hat{\mathbf{r}} \rangle$ and covariance matrix σ is

$$\boxed{\chi_G(\mathbf{r}) = e^{-\frac{1}{2}\mathbf{r}^\top \Omega^\top \sigma \Omega \mathbf{r}} e^{i\mathbf{r}^\top \Omega^\top \bar{\mathbf{r}}}.} \tag{4.85}$$

Since a state is Gaussian if and only if its characteristic function has the form described as above, this equation will be very useful to distinguish the Gaussianity of a state.

With the Gaussian characteristic function, we can obtain simple formulas for the quasi-probability distributions of Gaussian states. With the use of Eqs. (4.49) and (4.50), going to the quadrature eigenvalues space, we have that the s-ordered quasi probability distribution $W_s(\mathbf{r})$ in terms of the characteristic function $\chi(\mathbf{r})$ is

$$W_s(\mathbf{r}) = \frac{1}{(2\pi^2)^n} \int_{\mathbb{R}^{2n}} d\mathbf{r}' e^{i\mathbf{r}'^\top \Omega \mathbf{r}} e^{\frac{s}{4}\mathbf{r}'^\top \mathbf{r}'} \chi(\mathbf{r}'), \tag{4.86}$$

where n is the number of modes of the Gaussian state.

With the equation above and the Gaussian characteristic function of (4.85), we obtain (see Appendix C, Section C.17, for detailed calculation) the Glauber-Sudarshan P-function for the Gaussian state

$$\boxed{P_G(\mathbf{r}) = \frac{1}{(2\pi)^n} \frac{e^{-\frac{1}{2}\mathbf{r}^\top \left(\sigma - \frac{\mathbb{I}}{2}\right)^{-1} \mathbf{r}}}{\sqrt{\det\left(\sigma - \frac{\mathbb{I}}{2}\right)}};} \tag{4.87}$$

the Husimi Q-function for the Gaussian state

$$\boxed{Q_G(\mathbf{r}) = \frac{1}{(2\pi)^n} \frac{e^{-\frac{1}{2}\mathbf{r}^\top \left(\sigma + \frac{\mathbb{I}}{2}\right)^{-1} \mathbf{r}}}{\sqrt{\det\left(\sigma + \frac{\mathbb{I}}{2}\right)}};} \tag{4.88}$$

[11] This is done in details in Chapter 4 of Ref. [14].

and the Wigner W-function for the Gaussian state

$$\boxed{W_G(\mathbf{r}) = \frac{1}{(2\pi)^n} \frac{e^{-\frac{1}{2}\mathbf{r}^\top \sigma^{-1}\mathbf{r}}}{\sqrt{\det(\sigma)}}.} \tag{4.89}$$

Notice the resemblance of these quasi-probability distributions with the classical probability distribution of a multivariate Gaussian distribution of a $2n$-dimensional random variable

$$P(\mathbf{x}) = \frac{e^{-\frac{1}{2}(\mathbf{x}-\bar{\mathbf{x}})^\top \Sigma^{-1}(\mathbf{x}-\bar{\mathbf{x}})}}{\sqrt{(2\pi)^{2n}\det(\Sigma)}}, \tag{4.90}$$

where $\mathbf{x}$ is the multidimensional random variable, $\bar{\mathbf{x}}$ is the average of the random variable and Σ is the covariance matrix of the random variable. In particular, the Q-function of a quantum Gaussian state, which is a valid probability distribution describing the outcome of heterodyne measurements, has the same probability distribution as a classical random variable set with the addend of $\mathbb{I}/2$ in the covariance matrix.

These formulae will be useful for the second project of this thesis, in Chapter 8.

4.7 Gaussian operations

Given the very useful properties of Gaussian states pointed above, it is of our interest to find quantum operations (in the sense of quantum channels, defined at Section 2.2) that preserve this Gaussian status of the states. These operations are called *Gaussian operations* or *Gaussian channels*.

In this thesis we shall follow the Stinespring dilation protocol, as described in Section 2.2, for obtaining an open system evolution. This means that we will construct an initially uncorrelated joint system by making a tensor product between the system and the environment state, then we shall make the unitary evolution of the joint state and finally trace out the environment in order to obtain the open system description. In the following, we will prove that all of such operations: the tensor product, the unitary evolution (generated by second order Hamiltonians) and the partial trace, are Gaussian operations. This enables us to use only first moments and covariance matrices to completely describe our system during the Stinespring procedure, if our system and environment start at Gaussian states.

4.7.1 Tensor product

Suppose two Gaussian states ρ_A with m modes and ρ_B with n modes, first moments $\bar{\mathbf{r}}_A = \langle \hat{\mathbf{r}}_A \rangle$ and $\bar{\mathbf{r}}_B = \langle \hat{\mathbf{r}}_B \rangle$ and covariance matrices σ_A and σ_B respectively. Using the Gaussian characteristic function (Eq. (4.85)) and Eq. (4.42), we obtain

$$\begin{aligned}
\rho_A \otimes \rho_B &= \frac{1}{(2\pi)^{2(m+n)}} \int_{\mathbb{R}(2m)} d\mathbf{r}_A e^{-\frac{1}{4}\mathbf{r}_A^\top \Omega^\top \sigma_A \Omega \mathbf{r}_A} e^{i\mathbf{r}_A^\top \Omega^\top \bar{\mathbf{r}}_A} \hat{D}_{\mathbf{r}_A} \otimes \int_{\mathbb{R}(2n)} d\mathbf{r}_B e^{-\frac{1}{4}\mathbf{r}_B^\top \Omega^\top \sigma_B \Omega \mathbf{r}_B} e^{i\mathbf{r}_B^\top \Omega^\top \bar{\mathbf{r}}_B} \hat{D}_{\mathbf{r}_B} \\
&= \frac{1}{(2\pi)^{2(m+n)}} \int_{\mathbb{R}(2m+2n)} d\mathbf{r}_A d\mathbf{r}_B e^{-\frac{1}{4}\mathbf{r}_A^\top \Omega^\top \sigma_A \Omega \mathbf{r}_A - \frac{1}{4}\mathbf{r}_B^\top \Omega^\top \sigma_B \Omega \mathbf{r}_B + i\mathbf{r}_A^\top \Omega^\top \bar{\mathbf{r}}_A + i\mathbf{r}_B^\top \Omega^\top \bar{\mathbf{r}}_B} \hat{D}_{\mathbf{r}_A} \otimes \hat{D}_{\mathbf{r}_B} \\
&= \frac{1}{(2\pi)^{2(m+n)}} \int_{\mathbb{R}(2m+2n)} d\mathbf{r} e^{-\frac{1}{4}\mathbf{r}^\top \Omega^\top \sigma \Omega \mathbf{r} + i\mathbf{r}^\top \Omega^\top \bar{\mathbf{r}}} \hat{D}_{\mathbf{r}}, \qquad (4.91)
\end{aligned}$$

where $\mathbf{r} = \mathbf{r}_A \oplus \mathbf{r}_B$ and $\sigma = \sigma_A \oplus \sigma_B$. In the third equality, we regrouped the terms in the exponential and used that $\mathbf{r}_A^\top \Omega^\top \sigma_A \Omega \mathbf{r}_A + \mathbf{r}_B^\top \Omega^\top \sigma_B \Omega \mathbf{r}_B = \mathbf{r}^\top \Omega^\top \sigma \Omega \mathbf{r}$ and that $\mathbf{r}_A^\top \Omega^\top \bar{\mathbf{r}}_A + \mathbf{r}_B^\top \Omega^\top \bar{\mathbf{r}}_B = \mathbf{r}^\top \Omega^\top \bar{\mathbf{r}}$, which is a direct consequence of the definition of direct sum.[12] Finally, also in the third equality of the equation above, and we used that $\hat{D}_{\mathbf{r}} = \hat{D}_{\mathbf{r}_A} \otimes \hat{D}_{\mathbf{r}_B}$ which is a direct consequence from the definition of the Weyl operator (Eq. (4.22)).

Eq. (4.91) shows explicitly that the tensor product of two Gaussian states ρ_A and ρ_B is a Gaussian state since it has a characteristic function on the same form as Eq. (4.85). Moreover, it shows that we can construct a tensor product of two Gaussian states ρ_A and ρ_B by making the following operations in their first moments and covariance matrices

$$\langle \hat{\mathbf{r}} \rangle = \langle \hat{\mathbf{r}}_A \rangle \oplus \langle \hat{\mathbf{r}}_B \rangle \quad \text{and} \qquad (4.92)$$

$$\sigma = \sigma_A \oplus \sigma_B. \qquad (4.93)$$

4.7.2 Unitary operations

To show that unitary operators, generated by second order Hamiltonians, are Gaussian operations it is sufficient to show that if an initial state is of the form of Eq. (4.58), then its unitary evolution $\rho'_G = \hat{U} \rho_G \hat{U}^\dagger$ (where $\hat{U}$ is a unitary operator) will also be of the form of Eq. (4.58). Therefore, suppose that our initial state is given by Eq. (4.58), then

[12] We are implicitly assuming that Ω has the dimensions according to the vectors in which it is acting, i.e., switching the n in Eq. (4.10) in each case for convenience.

if we have an unitary evolution given by $\hat{U} = e^{-i\hat{H}'}$, where $\hat{H}'$ is a generic second order Hamiltonian, the evolution of the state will have the form

$$\begin{aligned}\rho'_G &= \hat{U}\frac{e^{-\beta\hat{H}}}{Z}\hat{U}^\dagger \\ &= \frac{e^{-\beta\hat{U}\hat{H}\hat{U}^\dagger}}{Z},\end{aligned}$$

now if we call $\hat{H}'' = \hat{U}\hat{H}\hat{U}^\dagger$, then we need only to show that $\hat{H}''$ is a second order Hamiltonian in order to complete our proof. In fact

$$\begin{aligned}\hat{H}'' &= \hat{U}\hat{H}\hat{U}^\dagger \\ &= e^{-i\hat{H}'}\hat{H}e^{i\hat{H}'} \\ &= \hat{H} - i[\hat{H}', \hat{H}] - \frac{1}{2!}[\hat{H}', [\hat{H}', \hat{H}]] + \frac{i}{3!}[\hat{H}', [\hat{H}', [\hat{H}', \hat{H}]]] + \cdots ,\end{aligned} \tag{4.94}$$

this is obtained with the use of another BCH formula.[13] This proof is completed by the fact that any commutator between second order operators is a second order operator (see Appendix C, Section C.18, for a proof of this statement), hence H'' is a second order Hamiltonian.

The unitary evolution for Gaussian states will be described by the symplectic transformations S_H as in Eq. (4.79). And it is sufficient to know the evolution of the first moments and covariance matrix from the following equations already obtained in Subsection 4.6.3

$$\boxed{\begin{aligned}\langle \mathbf{r}(t)\rangle &= S_H\langle \mathbf{r}(0)\rangle \qquad \text{and} \\ \sigma(t) &= S_H\sigma(0)S_H^\top,\end{aligned}} \tag{4.96}$$

$$\tag{4.97}$$

since the Gaussianity of the states is preserved.

[13] Given two operators $\hat{A}$ and $\hat{B}$, then

$$e^{\hat{A}}\hat{B}e^{-\hat{A}} = \hat{B} + [\hat{A}, \hat{B}] + \frac{1}{2!}[\hat{A}, [\hat{A}, B]] + \frac{1}{3!}[\hat{A}, [\hat{A}, [\hat{A}, \hat{B}]]] + \frac{1}{4!}[\hat{A}, [\hat{A}, [\hat{A}, [\hat{A}, \hat{B}]]]] + \cdots , \tag{4.95}$$

4.7.3 Partial trace

Suppose we have a global system AB composed of two subsystems A and B of m and n bosonic modes, respectively, and we prescribe the canonical operators of AB as $\hat{\mathbf{r}} = \hat{\mathbf{r}}_A \oplus \hat{\mathbf{r}}_B$, where $\hat{\mathbf{r}}_A$ and $\hat{\mathbf{r}}_B$ are the canonical operators of the subspace A and B, respectively. Then if the global state ρ_{AB} is Gaussian, it can be fully described by its first moments $\bar{\mathbf{r}} = \langle \hat{\mathbf{r}} \rangle$ and covariance matrix σ, which can be parametrized as

$$\bar{\mathbf{r}} = \bar{\mathbf{r}}_A \oplus \bar{\mathbf{r}}_B = \begin{pmatrix} \bar{\mathbf{r}}_A \\ \bar{\mathbf{r}}_B \end{pmatrix} \quad \text{and} \tag{4.98}$$

$$\sigma = \begin{pmatrix} \sigma_A & \xi_{AB} \\ \xi_{AB}^\top & \sigma_B \end{pmatrix}, \tag{4.99}$$

where $\bar{\mathbf{r}}_A$ and $\bar{\mathbf{r}}_B$ are vectors of $2m$ and $2n$ real numbers, respectively and σ_A, σ_B and ξ_{AB} are matrices of $2m \times 2m$, $2n \times 2n$ and $2m \times 2n$ real numbers, respectively. Moreover, the reduced state $\rho_A = \mathrm{Tr}_B(\rho_{AB})$ will also be a Gaussian state with its first moments given by $\bar{\mathbf{r}}_A$ and covariance matrix σ_A, completely describing the subsystem A. Analogously, the reduced state $\rho_B = \mathrm{Tr}_A(\rho_{AB})$ will also be a Gaussian state with first moments $\bar{\mathbf{r}}_B$ and covariance matrix σ_B.

The above affirmation can be proved as follows. Suppose we know the statistical moments of AB ($\bar{\mathbf{r}}$ and σ). Then, from the characteristic function of a Gaussian state (Eq. (4.85)), we have

$$\rho_{AB} = \frac{1}{(2\pi)^{m+n}} \int_{\mathbb{R}^{2(m+n)}} d\mathbf{r} e^{-\frac{1}{4}\mathbf{r}^\top \Omega^\top \sigma \Omega \mathbf{r} + i\mathbf{r}^\top \Omega \bar{\mathbf{r}}} \hat{D}_{\mathbf{r}}.$$

If we parametrize $\mathbf{r} = \mathbf{r}_A \oplus \mathbf{r}_B$ where $\mathbf{r}_A$ and $\mathbf{r}_B$ are $2m$ and $2n$ real vectors, respectively, then

$$\rho_{AB} = \frac{1}{(2\pi)^{m+n}} \int_{\mathbb{R}^{2m}} d\mathbf{r}_A \int_{\mathbb{R}^{2n}} d\mathbf{r}_B e^{-\frac{1}{4}(\mathbf{r}_A \oplus \mathbf{r}_B)^\top \Omega^\top \sigma \Omega (\mathbf{r}_A \oplus \mathbf{r}_B) + i(\mathbf{r}_A \oplus \mathbf{r}_B)^\top \Omega (\bar{\mathbf{r}}_A \oplus \bar{\mathbf{r}}_B)} \hat{D}_{\mathbf{r}_A} \otimes \hat{D}_{\mathbf{r}_B},$$

where we used Eq. (4.98) and that $\hat{D}_{\mathbf{r}} = \hat{D}_{\mathbf{r}_A \oplus \mathbf{r}_B} = \hat{D}_{\mathbf{r}_A} \otimes \hat{D}_{\mathbf{r}_B}$, from the definition of the Weyl operator (Eq. (4.22)). Computing the reduced state $\rho_A = \mathrm{Tr}_B(\rho_{AB})$ and

remembering that the partial trace Tr_B acts only on the operators that belong to the Hilbert space of B (thus all the exponential term and $\hat{D}_{\mathbf{r}_A}$ of the equation above remain unaffected by the trace) we obtain

$$\mathrm{Tr}_B\left(\rho_{AB}\right) = \\ \frac{1}{(2\pi)^{m+n}} \int_{\mathbb{R}^{2m}} d\mathbf{r}_A \int_{\mathbb{R}^{2n}} d\mathbf{r}_B e^{-\frac{1}{4}(\mathbf{r}_A\oplus\mathbf{r}_B)^\top\Omega^\top\sigma\Omega(\mathbf{r}_A\oplus\mathbf{r}_B)+i(\mathbf{r}_A\oplus\mathbf{r}_B)^\top\Omega(\bar{\mathbf{r}}_A\oplus\bar{\mathbf{r}}_B)}\hat{D}_{\mathbf{r}_A}\otimes\mathrm{Tr}_B\left(\hat{D}_{\mathbf{r}_B}\right). \tag{4.100}$$

From the orthogonality relation of Eq. (4.39), if we choose $\mathbf{s} = 0$ and use that $\hat{D}_0 = 1$, we obtain

$$\mathrm{Tr}\left(\hat{D}_{\mathbf{r}}\right) = (2\pi)^n\delta^{2n}(\mathbf{r}).$$

Applying the above equation in Eq. (4.100) results in

$$\mathrm{Tr}_B\left(\rho_{AB}\right) = \frac{1}{(2\pi)^m}\int_{\mathbb{R}^{2m}} d\mathbf{r}_A e^{-\frac{1}{4}(\mathbf{r}_A\oplus\mathbf{r}_B)^\top\Omega^\top\sigma\Omega(\mathbf{r}_A\oplus\mathbf{r}_B)+i(\mathbf{r}_A\oplus\mathbf{r}_B)^\top\Omega(\bar{\mathbf{r}}_A\oplus\bar{\mathbf{r}}_B)}\Big|_{\mathbf{r}_B=0}\hat{D}_{\mathbf{r}_A}. \tag{4.101}$$

Computing explicitly the exponential components

$$(\mathbf{r}_A\oplus\mathbf{r}_B)^\top\Omega^\top\sigma\Omega(\mathbf{r}_A\oplus\mathbf{r}_B) = \begin{pmatrix}\mathbf{r}_A^\top & \mathbf{r}_B^\top\end{pmatrix}\begin{pmatrix}\Omega_{m\times m}^\top & 0\\ 0 & \Omega_{n\times n}\end{pmatrix}\begin{pmatrix}\sigma_A & \sigma_{AB}\\ \sigma_{AB}^\top & \sigma_B\end{pmatrix}\begin{pmatrix}\Omega_{m\times m} & 0\\ 0 & \Omega_{n\times n}\end{pmatrix}\begin{pmatrix}\mathbf{r}_A\\ \mathbf{r}_B\end{pmatrix}$$
$$= \mathbf{r}_A^\top\Omega^\top\sigma_A\Omega\mathbf{r}_A + \mathbf{r}_B^\top\Omega^\top\sigma_{AB}\Omega\mathbf{r}_A + \mathbf{r}_A^\top\Omega^\top\sigma_{AB}\Omega\mathbf{r}_B + \mathbf{r}_B^\top\Omega^\top\sigma_B\Omega\mathbf{r}_B,$$

where again we stated that Ω has dimensions according to the vector in which it acts. Similarly, we have

$$\mathbf{r}^\top\Omega^\top\bar{\mathbf{r}} = \mathbf{r}_A^\top\Omega^\top\bar{\mathbf{r}}_A + \mathbf{r}_B^\top\Omega^\top\bar{\mathbf{r}}_B.$$

Consequently, the equations above imply

$$e^{-\frac{1}{4}(\mathbf{r}_A\oplus\mathbf{r}_B)^\top\Omega^\top\sigma\Omega(\mathbf{r}_A\oplus\mathbf{r}_B)+i(\mathbf{r}_A\oplus\mathbf{r}_B)^\top\Omega(\bar{\mathbf{r}}_A\oplus\bar{\mathbf{r}}_B)}\Big|_{\mathbf{r}_B=0} = e^{-\frac{1}{4}\mathbf{r}_A^\top\Omega^\top\sigma_A\Omega\mathbf{r}_A+i\mathbf{r}_A^\top\Omega\bar{\mathbf{r}}_A},$$

and using this equation in Eq. (4.101), we finally obtain

$$\mathrm{Tr}_B\left(\rho_{AB}\right) = \frac{1}{(2\pi)^m}\int_{\mathbb{R}^{2m}} d\mathbf{r}_A e^{-\frac{1}{4}\mathbf{r}_A^\top \Omega^\top \sigma_A \Omega \mathbf{r}_A + i\mathbf{r}_A^\top \Omega \bar{\mathbf{r}}_A}\hat{D}_{\mathbf{r}_A}. \tag{4.102}$$

This proves that the reduced state ρ_A is a Gaussian state completely described by the first moments $\bar{\mathbf{r}}_A$ and covariance matrix σ_A, since its characteristic function has the form of a Gaussian one (Eq. (4.85)) with the desired parameters. The proof is analogous for the reduced system ρ_B.

4.7.4 Gaussian CPTP-maps

We have completed the proof that all operations we shall use in our Stinespring dilation are Gaussian operators. Now we present the form of Gaussian CPTP-maps that the Stinespring dilation creates.

Suppose we have a Gaussian system of n bosonic modes initially at a state with first moments vector $\bar{\mathbf{r}}_S$ and covariace matrix σ_S. Similarly, initially we have a Gaussian environment of m bosonic modes with first moments $\bar{\mathbf{r}}_E$ and covariance matrix σ_E. If the initial system-environment joint state is uncorrelated they are described by a tensor product. Hence, from Eqs. (4.92) and (4.93), we have

$$\bar{\mathbf{r}}_{SE} = \bar{\mathbf{r}}_S \oplus \bar{\mathbf{r}}_E \;\text{ and }\; \sigma_{SE} = \sigma_S \oplus \sigma_E, \tag{4.103}$$

where $\bar{\mathbf{r}}_{SE}$ is the first moment vector of the initial joint state and σ_{SE} is the covariance matrix of the initial joint state.

Let the unitary evolution of the joint system be given by the symplectic matrix

$$S = \begin{pmatrix} A & B \\ C & D \end{pmatrix}, \tag{4.104}$$

where A is a $2n \times 2n$ real matrix, B is a $2n \times 2m$ real matrix, C is a $2m \times 2n$ real matrix

and D is a $2m \times 2m$ real matrix. Then, from Eqs. (4.96) and (4.97), we have

$$\bar{\mathbf{r}}'_{SE} = \begin{pmatrix} A\bar{\mathbf{r}}_S + B\bar{\mathbf{r}}_E \\ C\bar{\mathbf{r}}_S + D\bar{\mathbf{r}}_E \end{pmatrix}, \tag{4.105}$$

for the evolved first moments $\bar{\mathbf{r}}'_{SE}$. And

$$\sigma'_{SE} = \begin{pmatrix} A\sigma_S A^\top + B\sigma_E B^\top & A\sigma_S C^\top + B\sigma_E D^\top \\ C\sigma_S A^\top + D\sigma_E B^\top & C\sigma_S C^\top + D\sigma_E D^\top \end{pmatrix}, \tag{4.106}$$

for the evolved covariance matrix σ'_{SE}.

Finally, from taking the partial trace of the environment (see Subsection 4.7.3), we obtain

$$\bar{\mathbf{r}}'_S = A\bar{\mathbf{r}}_S + B\bar{\mathbf{r}}_E, \tag{4.107}$$

for the evolved first moments. And

$$\sigma'_S = A\sigma_S A^\top + B\sigma_E B^\top, \tag{4.108}$$

for the evolved covariance matrix.

If we define the $2n \times 2n$ real matrices $X = A$ and $Y = \sigma_E B^\top$ and the $2n$ vector $\mathbf{d} = B\bar{\mathbf{r}}_B$, we conclude that the following evolution

$$\boxed{\begin{aligned} &\bar{\mathbf{r}}_S \mapsto X\bar{\mathbf{r}}_S + \mathbf{d} \ \text{ and} && (4.109)\\ &\sigma_S \mapsto X\sigma_S X^\top + Y, \ \text{ with} && (4.110)\\ &Y + i\Omega \geq iX\Omega X^\top, && (4.111) \end{aligned}}$$

can represent any Gaussian CPTP-maps of a system n bosonic modes. The condition of Eq. (4.111) assures that the covariance matrices still satisfy the bona-fide condition. The necessity of this condition can be shown by demanding the Eq. (4.63) condition to the evolved covariance matrix of Eq. (4.110) and using the constrains on X and Y due to the fact that the matrix S (of Eq. (4.104)) is symplectic.

Conversely to the result above, one can show (see, for instance, Chapter 5 of Ref.

[14]) that any matrices X and Y satisfying Eq. (4.111) can represent a Stinespring dilation which acts on the system via the transformations of Eqs. (4.109) and (4.110). Furthermore, one can always consider the environment as a $2n$-modes state initially at the vacuum ($\sigma_E = \mathbb{I}/2$) to construct such Stinespring dilation (for this case, the quantum channel will have $\mathbf{d} = 0$).

The Stinespring dilation in bosonic modes will be the approach used in Chapter 6 to obtain the analytical results for the collisional model with initially correlated ancillae.

4.7.5 Applying a channel in only one partition

An useful result for further use is the following. Suppose that we have a Gaussian system with two parties A, with n modes, vector of first moments $\bar{\mathbf{r}}_A$ and covariance matrix σ_A, and B, with m modes, vector of first moments $\bar{\mathbf{r}}_B$ and covariance matrix σ_B. Now, suppose we have a quantum channel acting only in A given by Eqs. (4.109), (**??**) and (4.111) with the respective vector $\mathbf{d}$ and matrices X and Y (simultaneously, the identity operation acts in B). Then the global resulting map will be

$$\begin{pmatrix} \bar{\mathbf{r}}_A \\ \bar{\mathbf{r}}_B \end{pmatrix} \mapsto \begin{pmatrix} X\bar{\mathbf{r}}_A + \mathbf{d} \\ \bar{\mathbf{r}}_B \end{pmatrix} \quad \text{and} \tag{4.112}$$

$$\begin{pmatrix} \sigma_A & \xi \\ \xi^\top & \sigma_B \end{pmatrix} \mapsto \begin{pmatrix} X\sigma_A X^\top + Y & X\xi \\ \xi^\top X^\top & \sigma_B \end{pmatrix}. \tag{4.113}$$

The proof of this result can be found in Chapter 5 of Ref. [14].

4.7.6 One-mode Gaussian channels

As an important example of Gaussian channels, we present the classes of all possible Gaussian quantum channels acting in one-mode states. Any Gaussian quantum channel for one-mode bosonic systems can be described by a vector $\bar{\mathbf{d}} \in \mathbb{R}^2$ and 2×2 real matrices $\mathbf{T}$ (called *transmission matrix*) and $\mathbf{N}$ (called *noise matrix*) playing the role of X and Y, respectively, in Eqs. (4.109) and (4.110). Accordingly, the condition of Eq. (4.111) will

result in the conditions

$$\mathbf{N} = \mathbf{N}^{\top} \geq 0 \quad \text{and} \quad \det \mathbf{N} \geq (\det \mathbf{T} - 1)^2. \tag{4.114}$$

In Ref. [126], it was shown that the general structure of such transformations can be reduced to a simple set of classes of matrices $\mathbf{T}$ and $\mathbf{N}$ together with displacement operations to generate $\mathbf{d}$. The classes are the following

- Class A_1: $\mathbf{T} = 0$ and $\mathbf{N} = (\bar{n}+1/2)\mathbb{I}_2$, for $\bar{n} \geq 0$. This means that the state is turned completely into a thermal state, thus the channel is called *completely depolarizing channel*;

- Class A_2: $\mathbf{T} = \text{diag}(1, 0)$ and $\mathbf{N} = (\bar{n} + 1/2)\mathbb{I}_2$. This channel is *phase-sensitive*, i.e., the state's amplification of the second moments depends on the quadrature;

- Class B_1: $\mathbf{T} = \mathbb{I}_2$ and $\mathbf{N} = \text{diag}(0, 1)/2$, for $\bar{n} \geq 0$. This channel is also phase-sensitive;

- Class B_2: $\mathbf{T} = \mathbb{I}_2$ and $\mathbf{N} = \frac{\bar{n}}{2}\mathbb{I}_2$, for $\bar{n} \geq 0$. This is channel just add classical noise to the system, thus called *additive-noise channel*, it encompasses the case of the identity transformation for $\bar{n} = 0$;

- Class C: $\mathbf{T} = \sqrt{\tau}\ \mathbb{I}_2$ where $\tau > 0$ and $\tau \neq 1$. For the case of $0 \leq \tau \leq 1$, $\mathbf{N} = (1 - \tau)(\bar{n} + 1/2)$, for $\bar{n} \geq 0$, this case is called the *lossy channel* (this contemplates the *Beam-Splitter* case to be seen in Chapter 6). For the case of $\tau > 1$, $\mathbf{N} = (\tau - 1)(\bar{n} + 1/2)$, for $\bar{n} \geq 0$, this case is called the *amplifier channel* (this contemplates the *Two-Mode Squeezing* case.[14]

- Class D: $\mathbf{T} = \sqrt{|\tau|}\sigma_z$ for $\tau < 0$ and $\mathbf{N} = (1 + |\tau|)(\bar{n} + 1/2)\mathbb{I}_2$. This channel is also phase-sensitive and it can be seen as the environmental outcome of a two-mode squeezing operation.

This classification will be helpful to the construction of a method for computing the quantum discord in two-mode bosonic states exposed in Subsection 4.8.3. Also, it will be

[14] See Refs. [55, 118, 119] for the definition of the two-mode squeezing operation.

useful (in special the Class D) in the construction of two-mode bosonic locally thermal states that exchange heat in a reversed flow, in Chapter 8.

4.8 Entropic quantities for Gaussian states

Obtaining the entropy and related quantities, such as Mutual Information and Quantum Discord, of Gaussian states will be necessary to quantify correlations between bosonic modes in our second project of the thesis, specially in Chapter 8. Here we present how to compute these quantities. For obtaining the entropy of a Gaussian state, it will be useful to present the following diagonalization.

4.8.1 Diagonalization of Gaussian states to thermal states of free modes

Given a Gaussian state (Eq. (4.58)) with n bosonic modes and a general second order Hamiltonian in the form of Eq. (4.57), we can write the density matrix of the state as

$$\rho_G = \frac{e^{-(\hat{\mathbf{r}}-\bar{\mathbf{r}})^\top M(\hat{\mathbf{r}}-\bar{\mathbf{r}})}}{Z}, \tag{4.115}$$

where $Z = \mathrm{Tr}\left(e^{-(\hat{\mathbf{r}}-\bar{\mathbf{r}})^\top M(\hat{\mathbf{r}}-\bar{\mathbf{r}})}\right)$ and M is a positive definite $2n \times 2n$ matrix. We have, from Williamson's theorem (Eq. (4.83)), that

$$(\hat{\mathbf{r}}-\bar{\mathbf{r}})^\top M(\hat{\mathbf{r}}-\bar{\mathbf{r}}) = (\hat{\mathbf{r}}-\bar{\mathbf{r}})^\top S\mathbf{D}S^\top(\hat{\mathbf{r}}-\bar{\mathbf{r}}), \tag{4.116}$$

where $S \in S_{p_{2n,\mathbb{R}}}$ and $\mathbf{D} = \mathrm{diag}(d_1, d_1, \cdots, d_n, d_n)$ is the diagonal matrix of symplectic eigenvalues. From the fact that the transpose of a symplectic transformation is also symplectic,[15] we have that $\tilde{S} = S^\top$ is symplectic and hence

$$\begin{aligned}(\hat{\mathbf{r}}-\bar{\mathbf{r}})^\top M(\hat{\mathbf{r}}-\bar{\mathbf{r}}) &= (\hat{\mathbf{r}}-\bar{\mathbf{r}})^\top \tilde{S}^\top\mathbf{D}\tilde{S}(\hat{\mathbf{r}}-\bar{\mathbf{r}}) \\ &= \hat{S}^\dagger(\hat{\mathbf{r}}-\bar{\mathbf{r}})^\top \hat{S}\mathbf{D}\hat{S}^\dagger(\hat{\mathbf{r}}-\bar{\mathbf{r}})\hat{S} \\ &= \hat{S}^\dagger\hat{D}^\dagger_{\bar{\mathbf{r}}}\hat{\mathbf{r}}^\top\mathbf{D}\,\hat{\mathbf{r}}\hat{D}_{\bar{\mathbf{r}}}\hat{S},\end{aligned} \tag{4.117}$$

[15] This can be proved by taking the transpose of Eq. (4.81) and using that $\Omega^\top = -\Omega$.

where $\hat{D}_{\bar{\mathbf{r}}}$ is a displacement operator (and we used Eq. (4.23)) and $\hat{S}$ is a unitary such that $\hat{S}^\dagger \hat{\mathbf{r}} \hat{S} = \tilde{S}\hat{\mathbf{r}}$.[16] Finally, using the relation above in Eq. (4.115), we obtain

$$\boxed{\rho_G = \hat{S}^\dagger \hat{D}^\dagger_{\bar{\mathbf{r}}} \rho_{\text{free}} \hat{D}_{\bar{\mathbf{r}}} \hat{S},} \tag{4.118}$$

where

$$\rho_{\text{free}} = \frac{e^{-\hat{\mathbf{r}}^\top \mathbf{D}\ \hat{\mathbf{r}}}}{Z} \tag{4.119}$$

is a thermal state of n non-interacting modes with energies given by the symplectic eigenvalues of M. The density matrix of thermal n free bosonic modes is obtained in Appendix C (Eq. (C.33)). Explicitly, we have

$$\rho_{\text{free}} = \bigotimes_{j=1}^{n} \rho_{\text{free}_j}, \quad \text{with} \tag{4.120}$$

$$\rho_{\text{free}_j} = \frac{1}{\nu_j + 1/2} \sum_{n_j=0}^{\infty} \left(\frac{\nu_j - 1/2}{\nu_j + 1/2} \right)^{n_j} |n_j\rangle \langle n_j| , \tag{4.121}$$

where ν_j are the symplectic eigenvalues for the covariance matrix of the state ρ_G.[17]

4.8.2 Entropy of a Gaussian state

From Eq. (4.118) we observe that any Gaussian state can be described as a unitary transformation of a thermal state of free modes. Since the von Neumann Entropy is invariant under unitary transformations, we conclude

$$S(\rho_G) = S(\rho_{\text{free}}). \tag{4.122}$$

[16] This relation is possible since for any $S \in S_{p_{2n,\mathbb{R}}}$, there is a real and symmetric $2n \times 2n$ matrix H such that $H = \Omega^\top \log S$ and $\hat{S}^\dagger \hat{\mathbf{r}} \hat{S} = S\hat{\mathbf{r}}$, where $\hat{S} = e^{-i\frac{1}{2}\hat{\mathbf{r}}^\top H \hat{\mathbf{r}}}$ (see Appendix C, Section C.15, for the proof).

[17] A consequence of the parametrization of Eq. (4.82) is that the elements of the covariance matrix of the state ρ_{free} are the symplectic eigenvalues of the covariance matrix of ρ_G.

Using Eq. (4.120) we obtain[18]

$$S(\rho_G) = \sum_{j=1}^{n} S(\rho_{\text{free}_j}). \tag{4.123}$$

Finally, using Eq. (4.121), we have (see Appendix C, Section C.19, for a proof)

$$\boxed{S(\rho_G) = \sum_{j=1}^{n} g(\nu_j),} \tag{4.124}$$

where ν_j are the sympletic eigenvalues of the covariance matrix of ρ_G and

$$\boxed{g(x) = (x + 1/2)\log(x + 1/2) - (x - 1/2)\log(x - 1/2).} \tag{4.125}$$

4.8.3 Quantum discord between two Gaussian bosonic modes

With the formulae of Eqs. (4.124) and (4.125), it is possible to compute the entropy of any Gaussian state given its covariance matrix. Consequently, we can use this formula also to compute any entropy dependent quantity. Among these quantities is the Mutual Information, which is a quantifier of *total* correlations and can be computed with the use of Eq. (3.20). However, to compute a quantifier of *quantum* correlations for Gaussian states is a hard task [107, 127]. Therefore, in this section we only focus on the computation of Quantum Discord between two Gaussian bosonic modes, which will be used in Chapter 8, for the second project of this thesis.

There is no closed formula to compute the Quantum Discord between two Gaussian bosonic modes. Notwithstanding, in Ref. [128] it was obtained a closed formula for computing this quantity for a very rich and useful set of states. Here we present the main results of this paper. The main proofs of this Section are contained in the Supplemental Material of Ref. [128], which is a highly self contained and pedagogical text, so we make reference to this text when needed and to our proofs in Appendix C when we deem necessary.

[18] Here we used that $S(\bigotimes_n \rho_n) = \sum_n S(\rho_n)$. This is a consequence of the fact that $S(\rho_A \otimes \rho_B) = S(\rho_A) + S(\rho_B)$. Indeed $S(\rho_A \otimes \rho_B) = -\operatorname{Tr}((\rho_A \otimes \rho_B)\log(\rho_A \otimes \rho_B)) = -\operatorname{Tr}((\rho_A \otimes \rho_B)\log(\rho_A)) - \operatorname{Tr}((\rho_A \otimes \rho_B)\log(\rho_B)) = -\operatorname{Tr}_A(\rho_A \log(\rho_A)) - \operatorname{Tr}_B(\rho_B \log(\rho_B)) = S(\rho_A) + S(\rho_B)$.

First, we make a useful definition. It can be shown (see Appendix C, Section C.20) that any covariance matrix for a Gaussian state of two-modes can be transformed into the following form by means of single-mode symplectic transformations

$$\boxed{\sigma_S = \begin{pmatrix} a & 0 & c_+ & 0 \\ 0 & a & 0 & c_- \\ c_+ & 0 & b & 0 \\ 0 & c_- & 0 & b \end{pmatrix}}, \tag{4.126}$$

for a and b positive real numbers and c_+ and c_- are real numbers constrained so that the covariance matrix is bona-fide. This form is named *Simon normal form*. The normal form facilitates our treatment since each covariance matrix in a normal form represents a class of states which have the same amount of quantum correlations between the two parties (because each of these states can be transformed into another by successive local symplectic transformations, which represents local unitary transformations).

In order to make a clearer explanation for the method of Ref. [128] for obtaining the quantum discord between two bosonic modes, we start by showing how to compute the quantum discord for the *Two-mode squeezed thermal state (TMST)*. This state is represented by the following covariance matrix

$$\sigma_{\text{tmst}} = \begin{pmatrix} a & 0 & c & 0 \\ 0 & a & 0 & -c \\ c & 0 & b & 0 \\ 0 & -c & 0 & b \end{pmatrix}, \tag{4.127}$$

for positive a, b and c and null first moment (see Appendix **??** for a more detailed definition). Notice that the TMST's covariance matrix is simply the Simon normal form with opposite correlations terms c_+ and c_-.

The method can be described in two steps. First step: **state decomposition**. We construct our target Gaussian state ρ_{AB} (in this case, the TMST), made of two parties A and B (each being single-modes), as an application of a local quantum channel $\mathcal{E}$ in A of

an initial Gaussian state ρ_{aB}, i.e.,

$$\rho_{AB} = (\mathcal{E}_A \otimes \mathcal{I}_B)(\rho_{aB}), \tag{4.128}$$

where $\mathcal{I}$ represents the identity channel.

We chose the quantum channel $\mathcal{E}$ to be a *phase-insensitive Gaussian channel*, these are the classes A_1, B_2 and C described in Subsection 4.7.6. Given an input covariance matrix σ_{in} of the state, it will transform as

$$\sigma_{\text{in}} \to (\mathbf{T} \oplus \mathbb{I}_2)\sigma_{\text{in}}(\mathbf{T}^\top \oplus \mathbb{I}_2) + (\mathbf{N} \oplus \mathbf{0}), \tag{4.129}$$

where $\mathbf{T} = \sqrt{\tau}\,\mathbb{I}_2$, with $\tau \geq 0$ and $\mathbf{N} = \eta\mathbb{I}_2$, with $\eta \geq |1-\tau|$.

We also chose ρ_{aB} to be the *Einstein-Podolsky-Rosen* (EPR) state, which has null first moment, and has the following covariance matrix

$$\sigma_{aB} = \begin{pmatrix} \beta\mathbb{I}_2 & \sqrt{\beta^2-1}\mathbf{C} \\ \sqrt{\beta^2-1}\mathbf{C} & \beta\mathbb{I}_2 \end{pmatrix}, \tag{4.130}$$

where $\mathbf{C} = \text{sign}(c_+)\sigma_z$ and $\beta > 0$ (β here is not playing the role of the inverse of temperature). These choices ensure that the state decomposition of Eq. (4.128) correctly results in a TMST state parametrized as (see Suplemental Material of Ref. [128] for the proof)

$$\sigma_{AB} = \begin{pmatrix} (\tau\beta+\eta)\mathbb{I}_2 & \sqrt{\tau(\beta^2-1)}\mathbf{C} \\ \sqrt{\tau(\beta^2-1)}\mathbf{C} & \beta\mathbb{I}_2 \end{pmatrix}, \tag{4.131}$$

where $\tau \geq 0$ and $\eta \geq |1-\tau|$ are parameters of the phase-insensitive Gaussian channel.

Second: **remote preparation**. We make a local generalized measurement $\mathcal{M}_B = \{M_k\}_k$ in B. The application of such measurement in ρ_{aB} causes an ensemble $\mathcal{P} = \{p_k, \rho_{a|k}\}_k$ as its backaction in A. The resulting ensemble of applying the local generalized measurement $\mathcal{M}_B$ in ρ_{AB} is $\mathcal{A} = \{p_k, \rho_{a'|k}\}_k$, with

$$\rho_{a'|k} = \mathcal{E}(\rho_{a|k}), \tag{4.132}$$

as a consequence of Eq. (4.128) (see Fig. 4.1).

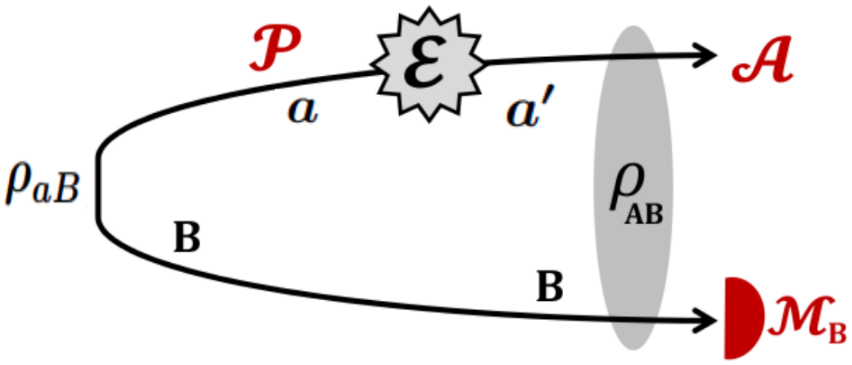

Figure 4.1: *State decomposition*: Depicted in black lines, the state ρ_{AB} can be decomposed as an initial state ρ_{aB} in which the first mode (in part A) passes trough a quantum channel $\mathcal{E}$. *Remote preparation* : Depicted in red symbols, the effect of the generalized measurement $\mathcal{M}_B$ in ρ_{aB} creates the ensemble $\mathcal{P} = \{p_k, \rho_{a|k}\}_k$ of states in A which, passing through the quantum channel, becomes the ensemble $\mathcal{A} = \{p_k, \rho_{a'|k}\}_k$. The ensemble $\mathcal{A}$ is also generated by the backaction, in A, of the generalized measurement $\mathcal{M}_B$ in ρ_{AB}. (This figure was taken from Ref. [128] with modifications.)

If we chose $\mathcal{M}_B = \text{het}_B$ to be an heterodyne measurement, the backaction of the state ρ_{aB} in A will result in an ensemble of coherent states $\mathcal{P} = \{Q(\alpha), \rho_{a|\alpha} = |\alpha\rangle\langle\alpha|\}_\alpha$, where $|\alpha\rangle$ are coherent states and $Q(\alpha)$ is the Husimi Q-function (see Supplemental Material of Ref. [128] for the proof of this statement). These coherent states are the inputs of the phase-insensitive Gaussian channel $\mathcal{E}$. Consequently, from Eq. (4.128) and from the definition of the quantum-classical conditional entropy (Eq. (3.31)), we obtain

$$\begin{aligned} S_{\text{het}_B}(A|B) &= \int_{\mathbb{C}} d^2\alpha\, Q(\alpha) S(\mathcal{E}(|\alpha\rangle\langle\alpha|)) \\ &= S(\mathcal{E}(|0\rangle\langle 0|)). \end{aligned} \tag{4.133}$$

The second equality of the equation above comes from the normalization of the Husimi Q-function and from the fact that $S(\mathcal{E}(|\alpha\rangle\langle\alpha|)) = S(\mathcal{E}(|0\rangle\langle 0|))$ for any coherent state $|\alpha\rangle$ (this statement is proved in Appendix C, Sec. C.21).

For computing the quantum discord, we must find the generalized measurement which minimizes the quantum-classical conditional entropy (Eq. (3.31)). In order to find this minimum, we use the seminal result of Refs. [129, 130], which states that the vacuum (or any translation of it, i.e., coherent states) minimizes the output entropy of a phase-

insensitive Gaussian channel $\mathcal{E}$ among all possible states, i.e.,

$$S\left[\mathcal{E}(|0\rangle\langle 0|)\right] = \inf_{\rho} S\left[\mathcal{E}(\rho)\right]. \tag{4.134}$$

From this result, we conclude that the heterodyne measurement is a strong candidate to minimize the quantum-classical conditional entropy. Indeed, Eqs. (4.133) and (4.134) imply

$$S_{\text{het}_B}(A|B) = \inf_{\rho} S[\mathcal{E}(\rho)]. \tag{4.135}$$

To complete the proof that $S_{\text{het}_B}(A|B)$ is the smaller quantum-classical conditional entropy, notice that, for any set $\{M_k\}_k$ of generalized measurements

$$\begin{aligned} S_M(A|B) &= \sum_k p_k S(\rho_{a'|k}) \\ &\geq \inf_{\mathcal{A}} S(\rho_{a'|k}) \\ &= \inf_{\mathcal{P}} S[\mathcal{E}(\rho_{a|k})] \\ &\geq \inf_{\rho} S(\mathcal{E}(\rho)), \end{aligned} \tag{4.136}$$

where the first equality above comes from the definition of Eq. (3.31), the first inequality says that the average is greater or equal to the infimum of $\mathcal{A}$, the second equality comes from Eq. (4.132) and the last inequality comes from the fact that $\mathcal{P}$ is contained in the set of all possible one-mode density matrices.

From the equation above and Eq. (4.135), we conclude that

$$S_M(A|B) \geq S_{\text{het}_B}(A|B), \tag{4.137}$$

for every generalized measurement $\{M_k\}_k$, implying that $S_{\text{het}_B}(A|B)$ is the minimum of the possible quantum-classical conditional entropy. Therefore, we have a closed formula for the quantum discord. From Eqs. (3.20) (3.32), (3.33) and (3.34), we have

$$\begin{aligned} \mathcal{D}(A|B) &= S(\rho_{AB}) + \min_{\{M_k^B\}_k} S_M(A|B) - S(\rho_B) \\ &= S(\rho_{AB}) + S(\mathcal{E}(|0\rangle\langle 0|)) - S(\rho_B), \end{aligned} \tag{4.138}$$

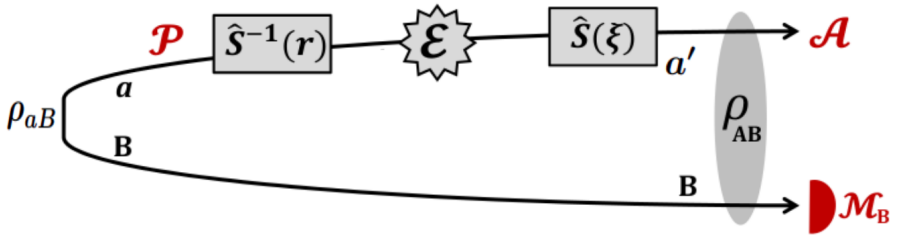

Figure 4.2: *State decomposition*: Depicted in black lines, the state ρ_{AB} can be decomposed as an initial state ρ_{aB} in which the first mode (in part A) passes trough an inverse squeezing operator $\hat{S}^{-1}(r)$, a quantum channel $\mathcal{E}$ and a sequeezing operator $\hat{S}(\xi)$. *Remote preparation* : Depicted in red symbols, the effect of the generalized measurement $\mathcal{M}_B$ in ρ_{aB} creates the ensemble $\mathcal{P} = \{p_k, \rho_{a|k}\}_k$ of states in A which, passing through the quantum channel and squeezing operators, becomes the ensemble $\mathcal{A} = \{p_k, \rho_{a'|k}\}_k$. The ensemble $\mathcal{A}$ is also generated by the backaction, in A, of the generalized measurement $\mathcal{M}_B$ in ρ_{AB}. (This figure was taken from Ref. [128] with modifications.)

where in the second equality we used Eqs. (4.133) and (4.137). Computing explicitly the entropies (see Appendix C, Section C.22), we have finally obtain

$$\boxed{\mathcal{D}(A|B) = g(\beta) - g(\nu_-) - g(\nu_+) + g\left(\frac{\tau+\eta}{2}\right),} \tag{4.139}$$

where ν_- and ν_+ are the symplectic eigenvalues of the TMST covariance matrix σ_{AB} (Eq. (4.131)) and $g(\bullet)$ is defined according to Eq. (4.125).

At this point, we can generalize the method described for computing the quantum discord of a TMST state in order to extend it to a larger set of correlated two-mode states. The two steps in the previous case will be modified as follows.

First step: **state decomposition**. In this case, we intend to construct a target Gaussian state ρ_{AB} in the Simon normal form (Eq. (4.126)). We first extend our phase-insensitive Gaussian channel $\mathcal{E}$ to include phase-sensitive channels with negative transmissivities, i.e., we can also have $\tau \leq 0$, this is the case D described in Subsection 4.7.6. Then, supposing again the initial state ρ_{aB} as being the EPR state, with covariance matrix given by Eq. (4.130), we generate our state ρ_{AB} by the following operation

$$\rho_{AB} = ((\mathcal{S}_\xi \mathcal{E} \mathcal{S}_r^{-1})_A \otimes \mathcal{I}_B)(\rho_{aB}), \tag{4.140}$$

where $\mathcal{S}_x(\rho) = \hat{S}(x)\rho\hat{S}^\dagger(x)$ is the unitary one-mode *squeezing operation* and $\hat{S}(x)$ is

the *squeezing operator* with $r \in [\beta^{-1}, \beta]$ and $\xi = r\frac{\sqrt{\eta r^{-1}+|\tau|\beta}}{\sqrt{\eta r+|\tau|\beta}}$.[19] The necessity of the additional squeezing operations in the decomposition made above and the choices of r and ξ will be explained in the next step. As consequence of Eq. (4.140), the state ρ_{AB} will have a covariance matrix σ_{AB} given in the Simon normal form (Eq. (4.126)), with the following parametrization

$$a = \theta(r)\theta(r^{-1}),\ \theta(r) = \sqrt{\eta r + |\tau|\beta}, \tag{4.141}$$

$$b = \beta, \tag{4.142}$$

$$c_+ = \pm\sqrt{|\tau|(\beta^2-1)\theta(r^{-1})/\theta(r)}, \tag{4.143}$$

$$c_- = \mp \text{sign}[\tau]\sqrt{|\tau|(\beta^2-1)\theta(r)/\theta(r^{-1})}, \tag{4.144}$$

where $\tau \in \mathbb{R}$, $\eta \geq |1-\tau|$, $r \in [\beta^{-1}, \beta]$ and the ambiguity in the sign of Eqs. (4.143) and (4.144) comes from the ambiguity of $\mathbf{C} = \text{sign}(\sigma_+)\sigma_z$.[20]

Second step: **remote preparation**. In this case we chose to make the local generalized measurement $\mathcal{M}_B$ in B such that $\{M_\alpha(u) = |\alpha, u\rangle\langle\alpha, u|\}_\alpha$, where $|\alpha, u\rangle = \hat{S}(u)|\alpha\rangle$ being $|\alpha\rangle$ a coherent state and $\hat{S}(u)$ the squeezing operator for $u > 0$. The backaction of this measurement in B will result in an ensemble $\mathcal{P} = \{p_\alpha, \rho_{a|\alpha}\}_\alpha$ in A such that the covariance matrix of the states $\rho_{a|\alpha}$ will be $\sigma_{a|\alpha} = \text{diag}(r^{-1}, r)$, where $r = (1+u\beta)(u+\beta)^{-1}$ (the proof of this affirmation can be found in the Supplemental Material of Ref. [128]). Moreover, we wish to turn these states into coherent states, so we apply the inverse squeezing unitary channel $\mathcal{S}_r^{-1}$. This enables us to use again the result of Refs. [129, 130] (Eq. (4.134)),[21] from which we conclude that

$$\begin{aligned}\inf_\rho S(\mathcal{E}(\rho)) &= S(\mathcal{E}(\mathcal{S}_r^{-1}(\rho_{a|\alpha}))) \\ &= S(\mathcal{E}(|0\rangle\langle 0|)),\end{aligned} \tag{4.145}$$

for every $\rho_{a|\alpha} \in \mathcal{P}$, since all $\mathcal{S}_r^{-1}(\rho_{a|\alpha})$ are coherent states.

[19] The action of the squeezing operation in Gaussian states is described by the symplectic matrix $S(x) = \begin{pmatrix} x^{1/2} & 0 \\ 0 & x^{-1/2} \end{pmatrix}$, for $x > 0$.

[20] The proof of the parametrization above can be found in details in the Supplemental Material of Ref. [128].

[21] Which is also valid for our extended phase-insensitive Gaussian channel $\mathcal{E}$ (for all $\eta \in \mathbb{R}$).

Proceeding in analogy with the argument of the TMST state, we conclude that the quantum discord of the state $((\mathcal{E}\mathcal{S}_r^{-1})_A \otimes \mathcal{I}_B)(\rho_{aB})$ is also given by Eq. (4.139). Finally, to turn the state into the Simon normal form, we apply the squeezing operation $\mathcal{S}_\xi$ in A, with $\xi = \frac{\sqrt{\eta r^{-1}+|\tau|\beta}}{\sqrt{\eta r+|\tau|\beta}}$, and we obtain the parametrization of Eqs. (4.141), (4.142), (4.143) and (4.144). The operation $\mathcal{S}_\xi$ is unitary and local in A, hence it does not interfere in any entropic quantity.

This method (see Fig. 4.2) gives the exact quantum discord between two modes for a large set of states in the Simon normal form. Such set generated by the parametrization of Eqs. (4.141), (4.142), (4.143) and (4.144) cannot range all possible bona-fide states in the Simon normal form, but encompasses a considerable amount of them. This can be seen in the plots of Fig. 4.3, where we randomly picked 2×10^5 values of τ and r having fixed different values of a and b.[22] The plots expose visually the range that can be accessible by the parametrization inside the region of possibles c_+ and c_- delimited by the bona-fide conditions. It also indicates the inability of such parametrization to achieve states with c_+ and c_- near to 0. For larger values of a and b, it can be seen that the parametrization is more capable to fill the region inside the bona-fide allowed states and can generate more points near to $c_+ = 0$ and $c_- = 0$. Although the regions exactly at $c_+ = 0$ and $c_- = 0$ are never accessible, this will not compromise our use of this method in Chapter 8.

[22] With a and b fixed, we choose randomly $r \in [b^{-1}, b]$. As a consequence of Eqs. (4.141), (4.142), (4.143) and (4.144), we will have $\eta = \frac{\sqrt{4a^2r^2+(r^2-1)\tau^2b^2}-(1+r^2)|\tau|b}{2r}$ defined in terms of a, b and r and τ will be restricted to $\tau \in [\tau_{\text{min}}, \tau_{\text{max}}]$, where $\tau_{\text{min}} = \frac{b+(br+2)r-\sqrt{(r^2-1)^2b^2+4a^2r(r+b)(rb+1)}}{2(r+b)(rb+1)}$ and $\tau_{\text{max}} = \frac{b+(br-2)r-\sqrt{(r^2-1)^2b^2-4a^2r(r-b)(rb-1)}}{2(r-b)(rb-1)}$ for $b \geq a$, which is also randomly chosen within this range.

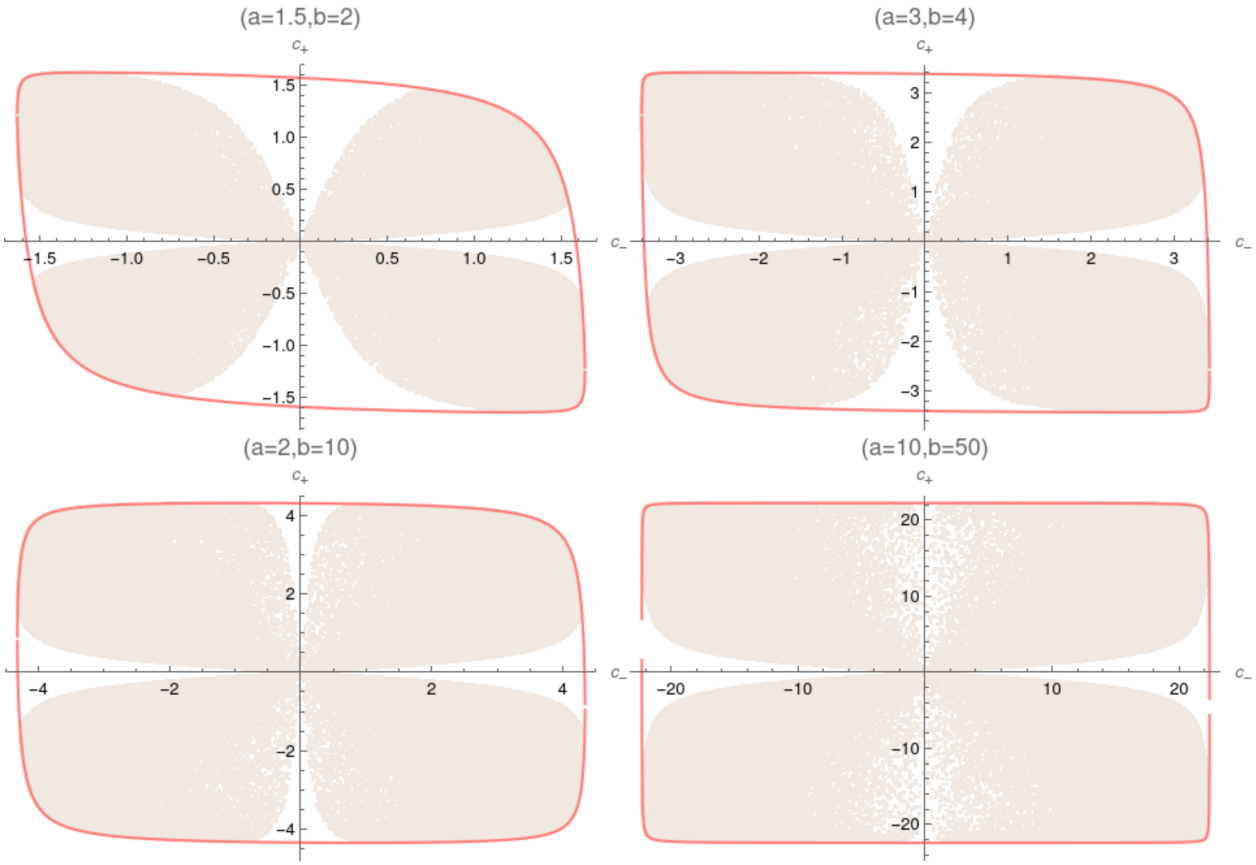

Figure 4.3: Plot of c_+ and c_- points, for different fixed a and b of states in the Simon normal form generated 2×10^5 times by random choices of r and τ, according to the parametrization of Eqs. (4.141), (4.142), (4.143) and (4.144). The pink curves delimit the bona-fide region of states.

Part II

Main projects

Chapter 5

Initially Correlated Ancillae - Minimal Qubit Model CM

As already anticipated in the Introduction and Sec. 2.3.1, our first project of this thesis focuses on dealing with Collisional Models (CMs) with initially correlated ancillae. This is the first Chapter concerning to the first project, and we will explore and obtain results for the evolution of a system interacting with correlated ancillae for the case where all the parties are made of qubits. The results of this Chapter will support the main results of Chapter 6 where we obtain a more complete description for the evolution of the system and ancillae in the case where all the parties are made of bosonic modes.

Initially correlated ancillae in a CM cause the system's evolution (given by Eq. (2.21)) to be described by a non-Markovian map, as already stressed in Subsection 2.3.1. We cannot treat it as a set of successive steps of separated maps, since in the very first interaction of the system with the first ancilla, all the other ancillae may start to be correlated with the system. Clearly, the problem will be much more intractable than the uncorrelated case, and maybe it would be impossible for one to find analytically the system's steady-state, just like it was done for some cases in Chapter 2, for qubits. For this reason, we computed Eq. (2.21) numerically for a (not very large, but sufficient) finite number of collisions in order to observe the effects of the initial ancillae correlations using the Partial SWAP (Eq. (2.44)) as the unitary dynamics of each collision. These results are contrasted with the case where the local ancillae states are the same, but are not correlated between themselves, and definitely show that the presence of correlations steer the system to a different

steady-state.

As it was presented in Sec. 2.3.6, a direct consequence of the fact that all ancillae are locally identical and from the Partial SWAP unitary in each collision, is that we have the following steady-state of the system

$$\rho_S^* = \lim_{n\to\infty} \rho_S^n = \rho_A, \tag{5.1}$$

where ρ_A is the local state of each ancillae. This phenomenon is called Homogenization [18, 19], described in Section 2.3.6, and in this Chapter we prove, for qubits, that the presence of initial correlations between the ancillae can prevent it to happen. Thus we conclude that the steering caused by the correlations can break Homogenization. The interesting point of it is that, as far as a local observer knows, the system is only interacting via a partial SWAP with locally identical parts, but the system is being driven to a different state then the local state of the ancillae. Therefore, the main goal of this Chapter and of Chapter 6 is to prove the presence of such steering.

In order to be able to simulate a setup physically feasible to implement such CM with initially correlated ancillae, we make use of *Hamiltonian graph states* [115, 131–135]. By putting the ancillae to interact with each other via such Hamiltonian, *before* the interaction with the system starts, we prepare an environment of correlated ancillae. This structure will be described as follows.

5.1 Preparing the correlated ancillae environment

5.1.1 Hamiltonian graph states

We want to have a structure that is capable of encompassing as many ancillae as we want, since Homogenization tends to happen for a large number of collisions. Also, we assume that our set of ancillae is translationally invariant. This means that, if $\rho_E = \rho_{A_1A_2\cdots A_n}$ is the environment global state made of all the N_A ancillae, then

$$\rho_{A_kA_{k+1}\cdots A_{k+l-1}} = \mathrm{Tr}_{E/\{k,\cdots,k+l-1\}}\,\rho_E = \rho_{A_1A_2\cdots A_l}, \text{ with } 1 \leq k \leq N_A, \tag{5.2}$$

where the subscript $E/\{k,\cdots,k+l-1\}$ means that all the ancillae but the ones at the set $\{k,\cdots,k+l-1\}$ are traced out.[1] The equation above means that the reduced state of any set of l neighbors ancillae is the same, no matter their position. Clearly this condition implies that the local state of each ancillae must be the same (which corresponds to $l=1$ in Eq. (5.2)).

The condition above can be accomplished if we start with a state of uncorrelated ancillae $|\Phi\rangle = \bigotimes_{k=1}^{N_A} |\phi\rangle$, where the state $|\phi\rangle$ is arbitrary, and then evolve it according to the Hamiltonian

$$H_G = k \sum_{i,j} G_{ij} H_{ij}, \tag{5.3}$$

where k is an interaction strength, G_{ij} are the matrix elements of the adjacency matrix of a graph (to be explained in a moment) and H_{ij} represents a certain Hamiltonian interaction between ancillae i and j. For concreteness, we choose

$$H_{ij} = \sigma_x^i \otimes \sigma_x^j, \tag{5.4}$$

where σ_x stands for the x Pauli matrix.

The adjacency matrix elements of a graph specifies the strength between the connection of each vertex of the graph. For instance, if G_{ij} is the element ij of a adjacency matrix G, its number is a measure of the strength of the connection between the vertex i and j of the graph. In our setup, we suppose that each vertex of the graph represent an ancilla and their edges, as well as the adjacency matrix elements, represent the interaction strength between them.

In general, we don't need to have $G_{ij} = G_{ji}$ which means that the connection between two vertices of a graph does not need to be symmetric. For instance, if the graph represents the traffic flow between two locations, the traffic can be stronger in one way than in the other. But, in our case, we only use symmetric graphs ($G_{ij} = G_{ji}$), this is due to the fact that, since $H_{ij} = H_{ji}$, then the sum of Eq. (5.3) will only affect the symmetric part of G. We also assume that our graph is *cyclic*, i.e., the connection strength between the vertices only depend on their distances, to ensure the translationally invariant character of the ancillae (Eq. (5.2)). This last restriction induces the adjacency matrix to be a *circu-*

[1] If $k+l$ surpass N_A, the sequence continues considering the first $k+l-N_A$ ancillae.

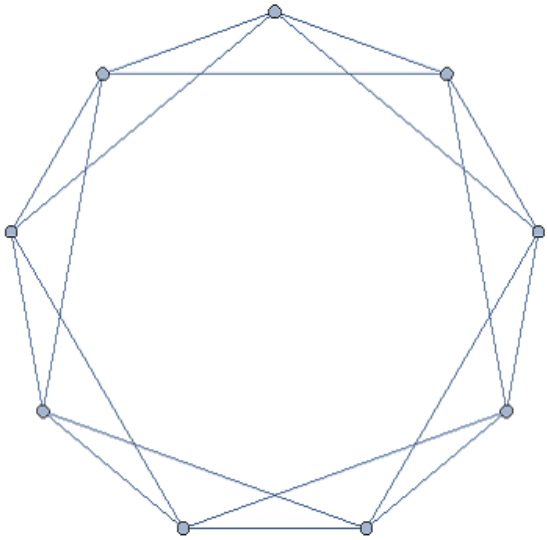

Figure 5.1: Cyclic graph with 9 ancillae (at the vertices), each interacting only with the first and second neighbors (interactions represented by the edges).

lant matrix [136], which means that the G_{ij} elements must depend only on the distance between i and j and we set the diagonal elements to 0. For instance, for $N_A = 5$ we have

$$G = \begin{pmatrix} 0 & c_1 & c_2 & c_3 & c_2 & c_1 \\ c_1 & 0 & c_1 & c_2 & c_3 & c_2 \\ c_2 & c_1 & 0 & c_1 & c_2 & c_3 \\ c_3 & c_2 & c_1 & 0 & c_1 & c_2 \\ c_2 & c_3 & c_2 & c_1 & 0 & c_1 \\ c_1 & c_2 & c_3 & c_2 & c_1 & 0 \end{pmatrix}, \tag{5.5}$$

where c_1, c_2 and c_3 are arbitrary real coefficients. As an example, if we want only first and second neighbors interactions in our graph (see Fig. 5.1), we put $c_j = 0,\ \forall j > 2$.

5.1.2 Properties of the initial ancillae and their correlations

In the previous section we outlined how to prepare the ancillae before the dynamics of the CM starts. Now, we show explicit examples of preparations and the correlations that this process causes between the ancillae.

As already indicated, the whole environment will be described by

$$\rho_E = |\psi_E\rangle \langle\psi_E| , \tag{5.6}$$

where

$$|\psi_E\rangle = e^{-iH_G t} |\phi\rangle , \tag{5.7}$$

and H_G is given by Eq. (5.3), generated by a specific cyclic graph that we choose in each case.

Next, we obtain the values for the density matrices of the reduced state of each individual ancilla, by tracing out the rest of the environment

$$\rho_A = \rho_{A_j} = \mathrm{Tr}_{\{A_2, A_3, \cdots, A_{N_A}\}} (\rho_E) , \ \forall j. \tag{5.8}$$

Additionally, we also compute the values for the joint density matrices for each pair of ancille 1 and j

$$\rho_{A_{1,j}} = \mathrm{Tr}_{E/\{1,j\}} (\rho_E) . \tag{5.9}$$

Finally, we compute the mutual information between the first ancilla and its neighbors,[2] from using Eq. (3.20) and the density matrices from the equations above, in order to measure their total correlations.

These computations are done numerically. We set the interaction time of Eq. (5.7) as $t = 1$, together with the interaction given by Eq. (5.4),[3] choose $|\phi\rangle = |0\rangle$ and obtained the following results.

- We studied the population of the individual ancilla ρ_A (Eq. (5.8)) for cyclic graphs where each ancillae interact only with their first nearest-neighbors (NN1) with equal intensities ($c_1 = 1$), only with their first and second nearest-neighbors (NN2) with equal intensities ($c_1 = c_2 = 1$) and only with their first, second and third nearest-

[2] The mutual information doesn't depend on which pair of ancillae we choose to compute it, but only on the distance between them, as a consequence of our translational invariant condition.

[3] This interaction turns the reduced qubits states ρ_A to be diagonal in the σ_z basis, i.e., a qubit thermal state. And thus it is sufficient to us only to study the population $p = \langle 1| \rho_A |1\rangle$ of the excited state, in order to describe the state ρ_A (see Appendix A, Section A.4). In other words, the ancilla local state will always be in the form $\rho_A = \begin{pmatrix} 1-p & 0 \\ 0 & p \end{pmatrix}$, with $0 \leq p \leq 1/2$.

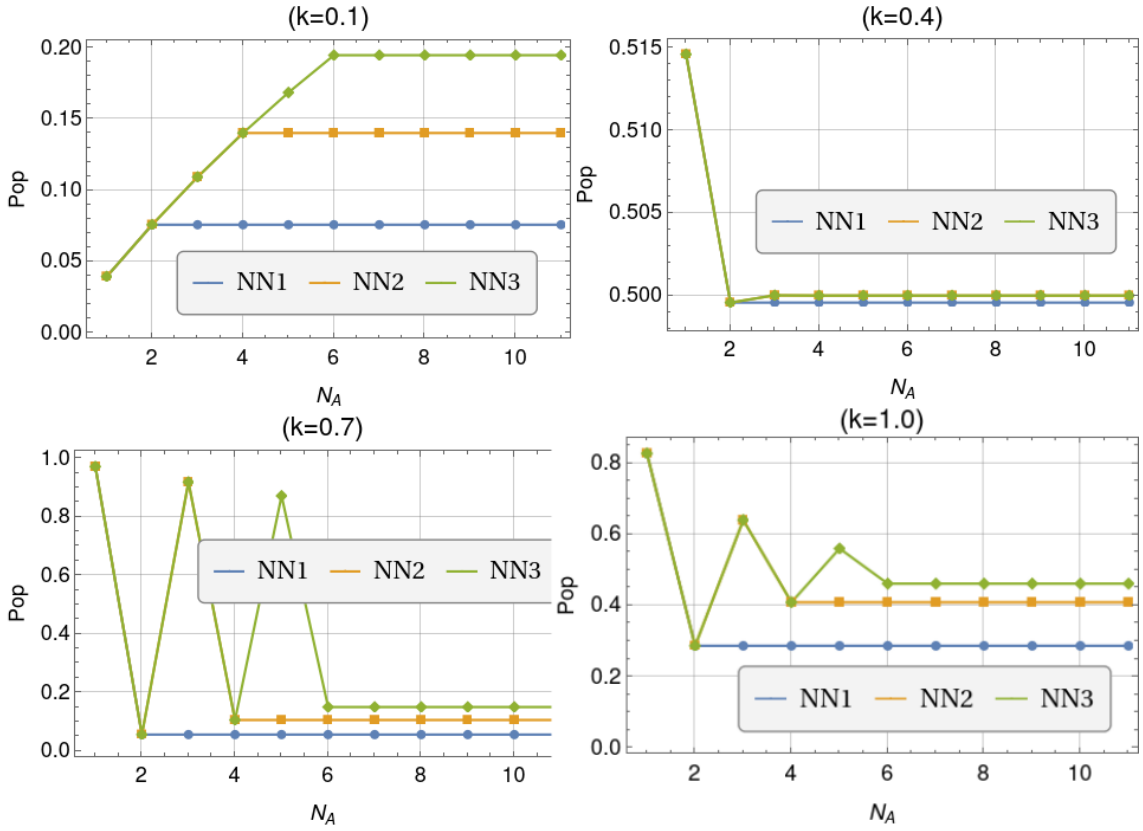

Figure 5.2: Population of the excited state of ρ_A $\times$ total number of ancillae N_A, for different values of k.

neighbors (NN3) with equal intensities ($c_1 = c_2 = c_3 = 1$). We investigated how the population of ρ_A depends on the total number of ancillae N_A. The answer is that, for a number of $N_A \gtrsim 6$, the population tends to stabilize independent of N_A. These observations are exemplified in the plots of Fig. 5.2.

- We studied the population dependence on the values of the interaction strength k in Eq. (5.3), obtaining a peak of the populations at $k = \pi/8$ when $p = 0.5$ (i.e. maximally mixed state and infinite temperature limit) and a minimum at $k = \pi/4$ when $p = 0$ (i.e. ground state and zero temperature limit) and then the population oscillates with a period of $\pi/4$ in k for NN1, NN2 and NN3. The plots of the populations versus k for different values of N_A are given in Fig. 5.3. These plots indicate that the maxima and minima of the population as a function of k are the same for any N_A and follow the same oscillatory pattern for NN1, NN2 and NN3;

- In Fig. 5.4, we compute the mutual information as a function of the distance be-

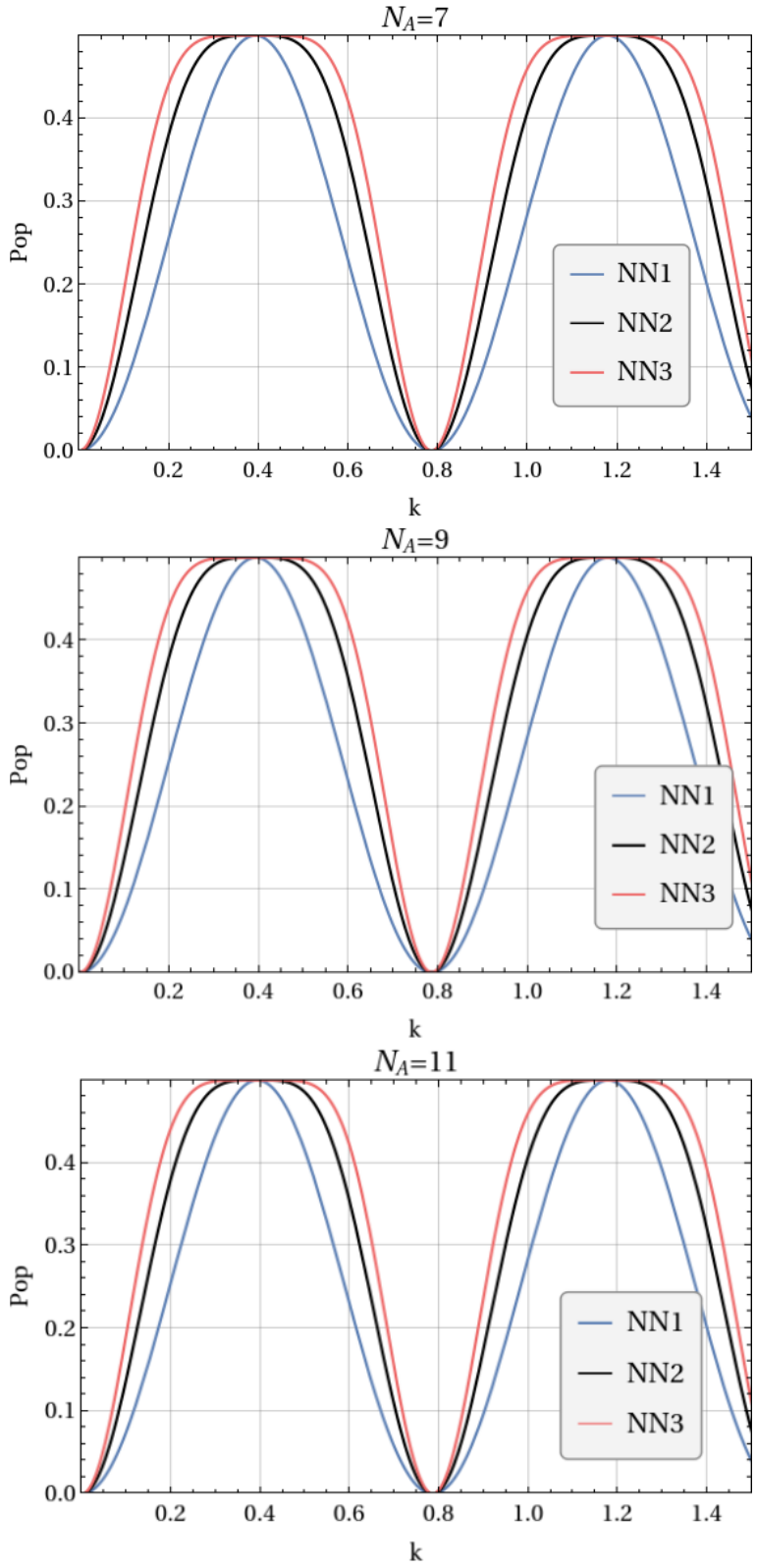

Figure 5.3: Population of ρ_A $\times$ values of k, for different values of N_A.

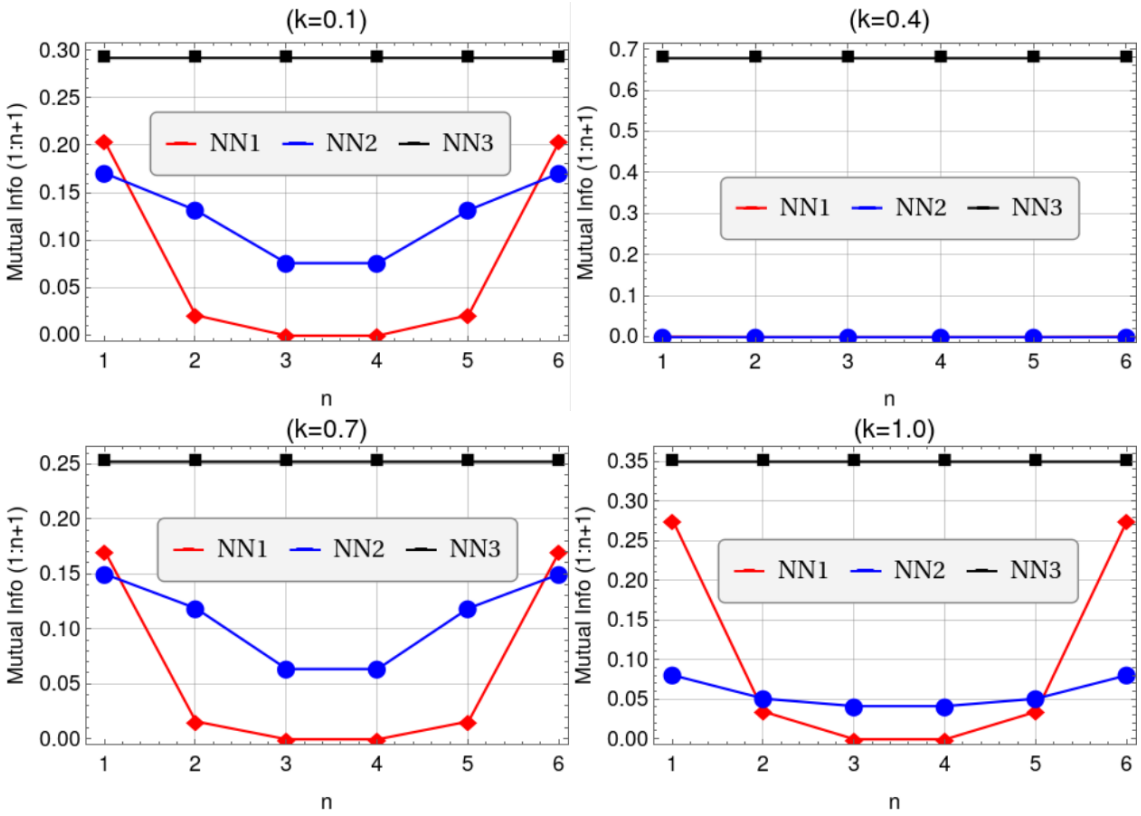

Figure 5.4: Mutual information between neighbors $\times$ distance between neighbors, for $N_A = 7$ and different values of k.

tween neighbors for NN1, NN2 and NN3. This shows that, in general, the ancillae get correlated with distant neighbors, even in the NN1 case. Intuitively, the mutual information between closest neighbors tend to be greater than with the more distant neighbors. An exception happens in the NN3 case with $N_A = 7$, where the mutual information tends to be very similar for any neighbor distance. Additionally, we can see that we have no mutual information between the neighbors in NN1 and NN2 for the case of $k = 0.4$, while in this case we have a higher mutual information in NN3 than for any other values of k;

- We analyzed the mutual information between nearest neighbors as a function of k for different values of N_A in Fig. 5.5. This exposes a periodic behaviour of the mutual information as a function of k (with a period of $\pi/4$), and peaks of maxima for the mutual information in regions close to $k = 0.1$ and $k = 0.7$ for NN1, and around $k = 0.15$ and $k = 0.65$ for NN2 and NN3. For $N_A \leq 7$, we observe a higher maximum peak of the mutual information at $k \approx 0.4$ in NN3, while this

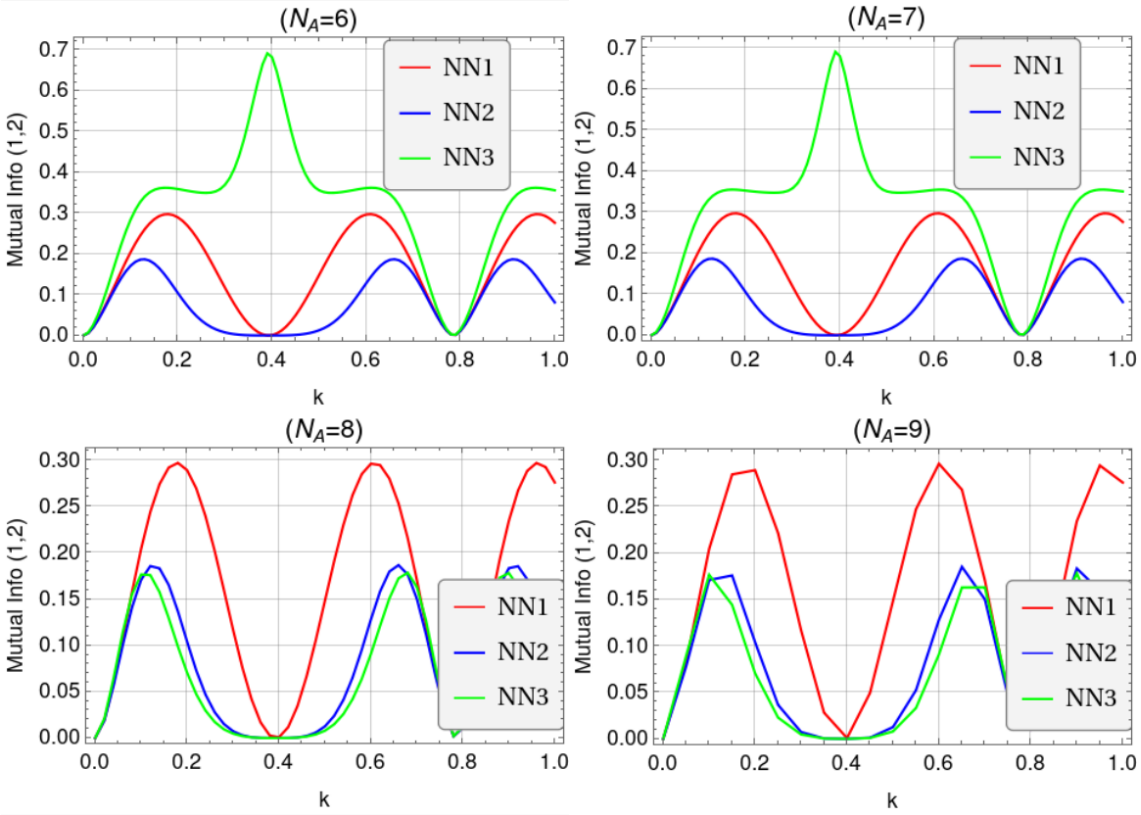

Figure 5.5: Mutual information between first neighbors $\times$ k, for different values of N_A. For larger values of N_A, the plots loose resolution since they are computationally more demanding.

region corresponds to a minimum for $NN1$ and $NN2$, which justifies the behaviour of the mutual information in Fig. 5.4 for $k = 0.4$. Interestingly, this maximum peak of the mutual information for NN3 seems to vanish for $N_A > 7$ and, as in NN1 and NN2, this region around $k \approx 0.4$ have a minimum for NN3. These observations about the correlations dependence on k will be useful to our choice of parameters in order to investigate the dynamics of the CM and the effects of the correlations in the evolution of the system, in the next Section.

5.2 Homogenization procedure with initial correlations between ancillae: Breaking Homogenization

Finally, we present the results for the CM evolution with a Partial SWAP unitary (Eq. (2.44)) describing the interaction between each locally identical ancilla and the system,

just like the Homogenization process described in Sec. 2.3.6. But now, we suppose the presence of initial correlations between the ancillae, which oblige us to compute directly Eq. (2.21) to obtain the system's evolution after each collision. In this case, we don't have the option of decomposing the evolution as the successive operation of simpler channels. Consequently, these computations using Eq. (2.21) needed to be done numerically.

We set the correlated ancillae forming the initial environment ρ_E^0 as being the hamiltonian graph states presented in the former Section, chosing the same set of cyclic graphs NN1, NN2 and NN3. We also constructed another environment by removing the correlations between the ancillae in these hamiltonian graph states, but keeping the same local ancilla reduced state ρ_A (such that $\rho_E = \rho_A^{\otimes N_A}$). This way, we prepare two environments, one causing a Non-Markovian evolution with correlated ancillae and the other with a Markovian evolution (exactly as the standard homogenization of Sec. 2.3.6), both having the ancillae in the same local state ρ_A.

As in standard CMs outlined in Sec. 2.3, we start at $t = 0$ and the stroboscopic evolution is given in steps of τ (for these computations we choose $\tau = 1$), which is the duration of each collision. We initialized the system's qubit at the ground state $\rho_S^0 = |0\rangle\langle 0|$ and we can again describe the system's state by its population of the excited state. We analyzed the dynamics for the hamiltonain graph states with different values of k (in the hamiltonian of Eq. (5.3)). From the analysis of Figs. (5.4) and (5.5) we searched for the the graph states that would maximize the initial correlations between the ancillae and, consequently, maximize the deviation of the system steady-state with respect to the case of independent ancillae, therefore breaking Homogenization. We also analyzed how different values of g for the strength of the Partial SWAP in Eq. (2.44) affected the desired steering. We present the following results:

- As can be seen in Figs. 5.6, 5.7 and 5.8, the parameter k has a central role in the steering effect of the correlations over the system's evolution, since it significantly affects the correlations between the ancillae, as was observed inf Fig. 5.5. From this same Figure we also deduced that the region around $k \approx 0.4$ may have a minimum for the mutual information of NN1, NN2 and NN3, and hence there would be less correlations to cause the steering. This fact can be seen in the plots of NN2 and NN3 (Figs. 5.7 and 5.8), where there is no breaking of homogeniztation for $k = 0.4$.

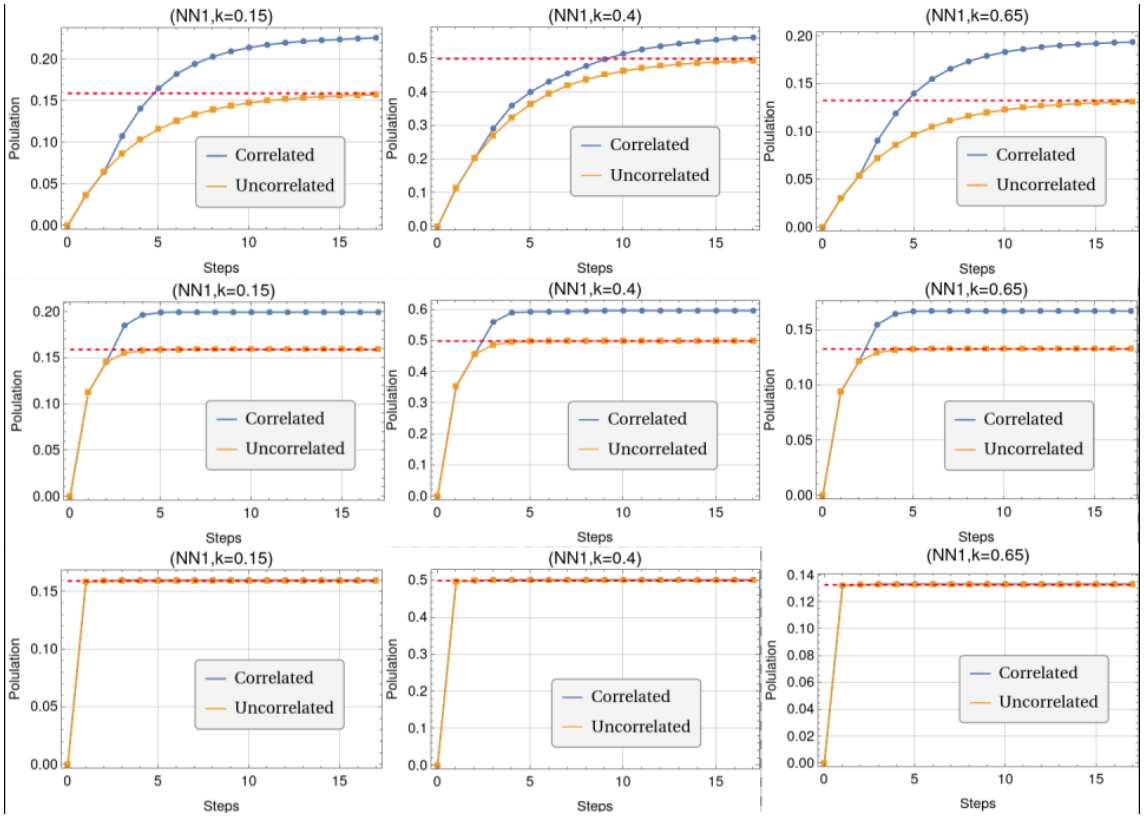

Figure 5.6: Plots of population of ρ_S $\times$ number of steps for ancillae prepared with the NN1 cyclic graph with $N_A = 17$, for different values of k. Each line correspond to a different value of g strength of the partial SWAP interaction, from top to bottom $g = 0.5$, $g = 1.0$ and $g = 1.5$. The red dashed lines indicate the value of the population of the respective ρ_A, which is the value in which the system's population converges if homogenizaton happens.

Adversely, for NN1 (Fig. 5.6) we see that the steering is still present in $k = 0.4$, which can be caused by a non-vanishing mutual information between the ancillae, since the behaviour of the mutual information can be different than in Fig. 5.5 for larger N_A. Also from Fig. 5.5, we suppose large correlation effects in the regions around $k = 0.15$ and $k = 0.65$ for NN1, $k = 0.15$ and $k = 0.7$ for NN2, and $k = 0.1$ and $k = 0.7$ for NN3. This is confirmed by the plots of Figs. 5.6, 5.7 and 5.8 since, for the initially correlated ancillae case with these values of k, clearly the system's steady-state deviates from the homogenization in the uncorrelated case;

- Finally, we also study different values of g (the strength of the Partial SWAP interaction, given in Eq. (2.44)) in the plots of Figs. 5.6, 5.7 and 5.8. They show the pattern that, for lower values of g, exemplified by $g = 0.5$, the homogeniza-

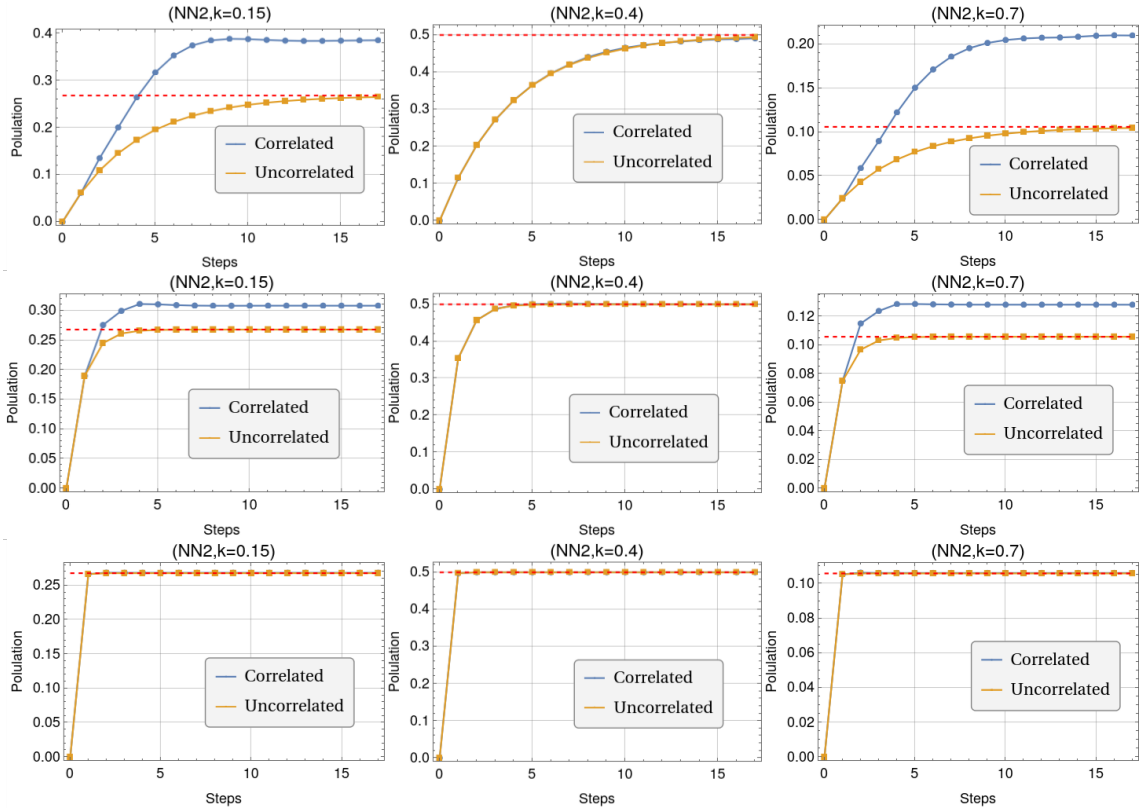

Figure 5.7: Plots of population of ρ_S $\times$ number of steps for ancillae prepared with the NN2 cyclic graph with $N_A = 17$, for different values of k. Each line correspond to a different value of g strength of the partial SWAP interaction, from top to bottom $g = 0.5$, $g = 1.0$ and $g = 1.5$. The red dashed lines indicate the value of the population of the respective ρ_A, which is the value in which the system's population converges if homogenizaton happens.

tion takes more steps to happen, but the effect of the correlations are stronger than for larger g's. This seems to suggest that a greater thermalization (or homogenization) time allows the correlations to act more in the system's evolution, for greater values of g, e.g. $g = 1.5$, the system homogenizes too rapidly, so the correlation effects are unseen. Lastly, the Partial SWAP depends trigonometrically on g (see Eq. (2.44)), therefore, the effects of g in the system's evolution will oscillate, as g grows, repeating the results in cycles of π.

The analysis above clearly confirm the steering effect on the system's evolution and the breaking of Homogenization caused by the presence of initial correlations between the ancillae, for the case where system and ancillae are qubits. These results are also published in [93].

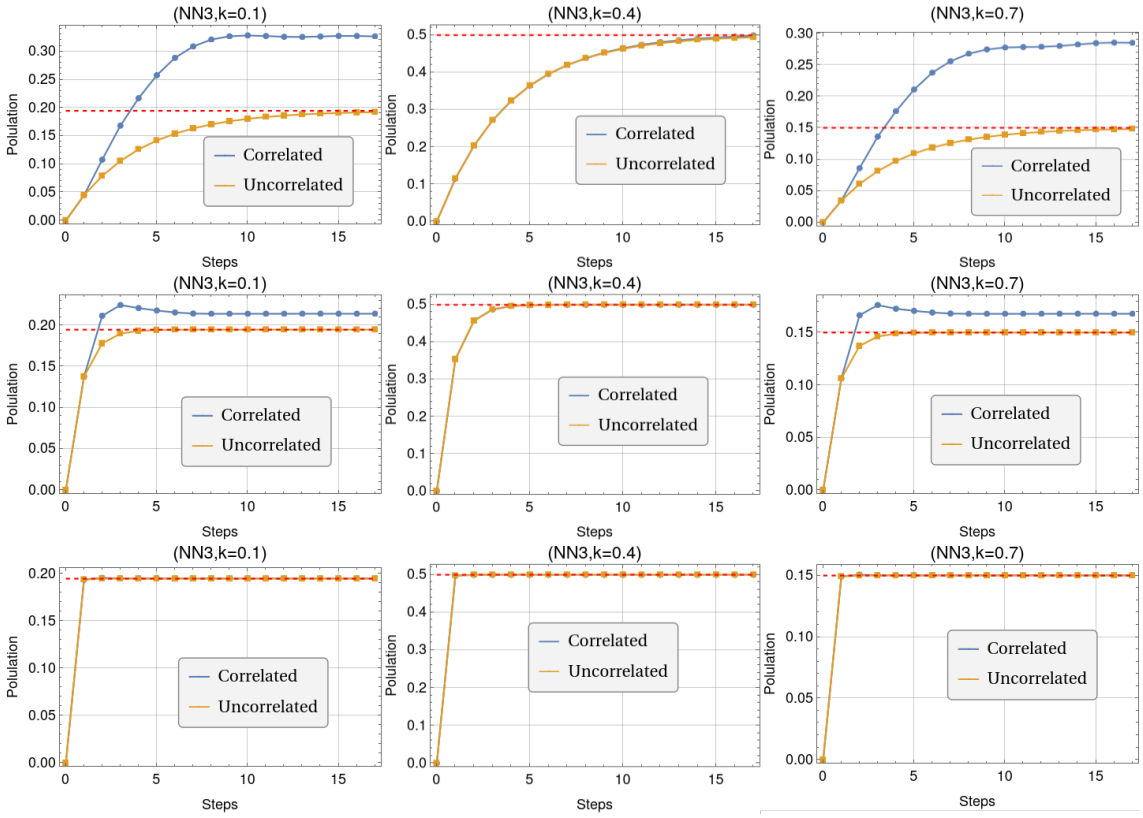

Figure 5.8: Plots of population of ρ_S $\times$ number of steps for ancillae prepared with the NN3 cyclic graph with $N_A = 17$, for different values of k. Each line correspond to a different value of g strength of the partial SWAP interaction, from top to bottom $g = 0.5$, $g = 1.0$ and $g = 1.5$. The red dashed lines indicate the value of the population of the respective ρ_A, which is the value in which the system's population converges if homogenizaton happens.

Chapter 6

Initially Correlated Ancillae - Gaussian States CM

In this Chapter, we present the main results of the second project of this thesis. We obtain simple analytical formulae for the evolution of the system for *any* number of initially correlated ancillae in the CM, as described in Sec. 2.3, with a Partial SWAP unitary in bosonic modes states. Here we observe a direct influence of the initial correlations between the ancillae in the system's evolution, which cause a linear (and independent of the initial system state) term on the system's steady-state. This presents a clear image of the steering caused by the correlations and the breaking of Homogenization. These results are also described in [93].

The results were possible since we consider the system and ancillae as bonsonic modes starting in Gaussian states. This simplifies remarkably the computations, as explained in Sec. 4.6. Now we only study the covariance matrices which will completely describe our system and environment.[1] Also, the continuous-variables formalism made possible a much more simple description of the dynamics, because now the evolution is given by the $2(N_A+1)\times 2(N_A+1)$ (where N_A is the total number of ancillae) sympletic matrices, instead of unitaries that act directly in the infinite dimensional Hilbert space. These characteristics of our object of study allows us to manipulate simple matrices analytically, for

[1] For instance, in Chapter 5 we were able to compute numerically a maximum of only 17 collisions in our CM since this would involve the preparation of 17 ancillae in the environment. In order to fully describe the environment density matrix the computations involved $2^{17}\times 2^{17}$ matrices. While for Gaussian states, an environment made of 100 ancillae can be fully described by a 200×200 covarince matrix.

a low number of ancillae and collisions, and then induce the results for arbitrary numbers. The procedure will be detailed in the following.

6.1 Preliminaries

6.1.1 The Stinespring dilation procedure

As we already pointed above, the system and environment are composed by bosonic modes. We have one mode for our system and N_A modes for the environment (each mode represents one ancilla). All of them start the evolution in Gaussian states, thus their initial states ρ_S^0 and ρ_E^0 will be fully described by their covariance matrices σ_S^0 and σ_E^0 and their firsts moments $\langle \hat{\mathbf{r}}_S^0 \rangle$ and $\langle \hat{\mathbf{r}}_E^0 \rangle$. Now we assume, without lost of generality, that $\langle \hat{\mathbf{r}}_S^0 \rangle = 0$ and $\langle \hat{\mathbf{r}}_E^0 \rangle = 0$ (where 0 here means a respective vector of 0 in all entries), which will ensure that the first moments will remain 0 during the evolution, remaining for us only the analysis of the covariance matrices.[2]

We will follow the Stinespring dilation described in Subsec. 2.3.1 to describe the dynamics of the CM. Since we are dealing with Gaussian states and quadratic-Hamiltonian unitaries (the Beam Splitter, to be presented in the next Subsection), all the following steps will maintain the Gaussian characeter of the states, as proved in Section 4.7. Further results from Section 4.7 will also be used.

We start by supposing that the system and environment start uncorrelated at time $t = 0$, so their joint state will be given by $\rho_{SE}^0 = \rho_S^0 \otimes \rho_E^0$. The tensor product is a Gaussian operation and the resulting covariance matrix will be

$$\sigma_{SE}^0 = \sigma_S^0 \oplus \sigma_E^0, \tag{6.1}$$

from Eq. (4.93).

Then we make a unitary evolution, which is described by a sympletic matrix S_H^1 (which will be related with the unitary used, in our case, the Partial SWAP), using Eq.

[2]This last restriction can contemplate the general analysis since, as we shall study the evolution under the Partial SWAP unitary, the evolution of the first moments is given by Eq. (4.73). So, if the system starts with some arbitrary first moment $\bar{\mathbf{r}}$, then we can always translate such first moment to 0 (which will not affect the covariance matrix since its evolution equation, Eq. (4.76), is decoupled from the first moments) and Eq. (4.73) guarantee that its evolution will be trivial.

(4.77)

$$\sigma_{SE}^{1} = S_H^1 \sigma_{SE}^{0} (S_H^1)^\top, \tag{6.2}$$

where σ_{SE}^{1} is the covariance matrix of the joint system plus environment state after the *first* collision.

Next, in order to obtain the system's evolution, we separate the joint covariance matrix as

$$\sigma_{SE}^{1} = \begin{pmatrix} \sigma_S^1 & \xi_{SE}^1 \\ (\xi_{SE}^1)^\top & \sigma_E^1 \end{pmatrix}, \tag{6.3}$$

where σ_S^1 is a 2×2 block matrix, σ_E^1 is a $2N_A \times 2N_A$ block matrix and ξ_{SE}^1 is a $2 \times 2N_A$ block matrix. As it is demonstrated in Sec. 4.7, σ_S^1 will be the covariance matrix of the reduced state of the system, i.e., the system obtained after tracing out the environment. For obtaining the following steps of the system's evolution, we just proceed evolving the joint system SE with the respective unitaries

$$\sigma_{SE}^{n} = S_H^n S_H^{n-1} \cdots S_H^1 \sigma_{SE}^{0} (S_H^1)^\top \cdots (S_H^{n-1})^\top (S_H^n)^\top \tag{6.4}$$

and again separate the evolved joint system as

$$\sigma_{SE}^{n} = \begin{pmatrix} \sigma_S^n & \xi_{SE}^n \\ (\xi_{SE}^n)^\top & \sigma_E^n \end{pmatrix}, \tag{6.5}$$

taking σ_S^n as the covariance matrix of our evolved reduced state. Notice that we can also use σ_E^n as the covariance matrix of the environment's reduced state.

The reason that we must evolve the *whole* joint system in Eq. (6.4) is that we cannot have a map from intermediate covariance matrices of the system to the final one since we must consider the non-Markovian effects caused by the initial correlations between the ancillae. This has the same reasoning of why we cannot break the map of Eq. (2.21) into a succession of intermediate maps. In fact, notice the resemblance between Eqs. (6.4) and (2.20) and note that Eq. (6.5) has the same role as Eq. (2.21).

6.1.2 The Beam Splitter interaction

Here, we present the unitary that we shall use in our CM for each collision. It is an interaction of immense importance in Quantum Optics, the so-called *Beam-Splitter (BS)* [14, 15, 55, 95, 118]. The BS can be defined by the following interaction Hamiltonian between two bosonic modes A and B

$$\hat{H}_{BS} = \frac{g}{2}(\hat{p}_A\hat{q}_B - \hat{q}_A\hat{p}_B), \tag{6.6}$$

where $g > 0$.

In the following, we will show that the unitary generated by this Hamiltonian satisfies the Partial SWAP conditions (Eqs. (2.45) and (2.46)) for the Gaussian bosonic modes case.

The interaction Hamiltonian above is quadratic in terms of canonical operators, hence it can be decomposed in terms of Eq. (4.55) with $\mu = 0$ and the Hamiltonian matrix

$$H_{BS} = \begin{pmatrix} 0 & -ig\sigma_y \\ ig\sigma_y & 0 \end{pmatrix}, \tag{6.7}$$

where each entry of the matrix above is a 2×2 matrix and σ_y is the y Pauli matrix. Therefore, the corresponding symplectic transformation will be

$$\begin{aligned} S_{BS} &= e^{\Omega H_{BS}\tau} \\ &= \begin{pmatrix} c & s \\ -s & c \end{pmatrix}, \end{aligned} \tag{6.8}$$

where $c = \cos(g\tau)$, $s = \sin(g\tau)$, τ is the duration of the interaction and each entry is multiplied by $\mathbb{I}_2$.

If the modes A and B are Gaussian, they can be described by covariance matrices σ_A and σ_B. And if they are uncorrelated and happen to be in the same local state ($\sigma_A = \sigma_B =$

σ), their joint covariance matrix will be

$$\sigma_{AB} = \begin{pmatrix} \sigma & 0 \\ 0 & \sigma \end{pmatrix}. \tag{6.9}$$

Hence, the unitary Beam Splitter operation in this state will be given by

$$\begin{aligned} S_{BS}\sigma_{AB}S_{BS}^{\top} &= \begin{pmatrix} c & -s \\ s & c \end{pmatrix} \begin{pmatrix} \sigma & 0 \\ 0 & \sigma \end{pmatrix} \begin{pmatrix} c & s \\ -s & c \end{pmatrix} \\ &= \begin{pmatrix} \sigma & 0 \\ 0 & \sigma \end{pmatrix}. \end{aligned} \tag{6.10}$$

Consequently, the partial traces in A and B will result in the same state as the initial, satisfying Eqs. (2.45) and (2.46). These Equations are necessary and sufficient conditions for a unitary operator to be a Partial SWAP [19].

6.1.3 Correlations block-matrices

Before presenting our results, we will expose important properties about the block matrices that will describe completely the correlations between our ancillae. Suppose two ancillae of our environment, representing the modes j and k, respectively. We can take a block matrix made of the covariance matrix terms

$$\begin{aligned} \xi_{j,k} &= \begin{pmatrix} \sigma_{2j-1,2k-1} & \sigma_{2j-1,2k} \\ \sigma_{2j,2k-1} & \sigma_{2j,2k} \end{pmatrix} \\ &= \begin{pmatrix} \langle q_j q_k \rangle - \langle q_j \rangle \langle q_k \rangle & \langle q_j p_k \rangle - \langle q_j \rangle \langle p_k \rangle \\ \langle p_j q_k \rangle - \langle p_j \rangle \langle q_k \rangle & \langle p_j p_k \rangle - \langle p_j \rangle \langle p_k \rangle \end{pmatrix}, \end{aligned} \tag{6.11}$$

where we used that canonical operators of different modes commute and Eq. (4.62). Now, if the canonical operators of j and k are statistically independent, then the components above must result in 0. Furthermore, given the reduced state $\rho_{j,k}$ of the modes j and k, its

covariance matrix will be

$$\sigma_{j,k} = \begin{pmatrix} \sigma_j & \xi_{j,k} \\ \xi_{j,k}^\top & \sigma_k \end{pmatrix}, \tag{6.12}$$

where $\sigma_{j(k)}$ is the local covariance matrix of $j(k)$. Now, from the deduction of Eq. (4.93), we have $\xi_{j,k} = 0$[3] if and only if $\rho_{j,k} = \rho_j \otimes \rho_k$ is the tensor product of the local density matrices. From Eq. (3.17), the mutual information between j and k is $\mathcal{I}(j:k) = 0$ when $\rho_{j,k} = \rho_j \otimes \rho_k$, consequently $\xi_{j,k} = 0$ is *necessary and sufficient* to $\mathcal{I}(j:k) = 0$.

For these reasons, we often name these components as *correlations* between bosonic modes of Gaussian states. For instance, for an environment made of 5 ancillae, we have

$$\sigma_E = \begin{pmatrix} \sigma_{A_1} & \xi_{1,2} & \xi_{1,3} & \xi_{1,4} & \xi_{1,5} \\ \xi_{1,2}^\top & \sigma_{A_2} & \xi_{2,3} & \xi_{2,4} & \xi_{2,5} \\ \xi_{1,3}^\top & \xi_{2,3}^\top & \sigma_{A_3} & \xi_{3,4} & \xi_{3,5} \\ \xi_{1,4}^\top & \xi_{2,4}^\top & \xi_{3,4}^\top & \sigma_{A_4} & \xi_{4,5} \\ \xi_{1,5}^\top & \xi_{2,5}^\top & \xi_{3,5}^\top & \xi_{4,5}^\top & \sigma_{A_5} \end{pmatrix}, \tag{6.13}$$

where all the terms inside the above matrix are actually 2×2 block matrices, σ_{A_n} are the covariance matrices of the n-th ancilla reduced state and $\xi_{j,k}$ represents the correlations between the ancillae j and k.

6.2 Main results

6.2.1 Correlated nearest-neighbors

We start with a simple, yet insightful result. We apply the Stinespring procedure presented in Subsection 6.1.1 for the case where we have N_A ancillae which are correlated only with their nearest-neighbors. Additionally, we start supposing that the ancillae are not necessarily identical for obtaining a more general result and then restricting it for identical ancillae and comparing it to Homogenization. This means that the correlation terms of the

[3] In this context, 0 means *null matrix*.

environment will be in the form $\xi_{j,k} = \xi_{j,k}\delta_{k,j+1}$. Therefore, the environment of correlated ancillae will initialize in a state with the following $2N_A \times 2N_A$ covariance matrix[4]

$$\sigma_E^0 = \begin{pmatrix} \sigma_{A_1} & \xi_{1,2} & 0 & \cdots & 0 \\ \xi_{1,2}^\top & \sigma_{A_2} & \xi_{2,3} & \cdots & 0 \\ 0 & \xi_{3,4}^\top & \sigma_{A_3} & \ddots & \vdots \\ \vdots & \ddots & \ddots & \ddots & \xi_{N_A-1,N_A} \\ 0 & 0 & \cdots & \xi_{N_A-1,N_A}^\top & \sigma_{A_{N_A}} \end{pmatrix}. \tag{6.14}$$

The joint system will start as

$$\begin{aligned} \sigma_{SE}^0 &= \sigma_S^0 \oplus \sigma_E^0 \\ &= \begin{pmatrix} \sigma_S^0 & 0 & 0 & \cdots & 0 \\ 0 & \sigma_{A_1} & \xi_{1,2} & \cdots & 0 \\ 0 & \xi_{1,2}^\top & \sigma_{A_2} & \ddots & \ddots \\ \vdots & \ddots & \ddots & \ddots & \xi_{N_A-1,N_A} \\ 0 & 0 & \cdots & \xi_{N_A-1,N_A}^\top & \sigma_{A_{N_A}} \end{pmatrix}. \end{aligned} \tag{6.15}$$

This joint state evolves as the system evolves unitarilly (collides) with each ancilla j. They interact via the Hamiltonian

$$\hat{H}_j = \hat{H}_S + \hat{H}_{A_j} + \hat{H}_{BS_j}, \tag{6.16}$$

where $\hat{H}_S = \frac{\omega}{2}(\hat{q}_S^2 + \hat{p}_S^2)$, $\hat{H}_{A_j} = \frac{\omega}{2}(\hat{q}_{A_j}^2 + \hat{p}_{A_j}^2)$, for $\omega > 0$, $\hat{q}_{S(A_j)}$ and $\hat{p}_{S(A_j)}$ are the quadrature operators of the system (ancilla j) and

$$\hat{H}_{BS_j} = \frac{g}{2}(\hat{p}_S\hat{q}_{A_j} - \hat{q}_S\hat{p}_{A_j}), \tag{6.17}$$

for $g > 0$, is the Beam Splitter interaction of the system with each ancillae j. We have that $\hat{H}_S$ and $\hat{H}_{A_j}$ are local Hamiltonians, so we can set them to 0 by going to the interaction picture (see Appendix A).

[4] In this Section, every matrix element is a 2×2 block matrix, or a number multiplied by $\mathbb{I}_2$.

Proceeding, we compute the sympletctic transformation corresponding to the unitary generated by the Hamiltonian $\hat{H}_j$ in the interaction picture

$$S_H^j = e^{\Omega H_{BS_j} \tau}, \tag{6.18}$$

where H_{BS_j} is the $(2N_A + 1) \times (2N_A + 1)$ Hamiltonian matrix corresponding to $\hat{H}_{BS_j}$ from Eq. (6.17) and τ is the duration of the collision. For $j = 1$ (first collision), we have the following matrix Hamiltonian matrix

$$H_{BS}^1 = \begin{pmatrix} 0 & -ig\sigma_y & 0 & \cdots & 0 \\ ig\sigma_y & 0 & 0 & \cdots & 0 \\ 0 & 0 & 0 & \cdots & 0 \\ \vdots & \vdots & \vdots & \ddots & \vdots \\ 0 & 0 & 0 & \cdots & 0 \end{pmatrix}, \tag{6.19}$$

where σ_y is the y Pauli matrix. Consequently, we have the following $(2N_A+1)\times(2N_A+1)$ symplectic matrix

$$S_H^1 = \begin{pmatrix} c & s & 0 & \cdots & 0 \\ -s & c & 0 & \cdots & 0 \\ 0 & 0 & 1 & \cdots & 0 \\ \vdots & \vdots & \vdots & \ddots & \vdots \\ 0 & 0 & 0 & \cdots & 1 \end{pmatrix}, \tag{6.20}$$

where $c = \cos(g\tau)$ and $s = \sin(g\tau)$.

In an completely analogous way, we have the Hamiltonian matrices corresponding to

the next collisions

$$H_{BS}^{2} = \begin{pmatrix} 0 & 0 & -ig\sigma_y & \cdots & 0 \\ 0 & 0 & 0 & \cdots & 0 \\ ig\sigma_y & 0 & 0 & \cdots & 0 \\ \vdots & \vdots & \vdots & \ddots & \vdots \\ 0 & 0 & 0 & \cdots & 0 \end{pmatrix},$$

$$\vdots$$

$$H_{BS}^{N_A-1} = \begin{pmatrix} 0 & 0 & \cdots & 0 & -ig\sigma_y \\ 0 & 0 & \cdots & 0 & 0 \\ \vdots & \vdots & \ddots & \vdots & \vdots \\ 0 & 0 & \cdots & 0 & 0 \\ ig\sigma_y & 0 & \cdots & 0 & 0 \end{pmatrix}, \tag{6.21}$$

and obtain the respective symplectic matrices

$$S_{H}^{2} = \begin{pmatrix} c & 0 & s & \cdots & 0 \\ 0 & 1 & 0 & \cdots & 0 \\ -s & 0 & c & \cdots & 0 \\ \vdots & \vdots & \vdots & \ddots & \vdots \\ 0 & 0 & 0 & \cdots & 1 \end{pmatrix},$$

$$\vdots$$

$$S_{H}^{N_A-1} = \begin{pmatrix} c & 0 & \cdots & 0 & s \\ 0 & 1 & \cdots & 0 & 0 \\ \vdots & \vdots & \ddots & \vdots & \vdots \\ 0 & 0 & \cdots & 1 & 0 \\ -s & 0 & \cdots & 0 & c \end{pmatrix}. \tag{6.22}$$

Next, we continue to follow the procedure described in Subsection 6.1.1 using the symplectic transformations above. Now we obtain the joint system's first collisional step evolution by computing $\sigma_{SE}^{1} = S_{H}^{1}\sigma_{SE}^{0}(S_{H}^{1})^{\top}$ and taking the system's covariance matrix

as in Eq. (6.5), obtaining

$$\sigma_S^1 = c^2\sigma_S^0 + s^2\sigma_{A_1}. \tag{6.23}$$

Doing the next step evolution $\sigma_{SE}^2 = S_H^2\sigma_{SE}^1(S_H^2)^\top$, we obtain

$$\sigma_S^2 = c^4\sigma_S^0 + c^2s^2\sigma_{A_1} + s^2\sigma_{A_2} + cs^2(\xi_{1,2} + \xi_{1,2}^\top).$$

And again, $\sigma_{SE}^3 = S_H^3\sigma_{SE}^2(S_H^3)^\top$ for the third step, obtaining

$$\sigma_S^3 = c^6\sigma_S^0 + c^4s^2\sigma_{A_1} + c^2s^2\sigma_{A_2} + s^2\sigma_{A_3} + c^3s^2(\xi_{1,2} + \xi_{1,2}^\top) + cs^2(\xi_{2,3} + \xi_{2,3}^\top).$$

From this we can begin to see a pattern, from which we can induce

$$\boxed{\sigma_S^n = c^{2n}\sigma_S^0 + \sum_{k=1}^{n} c^{2(n-k)}s^2\sigma_{A_n} + \sum_{k=1}^{n-1} c^{2k-1}s^2(\xi_{k-1,k} + \xi_{k-1,k}^\top),} \tag{6.24}$$

for the system's covariance matrix after the n^{th} collision.

Now, if we suppose that the ancillae are identical $\sigma_{A_k} = \sigma_A$, as in the Homogenization case, we obtain, after the use of the geometric sum and some simplifications

$$\sigma_S^n = c^{2n}\sigma_S^0 + (1 - c^{2n})\sigma_A + \sum_{k=1}^{n-1} c^{2k-1}s^2(\xi_{k-1,k} + \xi_{k-1,k}^\top).$$

The equation above indicates that, if the correlation terms are 0, Homogenization will happen. Indeed, for null correlation terms, if $g\tau$ are such that $|c| < 1$, then we will have the steady-state $\sigma_S^\infty = \sigma_A$.

Also supposing that the nearest-neighbor correlations have the same intensity $\xi_{k-1,k} = \xi$, for a 2×2 block-matrix ξ, we have

$$\boxed{\sigma_S^n = c^{2n}\sigma_S^0 + (1 - c^{2n})\sigma_A + c(1 - c^{2(n-1)})(\xi + \xi^\top).} \tag{6.25}$$

Finally, we obtain, for the case of identical ancillae and same intensity nearest-neighbor

correlations, the steady-state (considering that $|c| < 1$)

$$\boxed{\sigma_S^{\infty} = \sigma_A + c(\xi + \xi^{\top}).} \tag{6.26}$$

The equation above is our first result obtaining an analytical equation that describes the CM with the presence of initially correlated ancillae, computing the effects of such correlations. Also, by changing the entries of ξ we can have control over the steering of the entries of the steady-state, driving it away from the ancilla's covariance matrix σ_A. This shows a simple and clear visualization of how the correlations break Homogenization, and how we can obtain an additional term in the steady-state of the system which is completely dependent on global correlations, although the system interacts only locally with ancillae which are locally identical.

Another intriguing observation about the result above can be done. If we consider the initial state of the system and of the local ancillae as thermal states, the additional correlation term $\cos(g\tau)(\xi + \xi^{\top})$ can heat or cool down the system's steady-state, depending only on the sign of $\cos(g\tau)$. For instance, if the system and local ancillae initial states are thermal states at the same temperature, the term $\cos(g\tau)(\xi + \xi^{\top})$ can dictate the action of the CM as a thermal machine or a refrigerator depending only on the values of $g\tau$.

6.2.2 General case

Proceeding analogously as in the nearest-neighbor correlations case presented above, we can obtain the general evolution of a system interacting with N_A ancillae, all correlated with themselves, via BS interactions. Since the interactions are the same, the symplectic matrices used in the nearest-neighbor correlations case (Eqs. (6.20) and (6.22)) still describe the unitary dynamics. The only difference is in the initial environment state, its covariance matrix σ_E^0 will have the most general form, given, for instance, in Eq. (6.13) (for the case of $N_A = 5$). We initialize with the joint system's covariance matrix $\sigma_S^0 \otimes \sigma_E^0$ and, using Eq. (6.4), we proceed analogously as in the nearest-neighbor correlations case for obtaining the evolution of the system-environment joint state covariance matrix. This way, obtaining the local system's covariance matrices from Eq. (6.5), we achieve the

following chain of equations

$$\begin{aligned}
\sigma_S^1 =& s^2\sigma_{A_1} + c^2\sigma_S^0,\\
\sigma_S^2 =& c^4\sigma_S^0 + c^2s^2\sigma_{A_1} + s^2\sigma_{A_2} + cs^2(\xi_{1,2} + \xi_{1,2}^\top),\\
\sigma_S^3 =& c^6\sigma_S^0 + c^4s^2\sigma_{A_1} + c^2s^2\sigma_{A_2} + s^2\sigma_{A_3} + c^3s^2(\xi_{1,2} + \xi_{1,2}^\top) + c^2s^2(\xi_{1,3} + \xi_{1,3}^\top) + cs^2(\xi_{2,3} + \xi_{2,3}^\top),\\
\sigma_S^4 =& c^8\sigma_S^0 + c^6s^2\sigma_{A_1} + c^4s^2\sigma_{A_2} + c^2s^2\sigma_{A_3} + s^2\sigma_{A_4} + c^5s^2(\xi_{1,2} + \xi_{1,2}^\top) + c^4s^2(\xi_{1,3} + \xi_{1,3}^\top)\\
&+ c^3s^2(\xi_{1,4} + \xi_{1,4}^\top) + c^3s^2(\xi_{2,3} + \xi_{2,3}^\top) + c^2s^2(\xi_{2,4} + \xi_{2,4}^\top) + cs^2(\xi_{3,4} + \xi_{3,4}^\top),\\
&\vdots
\end{aligned} \tag{6.27}$$

from which, after some observation, we can induce the pattern for the system's covariance matrix after the n^{th} collision

$$\boxed{\sigma_S^n = c^{2n}\sigma_S^0 + \sum_{j=1}^{n} c^{2(n-j)}s^2\sigma_{A_j} + s^2\sum_{j=1}^{n-1}\sum_{\ell>j}^{n} c^{2n-j-\ell}(\xi_{j,\ell} + \xi_{j,\ell}^\top).} \tag{6.28}$$

Although the very general status of the solution above, it will give us more interesting results if we analyse more particular cases. First of all, if we suppose that again all ancillae are equal $\sigma_{A_j} = \sigma_A$ and using the geometric sum, we obtain

$$\sigma_S^n = c^{2n}\sigma_S^0 + (1 - c^{2n})\sigma_A + s^2\sum_{j=1}^{n-1}\sum_{\ell>j}^{n} c^{2n-j-\ell}(\xi_{j,\ell} + \xi_{j,\ell}^\top). \tag{6.29}$$

The equation above shows that Homogenization is indeed achieved again if we have no correlations, since in this case we have the steady-state $\sigma_S^\infty = \sigma$, if $|c| < 1$. Also, it is worth to note that the third term of right hand side will be fully responsible for the steering caused by the correlations and of the breaking of Homogenization. This term is completely independent from the system's initial state and from the ancillae local states.

6.2.3 Distance dependent correlations

We can proceed with a very intuitive restriction from the case above. That is, if the correlations terms depend only on the distance between the ancillae, i.e., they only depend

on $\ell - j = d$

$$\xi_{j,\ell} = \xi_{|j-\ell|} = \xi_d. \tag{6.30}$$

This simplifies Eq. (6.29) to

$$\boxed{\sigma_S^n = c^{2n}\sigma_S^0 + (1-c^{2n})\sigma_A + s^2 \sum_{m=1}^{n-1} c^{2m} \sum_{d=1}^{m} c^{-d}(\xi_d + \xi_d^\top).} \tag{6.31}$$

Here, we can have another way of computing the evolution of the system in the nearest-neighbors correlations case, by restricting $\xi_d = \delta_{1,d}\xi$ in the equation above, arriving in the same results. But another interesting application is for the *Algebraically decaying correlations* case, where we consider that the correlations decay exponentially with the distance

$$\xi_d = K^{1-d}\xi, \qquad d = 1, 2, \ldots, \tag{6.32}$$

for some 2×2 matrix ξ and $K > 1$. Using this choice in Eq. (6.31), we obtain

$$\sigma_S^n = c^{2n}\sigma_S^0 + (1-c^{2n})\sigma_A + \frac{Ks^2}{cK-1}\left(\frac{c^2 - c^{2n}}{s^2} - \frac{c^{n-1}K^{1-n} - 1}{1 - c^{-1}K}\right)(\xi + \xi^\top), \tag{6.33}$$

where we used the geometric sum twice and made a few algebraic manipulations. From the solution above, we obtain the system's steady-state (for $|c| < 1$)

$$\sigma_S^\infty = \sigma_A + \frac{cK}{K-c}(\xi + \xi^\top). \tag{6.34}$$

Now, notice that the case $K \gtrsim 1$ means long range correlations, while $K \gg 1$ are related to short range correlations. This short range correlations result is in total agreement with the nearest-neighbors correlations result. Indeed, if we take the limit of $K \to \infty$, the steady-state of Eq. (6.34) reduces to the nearest-neighbors correlations steady-state of Eq. (6.26), i.e.

$$\sigma_A + \frac{cK}{K-c}(\xi + \xi^\top) \xrightarrow{K\to\infty} \sigma_A + c(\xi + \xi^\top).$$

On the other hand, for the long range correlations case, we have large values of the correlations effects for small K. See, for instance, Fig. 6.1, which shows the behaviour of $\frac{cK}{K-c}$ in function of $g\tau$, for different values of K. For small values of K, the function $\frac{cK}{K-c}$

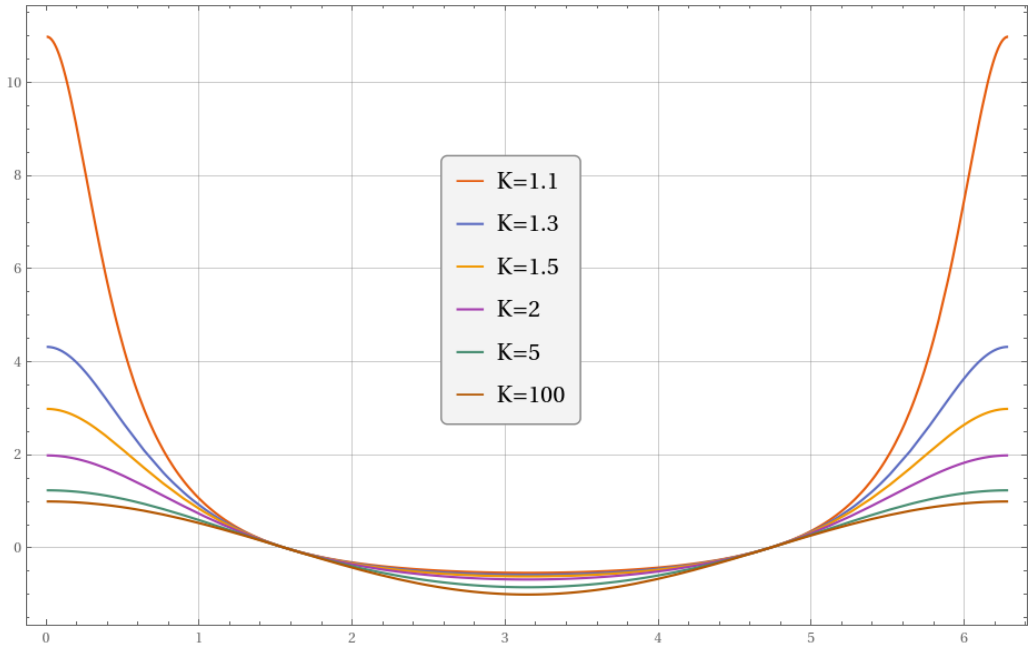

Figure 6.1: Values of $\frac{\cos(g\tau)K}{K-\cos(g\tau)} \times g\tau$ for different values of K in the interval $g\tau \in [0, 2\pi]$.

increases dramatically for $g\tau$ close to 0 or 2π, amplifying the effects of the correlation matrix ξ. As in the nearest-neighbor correlations case, the sign of the function multiplying $(\xi + \xi^{\top})$ can be positive or negative. Although in this case, for small values of K, we see a much larger potential to the positive sign case (heating the system) then negative sign case (cool down the system).

6.2.4 Ancillae evolution

Here we will obtain each ancilla local covariance matrix after it's collision with the state, for the general case of initially correlated ancillae. Importantly, these local ancillae states don't suffer any change before and after the collision with the system. This can be seen as a consequence of the *no-signaling theorem*.[5]

We use the exact same procedure used in Subsection 6.2.2. Analogously, we start with the most general environment σ_E^0 and evolve the joint system $\sigma_S^0 \otimes \sigma_E^0$ by using Eq. (6.4) with the symplectic matrices of Eqs. (6.20) and (6.22). In the final step, we separate the covariance matrix of the joint state as in Eq. (6.5), but we now take the local covariance matrix of the evolved ancilla (inside the covariance matrix of the evolved environemnt

[5]The no-signaling theorem have clear statement and proofs in [1, 2, 91].

σ_E^n), instead of taking the system's covariance matrix. The result for the first four evolved ancillae after their collisions is given in the following chain of equations

$$
\begin{aligned}
\sigma'_{A_1} &= s^2\sigma_S + c^2\sigma_{A_1}, \\
\sigma'_{A_2} &= c^2s^2\sigma_S + c^2\sigma_{A_2} + s^4\sigma_{A_1} - cs^2(\xi_{1,2} + \xi_{1,2}^\top), \\
\sigma'_{A_3} &= c^4s^2\sigma_S + c^2\sigma_{A_3} + s^4\sigma_{A_2} + c^2s^4\sigma_{A_1} + cs^4(\xi_{1,2} + \xi_{1,2}^\top) - c^2s^2(\xi_{1,3} + \xi_{1,3}^\top) - cs^2(\xi_{2,3} + \xi_{2,3}^\top), \\
\sigma'_{A_4} &= c^6s^2\sigma_S + c^2\sigma_{A_4} + s^4\sigma_{A_3} + c^2s^4\sigma_{A_2} + c^4s^4\sigma_{A_1} + c^3s^4(\xi_{1,2} + \xi_{1,2}^\top) + c^2s^4(\xi_{1,3} + \xi_{1,3}^\top) \\
&\quad - c^3s^2(\xi_{1,4} + \xi_{1,4}^\top) + cs^4(\xi_{2,3} + \xi_{2,3}^\top) - c^2s^2(\xi_{2,4} + \xi_{2,4}^\top) - cs^2(\xi_{3,4} + \xi_{3,4}^\top),
\end{aligned} \tag{6.35}
$$

where σ'_{A_j} is the covariance matrix of the ancilla j after its collision with the system. Analyzing the equations above, we induce that the covariance matrix an ancilla $n \geq 2$ after its collision with the system is given by

$$
\begin{aligned}
\sigma'_{A_n} &= c^{2n-1}s^2\sigma_S + s^4\sum_{k=1}^{n-1} c^{2(n-k-1)}\sigma_{A_k} + c^2\sigma_{A_n} + \sum_{m=1}^{n-1}\sum_{n'>m}^{n-1} c^{2n-2-n'-m}s^4(\xi_{m,n'} + \xi_{m,n'}^\top) \\
&\quad - \sum_{m=1}^{n-1} c^{n-m}s^2(\xi_{m,n} + \xi_{m,n}^\top).
\end{aligned} \tag{6.36}
$$

The equation above is quite general, but we can obtain more conclusive analysis by making some restrictions. For studying the Homogenization case, we suppose that all ancillae are initially identical $\sigma_{A_j} = \sigma_A$ for every j. After supposing it in the equation above, using the geometric sum and making algebraic simplifications, we obtain

$$
\begin{aligned}
\sigma'_{A_n} &= c^{2(n-1)}s^2(\sigma_S - \sigma_A) + \sigma_A + \sum_{m=1}^{n-1}\sum_{n'>m}^{n-1} c^{2n-n'-m-2}s^4(\xi_{m,n'} + \xi_{m,n'}^\top) \\
&\quad - \sum_{m=1}^{n-1} c^{n-m}s^2(\xi_{m,n} + \xi_{m,n}^\top).
\end{aligned} \tag{6.37}
$$

Clearly, for this case of initially identical ancillae, if we have null correlations terms and $|c| < 1$, then $\sigma_S^\infty = \sigma$. This means that, after a large number of collisions, the ancilla will practically not modify it's state after interacting with the system. This agrees with the last Homogenization condition (Eq. (2.48)) and it is the final step in order to show that, in the absence of initial correlations between the ancillae, our CM of system and

initially identical ancillae of bosonic modes, interacting via the BS, indeed corresponds to the Homogenization in the bosonic case.

Again, if we make a restriction over the correlations matrix, making it only distance dependent (Eq. (6.30)), we obtain

$$\sigma'_{A_n} = c^{2(n-1)}s^2(\sigma_S - \sigma_A) + \sigma_A + \sum_{m=1}^{n-1}\sum_{d=1}^{n-m-1} c^{2n-d-2m-2}s^4(\xi_d + \xi_d^\top) - \sum_{m=1}^{n-1} c^d s^2(\xi_d + \xi_d^\top). \tag{6.38}$$

In order to consider the cases studied in the previous Subsection for the system's evolution, we suppose Algebraically decaying correlations, given by Eq. (6.32). Using this type of correlations in the Equation above, we have, after using the geometric sum twice and making algebraic manipulations

$$\sigma'_{A_n} = c^{2(n-1)}s^2(\sigma_S - \sigma_A) + \sigma_A + \Gamma_n(K, gt)(\xi + \xi^\top), \tag{6.39}$$

where

$$\Gamma_n(K,\tau) = -s^2K\frac{cK^{-1} - (cK^{-1})^n}{1 - cK^{-1}} + \frac{s^4K}{c^2}\left(\frac{1}{cK-1}\frac{c^2 - c^{2n}}{s^2} - \frac{cK(c^{-1}K)^{1-n} - cK}{(cK-1)(1-c^{-1}K)}\right),$$
$$c = \cos(\tau),$$
$$\text{and} \quad s = \sin(\tau). \tag{6.40}$$

The function $\Gamma_n(K,\tau)$ will dictate the correlations effects on the n^{th} ancilla state after its collision with the system. This function vanishes at the limit of large n, verily

$$\begin{aligned}\Gamma_\infty(K,\tau) &= -s^2K\frac{cK^{-1}}{1-cK^{-1}} + s^4K\left(\frac{1}{(cK-1)s^2} + \frac{c^{-1}K}{(cK-1)(1-c^{-1}K)}\right)\\ &= -s^2K\frac{cK^{-1}}{1-cK^{-1}} + s^2K\left(\frac{cK^{-1}}{1-cK^{-1}}\right)\\ &= 0.\end{aligned} \tag{6.41}$$

Additionally, we see, from the plots of Figs. 6.2 and 6.3, that after oscillating in the first collision, the function $\Gamma_n(K,\tau)$ converges monotonically to 0 for large n. Therefore, the

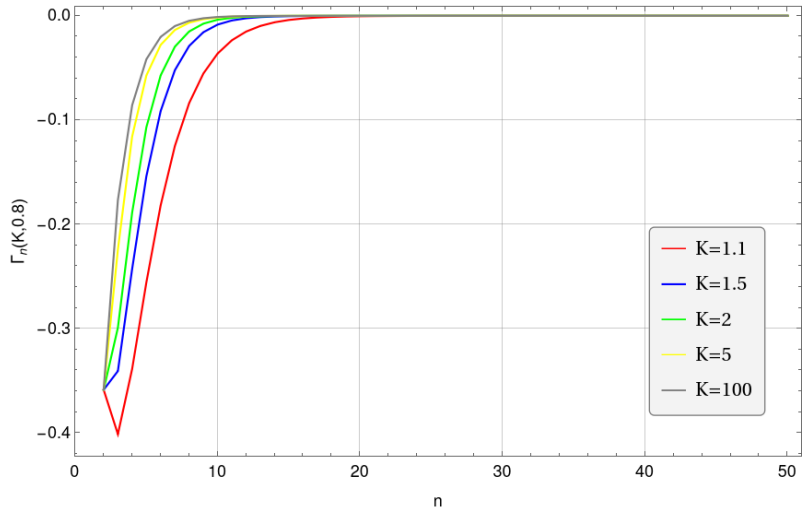

Figure 6.2: $\Gamma_n(K, gt) \times n$ for different values of K, for $g = 0.8$ and $t = 1$ fixed.

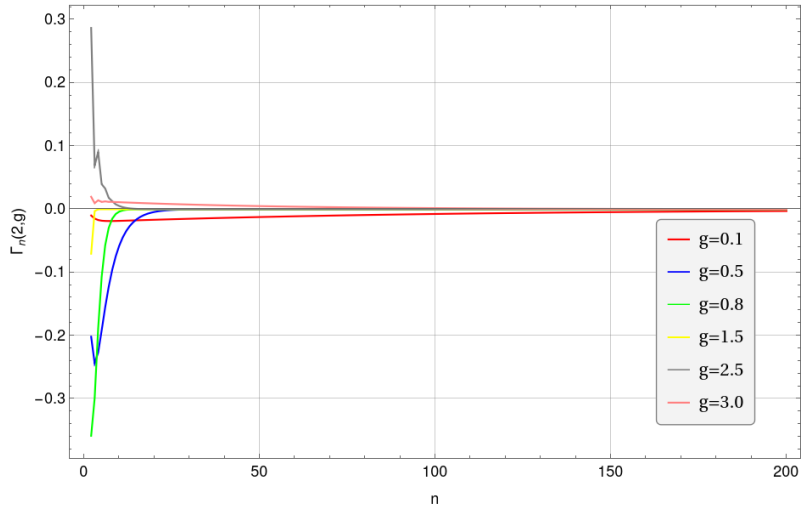

Figure 6.3: $\Gamma_n(K, gt) \times n$ for different values of g, for $K = 2$ and $t = 1$ fixed.

effects of correlations in each ancilla decrease as the ancillae collides with the system until they eventually vanish.

6.3 Constructing initially correlated ancillae from H-Graphs

In this Section, we describe a method for constructing an environment of bosonic ancillae whose correlations depend only on the distance between the ancillae. This justifies the form of the environment correlations supposed in the last Section (specially in Subsection 6.2.3) by means of a construction made with known systems and operations.

The procedure to create such environments is again by making use of *Hamiltonian*

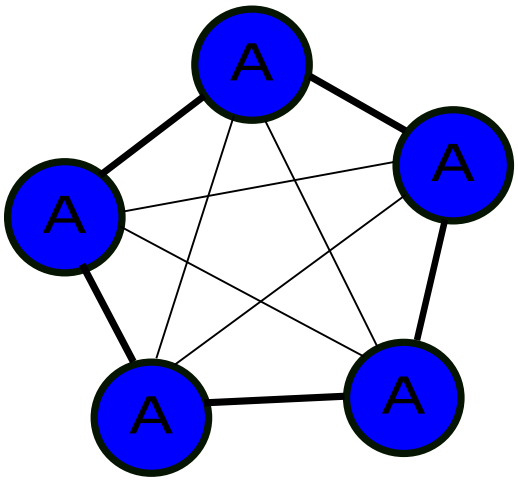

Figure 6.4: Example of a graph with ancillae in the vertices and the thickness of the edges between them represent the strength of the correlations (in this case the correlations are weaker for more distant ancillae), given by the adjacency matrix.

graph states or *H-graphs* [115, 131–135] and is completely analogous to the procedure presented in Section 5.1 for qubits ancillae. However, due to the versatile tools of continuous-variables, here we create a protocol of constructing environments with the desired form of distance dependent correlations by using H-graphs. The protocol is described as follows.

6.3.1 Constructing covariance matrix elements

If we want an environment with n bosonic modes, suppose initially that the environment state is in the n-mode vacuum $|\phi\rangle = |0\rangle^{\otimes n}$. To create graph states, first we define the unitary operator

$$\mathcal{V} = e^{-ik\sum_{i,j} G_{ij} H_{ij}}, \tag{6.42}$$

where G_{ij} are the elements of the adjacency matrix G representing a graph where the vertices are the ancillae and the edges represent the interactions between them (see Fig. 6.4) and

$$H_{ij} = \frac{i}{2}\sum_{ij}(\hat{a}_i^\dagger \hat{a}_j^\dagger - \hat{a}_i \hat{a}_j), \tag{6.43}$$

is the two-mode squeezing interaction Hamiltonian between the modes i and j, the operator $\hat{a}_i(\hat{a}_i^\dagger)$ correspond to the anihilattor (creator) operator of the mode i. And the graph

state is defined as the the application of this unitary in the vacuum

$$|\psi_E\rangle = \mathcal{V}\,|\phi\rangle\,. \tag{6.44}$$

With the canonical commutation relations, one can show that evolution of the canonical operators for each mode i will be given by

$$\mathcal{V}^\dagger \hat{q}_i \mathcal{V} = \sum_j M_{ij}\hat{q}_j \quad \text{and} \tag{6.45}$$

$$\mathcal{V}^\dagger \hat{p}_i \mathcal{V} = \sum_j M^{-1}_{ij}\hat{p}_j, \tag{6.46}$$

where

$$M = e^{Gk}. \tag{6.47}$$

Consequently, we can compute the average of the anti-commutators of the canonical operators, resulting in

$$\frac{1}{2}\langle\{q_i, q_j\}\rangle = \frac{1}{2}(MM^\top)_{ij}, \tag{6.48}$$

$$\frac{1}{2}\langle\{p_i, p_j\}\rangle = \frac{1}{2}[(M^\top M)^{-1}]_{ij}, \quad \text{and} \tag{6.49}$$

$$\langle q_i p_j\rangle = 0. \tag{6.50}$$

Supposing now that G is the adjacency matrix of a cyclic graph, then it must be a circulant matrix [136].[6] The diagonalization of such matrix is given by

$$G = \mathcal{O}\Lambda\mathcal{O}^\dagger, \tag{6.51}$$

where the elements of $\mathcal{O}$ are discrete Fourier transforms

$$\mathcal{O}_{l,m} = \frac{e^{i2\pi lm/n}}{\sqrt{n}},\ l, m = 0, \cdots, n-1, \tag{6.52}$$

[6] Remembering, cyclic graphs are graphs in which the connection strength between the vertices only depend on their distances. Hence the coefficients have the same value c_j for each diagonal and $c_j = c_{n-j}$, for every $0 \leq j \leq n-1$, since we demand that the adjacency matrix must be symmetric. See, for instance, Eq. (5.5).

and Λ is the matrix of eigenvalues $\Lambda_{l,m} = \delta_{l,m}\lambda_k$, where

$$\lambda_j = 2 \sum_{l=0}^{(n-1)/2} c_l \cos(2\pi l j/n), \tag{6.53}$$

assuming n odd for convenience.

From these equations and Eqs. (6.48), (6.49) and (6.50), we obtain, for cyclic graphs, after algebraic manipulations

$$\langle q_j q_{j'} \rangle = \frac{1}{2n} \sum_l \exp\left[i\frac{2\pi l}{n}(j-j') + 2k\lambda_l \right] \text{ and}$$
$$\langle p_j p_{j'} \rangle = \frac{1}{2n} \sum_l \exp\left[i\frac{2\pi l}{n}(j-j') - 2k\lambda_l \right].$$

This results in equal local covariance matrices for the ancillae

$$\sigma_A = \frac{1}{2n} \begin{pmatrix} \sum_{m=0}^{n-1} e^{2k\lambda_m} & 0 \\ 0 & \sum_{m=0}^{n-1} e^{-2k\lambda_m} \end{pmatrix}. \tag{6.54}$$

And correlations block matrices depending only on the distance between the ancillae

$$\xi_d = \begin{pmatrix} \xi_d^{(q)} & 0 \\ 0 & \xi_d^{(p)} \end{pmatrix}, \tag{6.55}$$

where

$$\xi_d^{(q)} = \langle q_j q_{j+d} \rangle = \frac{1}{2n} \sum_{m=0}^{n-1} e^{i2\pi dm/n + 2k\lambda_m} \text{ and} \tag{6.56}$$

$$\xi_d^{(p)} = \langle p_j p_{j+d} \rangle = \frac{1}{2n} \sum_{m=0}^{n-1} e^{i2\pi dm/n - 2k\lambda_m}. \tag{6.57}$$

6.3.2 Constructing desired correlations from choosing the cyclic graph

Here we describe a protocol of obtaining a desired form of correlation term $\xi_d^{(q)}$ by choosing properly the coefficients of the adjacency matrix.

First notice that we can rewrite Eq. (6.56) as

$$\xi_d^{(q)} = \sum_{l=0}^{n-1} a_l e^{i\theta_d l}, \tag{6.58}$$

where $a_l = \frac{e^{2k\lambda_l}}{2n}$ and $\theta_d = \frac{2\pi d}{n}$. Now, since $\lambda_{n-l} = \lambda_l$, we have that $a_{n-l} = a_l$, additionally, from $\lambda_l = \lambda_{-l}$ we also have $a_l = a_{-l}$. Using these facts, we can write[7]

$$\sum_{l=0}^{n-1} a_l e^{i\theta_d l} = \sum_{l=-(n-1)/2}^{(n-1)/2} a_l e^{i\theta_d l}. \tag{6.59}$$

Therefore, for large number of ancillae n, we can approximate $\xi_d^{(q)}$ to a Fourier Series

$$\xi_d^{(q)} = \sum_{l=-\infty}^{\infty} a_l e^{i\theta_d l}, \tag{6.60}$$

from which we can obtain the coefficient of the series

$$\boxed{a_l = \frac{1}{2\pi} \int_0^{2\pi} \xi_d^{(q)} e^{-i\theta_d l} d\theta_d,} \tag{6.61}$$

where $\theta_d = \frac{2\pi d}{n}$ approaches to a continuous variable due to the large n approximation.

We therefore obtained a formula for a_l given a desired form of distance dependent correlation $\xi_d^{(q)}$. Inverting the definition of a_l, we obtain the adjacency matrix G eigenvalues in function of $\xi_d^{(q)}$

$$\lambda_l = \frac{\log(2na_l)}{2k}. \tag{6.62}$$

Finally, from the eigenvalues of the circulant adjacency matrix G, we can obtain its coefficients by noticing that, from Eq. (6.53), if we go to the large n limit, the eigenvalues will also be a Fourier Series

$$\lambda(\theta_l) = \sum_{l=0}^{\infty} 2c_j \cos(j\theta_l), \tag{6.63}$$

where $\theta_l = \frac{2\pi l}{n}$. From this Fourier Series we obtain the coefficients

[7] One can prove this equation by noticing that $\sum_{l=0}^{n-1} a_l e^{i\theta_d l} = \sum_{l=0}^{(n-1)/2} a_l e^{i\theta_d l} + \sum_{l=(n+1)/2}^{n-1} a_l e^{i\theta_d l}$ and using $a_{n-l} = a_l$, $a_l = a_{-l}$ and $\theta_d = \frac{2\pi d}{n}$ to show that $\sum_{l=(n+1)/2}^{n-1} a_l e^{i\theta_d l} = \sum_{l=-(n-1)/2}^{-1} a_l e^{i\theta_d l}$.

$$c_0 = \frac{1}{4\pi}\int_{-\pi}^{\pi}\lambda(\theta_l)d\theta_l \text{ and} \tag{6.64}$$

$$c_j = \frac{1}{2\pi}\int_{-\pi}^{\pi}\lambda(\theta_l)\cos(j\theta_l)d\theta_l \text{ for } j \geq 1, \tag{6.65}$$

where θ_j approaches to a continuous variable for large n. Whence, from Eqs. (6.61), (6.62), (6.64) and (6.65) we have a procedure of obtaining the coefficients of the circulant adjacency matrix G from a desired correlation term $\xi_d^{(q)}$ depending on the distance between the ancillae.

6.3.3 Application to the Algebraically decaying correlations case

As an important example, which generate an environment as the one used in Subsection 6.2.3, we apply these results to find the coefficients for the adjacency matrix of the cyclic graph which generates the graph state environment with correlations depending on the distance d described by

$$\xi_d^{(q)} = K^{1-d}\xi_0^{(q)}, \tag{6.66}$$

where $\xi_0^{(q)}$ is a real number and $K > 1$.

From using Eq. (6.61), we obtain

$$a_l = 2nK\log(K)\frac{1-(-1)^l K^{-n/2}}{4\pi^2 l^2 + n^2\log^2(K)}\xi_0^{(q)}, \tag{6.67}$$

and after some manipulations we can write, for large n

$$a(\theta_l) = \frac{2K\log(K)}{n}\frac{1}{\theta_l^2 + \log^2(K)}\xi_0^{(q)},$$

where $\theta_l = \frac{2\pi l}{n}$. Moreover, from Eq. (6.62) we obtain

$$\lambda(\theta_l) = \left[\frac{1}{2k}\log(4K\log(K)) - \frac{1}{2k}\log\left(\theta_l^2 + \log^2(K)\right)\right]\xi_0^{(q)}.$$

Finally, for obtaining the coefficients of G, we must evaluate the integrals from Eqs.

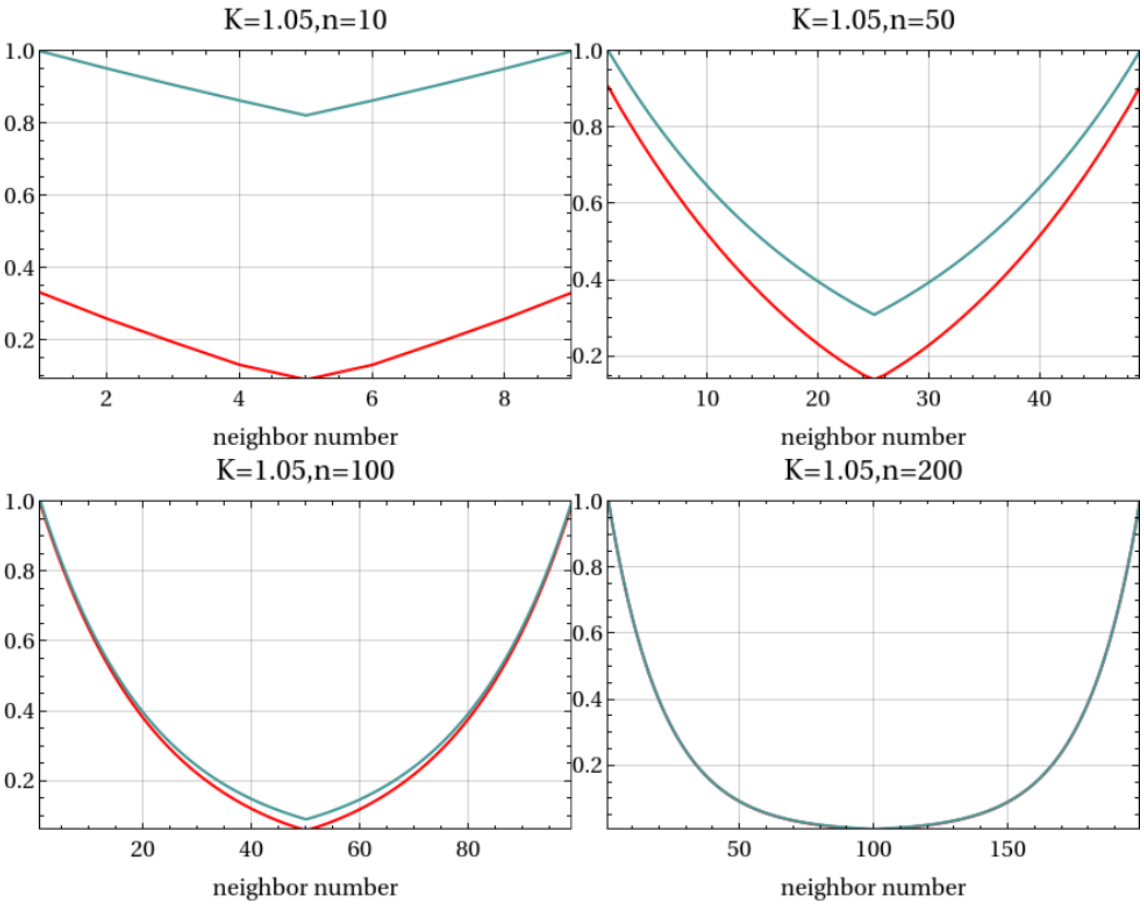

Figure 6.5: Correlations $(\xi_d^{(q)}) \times d$: distance of the neighbor ancilla from the first ancilla. The blue line is the correlation given by Eq. (6.66) mirrored from $n/2$, while the red line is the correlation of the graph state generated by our method. The parameters are $k = 1.0$, $\xi_0^{(q)} = 1.0$ and $K = 1.05$, with n indicated above the plots.

(6.64) and (6.65)

$$c_0 = \frac{1}{4\pi}\int_{-\pi}^{\pi}\left[\frac{1}{2k}\log(4K\log(K)) - \frac{1}{2k}\log\left(\theta_l^2 + \log^2(K)\right)\right]\xi_0^{(q)}d\theta_l \quad \text{and} \tag{6.68}$$

$$c_j = \frac{1}{2\pi}\int_{-\pi}^{\pi}\left[\frac{1}{2k}\log(4K\log(K)) - \frac{1}{2k}\log\left(\theta_l^2 + \log^2(K)\right)\right]\xi_0^{(q)}\cos(j\theta_l)d\theta_l \text{ for } j \geq 1. \tag{6.69}$$

To obtain such coefficients, these integrals must be computed numerically.

A cyclic graph has its vertices disposed in a form of a ring (see, for instance, Figs. 5.1 and 6.4). Therefore, if we want correlations in the form of Eq. (6.66), the correlations of the first ancilla with its neighbors will decay in relation to its nearest-neighbors and then raise again, since the last neighbors close the ring. In Figs. 6.5, 6.6, 6.7 and 6.8 we

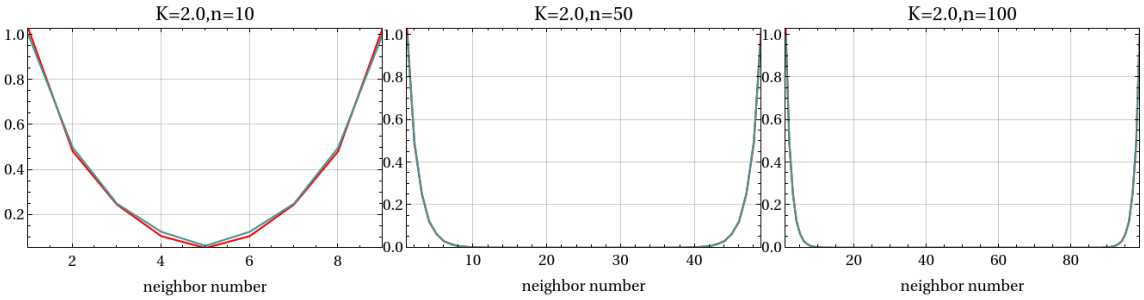

Figure 6.6: Correlations $(\xi_d^{(q)}) \times d$: distance of the neighbor ancilla from the first ancilla. The blue line is the correlation given by Eq. (6.66) mirrored from $n/2$, while the red line is the correlation of the graph state generated by our method. The parameters are $k = 1.0$, $\xi_0^{(q)} = 1.0$ and $K = 2.0$, with n indicated above the plots.

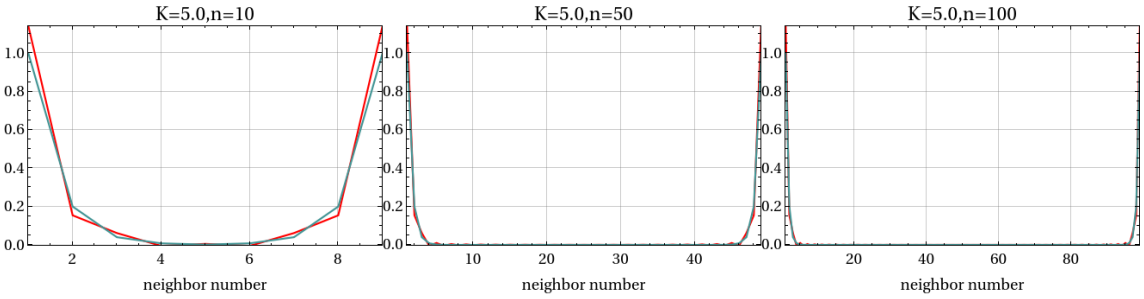

Figure 6.7: Correlations $(\xi_d^{(q)}) \times d$: distance of the neighbor ancilla from the first ancilla. The blue line is the correlation given by Eq. (6.66) mirrored from $n/2$, while the red line is the correlation of the graph state generated by our method. The parameters are $k = 1.0$, $\xi_0^{(q)} = 1.0$ and $K = 5.0$, with n indicated above the plots.

plotted the values of the correlations of the first ancilla with its neighbors. We computed the correlations according to Eq. (6.66) mirrored in $n/2$, mimicking the behaviour of the correlations between ancillae disposed in a ring form, and computed the correlations of the graph states generated by using Eqs. (6.68) and (6.69) to prepare the coefficients for the adjacency matrix G and using Eqs. (6.48), (6.49) and (6.50) to obtain the covariance matrix elements (and correlations) of the graph state. In these plots we can see a good match between the correlations generated by the graph states and the desired form of the mirrored Eq. (6.66).

From choosing the parameters $k = 1.0$ and $\xi_0^{(q)} = 1.0$ we see that our method using graph states creates the desired correlations mostly if K is not too close to 1.0, but for $K = 1.05$ a number of $n = 100$ of ancillae causes a match between the correlations which is almost perfect, as can be seen in Fig. 6.5. However, for values of K too big, we don't have a very satisfactory match, even for a number of $n = 100$ ancillae, as can be

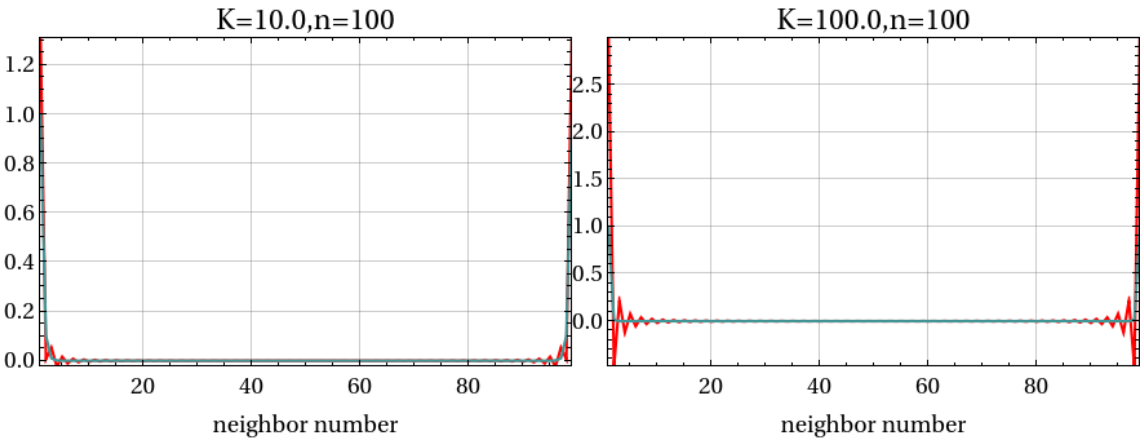

Figure 6.8: Correlations $(\xi_d^{(q)}) \times d$: distance of the neighbor ancilla from the first ancilla. The blue line is the correlation given by Eq. (6.66) mirrored from $n/2$, while the red line is the correlation of the graph state generated by our method. The parameters are $k = 1.0$, $\xi_0^{(q)} = 1.0$ and $n = 100$, with K indicated above the plots.

seen in Fig. 6.8.

Therefore, we conclude that for a region of $1.5 \lesssim K \lesssim 10.0$ and $n \gtrsim 50$, our method of creating an environment with correlations in the form of Eq. (6.66) with graph states is satisfactory.

6.3.4 Analysing $\xi_d^{(p)}$

If we use the method described above to create the desired correlations $\xi_d^{(q)}$ in graph states, we automatically constrain the correlations referring to the $\xi_d^{(p)}$ canonical operators $\hat{p}$. In fact, from Eq. (6.57), we can write

$$\xi_d^{(p)} = \sum_{l=-(n-1)/2}^{(n-1)/2} b_l e^{i2\pi dl/n}, \tag{6.70}$$

where $b_l = \frac{e^{-2k\lambda_k}}{2n}$. And we also have, by definition, that the coefficient of the correlation $\xi_d^{(q)}$ is $a_l = \frac{e^{2k\lambda_k}}{2n}$, therefore we can relate them by

$$\boxed{b_l = \frac{1}{4a_l n^2},} \tag{6.71}$$

from which we conclude that $\xi_d^{(p)}$ is completely fixed by $\xi_d^{(q)}$.

As an example, we take again the case of Algebraic correlations from Eq. (6.66). In

this case we have, from the equation above and from Eq. (6.67), for large n

$$b_l = \frac{4\pi^2 l^2 + n^2 \log(K)^2}{2nK\log(K)} \frac{1}{4n^2}. \tag{6.72}$$

Applying this in Eq. (6.70) and making a large n approximation, we obtain

$$\begin{aligned} \xi_d^{(p)} &= \sum_{l=-(n-1)/2}^{(n-1)/2} \frac{4\pi^2 l^2 + n^2 \log(K)^2}{2nK\log(K)} \frac{1}{4n^2} e^{i2\pi dl/n} \\ &\approx \int_{-\pi}^{\pi} \frac{\theta^2 + \log(K)^2}{16\pi K \log(K)} e^{i\theta d} d\theta \\ &= \frac{(-1)^d}{4\pi K \log(K) d^2}. \end{aligned} \tag{6.73}$$

Therefore, for creating a correlation of Eq. (6.66) type for $\xi_d^{(q)}$, we must obtain an oscillating correlation decaying with d^2 type for $\xi_d^{(p)}$. This oscillating $\xi_d^{(p)}$ is also obtained, for instance, if we create prepare the correlations from a nearest-neighbor interaction graph state (see Ref. [93]).

Fortunately, despite we cannot create correlation terms $\xi_d^{(q)}$ and $\xi_d^{(p)}$ which decay equally with the distance, their effect in the initially correlated CM always act linearly in the system's evolution (see Eq. (6.31)). Hence, such correlations affect differently the system's evolution and can be computed separately.

Chapter 7

Obtaining Observables Shifts Using QBNs

This is the first Chapter about the second main project of this thesis. This project has as its principal goal to compute the statistics of the heat distribution between two initially correlated parties using Quantum Bayesian Networks (QBNs), described in Subsection 3.4.2. The QBN formalism, inspired mostly in Ref. [48], has the advantage of estimating a probability distribution for a *process* to happen during a system's evolution without supposing that a measurement is made. This is opposite to the most commonly used *Two-Point Measurement (TPM)* protocol [33–35]. For the TPM protocol, two measurements are made to obtain the outcome of a desired observable for the party of interest at two points in time, this way the change of the observable is obtained during the process. The unwanted character of this procedure is the fact that after each measurement the backaction completely destroys the coherence of the joint state density matrix, therefore consuming the quantum correlation between the parties. The presence of initial correlations can cause interesting effects on thermodynamic processes, one of our main influences is the inversion of heat flow caused by initial correlations [50–53]. Hence, finding a reliable way of computing the statistics of observable in such processes can be a fruitful objective.

The major goal of finding the heat distribution with the use of QBNs is achieved for a particular case in Chapter 8, when we compute the heat distribution between two initially correlated bosonic modes. In this present Chapter we construct a more general formalism used to compute the statistics for the change of any local observable during a process in

which the party of a joint system evolves. In the second part of the Chapter we apply, as an example, such general results for the case where the two parties are qubits, recovering part of the results of Refs. [48] and [54]. In the final part of the Chapter, we bring our analysis about the consequences of choosing different ensembles for the initial density matrix of the joint system over the QBN statistics, since we found out that this statistics is dependent on the initial density matrix ambiguity of mixtures. This last enquiry creates important interpretative caveats and thus will be one of the main questionings of this project.

7.1 General results

7.1.1 Statement of the problem

The setup is the same as the one described in Subsection 3.4.2. As already stated, the system is composed by to parties A and B and we suppose that they evolve according to a unitary operator $U(t)$. The joint system starts its evolution in the state

$$\rho_{AB}(0) = \sum_s P_s \left|\psi_s(0)\right\rangle \left\langle\psi_s(0)\right|, \tag{7.1}$$

where $\{P_s, |\psi_s(0)\rangle\}_s$ is an ensemble of quantum states, and we have the observable $\mathcal{O}_A(t)$ (which can be time dependent) acting in A and $\mathcal{O}_B(t)$ in B with eigenvalues (eigenvectors) $\{a_i(t)\}_i$ ($\{|a_i(t)\rangle\}_i$) and $\{b_j(t)\}_j$ ($\{|b_j(t)\rangle\}_j$), respectively. Then, the QBN infer that the probability of the joint system to be in the states $(|a_0, b_0\rangle, |a_1, b_1\rangle \cdots, |a_n, b_n\rangle)$ in the respective time instants $(0, t_1, \cdots, t_n)$ is (see the deduction of Eq. (3.44) and Fig. 3.4 for the Beaysian Network graph)

$$P(a_0, b_0, a_1, b_1, \cdots, a_n, b_n) = \sum_s P_s P(a_0, b_0|\psi_s(0)) P(a_1, b_1|\psi_s(t_1)) \cdots P(a_n, b_n|\psi_s(t_n)), \tag{7.2}$$

where

$$\begin{aligned} P(a_k, b_k|\psi_s(t)) &= |\langle a_k, b_k|\psi_s(t)\rangle|^2 \\ &= |\langle a_k, b_k| U(t) |\psi_s(0)\rangle|^2 \end{aligned} \tag{7.3}$$

is the conditional probability for the joint state to be in $|a_k, b_k\rangle$ given that the system started at $|\psi_s(0)\rangle$.

Here we use the BQN formalism to infer the statistics of the observable $\mathcal{O}_A(t)$ *change* $\Delta\mathcal{O}_A$ during a proces, i.e., as the system evolves between two points in time. Accordingly, we only need the conditional trajectory probability distribution of Eq. (7.2) for two points in time

$$\mathcal{P}(a_0, b_0, a_t, b_t) = \sum_s P_s P(a_0, b_0|\psi_s(0)) P(a_t, b_t|\psi_s(t)), \tag{7.4}$$

where we rename $t_1 = t$ and $a_1(b_1) = a_t(b_t)$.

Importantly, this conditional trajectory probability distribution satisfies standard probability distribution marginalization properties. Consider, for instance,

$$\begin{aligned} \sum_{b_0,b_t} \mathcal{P}(a_0, b_0, a_t, b_t) &= \sum_{b_0,b_t,s} P_s |\langle a_0, b_0|\psi_s(0)\rangle|^2 |\langle a_t, b_t|\psi_s(t)\rangle|^2 \\ &= \sum_s P_s \langle\psi_s(0)|a_0\rangle \left(\sum_{b_0} |b_0\rangle\langle b_0|\right) \langle a_0|\psi_s(0)\rangle \langle\psi_s(t)|a_t\rangle \left(\sum_{b_t} |b_t\rangle\langle b_t|\right) \langle a_t|\psi_s(t)\rangle \\ &= \sum_s P_s |\langle a_0|\psi_s(0)\rangle|^2 |\langle a_t|\psi_s(t)\rangle|^2 \\ &= \mathcal{P}(a_0, a_t). \end{aligned} \tag{7.5}$$

And analogously, we have $\sum_{a_0,a_t} \mathcal{P}(a_0, b_0, a_t, b_t) = \mathcal{P}(b_0, b_t)$. Furthermore, consider the

sum

$$\begin{aligned}\sum_{a_0,b_0}\mathcal{P}(a_0,b_0,a_t,b_t) &= \sum_{s,a_0,b_0} P_s|\left\langle a_0,b_0|\psi_s(0)\right\rangle|^2|\left\langle a_t,b_t|\psi_s(t)\right\rangle|^2 \\ &= \sum_s P_s\left\langle\psi_s(0)\right|\left(\sum_{a_0,b_0}|a_0,b_0\rangle\left\langle a_0,b_0\right|\right)|\psi_s(0)\rangle\left\langle\psi_s(t)|a_t,b_t\right\rangle\left\langle a_t,b_t|\psi_s(t)\right\rangle \\ &= \left\langle a_t,b_t\right|\left(\sum_s P_s|\psi_s(t)\rangle\left\langle\psi_s(t)\right|\right)|a_t,b_t\rangle \\ &= \left\langle a_t,b_t\right|\rho_{AB}(t)\,|a_t,b_t\rangle\,, \end{aligned} \tag{7.6}$$

which is the standard probability distribution $P(a_t,b_t)$ obtained from the postulates of Quantum Mechanics. Analogously we also obtain $\sum_{a_t,b_t}\mathcal{P}(a_0,b_0,a_t,b_t) = \left\langle a_0,b_0\right|\rho_{AB}(0)\,|a_0,b_0\rangle$.

With the use of this conditional probability, we can construct the probability of obtaining a change Δa in the observable $\mathcal{O}_A(t)$ during two points in time

$$\boxed{p(\Delta\mathcal{O}_A=\Delta a)=\sum_{a_t,a_0}\delta(\Delta a-(a_t-a_0))\mathcal{P}(a_0,a_t).} \tag{7.7}$$

Our main enquiry in this Chapter and in Chapter 8 is to investigate the aspects of this probability distribution, and how the initial correlations between the parts of the global system affect it. Notice that this change can represent thermodynamic quantities. For instance, for the case where $\mathcal{O}_A$ is the Hamiltonian of the subsystem A, for a global time-independent Hamiltonian, the quantity $\Delta\mathcal{O}_A$ will be the heat.

7.1.2 Characteristic function of the change probability distribution

In order to obtain an useful expression for the probability distribution of Eq. (7.7), we can resort to the characteristic function of it

$$G_{\mathcal{O}_A}(k)=\int_{-\infty}^{\infty}(d\Delta a)\,e^{ik\Delta a}\,p(\Delta\mathcal{O}_A=\Delta a). \tag{7.8}$$

Using Eq. (7.7) in the definition above, we obtain

$$G_{\mathcal{O}_A}(k)=\sum_{a_0,a_t}e^{ik(a_t-a_0)}\mathcal{P}(a_0,a_t). \tag{7.9}$$

Proceeding, we expand the distribution $\mathcal{P}(a_0, a_t)$ in the equation above, then we have[1]

$$\begin{aligned}
G_{\mathcal{O}_A}(k) &= \sum_{a_t,a_0,s} e^{ik(a_t-a_0)} P_s |\langle a_0|\psi_s\rangle|^2 |\langle a_t| U(t) |\psi_s\rangle|^2 \\
&= \sum_{a_t,a_0,s} P_s \langle a_0|\psi_s\rangle\langle\psi_s|e^{-ika_0}|a_0\rangle\langle a_t|U(t)|\psi_s\rangle\langle\psi_s|U^\dagger(t)e^{ika_t}|a_t\rangle \\
&= \sum_{a_t,a_0,s} P_s \langle a_0|\psi_s\rangle\langle\psi_s|e^{-ik\mathcal{O}_A(0)}|a_0\rangle\langle a_t|U(t)|\psi_s\rangle\langle\psi_s|U^\dagger(t)e^{ik\mathcal{O}_A(t)}|a_t\rangle \\
&= \sum_s P_s \langle\psi_s|e^{-ik\mathcal{O}_A(0)} \left(\sum_{a_0} |a_0\rangle\langle a_0|\right) |\psi_s\rangle\langle\psi_s|U^\dagger(t)e^{ik\mathcal{O}_A(t)} \left(\sum_{a_t} |a_t\rangle\langle a_t|\right) U(t)|\psi_s\rangle \\
&= \sum_s P_s \langle\psi_s| e^{-ik\mathcal{O}_A(0)} |\psi_s\rangle \langle\psi_s| U^\dagger(t)e^{ik\mathcal{O}_A(t)}U(t) |\psi_s\rangle . \qquad (7.10)
\end{aligned}$$

From which we obtain the result

$$\boxed{G_{\Delta\mathcal{O}_A}(k) = \sum_s P_s \langle\psi_s| e^{-ik\mathcal{O}_A(0)} |\psi_s\rangle \langle\psi_s| e^{ik\mathcal{O}_{A_H}(t)} |\psi_s\rangle .} \qquad (7.11)$$

where

$$\mathcal{O}_{A_H}(t) = U^\dagger(t)\mathcal{O}_A(t)U(t) \qquad (7.12)$$

is the operator $\mathcal{O}_A(t)$ in the Heisenberg picture.

An important comment that can be made here about the characteristic function of Eq. (7.11) is that it has a non-trivial dependence on the choice for the ensemble of pure states to represent the initial density matrix of the joint state (Eq. (7.1)).

7.1.3 Statistical moments of the change probability distribution

An important utility for the characteristic function is that we can easily obtain formulae for the statistic moments of the random variables from it. This can be done, for the characteristic function of the distribution above, by the equation[2]

$$\langle(\Delta\mathcal{O}_A)^n\rangle = (-i)^n \frac{\partial^n \left(G_{\mathcal{O}_A}(k)\right)}{\partial k^n}\Big|_{k=0}. \qquad (7.13)$$

[1] From now on, we call $|\psi_s\rangle = |\psi_s(0)\rangle$ for simplicity.

[2] This relation between statistical moments and the characteristic function can be obtained simply by direct differentiation of Eq. (7.8) and setting $k = 0$.

Using this equation in the result of Eq. (7.11), we obtain the average of $\mathcal{O}_A(t)$

$$\boxed{\langle \Delta \mathcal{O}_A \rangle = \sum_s P_s \langle \psi_s | \left(\mathcal{O}_{A_H}(t) - \mathcal{O}_A(0) \right) | \psi_s \rangle ,} \tag{7.14}$$

which can be rewritten as

$$\boxed{\langle \Delta \mathcal{O}_A \rangle = \mathrm{Tr} \left\{ (\mathcal{O}_{A_H}(t) - \mathcal{O}_A(0)) \rho_{AB}(0) \right\} .} \tag{7.15}$$

And obtain the second moment of $\mathcal{O}_A(t)$

$$\boxed{\langle (\Delta \mathcal{O}_A(t))^2 \rangle = \sum_s P_s \left(\langle \psi_s | \left((\mathcal{O}_{A_H}(t))^2 + (\mathcal{O}_A(0))^2 \right) | \psi_s \rangle - 2 \langle \psi_s | \mathcal{O}_A(0) | \psi_s \rangle \langle \psi_s | \mathcal{O}_{A_H}(t) | \psi_s \rangle \right) .} \tag{7.16}$$

For higher moments the results will be more complex, but with similar aspect. We restrict the focus to these two moments since they will already expose the desired attributes of the probability distribution for our analysis.

7.1.4 Comparison with TPM

Here we will compare our results for the statistics obtained using QBN with the standard TPM statistics.[3] The TPM supposes that measurements are made for two points in time in order to obtain the variation (or change) of some observable. So, supposing the same bipartite setup presented to the QBN case in Subsection 7.1.1, we additionally suppose that a projective measurements is made initially in the eigenbasis $\{|a_0\rangle\}_{a_0}$ of the operator $\mathcal{O}_A(0)$ and finally in the eigenbasis $\{|a_t\rangle\}_{a_t}$ of the operator $\mathcal{O}_A(t)$. The probability of the initial global system $\rho_{AB}(0)$ to have outcomes a_0 and a_t, respectively, in these two measurements is

$$\mathcal{P}_{\text{TPM}}(a_0, a_t) = P(a_t|a_0)P(a_0), \tag{7.17}$$

where $P(a_0) = P_{a_0} = \langle a_0 | \rho_A(0) | a_0 \rangle$, with $\rho_A = \mathrm{Tr}_B(\rho_{AB}(0))$, is the probability of the first measurement to have an outcome a_0. While $P(a_t|a_0)$ is the probability of having an outcome a_t for the second measurement after the backaction of the first measurement and

[3] In Section II of Ref. [34] the TPM statistics is presented in details.

the evolution between them

$$P(a_t|a_0) = \mathrm{Tr}\left\{|a_t\rangle\langle a_t| U(t)\rho'_{AB}(0)U^\dagger(t)|a_t\rangle\langle a_t|\right\}, \tag{7.18}$$

where $\rho'_{AB}(0) = \frac{|a_0\rangle\langle a_0|\rho_{AB}(0)|a_0\rangle\langle a_0|}{P_{a_0}}$ is the backaction of ρ after the first measurement and $U(t)$ is the unitary evolution operator between the two measurements.

If now we desire to obtain the probability of a change Δa in the observable $\mathcal{O}_A(t)$ with this probability distribution, we define

$$p_{\text{TPM}}(\Delta\mathcal{O}_A = \Delta a) = \sum_{a_t,a_0} \delta(\Delta a - (a_t - a_0))\mathcal{P}_{\text{TPM}}(a_0, a_t). \tag{7.19}$$

Using Eqs. (7.17) and (7.18), we obtain (see Appendix D for the computation) the following characteristic function for this probability distribution

$$G_{\mathcal{O}_{A_{\text{TPM}}}}(k) = \mathrm{Tr}\left\{e^{ik\mathcal{O}_{A_H}(t)}e^{-ik\mathcal{O}_A(0)}\mathcal{D}_{\mathcal{O}_A(0)}(\rho_{AB}(0))\right\}, \tag{7.20}$$

where $\mathcal{D}_{\mathcal{O}_A(0)}(\bullet) = \sum_{a_0}|a_0\rangle\langle a_0|\bullet|a_0\rangle\langle a_0|$ is the *dephasing operator* for the eigenvectors $\{|a_0\rangle\}_{a_0}$ of $\mathcal{O}_A(0)$.

The only dependence of the joint system initial state in this characteristic functions is given by $\mathcal{D}_{\mathcal{O}_A(0)}(\rho_{AB}(0))$. Thus all contributions from the initial coherence, in the eigenbasis of $\mathcal{O}_A(0)$ vanish in contrast with the QBN characteristic function of Eq. (7.11) which takes into account the coherence of the initial state. Importantly, the QBN characteristic function of Eq. (7.11) *is equivalent* to the TPM characteristic function in Eq. (7.20) for the case where $[\rho_{AB}(0), \mathcal{O}_A(0)] = 0$, which is the case where there is no coherence for the initial state in the eigenbasis of $\mathcal{O}_A(0)$.

7.2 Application to qubits

Here we apply our general results to the case where the systems A and B are qubits. As already said, our main goal is to obtain the heat probability distribution during an interaction taking into account the effects of the initial correlations between the parties. Among other results, this predicts the inversion of the heat flow caused by initial correlations.

The first experimental observation of this fact was obtained for this two-qubit setup in Ref. [54] and we describe this statistics with our results using QBNs. Reference [48], which initially proposed QBNs, also described the statistics of [54] using QBNs. Thus our analysis with two-qubit systems will serve as a sanity check for our methods of obtaining the statistical moments of the heat probability distribution and its characteristic function.

7.2.1 Setup and statistical moments

We suppose that the two qubits have local Hamiltonians $H_{A(B)} = \omega_0(1 - \sigma_z^{A(B)})/2$, interacting via the unitary

$$U(g,t) = e^{-it\frac{\pi}{2g}(\sigma_+^A \otimes \sigma_-^B + \sigma_-^A \otimes \sigma_+^B)}, \tag{7.21}$$

for $\sigma_{+(-)}$ defined according to Eq. (2.33). The joint system starts at the state

$$\rho_{AB}(0) = \rho_{\text{th}}^A \otimes \rho_{\text{th}}^B + \chi_{AB}, \tag{7.22}$$

where

$$\rho_{\text{th}}^{A(B)} = \frac{1}{(1 + e^{-\omega_0 \beta_{A(B)}})} \begin{pmatrix} 1 & 0 \\ 0 & e^{-\omega_0 \beta_{A(B)}} \end{pmatrix},$$

are the locally thermal states[4] and the term

$$\chi_{AB} = \begin{pmatrix} 0 & 0 & 0 & 0 \\ 0 & 0 & \alpha & 0 \\ 0 & \alpha^* & 0 & 0 \\ 0 & 0 & 0 & 0 \end{pmatrix},$$

is responsible for the coherence and correlations between the parties with α satisfying $|\alpha| \leq \exp\left[-\omega_0(\beta_A + \beta_B)\right] / \left((1 + e^{-\omega_0 \beta_A})(1 + e^{-\omega_0 \beta_B})\right)$ for the positivity of the density

[4] These locally thermal states are different from the one described at Appendix A, Section A.4, only due their local Hamiltonians. Also, the unitary of Eq. (7.21) is simply the Partial SWAP of Eq. (2.44) multiplied by a phase. The slight differences in these definitions from the previous Chapters are made in order to have a better comparison with the results of Ref. [48].

matrix. In fact, the mutual information between the parties is 0 when α is null and reaches its maximum when $|\alpha| = |\alpha^*| = \exp\left[-\omega_0(\beta_A+\beta_B)\right] / \left((1+e^{-\omega_0\beta_A})(1+e^{-\omega_0\beta_B})\right)$, as well its *geometrical quantum discord*[5] has its maximum when $\alpha = \pm i|\alpha^*|$ [54].

We define the *heat* received by the subsystem A as the change of the local Hamiltonian H_A during the evolution from time 0 to t

$$\mathcal{Q}_A(t) = \Delta H_A. \tag{7.23}$$

Using the result of Eq. (7.14) for the average of the change of an operator, we have

$$\langle \mathcal{Q}_A(t) \rangle = \mathrm{Tr}\left\{ \left(U^\dagger(g,t) H_A U(g,t) - H_A \right) \rho_{AB}(0) \right\}. \tag{7.24}$$

Computing the trace under the conditions described above, we obtain

$$\langle \mathcal{Q}_A(t) \rangle = \omega_0 \left[\mathrm{Im}(\alpha) \sin\left(\frac{\pi t}{g}\right) + \frac{1}{2}\sin^2\left(\frac{\pi t}{2g}\right)\left(\tanh\left(\frac{\omega_0\beta_A}{2}\right) - \tanh\left(\frac{\omega_0\beta_B}{2}\right)\right)\right]. \tag{7.25}$$

This result describes correctly the heat flow inversion caused by the initial correlations between the two qubits. This can be achieved for negative values of $\mathrm{Im}(\alpha)$, as can be seen in Fig. 7.1. In this figure we can spot the heat average initially going from the colder system A to the hotter system B for the cases where $\mathrm{Im}(\alpha) < 0$ and a stronger manifestation of such effect for the case with maximum correlation, i.e., for $\mathrm{Im}(\alpha) = -\frac{e^{-\omega_0(\beta_A+\beta_B)/2}}{(1+e^{-\omega_0\beta_A})(1+e^{-\omega_0\beta_B})}$.

Additionally, with the result of Eq. (7.16), we can obtain the second moment of the heat probability distribution

$$\begin{aligned}\langle \mathcal{Q}_A^2(t) \rangle = &\sum_i \lambda_i (\langle\lambda_i| \left((U^\dagger(g,t) H_A U(g,t))^2 + H_A^2 \right) |\lambda_i\rangle \\ &- 2\langle\lambda_i| H_A |\lambda_i\rangle \langle\lambda_i| U^\dagger(g,t) H_A U(g,t) |\lambda_i\rangle),\end{aligned} \tag{7.26}$$

where $\{\lambda_i\}_i$ and $\{|\lambda_i\rangle\}_i$ are the eigenvalues and eigenvectors of the initial density matrix $\rho_{AB}(0)$. We *choose* to compute the second moment in the eigenvector ensemble of the initial density matrix since it is the ensemble which causes the smaller variance (to

[5] An alternative quantifier of quantum discord [137, 138]

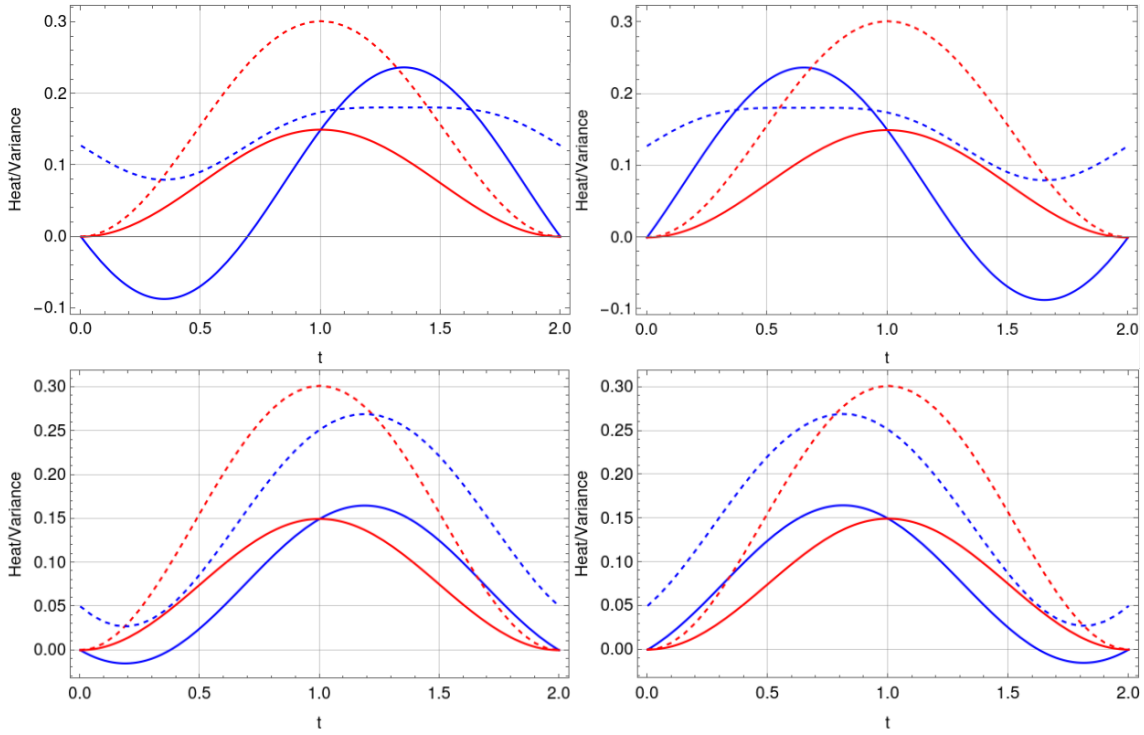

Figure 7.1: Heat (in unites of ω_0)/ Variance of the heat (in unites of ω_0^2) $\times$ t. The blue lines represent the heat received by A and the blue dashed lines represent the variance of the heat when the the qubits are initially correlated. The red lines represent the heat received by A and the red dashed lines represent the variance of the heat when the the qubits are initially uncorrelated. The parameters are $g = 1$, $\beta_A = 2/\omega_0$ and $\beta_B = 1/\omega_0$. Each plot has a different value of α. In the first line we have, from left to right, $\mathrm{Im}(\alpha) = -\frac{e^{-\omega_0(\beta_A+\beta_B)/2}}{(1+e^{-\omega_0\beta_A})(1+e^{-\omega_0\beta_B})}$ and $\mathrm{Im}(\alpha) = +\frac{e^{-\omega_0(\beta_A+\beta_B)/2}}{(1+e^{-\omega_0\beta_A})(1+e^{-\omega_0\beta_B})}$, and in the second line $\mathrm{Im}(\alpha) = -1/20$ and $\mathrm{Im}(\alpha) = +1/20$.

be seen in the next section). With this, we compute (see Fig. 7.1) numerically the heat variance $\mathrm{Var}(\mathcal{Q}_A)(t) = \langle \mathcal{Q}_A^2(t) \rangle - \langle \mathcal{Q}_A(t) \rangle^2$ for different choices of α for $\beta_A = 2/\omega_0$ and $\beta_B = 1/\omega_0$, i.e., initially A colder than B. For both negative and positive values of $\mathrm{Im}(\alpha)$, the presence of correlations decreases considerably the maximum of the variance. Interestingly, for the cases where the mutual information has its maximum $\mathrm{Im}(\alpha) = \pm \frac{e^{-\omega_0(\beta_A+\beta_B)/2}}{(1+e^{-\omega_0\beta_A})(1+e^{-\omega_0\beta_B})}$ we have a higher diminishing of the variance than in the smaller correlation case of $\mathrm{Im}(\alpha) = \pm 1/20$. This seems to indicate that the greater the correlations, the smaller the variance.

7.2.2 Obtaining the probability distribution

We can compute the characteristic function for the heat probability distribution using the result of Eq. (7.11) to the conditions above, obtaining

$$G_{\mathcal{Q}_A}(k) = \sum_s \lambda_s \langle \lambda_s | e^{-ikH_A} | \lambda_s \rangle \langle \lambda_s | e^{ikU^\dagger(g,t)H_A U(g,t)} | \lambda_s \rangle . \tag{7.27}$$

As a sanity check, we computed the probability distribution of the heat from this characteristic function numerically by applying the inverse Fourier transform on it for a set of parameters. We compared it to the probability distributions obtained in Ref. [48] and they matched perfectly.

The probability distributions of Ref. [48] are

$$P(\mathcal{Q}_A = -\omega_0) = \frac{e^{\omega_0\beta_B}\left(e^{\omega_0\beta_A/2}\cos\left(\frac{\pi t}{2g}\right) + e^{\omega_0\beta_B/2}\sin\left(\frac{\pi t}{2g}\right)\right)^2}{\left(e^{\omega_0\beta_A}+1\right)\left(e^{\omega_0\beta_B}+1\right)\left(e^{\omega_0\beta_A}+e^{\omega_0\beta_B}\right)},$$

$$P(\mathcal{Q}_A = 0) = \frac{\left(e^{\omega_0\beta_A}+e^{\omega_0\beta_B}\right)\left(2+e^{\omega_0\beta_A}+e^{\omega_0\beta_B}+2e^{\omega_0(\beta_A+\beta_B)}\right) + \left(e^{\omega_0\beta_A}-e^{\omega_0\beta_B}\right)^2\cos\left(\frac{\pi t}{g}\right)}{2\left(e^{\omega_0\beta_A}+1\right)\left(e^{\omega_0\beta_B}+1\right)\left(e^{\omega_0\beta_A}+e^{\omega_0\beta_B}\right)}$$
$$+ \frac{2e^{\omega_0(\beta_A+\beta_B)/2}\left(e^{\omega_0\beta_A}-e^{\omega_0\beta_B}\right)\sin\left(\frac{\pi t}{g}\right)}{2\left(e^{\omega_0\beta_A}+1\right)\left(e^{\omega_0\beta_B}+1\right)\left(e^{\omega_0\beta_A}+e^{\omega_0\beta_B}\right)},$$

$$P(\mathcal{Q}_A = +\omega_0) = \frac{e^{\omega_0\beta_A}\left(e^{\omega_0\beta_B/2}\cos\left(\frac{\pi t}{2g}\right) - e^{\omega_0\beta_A/2}\sin\left(\frac{\pi t}{2g}\right)\right)^2}{\left(e^{\omega_0\beta_A}+1\right)\left(e^{\omega_0\beta_B}+1\right)\left(e^{\omega_0\beta_A}+e^{\omega_0\beta_B}\right)}.$$

As an example, in Fig. 7.2 we plot the probability distributions of $\mathcal{Q}_A = -\omega_0$, $\mathcal{Q}_A = 0$ and $\mathcal{Q}_A = +\omega_0$ computed numerically for initial states $\rho_{AB}(0)$ with $\beta_A = 2/\omega_0$, $\beta_B =$

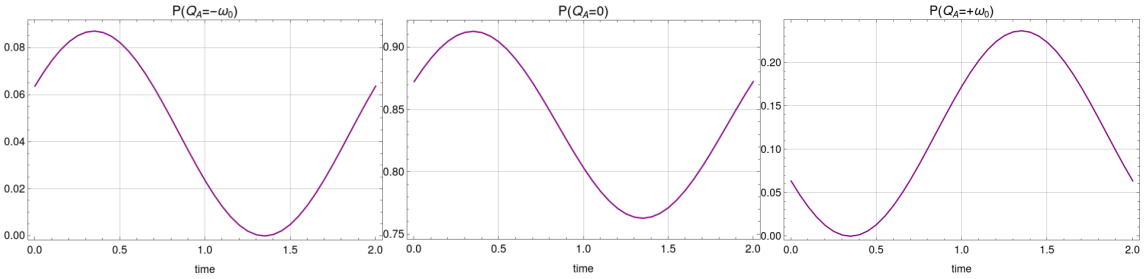

Figure 7.2: $P(\mathcal{Q}_A) \times t$, for different values of $\mathcal{Q}_A$, computed numerically with the inverse Fourier transform of the characteristic function of Eq. (7.27). The initial joint state is prepared at $\rho_{AB}(0)$ of Eq. (7.22) with $\beta_A = 2/\omega_0$, $\beta_B = 1/\omega_0$, $\alpha = -i\frac{e^{-\omega_0(\beta_A+\beta_B)/2}}{(1+e^{-\omega_0\beta_A})(1+e^{-\omega_0\beta_B})}$ and we have $g = 1$.

$1/\omega_0$ and $\alpha = -i\frac{e^{-\omega_0(\beta_A+\beta_B)/2}}{(1+e^{-\omega_0\beta_A})(1+e^{-\omega_0\beta_B})}$ during an evolution in time. These plots match perfectly with the curves of the probabilities above.

7.3 Dependence on the ambiguity of mixtures

In the results of Eqs. (7.11) and (7.16) an explicit dependence can be verified of the characteristic function and of the second moment of the change $\Delta\mathcal{O}_A$ on the choice of the ensemble of states $\{P_s,\ |\psi_s\rangle\}_s$ for the mixture of states in the initial density matrix of Eq. (7.1).[6] Therefore, this dependence is present in the probability distribution of $\Delta\mathcal{O}_A$. The dependence is a consequence from the fact that our construction of the QBN is a causal network stemming from different possible initial states. Although different choices of these initial states result in the same initial density matrix, they don't necessarily cause the same chain of events with the same chances of occurring.

A compelling result is that, although we have a probability distribution dependence on the ambiguity of mixtures, the average of the $\Delta\mathcal{O}_A$ has not. This can be clearly seen in the result of Eq. (7.15). On the other hand, the second moment does depend on the ensemble choice for the initial density matrix, and thus the variance will also depend on it.

[6] Remember that in further equations after Eq. (7.1) we omitted the (0) in $|\psi_s(0)\rangle$ for simplicity of notation.

7.3.1 The variance for the qubits case

Due to its importance on the statistics of a random variable, we analyse in more details the variance dependence on the ambiguity of mixtures. We compute its values for different choices of ensembles of the initial density matrix for the case of qubits states described in Sec. 7.2. Here, the random variable under analysis is the heat received by A: $\Delta H_A = \mathcal{Q}_A$. We obtain the variance of the heat

$$\text{Var}(\mathcal{Q}_A)(t) = \langle \mathcal{Q}_A^2(t) \rangle - \langle \mathcal{Q}_A(t) \rangle^2, \tag{7.28}$$

from Eq. (7.24) for computing the average and Eq. (7.16) for computing the second moment, from which we have

$$\begin{aligned} \langle \mathcal{Q}_A^2(t) \rangle &= \text{Tr}\left\{ \left((U^\dagger(g,t) H_A U(g,t))^2 + H_A^2 \right) \rho_{AB}(0) \right\} \\ &- 2 \sum_s P_s \langle \psi_s | H_A | \psi_s \rangle \langle \psi_s | U^\dagger(g,t) H_A U(g,t) | \psi_s \rangle , \end{aligned} \tag{7.29}$$

depending on the ensemble $\{P_s, \ |\psi_s\rangle\}_s$ of the initial density matrix.

For generating a set of different ensembles for the same initial density matrix $\rho_{AB}(0)$, we recall a seminal result from Ref. [139]. This Reference reveals that, given a density matrix ρ with an *eigen-ensemble*[7] $\{\lambda_i, \ |\lambda_j\rangle\}_j$, we can generate an ensemble $\{P_i, \ |\psi_i\rangle\}_i$ of ρ with the formula

$$\boxed{\sqrt{P_i} |\psi_i\rangle = \sum_{i=1}^{k} \sqrt{\lambda_j} M_{ij} |\lambda_i\rangle , \ \ i = 1, \cdots, r,} \tag{7.30}$$

where $k = \dim(\text{Support}(\rho))$,[8] $r \geq k$ and M_{ij} are the elements of any $r \times k$ matrix M

[7] An *eigen-ensemble* of a density matrix ρ is an ensemble of ρ in which all elements are orthonormal eigenvectors.

[8] The set Support(ρ) is the linear space spanned by the set of eigenvectors or ρ with non-zero eigenvalues.

whose columns are orthonormal vectors in $\mathbb{C}^r$.[9]

Using this result, we suppose an initial state $\rho_{AB}(0)$ given by Eq. (7.22) with $\beta_A = 2/\omega_0$, $\beta_B = 1/\omega_0$ and $\alpha = -i \exp\left[-\omega_0(\beta_A + \beta_B)\right] / \left((1 + e^{-\omega\beta_A})(1 + e^{-\omega\beta_B})\right)$. For the generation of eight different equivalent ensembles of $\rho_{AB}(0)$, we used Eq. (7.30) with eight different choices of matrices M (see the matrices chosen in Appendix D). In Fig. 7.3 we see the variance in function of time computed using such ensembles in Eq. (7.29) and compared with the computation of the variance using the eigen-ensemble. We clearly see the pattern that the variance computed in general ensembles are greater than or equal to to the variance computed in an eigen-ensemble.

From these results and from further results of Chapter 8, we postulate that:

> The eigen-ensemble is the choice of ensemble which minimizes the variance of the probability distribution for a change of an observable using a QBN.

The meaning of this postulate is in our supposition that the presence of indistinguishability between non-orthogonal states of an ensemble can increase the variance of a distribution generated by such ensemble. Therefore, the postulate is a consequence of noticing that the eigen-ensembles are the only ones without such superpositions. In Fig. 7.3 we see that, for the case of the matrices M_7 and M_8 (see Appendix D), the ensembles are also composed by eigenvectors of $\rho_{AB}(0)$ but they are non-orthogonal to each other. Consequently, their variances have higher values than the ones generated for an eigen-ensemble.[10] Furthermore, the matrix M_8 generates a more superposed ensemble than the one generated by M_7, hence we can see a larger variance in this case.

[9] This can be proved simply by noticing that, given P_i and $|\psi_i\rangle$ defined by Eq. (7.30), we have

$$\begin{aligned}\sum_{i=1}^{r} P_i \left|\psi_i\right\rangle \left\langle\psi_i\right| &= \sum_{i=1}^{r} \sum_{l=1,m=1}^{k,k} M_{il}^* M_{im} \sqrt{\lambda_m \lambda_l} \left|\lambda_m\right\rangle \left\langle\lambda_l\right| \\ &= \sum_{m=1}^{k} \lambda_m \left|\lambda_m\right\rangle \left\langle\lambda_m\right| \\ &= \rho, \end{aligned} \tag{7.31}$$

where in the second equality we used that the columns of M are orthonormal vectors.

[10] Remember that the eigen-enesemble definition demands that the vectors are orthogonal among them, in addition to be eigenvectors.

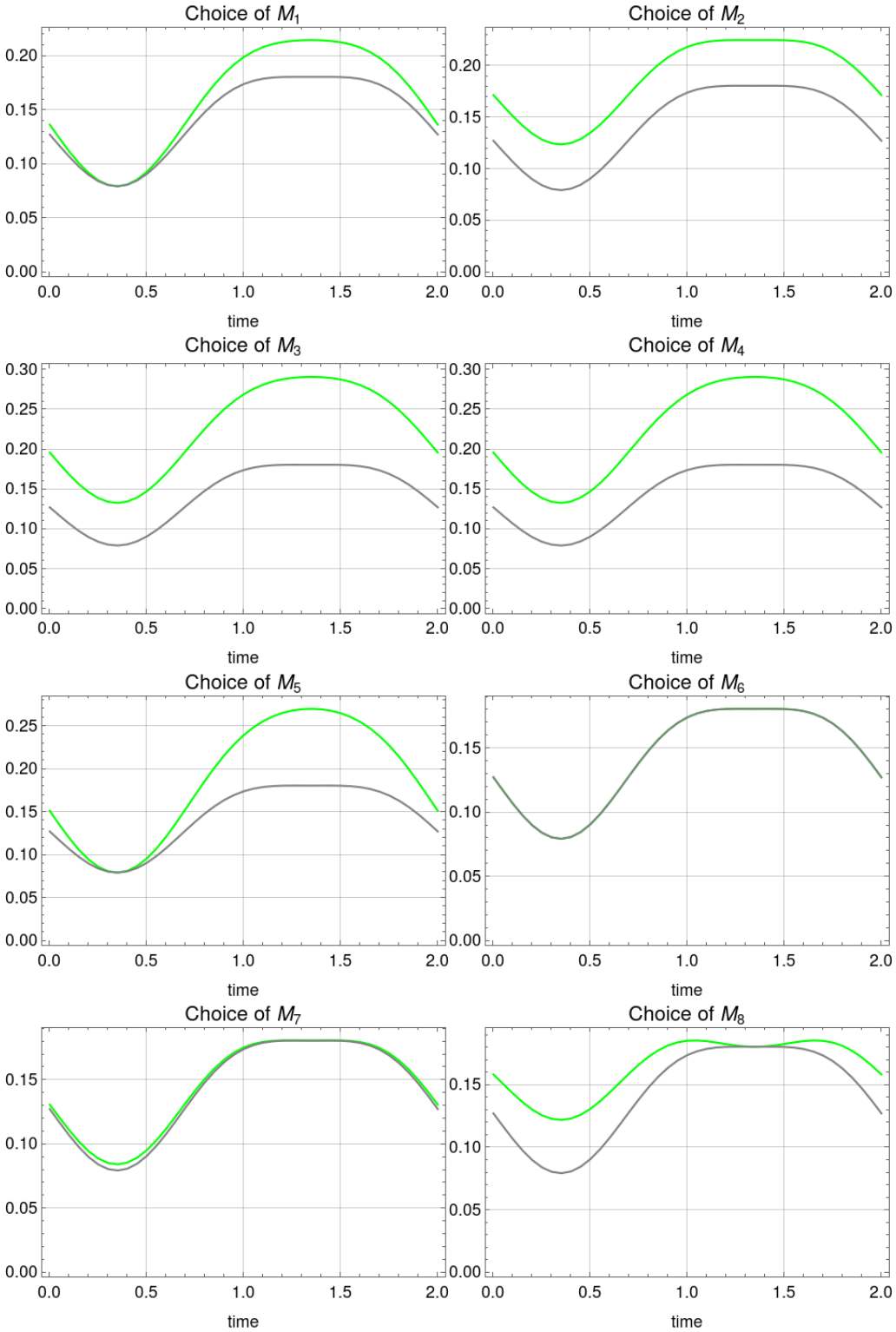

Figure 7.3: Variance of $\mathcal{Q}_A$ (in units of ω_0^2) $\times\ t$. The green curves represent the variance computed with the ensembles generated by the respective matrix M (see Appendix D) with the use of Eq. (7.30) while the gray curves represent the variance computed in an eigen-ensemble. The initial state $\rho_{AB}(0)$ is given by Eq. (7.22) with $\beta_A = 2/\omega_0$, $\beta_B = 1/\omega_0$ and $\alpha = -i \exp\left[-\omega_0(\beta_A + \beta_B)\right] / \left((1 + e^{-\omega\beta_A})(1 + e^{-\omega\beta_B})\right)$. For the unitary $U(g,t)$ we have $g = 1$.

Chapter 8

Heat Exchanged Between Bosonic Modes

As already mentioned, the second project of this thesis has as its main goal to obtain the probability distribution of the heat exchanged by two systems using QBNs due to its advantage to describe the statistics of initially correlated quantum systems. In this Chapter we obtain analytical results for the probability distribution of the heat exchanged between two initially correlated bosonic modes. The analytical formulae are possible thanks to the continuous-variables methods and we use them to analyze some of the general QBNs probability distributions characteristics given in Chapter 7 and specific meaningful results concerning bosonic systems heat exchange.

We begin this Chapter by exposing our main results concerning the characteristic function of the heat distribution, its average and its variance and exploring some features of such results. In the final part of the Chapter we discuss the consequences of the ambiguity of mixing of the initial density matrix in the heat statistics obtained.

8.1 Probability distribution for the heat exchanged

8.1.1 Statement of the problem

We suppose that the systems A and B are bosonic modes with local Hamiltonians

$$H_{A(B)} = \omega \left(\hat{a}^\dagger(\hat{b}^\dagger)\hat{a}(\hat{b}) + \frac{1}{2} \right), \tag{8.1}$$

where $\hat{a}(\hat{a}^\dagger)$ and $\hat{b}(\hat{b}^\dagger)$ are the annihilator (creator) operators of the modes in A and B, respectively. Their interaction is given by the Beam-Splitter unitary

$$U(t) = e^{-itH_{BS}}, \tag{8.2}$$

where

$$H_{BS} = ig(\hat{a}^\dagger\hat{b} - \hat{b}^\dagger\hat{a}). \tag{8.3}$$

Let the initial density matrix of the joint system be

$$\rho_{AB}(0) = \sum_s P_s \left|\psi_s\right\rangle \left\langle\psi_s\right|, \tag{8.4}$$

where $\{P_s, |\psi_s\rangle\}_s$ is an ensemble of states. The heat will again be defined as the change of the local Hamiltonian of A, i. e., $\mathcal{Q}_A = \Delta H_A$ and therefore the probability distribution of this quantity can be obtained from

$$P(\mathcal{Q}_A = \Delta a) = \sum_{a_0,a_t} \delta(\Delta a - (a_t - a_0))\mathcal{P}(a_0, a_t), \tag{8.5}$$

where $\{a_i\}_i$ are the eigenvalues of H_A. The probability distribution above $\mathcal{P}(a_0, a_t)$ is obtained from the QBN methods described in Sections 3.4 and 7.1. The distribution is given by

$$\mathcal{P}(a_0, a_t) = \sum_{b_0,b_t} \mathcal{P}(a_0, a_t, b_0, b_t), \tag{8.6}$$

where $\{b_j\}_j$ are the eigenvalues of H_B and

$$\mathcal{P}(a_0, a_t, b_0, b_t) = \sum_s P_s |\langle a_0, b_0|\psi_s\rangle|^2 |\langle a_t, b_t| U(t) |\psi_s\rangle|^2, \tag{8.7}$$

is a result from the QBN, where $\{|a_i(b_j)\rangle\}_{i(j)}$ are the eigenvectors of $H_A(H_B)$.

8.1.2 Choosing the ensemble and the seed probability

A tricky issue is to choose the more suitable ensemble of the initial density matrix to make the computations concerning this probability distribution. We have from Chapter 7 our postulate that the probability distribution with smaller variance is the one generated by the eigen-ensemble of the initial density matrix. But, due to the infinite dimensional nature of bosonic modes, obtain the diagonalization of the density matrix, specially in cases where correlations terms are relevant, is in general a highly intricate problem. We choose to utilize the ensemble made of coherent states for the initial density matrix in order to be able to apply continuous-variables methods. With this choice, the initial density matrix has the following form

$$\rho_{AB}(0) = \int_{\mathbb{C}^2} d^2\alpha \, d^2\beta \, P(\alpha, \beta) \, |\alpha, \beta\rangle \langle \alpha, \beta| \,, \tag{8.8}$$

where $P(\alpha, \beta) = W_1(\alpha, \beta)$ is the Glauber-Sudarshan P-function (see Eqs. (4.86) and (4.52)) and $|\alpha, \beta\rangle = |\alpha\rangle_A \otimes |\beta\rangle_B$ when $|\alpha(\beta)\rangle_{A(B)}$ is a coherent state in $A(B)$ with eigenvalues $\alpha(\beta)$.

With this choice of ensemble of coherent states we took the caveat of determining the adequate function P_s of Eqs. (8.4) and (8.7), which we will call the *seed probability*. The QBN developed in Sections 3.4 and 7.1 is the sum of successive products of conditional probabilities for possible evolution of hidden layers states times the seed probability (see Fig. 3.4 and Eq. (3.44)). One could interpret these conditional probabilities as the probabilities of obtaining a result if a projective measurement were made in the system, but without assuming that such measurement is indeed made, which would disturb the hidden layer state. As for the seed probability P_s, one could understand it as representing the *probability distribution* for the mixed initial state to be in each of the pure states of the

initial hidden layer. However, as we shall see, the most suitable choice for representing the seed probability P_s for the case where the vectors of the ensemble choice of the initial density matrix ($|\psi_s\rangle$) are coherent states $|\alpha,\beta\rangle$ is the Glauber-Sudarshan P-function $P(\alpha,\beta)$, which is a *quasi-probability* distribution.

We can argue in favor of the last sentence above by supposing that we want our probability distribution to respect the marginalization conditions given in Eqs. (7.5) and (7.6). Let the probability distribution $\mathcal{P}(a_0,a_t,b_0,b_t)$ of Eq. (8.7) for the choice of coherent states ensemble be of the form

$$\mathcal{P}(a_0,a_t,b_0,b_t)=\int_{\mathbb{C}^2} d^2\alpha\, d^2\beta\, f(\alpha,\beta)|\,\langle a_0,b_0|\alpha,\beta\rangle\,|^2|\,\langle a_t,b_t|\,U(t)\,|\alpha,\beta\rangle\,|^2. \tag{8.9}$$

We want to find the function $f(\alpha,\beta)$ for the seed probability from imposing Eq. (7.6) to the probability distribution above.

Consider the sum

$$\begin{aligned}\sum_{a_0,b_0}\mathcal{P}(a_0,b_0,a_t,b_t)&=\int_{\mathbb{C}^2} d^2\alpha\, d^2\beta\, f(\alpha,\beta)|\,\langle a_t,b_t|\,U(t)\,|\alpha,\beta\rangle\,|^2\\&=\langle a_t,b_t|\,U(t)\left(\int_{\mathbb{C}^2} d^2\alpha\, d^2\beta\, f(\alpha,\beta)\,|\alpha,\beta\rangle\,\langle\alpha,\beta|\right)U^\dagger(t)\,|a_t,b_t\rangle\,,\end{aligned} \tag{8.10}$$

hence this sum is equal to $\langle a_t,b_t|\,U(t)\rho_{AB}(0)U^\dagger(t)\,|a_t,b_t\rangle$ (in order to satisfy Eq. (7.5)) if and only if $f(\alpha,\beta)=P(\alpha,\beta)$ (see Eq. (8.8)). The marginalization condition Eq. (7.5) is also satisfied by direct application of $f(\alpha,\beta)=P(\alpha,\beta)$.

One could guess that the most suitable function to play the role of $f(\alpha,\beta)$ would be the Husimi Q-function $Q(\alpha,\beta)$, since it is a valid probability distribution for every α and β. However, this function represents the probability of obtaining outcomes α and β for heterodyne measurements in A and B and the seed probability need not to assume that a measurement is indeed made. In fact, if we suppose in Eq. (8.10) that $f(\alpha,\beta)=Q(\alpha,\beta)$, then we have

$$\sum_{a_0,b_0}\mathcal{P}(a_0,b_0,a_t,b_t)=\langle a_t,b_t|\,U(t)\rho'_{AB}U^\dagger(t)\,|a_t,b_t\rangle\,, \tag{8.11}$$

where

$$\rho'_{AB} = \int_{\mathbb{C}^2} d^2\alpha \, d^2\beta \, Q(\alpha,\beta) \left|\alpha,\beta\right\rangle \left\langle\alpha,\beta\right| . \tag{8.12}$$

This density matrix is the result of performing the heterodyne measurement $\{M_{\alpha,\beta} = \frac{1}{\pi}\left|\alpha,\beta\right\rangle\left\langle\alpha,\beta\right|\}_{\alpha,\beta}$ in $\rho_{AB}(0)$ without revealing the outcome (see Appendix E). Therefore, the correct interpretation for the QBN probability distribution

$$\mathcal{P}_Q(a_0,a_t,b_0,b_t) = \int_{\mathbb{C}^2} d^2\alpha \, d^2\beta \, Q(\alpha,\beta) |\left\langle a_0,b_0|\alpha,\beta\right\rangle|^2 |\left\langle a_t,b_t\right| U(t)\left|\alpha,\beta\right\rangle|^2, \tag{8.13}$$

is that this corresponds to the trajectory probability of the joint system after a heterodyne measurement $\{M_{\alpha,\beta} = \frac{1}{\pi}\left|\alpha,\beta\right\rangle\left\langle\alpha,\beta\right|\}_{\alpha,\beta}$ is made in the initial state without revealing its outcome.

8.1.3 The characteristic function

With the QBN probability distribution

$$\mathcal{P}(a_0,a_t,b_0,b_t) = \int_{\mathbb{C}^2} d^2\alpha \, d^2\beta \, P(\alpha,\beta) |\left\langle a_0,b_0|\alpha,\beta\right\rangle|^2 |\left\langle a_t,b_t\right| U(t)\left|\alpha,\beta\right\rangle|^2, \tag{8.14}$$

we have the heat probability distribution $P(\mathcal{Q}_A)$ from Eq. (8.5). With the result of Eq. (7.11), we obtain

$$G_{\mathcal{Q}_A}(k) = \int_{\mathbb{C}^2} d^2\alpha d^2\beta \, P(\alpha,\beta) \left\langle\alpha,\beta\right| e^{-ik\omega\hat{a}^\dagger\hat{a}} \left|\alpha,\beta\right\rangle \left\langle\alpha,\beta\right| e^{ik\omega U(t)\hat{a}^\dagger\hat{a}U^\dagger(t)} \left|\alpha,\beta\right\rangle . \tag{8.15}$$

The computation of the quantities $\left\langle\alpha,\beta\right| e^{-ik\omega\hat{a}^\dagger\hat{a}} \left|\alpha,\beta\right\rangle$ and $\left\langle\alpha,\beta\right| e^{ik\omega U(t)\hat{a}^\dagger\hat{a}U^\dagger(t)} \left|\alpha,\beta\right\rangle$ are extensive, so we present them in Appendix E, Section E.2. They result in

$$\left\langle\alpha,\beta\right| e^{-ik\omega\hat{a}^\dagger\hat{a}} \left|\alpha,\beta\right\rangle = \exp\{-|\alpha|^2(1-e^{-ik\omega})\}, \tag{8.16}$$

and

$$\left\langle\alpha,\beta\right| e^{ik\omega U(t)\hat{a}^\dagger\hat{a}U^\dagger(t)} \left|\alpha,\beta\right\rangle = \exp\left\{-\vec{\alpha}^\dagger\left(\mathbb{I}_2 - e^{ik\omega M}\right)\vec{\alpha}\right\}, \tag{8.17}$$

where

$$\vec{\alpha} = \begin{pmatrix} \alpha \\ \beta \end{pmatrix} \text{ and } M = \begin{pmatrix} \cos^2(gt) & \cos(gt)\sin(gt) \\ \cos(gt)\sin(gt) & \sin^2(gt) \end{pmatrix}.$$

Therefore, the characteristic function of the heat probability distribution is

$$\boxed{G_{\mathcal{Q}_A}(k) = \int_{\mathbb{C}^2} d^2\alpha d^2\beta \; P(\alpha,\beta) \exp\{-|\alpha|^2(1-e^{-ik\omega})\} \exp\left\{-\vec{\alpha}^\dagger \left(1 - e^{ik\omega M}\right)\vec{\alpha}\right\}.} \tag{8.18}$$

8.2 Heat statistical moments

At this point, it is useful to describe the characteristic function in terms of the phase space of the eigenvalues for canonical operators. Let $\mathbf{r}^\top = (\mathbf{r}_A^\top, \mathbf{r}_B^\top) = (q_A, p_A, q_B, p_B)^\top$ be the vector of eigenvalues of the canonical operators $(\hat{q}_A, \hat{p}_A, \hat{q}_B, \hat{p}_B)$ and satisfy $\alpha = (q_A + ip_A)/\sqrt{2}$ and $\beta = (q_B + ip_B)/\sqrt{2}$. With this change of variables, the characteristic function is

$$\boxed{\begin{aligned} G_{\mathcal{Q}_A}(k) &= \int_{\mathbb{R}^4} d\mathbf{r} \; P(\mathbf{r}) \exp\left\{-\frac{1}{2}\left(1-e^{-ik\omega}\right)|\mathbf{r}_A|^2\right\} \\ &\times \exp\left\{-\frac{1}{4}\left(1-e^{ik\omega}\right)\left(|\mathbf{r}_A|^2 + |\mathbf{r}_B|^2 + (|\mathbf{r}_A|^2 - |\mathbf{r}_B|^2)\cos(2gt) + 2\mathbf{r}_A\cdot\mathbf{r}_B\sin(2gt)\right)\right\}. \end{aligned}} \tag{8.19}$$

8.2.1 Average of heat

With the characteristic function we compute the statistical moments with Eq. (7.13), hence the average of the heat will be

$$\begin{aligned} \langle \mathcal{Q}_A(t)\rangle &= -i\frac{\partial G_{\mathcal{Q}_A}(k)}{\partial k}\bigg|_{k=0} \\ &= \int_{\mathbb{R}^4} d\mathbf{r} P(\mathbf{r}) \left[\frac{\omega}{2}\left(\sin^2(gt)(|\mathbf{r}_B|^2 - |\mathbf{r}_A|^2) + \sin(2gt)\mathbf{r}_A\cdot\mathbf{r}_B\right)\right]. \end{aligned} \tag{8.20}$$

Now we suppose that our initial state $\rho_{AB}(0)$ is a Gaussian state. Therefore from Eq. (4.87) we conclude that the Glauber-Sudarshan P-function must be completely described by the covariance matrix σ_{AB} corresponding to the initial state $\rho_{AB}(0)$. Moreover, from Eq. (4.90) we have that the P-function $P(\mathbf{r})$ can be understood as a $\mathbb{R}^4$ probability distribution of a classical Gaussian probability distribution with covariance matrix $\Sigma = \sigma_{AB} - \mathbb{I}_4/2$. This implies that the average for polynomials of (q_A, p_A, q_B, p_B) are elements of the classical covariance matrix Σ, for instance

$$\int_{\mathbb{R}^4} d\mathbf{r} P(\mathbf{r}) q_B^2 = \Sigma_{2,2} = \sigma_{AB_{2,2}} - \frac{1}{2}.$$

Accordingly, the heat average will be

$$\langle \mathcal{Q}_A(t) \rangle = \frac{\omega}{2} \left(\sin^2(gt)(\sigma_{AB_{4,4}} + \sigma_{AB_{3,3}} - (\sigma_{AB_{2,2}} + \sigma_{AB_{1,1}})) + \sin(2gt)(\sigma_{AB_{1,3}} + \sigma_{AB_{2,4}}) \right). \tag{8.21}$$

As we intend to explore effects of quantum correlations, we suppose that the initial joint state is in the normal Simon form (Eq. (4.126)). Therefore the joint system's initial covariance matrix is

$$\sigma_{AB} = \begin{pmatrix} \mathbf{a} & 0 & c_+ & 0 \\ 0 & \mathbf{a} & 0 & c_- \\ c_+ & 0 & \mathbf{b} & 0 \\ 0 & c_- & 0 & \mathbf{b} \end{pmatrix}, \tag{8.22}$$

where a and b are positive real numbers. Beyond the fact that any two-mode Gaussian state can be transformed by means of local unitaries in a state with covariance matrix in the Simon form, this form also assumes that the local states are thermal. The parameters $\mathbf{a}$ and $\mathbf{b}$ are related to their local inverse of temperatures β_A and β_B by means of

$$\mathbf{a}(\mathbf{b}) = \frac{1}{2} \coth\left(\frac{\omega \beta_{A(B)}}{2} \right), \tag{8.23}$$

hence the parameters $\mathbf{a}$ and $\mathbf{b}$ are directly proportional to their systems temperature.[1]

[1] This relation is a consequence of Eq. (C.35) and from Section C.13 discussion for the case of local Hamiltonians $H_{A(B)}$ given by Eq. (8.1) and locally thermal states $\rho_{A(B)} = e^{-\beta_{A(B)} H_{A(B)}}/Z_{A(B)}$, where $Z_{A(B)} = \mathrm{Tr}\{e^{-\beta_{A(B)} H_{A(B)}}\}$.

In terms of these parameters, the heat average is

$$\boxed{\langle \mathcal{Q}_A(t) \rangle = \omega \left(\sin^2(gt)(\mathbf{b} - \mathbf{a}) + \frac{1}{2} \sin(2gt)(c_+ + c_-) \right).} \tag{8.24}$$

This formula for the average pinpoints important aspects about the heat flow between two bosonic modes interacting via a Beam Splitter. The first term $\omega \sin^2(gt)(\mathbf{b} - \mathbf{a})$ indicates the ordinary heat flowing from the hot system to the cold system disregarding the initial correlations. As for the second term $\frac{\omega}{2} \sin(2gt)(c_+ + c_-)$, the effect of the correlations is completely manifest. The sign of the sum $c_+ + c_-$ dictate the tendency of the correlations to reverse the heat flow or to increase the ordinary flow. Intriguingly, for the most usual way of entangling two locally thermal bosonic modes, i.e., for two-mode squeezed thermal states, we have $c_- = -c_+$ (see Eq. (4.127)) causing the effect of the correlations in the average heat flow to be null. However, in Appendix C, Subsection E.4, we construct the *D-plus thermal state* and *D-minus thermal state* in which it is possible to use the correlation terms to cause the inversion of the heat flow. Importantly, the construction of these two states are possible only with the use of the one-mode bosonic channel D (see Subsection 4.7.6), which represents the environmental outcome of a two-mode squeezing acting in the mode. The unitary two-mode squeezing channel, together with any other two-mode unitaries, is by itself unable to construct correlations terms that do not cancel with themselves in the heat average.

In the case of the D-plus thermal state, the covariance matrix in the Simon form is

$$\sigma_{AB}^{D+} = \begin{pmatrix} \mathbf{a} & 0 & c & 0 \\ 0 & \mathbf{a} & 0 & c \\ c & 0 & \mathbf{b} & 0 \\ 0 & c & 0 & \mathbf{b} \end{pmatrix}, \tag{8.25}$$

with positive $\mathbf{a}$, $\mathbf{b}$ and c. For this case it is possible to make the system A locally hotter then the system B (see Subsection E.4), thus the standard heat flow would cause the average of Eq. (8.24) to be negative. But the correlation terms are always positive and their influence is capable of reversing the heat flow direction (see Fig. 8.1).

Alternatively, for case of the D-minus thermal state, the covariance matrix in the Si-

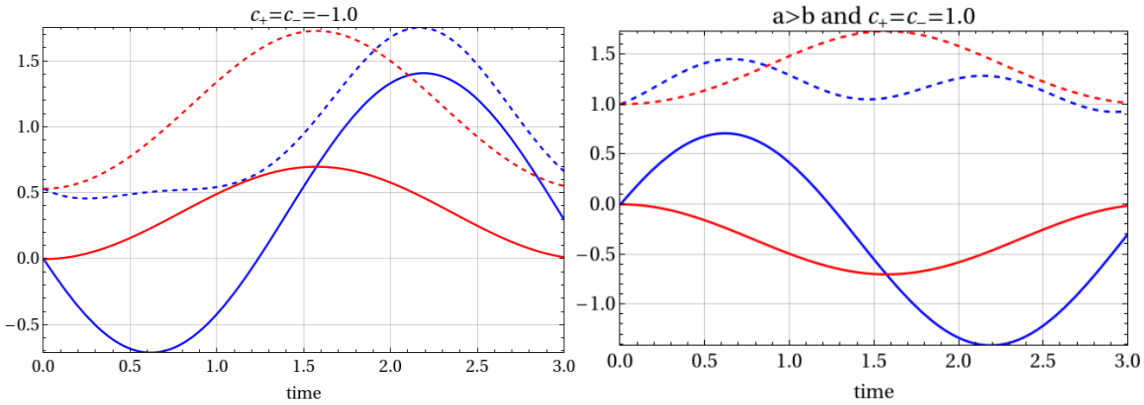

Figure 8.1: $\langle \mathcal{Q}_A \rangle$ in units of ω (solid lines) and var$(\mathcal{Q}_A)$ in units of $\omega^2/3$ (dashed lines) $\times$ interaction time. For the blue curves in the plot on the left we have an initial state in the Simon form with $\mathbf{a} = 1.3$, $\mathbf{b} = 2.0$ and $c_+ = c_- = -1.0$, this state is correspondent to a D-minus thermal state. For the blue curves in the plot on the right we have an initial state in the Simon form with $\mathbf{a} = 2.0$, $\mathbf{b} = 1.3$ and $c_+ = c_- = 1.0$, this state is correspondent to a D-plus thermal state. The red curves correspond to initial locally thermal states but with no correlations ($c_+ = c_- = 0$) with $\mathbf{a} = \mathbf{1.3}$ and $\mathbf{a} = \mathbf{2.0}$ on the left and $\mathbf{a} = 2.0$ and $\mathbf{b} = 1.3$ on the right. The interaction strength is $g = 1.0$.

mon form is

$$\sigma_{AB}^{D-} = \begin{pmatrix} \mathbf{a} & 0 & -c & 0 \\ 0 & \mathbf{a} & 0 & -c \\ -c & 0 & \mathbf{b} & 0 \\ 0 & -c & 0 & \mathbf{b} \end{pmatrix}, \tag{8.26}$$

with positive $\mathbf{a}$, $\mathbf{b}$ and c. Here it is possible to make the system B hotter than A, but again it is possible to reverse the direction of the heat flow due to the sign of the correlation terms (see Fig. 8.1).

8.2.2 Heat variance

From Eq. (8.19) we can obtain the heat second moment

$$\langle \mathcal{Q}_A^2 \rangle = -\frac{\partial^2 G_{\mathcal{Q}_A}(k)}{\partial k^2}\bigg|_{k=0}. \tag{8.27}$$

After evaluating the second derivative, we obtain

$$\langle \mathcal{Q}_A^2 \rangle = \int_{\mathbb{R}^4} d\mathbf{r} P(\mathbf{r}) \frac{\omega^2}{4} \Big[\left(3|\mathbf{r}_A|^2 + |\mathbf{r}_B|^2 + (|\mathbf{r}_A|^2 - |\mathbf{r}_B|^2)\cos(2gt) + 2\mathbf{r}_A \cdot \mathbf{r}_B \sin(2gt)\right) + \frac{1}{4}\left(|\mathbf{r}_B|^2 - |\mathbf{r}_A|^2 + (|\mathbf{r}_A|^2 - |\mathbf{r}_B|^2)\cos(2gt) + \mathbf{r}_A \cdot \mathbf{r}_B \sin(2gt)\right)^2 \Big]. \tag{8.28}$$

Since $P(\mathbf{r})$ is a classical Gaussian probability distribution with covariance matrix $\Sigma = \sigma_{AB} - \mathbb{I}_4/2$, all averages for polynomials of $(\hat{q}_A, \hat{p}_A, \hat{q}_B, \hat{p}_B)$, with respect to the function $P(\mathbf{r})$, are dependent only on the covariance matrix. This is a consequence of the *Isserlis' Theorem* (See Appendix E, Section E.3), which gives the relation between the average of higher order polynomials and the covariance matrix terms. We use this theorem together with Eq. (8.28) to obtain the analytical result for the second moment of the heat distribution. The solution's formula is too extensive and not very clarifying by itself, therefore in Appendix E, Section E.3, we explain in more details how we computed this quantity and here we present some plots with physical interpretations of this function.

We present the plots for the variance of the heat

$$\text{var}(\mathcal{Q}_A) = \langle \mathcal{Q}_A^2 \rangle - \langle \mathcal{Q}_A \rangle^2, \tag{8.29}$$

using our analytical results for the ensemble of coherent states $\{P(\alpha,\beta), |\alpha,\beta\rangle\}_{\alpha,\beta}$ obtained from Eqs. (8.24) and (8.28). In Fig. 8.1 the plots are made relative to states correspondent to D-minus and D-plus thermal states in which the reversal of the heat flow is achieved. Curiously, for the case of the D-minus state, at the same time that the initial correlations reverse the heat flow, they seem to decrease the variance in relation to the initially uncorrelated case. However, this decreasing of the variance seems not to happen for the D-plus state case, even during the initial heat flow inversion. This is not a fact for all ensemble choices generationg the QBN, as we will show in the next Subsection. For the eigen-ensemble choice, the variance also decreases while the heat flow inversion happens for the D-plus case.

Moreover, in Fig. 8.2 we have the plots of the heat average and variance for states prepared initially at two-mode squeezed thermal states. For these states, the correlation terms in the average completely cancel, so its curve coincides with the initially uncorre-

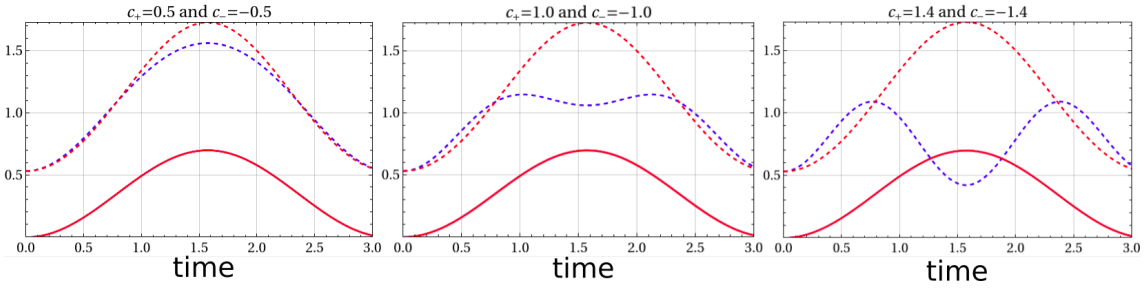

Figure 8.2: $\langle \mathcal{Q}_A \rangle$ in units of ω (solid lines) and var$(\mathcal{Q}_A)$ in units of $\omega^2/3$ (dashed lines) $\times$ interaction time. For all the curves in the plots we have initial states in the Simon form with $\mathbf{a} = 1.3$ and $\mathbf{b} = 2.0$. For the blue curves we have the respective values of $c_- = -c_+$ indicated above each plot, these initial states correspond to two-mode squeezed thermal states (see Appendix C, Section C.72). The red curves correspond to the same initial locally thermal states but with no correlations ($c_+ = c_- = 0$). The interaction strength is $g = 1.0$.

lated state curve. Conversely, the initial correlations effects are manifest in the variance. These plots show that as the initial correlations increase, the variance decreases significantly at the heat's average peak. In Section 8.4, we also identify this region as a peak of mutual information between the modes.

8.3 The variance for different QBN choices

8.3.1 The ambiguity of mixing

As already mentioned, we have from Eqs. (7.11) and (7.16) that the probability distribution generated by a QBN is dependent on the initial density matrix ensemble choice. An analysis of the variance dependence on the ensemble choice was made in Section 7.3 for the case of two initially correlated qubits. Here we compare our analytical computations for the coherent states ensemble choice $\{P(\alpha,\beta), |\alpha,\beta\rangle\}_{\alpha,\beta}$ to numerical computations for the statistical moments obtained using the QBN with the eigen-ensemble of the initial density matrix for two interacting bosonic modes.

The numerical computations are made supposing a finite Fock space, i.e., we consider in the trace computations all the Fock basis elements from the ground state $|0\rangle$ to a higher energy state $|N\rangle$ for each mode. The adequate value of N for a good approximation depends on the temperature of the state in question. The higher the temperature of the state, the higher the states of the Fock basis need to be considered. For our computations,

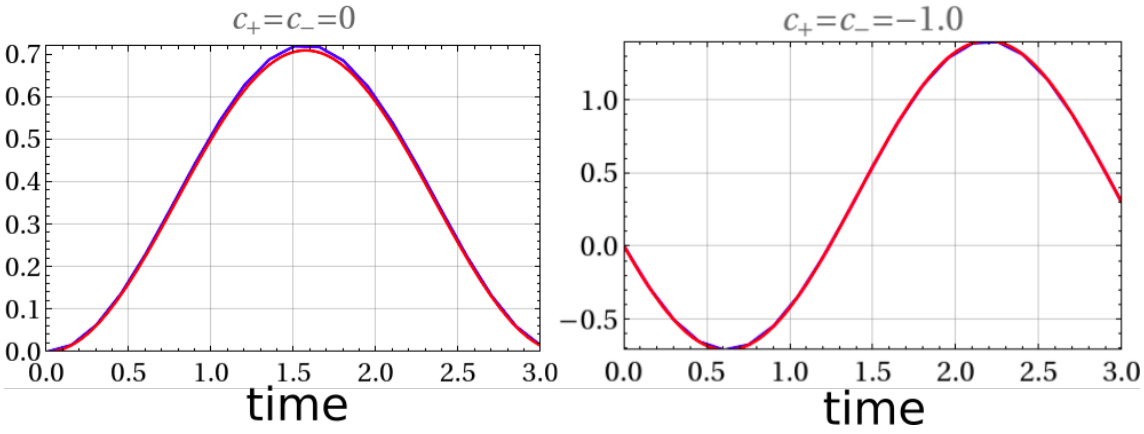

Figure 8.3: $\langle \mathcal{Q}_A \rangle$ in units of $\omega \times$ interaction time. The states are initially in the Simon form with $\mathbf{a} = 1.3$, $\mathbf{b} = 2.0$ and the values of the correlation parameters are indicated above the plots. For the blue curves we have the numerical calculation of the average by computing the trace in the finite Fock basis and for the red curves we have the plot of the average computed using the result of Eq. (8.24). The interaction strength is $g = 1.0$.

the number $N = 25$ of first Fock basis elements is sufficient for the convergence of the trace for its correct value.

From the result of Eq. (7.15) we have that the heat average obtained by the QBN is independent of the ensemble choice. We confirm this result by comparing the heat average of Eq. (8.24) obtained using the coherent states ensemble with the trace of Eq. (7.15) computed numerically. In Fig. 8.3 we present two examples of such comparison.

The numerical computations for the second moment of the heat are made using Eq. (7.16) from which we have

$$\begin{aligned}\langle \mathcal{Q}_A^2(t) \rangle = \sum_i \lambda_i (\langle \lambda_i | \left((U^\dagger(t) H_A U(t))^2 + H_A^2 \right) | \lambda_i \rangle \\ - 2 \langle \lambda_i | H_A | \lambda_i \rangle \langle \lambda_i | U^\dagger(t) H_A U(t) | \lambda_i \rangle),\end{aligned} \tag{8.30}$$

where $\{\lambda_i, |\lambda_i\rangle\}_i$ is the eigen-ensemble of the initial state $\rho_{AB}(0)$. Given the initial state covariance matrix σ_{AB} (and supposing null first moments) we obtain its density matrix $\rho_{AB}(0)$ by using Eq. (4.82) which is computed in the Fock basis with its first $N = 25$ elements for each of the two modes. After obtaining the eigenvalues and eigenvectors of $\rho_{AB}(0)$ in this finite Fock basis, we are able to compute $\langle \mathcal{Q}_A^2(t) \rangle$ from Eq. (8.30).

Using these numerical computations for $\langle \mathcal{Q}_A^2(t) \rangle$ and $\langle \mathcal{Q}_A(t) \rangle$ in the eigen-ensemble of the initial density matrix and our analytical results from Section 8.2 for the ensemble

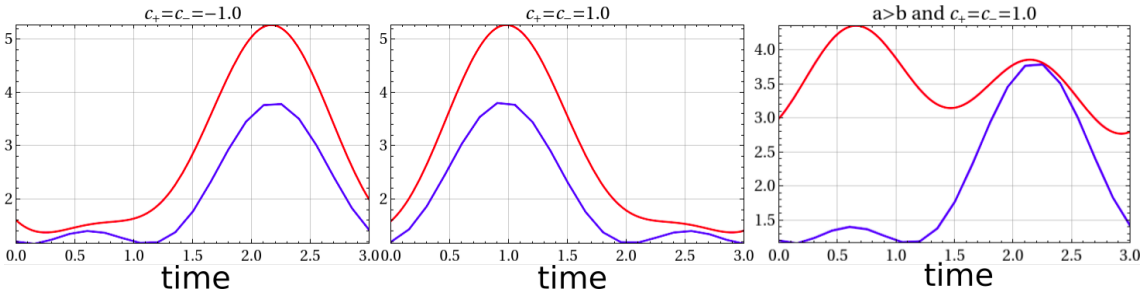

Figure 8.4: $\mathrm{var}(\mathcal{Q}_A)$ in units of $\omega^2 \times$ interaction time. For the two plots in the left, the states are initially in the Simon form with $\mathbf{a} = 1.3$, $\mathbf{b} = 2.0$ and the values of the correlation parameters are indicated above the plots. For the plot in the right, the state is initially in the Simon form with $\mathbf{a} = 2.0 > \mathbf{b} = 1.3$ and $c_+ = c_- = 1.0$. For the blue curves we have the numerical computations using the eigen-ensemble choice while in the red curves we use our analytical results in the coherent states ensemble choice. The interaction strength is $g = 1.0$.

of coherent states, we obtain heat variance (Eq. (8.29)) for such ensembles. In Fig. 8.4 we contrast the variance computed in these two ensembles for different initial states. The plot on the left of Fig. 8.4 represents a D-minus state while the plot on the right represent a D-plus state, notice that in this plot the variance for $t < 1.5$ is clearly much smaller for the eigein-ensemble then for the coherent states ensemble. Therefore, for the eingen-ensemble the variance decreases as the heat flux inversion happens for an intial D-plus state. This is the opposite as Fig. 8.1 seemed to indicate for the coherent states ensemble. This is because the coherent state ensemble has an additional variance term related only to the mode in which the heat statistics is being computed. For instance, for any initial state with covariance matrix in the Simon form, the initial heat variance will be $\mathrm{var}(\mathcal{Q}_A(0)) = 2\mathbf{a} - 1$ for the coherent states ensemble choice.[2]

The results presented above seem to agree with our postulate made in Subsection 7.3.1 which affirms that the heat variance of the eigen-ensemble is always smaller than the variance of the probability distribution generated by any other ensemble of the initial state. Nevertheless, the coherent states ensemble choice suggests to refute this postulate as can be seen in Fig. 8.5. In this figure we have plots of the variance computed for the eigen-ensemble and for the coherent states ensemble for four different initial states which represent two-mode squeezed thermal states. For all of these initial states, in-

[2]Conversely, if we construct an equivalent QBN to compute the heat received from B, i.e., $\mathcal{Q}_B$, its variance for the coherent states ensemble choice will be initially $\mathrm{var}(\mathcal{Q}_B(0)) = 2\mathbf{b} - 1$.

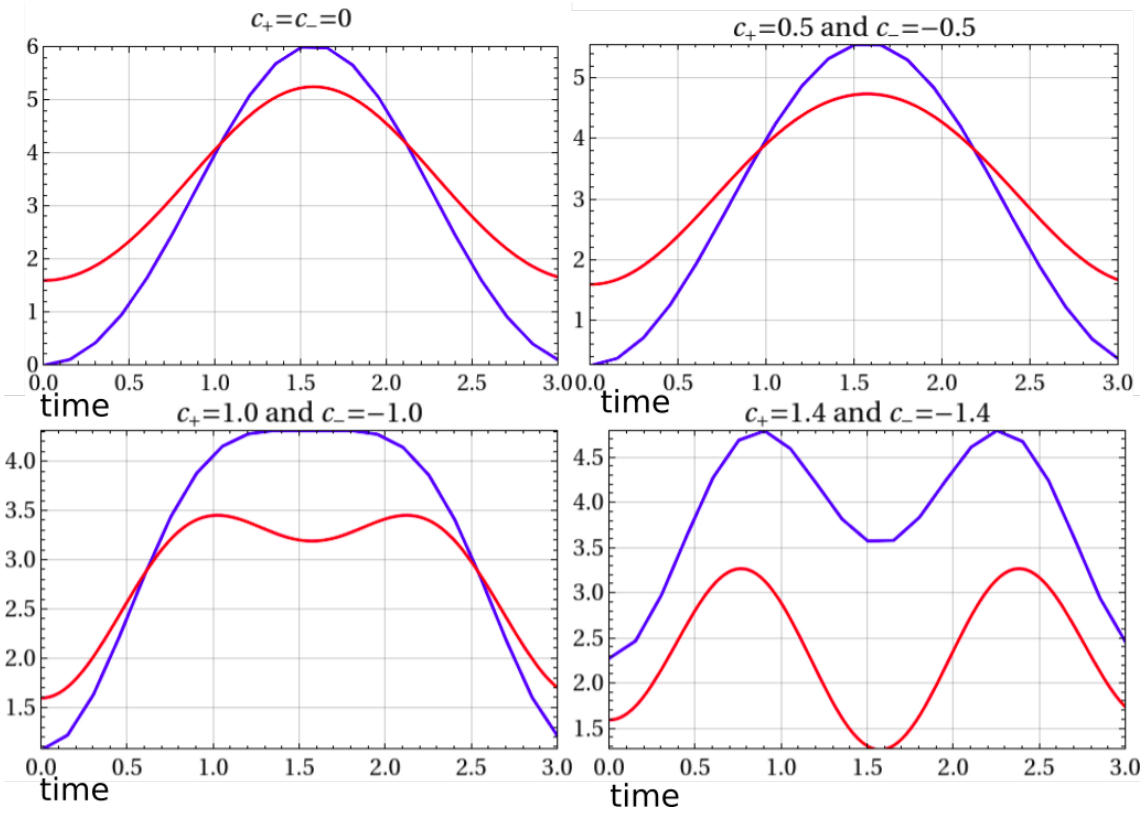

Figure 8.5: $\mathrm{var}(\mathcal{Q}_A)$ in units of $\omega^2 \times$ interaction time. For all the plots the states are initially in the Simon form with $\mathbf{a} = 1.3$, $\mathbf{b} = 2.0$ and the values of the correlation parameters are indicated above the plots. For the blue curves we have the numerical computations using the eigen-ensemble choice while in the red curves we use our analytical results in the coherent states ensemble choice. The interaction strength is $g = 1.0$.

cluding the case of uncorrelated two locally thermal states, the variance is bigger for the eigen-ensemble choice than for the coherent states ensemble choice in the region of the peak for the heat average. We suspect that this rebut of our postulate can occur due to the fact that the coherent state ensemble is associated to the *quasi*-probability distribution P-function rather than a well behaved probability distribution.

8.3.2 Different seed probability choices

Additionally, as we discussed in Subsection 8.1.2, we can construct further QBNs with different seed probability choices. Of course, these QBNs would represent different initial density matrices than $\rho_{AB}(0)$. But, as it is shown in Appendix E, Section E.1, these states can represent the initial state after a projective measurement is made without a revealed outcome. Surprisingly, for the coherent states ensemble, if we choose the Husimi Q-

function or the Wigner W-function as the seed probability instead of the P-function, the heat average will remain the same.[3] Therefore, it would be also instructive to compute the heat deviation from the average in these cases.

In Fig. 8.6 we plot the variance computed numerically for the eigen-ensemble choice and analytically for the coherent states ensemble choice with the choice of the P-function, Q-function and W-function as seed probability. The analytical results of the variance using the Q-function and W-function as seed probability can be obtained analogously as it is obtained for the P-function as described in Appendix E, Section E.3. Here we switch $P(\mathbf{r})$ by $Q(\mathbf{r})$ or $W(\mathbf{r})$ and using Eqs. (4.88) and (4.89) to treat $Q(\mathbf{r})$ or $W(\mathbf{r})$ as classical probability distributions and use Isserlis' Theorem to compute the integrals.

It is important to recall that the *correct* choice of the quasi-probability distribution to represent the coherent states ensemble of the initial state $\rho_{AB}(0)$ is the P-function. As the Q-function and W-function represent different density matrices which are the evolution of the initial $\rho_{AB}(0)$ after a projective measurement (respectively, an heterodyne and an homodyne measurement) is made, we expect their von Neumann entropy to be bigger than $S(\rho_{AB}(0))$ [1, 2]. This can be an interpretation to the fact that in Fig. 8.6 the variance generated by the seed probabilities of the Q-function and W-function are always bigger than the one generated by the P-function. In particular, notice that the P-function is the only seed function which causes smaller variance than the eigen-ensemble choice for the initial two-mode squeezed thermal state (plot on the right in Fig. 8.6).

8.4 Investigations on correlations

8.4.1 Profile of correlations in the initial state

Since we observed different behaviour of the heat flow and of the heat variance for initially different states at the Simon form, we explore the content of the correlations for different states in the Simon form. In Fig. 8.7 we plot the mutual information (representing the total correlation content) between the modes as well as the quantum discord and the classical correlations content between the modes for different values of c_+ and c_- for fixed local

[3] This can be seen if we switch $P(\mathbf{r})$ by $Q(\mathbf{r})$ or $W(\mathbf{r})$ in Eq. (8.20) and use Eqs. (4.88) and (4.89) to treat $Q(\mathbf{r})$ or $W(\mathbf{r})$ as classical probability distributions.

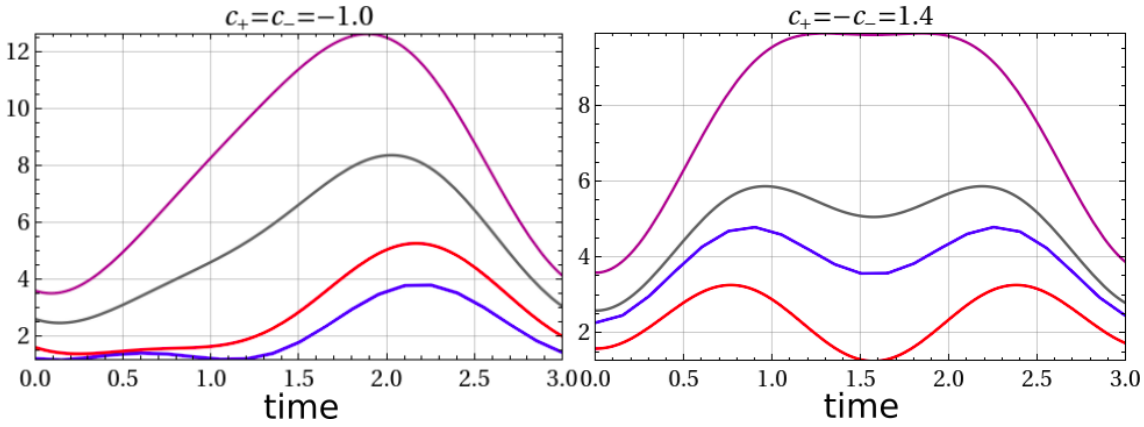

Figure 8.6: var$(\mathcal{Q}_A)$ in units of ω^2 $\times$ interaction time. For all the plots, the states are initially in the Simon form with $\mathbf{a} = 1.3$, $\mathbf{b} = 2.0$ and the values of the correlation parameters are indicated above the plots. For the blue curves we have the numerical computations using the eigen-ensemble choice while in the red, gray and purple curves we use our analytical results in the coherent states ensemble choice for the P-function, W-function and Q-function chosen as seed probabilities. The interaction strength is $g = 1.0$.

temperatures $a = 2$ and $b = 10$.

To prepare the plots we randomly peaked $100,000$ points of $r \in [1/10, 10]$ and $\tau \in [\tau_{\text{min}}, \tau_{\text{max}}]$ where τ_{min} and τ_{max} are defined in the footnote of Page 85. This way, we create $100,000$ Simon states with $a = 2$, $b = 10$ and c_+ and c_+ given by the parametrization of Eqs. (4.143) and (4.144). With the covariance matrices, we compute the mutual information with the use of Eqs. (4.124), (4.125) and (3.20). Additionally, we use the values of $\mathbf{a}$, $\mathbf{b}$, r and τ from each state to obtain the value of η (see footnote of Page 85) and finally we use Eq. (4.139) to compute the quantum discord of each state. The quantity we call *classical correlation content* ($\mathcal{J}(A|B)$) is the difference between the mutual information and the quantum discord computed to each state $\mathcal{J}(A|B) = \mathcal{I}(A:B) - \mathcal{D}(A|B)$. From Eqs. (3.32), (3.33) and (3.34) we can interpret $\mathcal{J}(A|B)$ as the maximum information one can obtain for the mode A with the outcomes of a quantum measurement in the mode B.

We see from Fig. 8.7 that the mutual information is almost radially equally distributed for different values of c_+ and c_-, i.e., the total correlations seem to increase as $|c_+| + |c_-|$ increases. Differently, the quantum discord has not this radial pattern, it seems to decrease as c_- and c_+ approaches to the $c_+ = 0$ and $c_- = 0$ axes. Also, the quantum discord increases substantially at the border regions with higher $|c_-|$ and $|c_+|$ and with $|c_-| \approx |c_+|$.

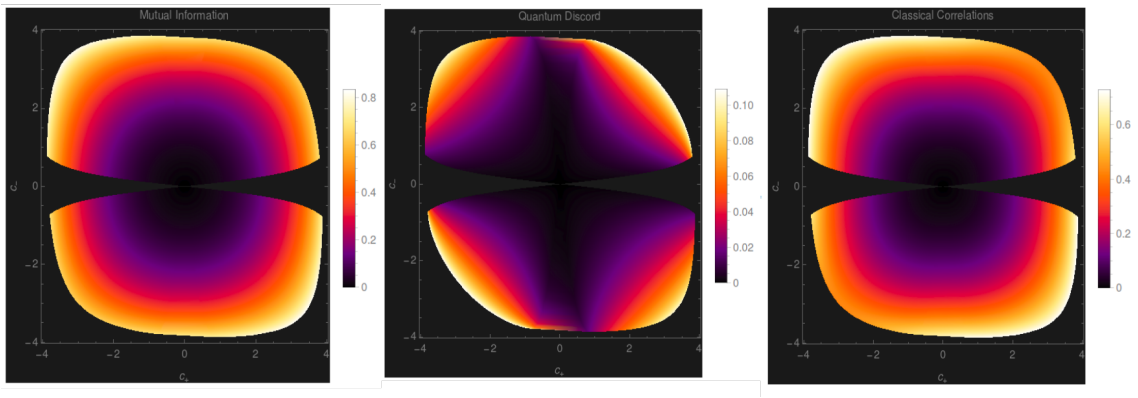

Figure 8.7: From left to right: mutual information, quantum discord and classical information content in function of c_+ (horizontal axis) and c_- (vertical axis), for Simon states prepared with $a = 2$ and $b = 10$.

These richer regions in quantum discord are correspondent to the D-plus and D-minus thermal states ($c_- = c_+$) and two-mode squeezed thermal states $c_- = -c_+$ and this can be a justification about why these initial states cause the higher correlations effects in the statistical moments of the heat. Curiously, the D-plus and D-minus thermal states regions are slightly richer in quantum discord than the two-mode squeezed thermal states and the classical correlations content is more present in two-mode squeezed thermal states than in the D-plus and D-minus thermal states.

8.4.2 Correlations behaviour during evolution

We analyze the correlation quantifiers during the evolution of the system. For our results, the mutual information is computed according to the evolution of the covariance matrix using Eqs. (4.124), (4.125) and (3.20). The quantum discord is obtained by inverting Eqs. (4.141), (4.142), (4.143) and (4.144) numerically to obtain the parameters τ and η and use Eq. (4.139) to the computation for each covariance matrix during the evolution. Again, we define the classical correlations content as $\mathcal{J}(A|B) = \mathcal{I}(A:B) - \mathcal{D}(A|B)$.

In Fig. 8.8 we plot the quantifiers for two different initial states in D-minus thermal states and for an initially uncorrelated thermal state together with the heat average evolution. As already expected [50–53], and analogously as founded in Ref. [54] for qubits, the mutual information as well as the quantum discord are completed *consumed* so that the heat flow inversion happens in the cases of initial D-minus thermal states. After this

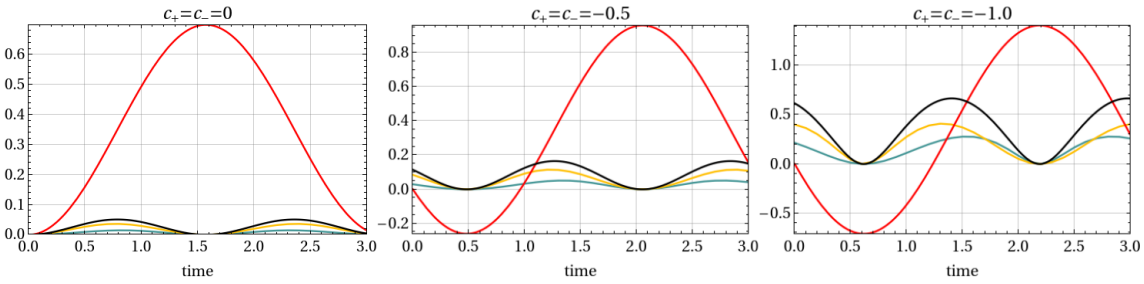

Figure 8.8: Heat average in units of ω (red), mutual information (black), quantum discord (blue) and classical correlations content (yellow) $\times$ time of interaction. Each plot represents a different initial state, all the initial states are in the Simon form with $a = 1.3$, $b = 2.0$ and with the correlation terms are described above each plot.

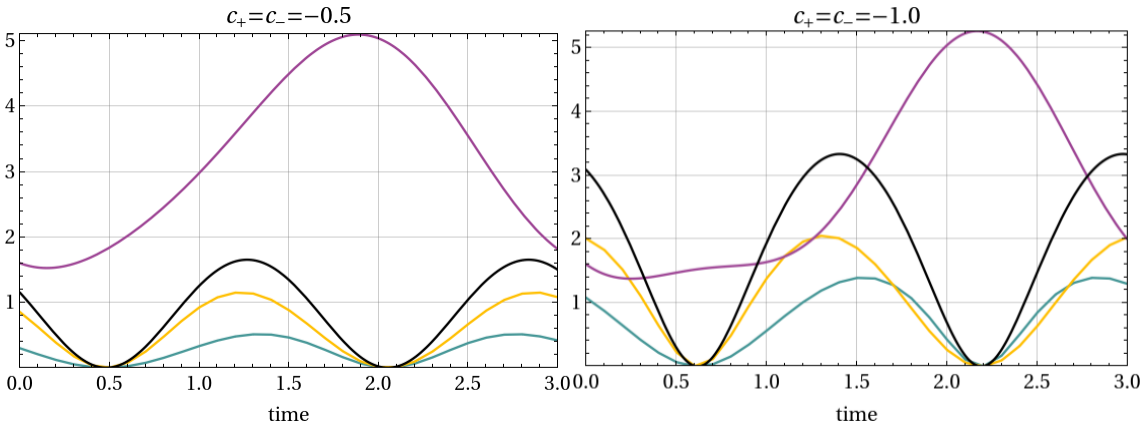

Figure 8.9: Heat variance in units of ω^2 (purple), mutual information (black), quantum discord (blue) and classical correlations content (yellow) $\times$ time of interaction. Each plot represents a different initial state, all the initial states are in the Simon form with $a = 1.3$, $b = 2.0$ and with the correlation terms are described above each plot.

consumption the correlations and the heat average oscillate due to the unitary nature of the interaction. As for the initially uncorrelated state, the correlations are created and start to oscillate with the unitary evolution.

In Fig. 8.9 we plot the variance as well as the evolution of the correlations quantifiers for the same initial D-minus states as in Fig. 8.8. During the heat flow inversion and the first correlations consumption, the variance shows a slight decrease. As the oscillatory evolution starts, the variance peaks are approximately following the consumption of correlations.

Unfortunately, if initially we have a state with covariance matrix in the Simon form, but we don't have $c_- = c_+$, the Beam-Splitter unitary evolution causes the local states not to be locally thermal during the evolution. This precludes the use of the method from

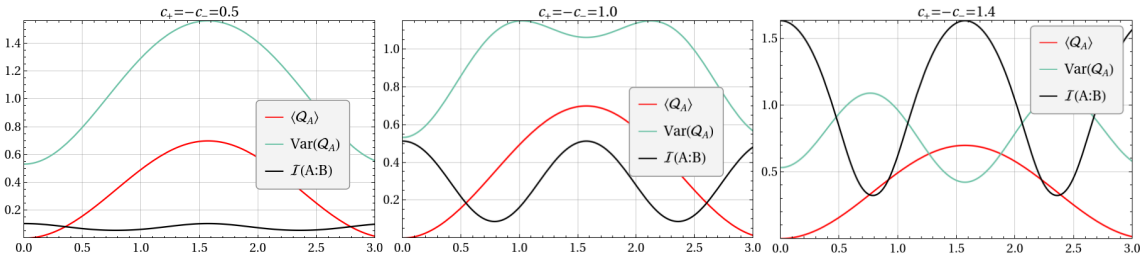

Figure 8.10: Heat average (red), heat variance in units of ω^2 (blue) and mutual information (black) $\times$ time of interaction. Each plot represent a different initial state, all the initial states are in the Simon form with $a = 1.3$, $b = 2.0$ and with the correlation terms are described above each plot.

Ref. [128] described in Subsection 4.8.3 to compute the quantum discord for two-mode Gaussian states, since it only considers locally thermal states. Hence, in Fig. 8.10 we compute only the mutual information evolution as a quantifier of correlations, together with the heat average and the heat variance for three initial two-mode squeezed thermal states. However, with the plots of the mutual information it is possible to see again the tendency of the correlations minima to be aligned with the peaks of the heat variance, as it is seen in Fig. 8.9.

Another interesting feature that can be seen in the plots of Fig. 8.10 is the alignment between a mutual information peak, the heat average peak and a meaningful decreasing of the heat variance, visible specially for the cases of $c_+ = -c_- = 1.0$ and $c_+ = -c_- = 1.4$. This is the same decreasing pattern of the heat variance spotted in Fig. 8.2 and it is clearly an effect that happens only due to the presence of correlations in the initial state. This could indicate that the increasing of correlations can reduce the variance of the heat.

Chapter 9

Conclusions and further perspectives

The main motivations of this thesis was to explore new effects of quantum correlations in two distinct situations.

The first project, relative to chapters 5 and 6, explored the effects of initial global correlations between the ancillae in the evolution and thermalization of a system that interacts locally with them in a collisional model setup. As a benchmark for comparison, we contrasted our results to well-known papers concerning collisional models and the asymptotic behaviour of the system, leading us to a comparison with Refs. [18, 19], in which the model studied is very similar to our model explored in Chapter 5. The new component introduced in our studies (the initial ancillae correlations) revealed highly non-negligible effects, steering the system towards different steady-states and breaking the Homogenization proposed in [19]. These facts were numerically glimpsed in the qubit model and fully described for the bosonic modes case thanks to the very feasible description of Gaussian bosonic states. It was our initial intention to obtain the full description of the initial correlations effects in bosonic Gaussian modes and to construct a physical model capable of mimicking the initial correlations between the ancillae. Both goals were achieved and lead us to the use of H-Graphs to prepare correlated bosonic modes. From Chapter 5 we can conclude that it is possible to create an environment with distance dependent correlated ancillae with the use of H-graphs in qubits. We couldn't obtain analytical closed expressions for preparing environments with the desired correlations, however, with numerical approaches it was possible to visualize non-trivial correlation patterns, as it is shown in Section 5.1. In Chapter 6, Section 6.3, we obtained a

satisfactory method for such preparation of correlated ancillae for the Gaussian bosonic case, additionally it would be stimulating to suggest in detail a platform for physical implementation. This is a future work perspective and possibly a feasible candidate is to implement it in the context of waveguide-QED [100, 101]. Another alternative would be to recycle the ancillae and apply a periodic set of gates in them before they interact with the system to prepare the initial correlations between neighbors ancillae. This "on the go" scheme of preparing correlations between ancillae can be applied, for the qubits case, can be implemented in recent quantum computer platforms. Additionally, the very structure of continuous-variables graph-states itself [48], used in Section 6.3, is proposed under the possibility of optical preparation with offline squeezing plus interferometry [140, 141] or optical parametric oscillators [142].

The analytical results obtained in the Gaussian case raise a variety of enquiries. A special enquiry is about the underlying mechanisms of the steering effects since there is still a lack of interpretation about how correlations can deviate the system towards the specific forms of Eqs. (6.26) and (6.34), for instance. One possible future research is to analyze this model from the perspective of Quantum Trajectories [8, 57, 143].

It is also important to remember that such kind of deviations can be present in a wide variety of collisional models rather then in the Homogenization context due to the generality of Eq. (6.24), and this could indicate the presence of such effects in a diversity of physical situations. For instance, one could consider not locally identical initial ancillae, but ancillae whose states fluctuate around an average. In this case the steady-state of the system without the initial ancillae correlations would be the average of the ancillae state, however if we consider the initial correlations, the steady-state would be steered in the same way. Therefore, exploring the possibility of new environmental correlations inducing steering in a system can be a fruitful direction for research.

A very relevant question to be asked is about the necessity for the ancillae correlations to be of quantum nature. This is also a future work possibility which can be very challenging for qubits ancillae but feasible for bosonic systems with the use of continuous-variables methods [14–16, 128]. Another possible exploration about the internal correlations of the ancillae with the use of our results is to analyze how the many-body *weaving* of the ancillae set can be changed with the collisions. This concept, proposed in [144],

characterizes multipartite correlations and describe how correlations scale with the size of the many-body system.

Furthermore, Eqs. (6.26) and (6.34) give non-trivial results for thermodynamics. As already indicated in Section 6.2, we could have initial locally thermal system and ancillae (it could also be possible to have them in the same temperature), and Eqs. (6.26) and (6.34) indicate that, depending on the collisions strength and on the ancillae initial correlations configuration, the system could get dramatically warmer or colder in the steady-state. These predictions could result in a thermal machine or refrigerator in which correlations are consumed, rather than work. Therefore, a deeper study in this feature can give interesting insights in thermodynamics. Finally, a random distribution in the initial correlations of the ancillae could nullify or interfere in the steering effect on the system. A further analysis in this subject could clarify this steering effect in physical systems.

In chapters 7 and 8, regarding to the second project, we refer to the statistics of thermodynamic quantities using QBNs and our main search was to estimate an adequate probability distribution for the heat distribution which fully considered the effects of initial quantum correlations. We aimed to achieve this goal using QBNs initially proposed in Ref. [48]. In Chapter 7 we obtained, inspired by this main question, a general framework using QBNs to estimate probability distributions to describe observable variations (or *changes*) during a physical process. This framework was further reduced to the particular case for our studies of the heat distribution, but we can have a wide variety of applications due to the generality of the observable whose change can be explored. For instance, with this framework we are able estimate the probability distribution variation of the number of particles (when the observable is the number operator) or work (in the presence of external time-dependent force on the Hamiltonian), being a possibly fruitful road for future research. The characteristic function of such distribution obtained in Eq. (7.11), as well as the statistical moments resulting from it, takes under consideration the initial quantum coherences of the system to describe the full statistics of the changes and reduces to the TPM statistics for the case where there is no initial coherence in the eigenbasis of the initial observable in question. Additionally, this formalism is feasible to quantum fluctuation theorems [48] and has an experimental validation protocol based on the postselection of independent multiple copies [49]. Therefore, we expect that this formalism can be useful

for further explorations for the statistics of thermodynamic quantities when one desires to consider entirely the effects of initial quantum correlations and quantum coherence.

Another important aspect observed from the result of the QBN characteristic function for the observable changes, obtained in Eq. (7.11), is it's dependence on the choice of the ensemble to describe the initial covariance matrix. As a consequence, the statistical moments will also depend on this choice, with the notable exception of the average. Part of our analysis focus on the behaviour of the variance under this ensemble choice dependence, since it is in our interest to understand which choice of initial ensemble causes in the probability distribution a smaller deviation from the average. In our analysis for the statistic of the heat exchanged between two interacting qubits, which we proved to agreed with the results of Refs. [48, 54], we concluded that the probability distribution generated by the eigen-ensemble of the initial density matrix would minimize the variance in relation to any other ensemble choice. We postulated this conclusion from testing it for a variety of examples and from the intuitive perspective that non-orthogonal ensembles would engender a larger variance distribution due to the indistinguishability of states. An ongoing research effort to prove analytically this statement or to discover counterexamples continues. And further researches relating this feature to related papers as, for instance, Refs. [139, 145, 146] could illuminate this quest.

Continuing to pursue our main goal in this second project, we focused in obtaining the statistics of the heat exchanged between two initially correlated Gaussian bosonic modes during a Beam-Splitter interaction. This led us to the use of coherent-states as the ensemble of the initial density matrix to be used in the QBN due to it usefulness when applying continuous-variables methods. From the marginalization conditions we concluded that the suitable seed probability distribution to the coherent-states ensemble is the Glauber-Sudarshan P-function. We obtained analytically the heat probability distribution characteristic function for this choice of ensemble in Eq. (4.85) and, consequently, their first moments. The heat average predicts a heat flow inversion caused by the initial correlations between the bosonic modes, analogous to the already experimentally proved qubits case [54]. We discovered that this heat flow inversion cannot happen if the initial global state is the well-known two-mode squeezed thermal state. Therefore, we proposed a construction of initial locally thermal states from known methods in which this inver-

sion is possible, calling them *D-plus* and *D-minus thermal states*. However, it still an open question and future query to interpret why an initial two-mode squeezed thermal state is unable to cause the heat flow inversion while the D-plus and D-minus thermal states can, since both are rich in quantum correlations (quantum discord) and mutual information between the modes (see Section 8.4). Is there a feature or resource created during the preparation of the D-plus and D-minus thermal states which isn't present in a two-mode squeezed state?

As for our analysis of the variance for the heat exchanged between two bosonic modes, we spotted that the variance decreases while the correlations (classical and quantum) are consumed for the heat flow inversion and it oscillates achieving its maxima when the correlations are at their minima and its minima when the correlations reaches its maxima. Therefore, a conclusion is that the presence of correlations decreases the variance. Notwithstanding, our examination on contrasting the variance computed numerically using the eigen-ensemble of the initial state with the variance computed with our analytical results from coherent-states ensemble showed unexpected conclusions which signal the need for for more enquiries and future researches. We observed that the heat variance computed using the coherent states ensemble choice can be smaller than the variance computed using the eigen-ensemble, apparently contradicting our earlier postulate. However, we suppose that this may not be considered a an counterexample since the seed probability associated to this ensemble is a *quasi*-probability distribution. Despite generating a valid heat probability distribution, our use of quasi-probabilities as seed probabilities still lack of better interpretations and an ongoing research direction is to enlighten these results, be it extending the measurement proposals [49] or relating it to other interpretations of quasi-probabilities [42, 147, 148].

Finally, it can be a worthwhile research to relate our QBN probability distributions results concerning to its dependence on initial density matrices ensemble choice to measurement schemes. This is done in Ref. [49] concerning to the eigen-ensemble choice and a possible generalization can be explored.

Appendix A

Some proofs and definitions in Open Quantum Systems and Collisional Models

A.1 Some properties of purity

Given a density matrix ρ, we can make its spectral decomposition (since it is an hermitian operator)

$$\rho = \sum_k \lambda_k \left|\lambda_k\right\rangle \left\langle\lambda_k\right|, \tag{A.1}$$

where λ_k and $\left|\lambda_k\right\rangle$ are respectively the eigenvalues and eigenvectors of ρ. Notice that, from the semipositivity and normalization condition (Eqs. (2.4) and (2.5)), we obtain

$$\lambda_k \geq 0 \ \text{ and } \ \sum_k \lambda_k = 1, \tag{A.2}$$

which implies that we can treat λ_k as the probabilities. Now, computing the purity of ρ, we obtain

$$\mathcal{P}(\rho) = \mathrm{Tr}\left\{\sum_k \sum_l \lambda_k \lambda_l \left|\lambda_k\right\rangle \left\langle\lambda_k|\lambda_l\right\rangle \left\langle\lambda_l\right|\right\} = \sum_k \lambda_k^2 \leq 1, \tag{A.3}$$

the above quantity is less or equal than 1 since it is a sum of probabilities squared and can be 1 *if and only if* all the probabilities are 0 except one λ_k which is 1, and in this case we arrive at a pure state.

Moreover, we can argue that the case where the purity is at its minimum is the situation where the state is more mixed. This is the case where we have no information that gives preference for the system to be in one state or another, so $\lambda_k = 1/d,\ \forall k$ (since λ_k represents the probability of the system being in the element of basis $|\lambda_k\rangle$), where d is the dimension of the Hilbert space of the system. Consequently we shall have

$$\mathcal{P}(\rho) = \sum_k \lambda_k^2 = \sum_k \frac{1}{d^2} = \frac{1}{d}, \tag{A.4}$$

and thus we have the lower bound for $\mathcal{P}(\rho)$. This result can also be obtained by using Lagrange multipliers for minimizing $\mathcal{P}(\rho)$ under the constraint of ρ normalization (Eq. (2.5)).

A.2 The partial trace

If we treat a bipartite system AB in a Hilbert space $\mathcal{H}_{AB} = \mathcal{H}_A \otimes \mathcal{H}_B$, the partial trace comes from the idea of creating the adequate description for the subsystem A by summing the average effects of B. For accounting the effects of B, one can proceed as follows, suppose the most general linear operator $\mathcal{O}$ that acts on $\mathcal{H}_{AB}$

$$\mathcal{O} = \sum_k A_k \otimes B_k, \tag{A.5}$$

where A_k and B_k are generic operators that act in $\mathcal{H}_A$ and $\mathcal{H}_B$ respectively. The partial trace with respect to B is defined to be *the trace of all the operators that act only on $\mathcal{H}_B$ space*

$$\mathrm{Tr}_B\, \mathcal{O} = \sum_k A_k \otimes \mathrm{Tr}\{B_k\}, \tag{A.6}$$

or, equivalently

$$\mathrm{Tr}_B\, \mathcal{O} = \sum_k \sum_\alpha \langle\alpha|_B\, A_k \otimes B_k\, |\alpha\rangle_B\,, \tag{A.7}$$

where $\{|\alpha\rangle_B\}$ is some basis of $\mathcal{H}_B$. Evidently, $\mathrm{Tr}_B\,\mathcal{O}$ is not a number, but an operator acting on $\mathcal{H}_A$ and

$$\mathrm{Tr}\{\mathcal{O}\} = \mathrm{Tr}_A\{\mathrm{Tr}_B\{\mathcal{O}\}\}. \tag{A.8}$$

Together with the definition of partial trace we have the notion of *reduced density matrix* of a state ρ in AB

$$\rho_A = \mathrm{Tr}_B\,\rho, \tag{A.9}$$

which describes the system that we would see if we only looked at A making an average of the effects of B. The intuition may come from the fact that if $\mathcal{O}_A$ is an operator acting in $\mathcal{H}_A$, then

$$\langle\mathcal{O}_A\rangle = \mathrm{Tr}\{\mathcal{O}_A\rho\} = \mathrm{Tr}_A\{\mathcal{O}_A\,\mathrm{Tr}_B\{\rho\}\} = \mathrm{Tr}_A\{\mathcal{O}_A\rho_A\} = \mathrm{Tr}\{\mathcal{O}_A\rho_A\}, \tag{A.10}$$

where in the last equality we exchange Tr_A for the full trace Tr since all the operator inside the trace acts only on $\mathcal{O}_A$.The above equation means that ρ_A acts just like a density matrix should act for computing averages only on A.

A.3 Interaction Picture

We shall make the description of this formalism just for completeness, here we are strictly following Ref. [91].

Notice that the von Neumann Equation (Eq. 2.11), just like Schödinger's Equation, also describes a closed system evolving under a *time-dependent* Hamiltonian $H(t)$. So, given a quantum state ρ that evolves under such time-dependent Hamiltonian, we can define a new density matrix given by

$$\tilde{\rho} = S(t)\rho S^\dagger(t), \tag{A.11}$$

where $S(t)$ is an arbitrary time-dependent unitary.

The density matrix $\tilde{\rho}$ is now a state that describes the system ρ in a *rotating frame* and

evolves acording to a von Neumann equation

$$\boxed{\frac{d\tilde{\rho}}{dt} = -i[\tilde{H}(t), \tilde{\rho}],} \tag{A.12}$$

where

$$\boxed{\tilde{H}(t) = i\frac{dS(t)}{dt}S^{\dagger}(t) + S(t)H(t)S^{\dagger}(t).} \tag{A.13}$$

To prove Eqs. A.12 and A.13, we need only to differentiate $\tilde{\rho}$ in function of t

$$\begin{aligned}
\frac{d\tilde{\rho}}{dt} &= \frac{dS(t)}{dt}\rho S^{\dagger}(t) + S(t)\frac{d\rho}{dt}S^{\dagger}(t) + S(t)\rho\frac{dS^{\dagger}(t)}{dt} \\
&= \frac{dS(t)}{dt}S^{\dagger}(t)\tilde{\rho} - iS(t)[H(t), \rho]S^{\dagger}(t) + \tilde{\rho}S(t)\frac{dS^{\dagger}(t)}{dt} \\
&= \frac{dS(t)}{dt}S^{\dagger}(t)\tilde{\rho} - i[S(t)H(t)S^{\dagger}(t), \tilde{\rho}] - \tilde{\rho}\frac{dS(t)}{dt}S^{\dagger}(t) \\
&= -i[S(t)H(t)S^{\dagger}(t) + i\frac{dS(t)}{dt}S^{\dagger}(t), \tilde{\rho}] = -i[\tilde{H}(t), \tilde{\rho}],
\end{aligned}$$

where in the second equality we used the von Neumann Equation for ρ and in the third equality we used that $\frac{dS(t)}{dt}S^{\dagger}(t) = -S(t)\frac{dS^{\dagger}(t)}{dt}$ since $\frac{d}{dt}(S(t)S^{\dagger}(t)) = 0$.

The appropriate choice of $S(t)$ can make a time-dependent Hamiltonian become time-independent and vice-versa. If we have a time-independent Hamiltonian that can be divided in

$$H = H_0 + V, \tag{A.14}$$

then, if we chose

$$\boxed{S(t) = e^{iH_0 t},} \tag{A.15}$$

we obtain

$$\tilde{H}(t) = e^{iH_0 t}Ve^{-iH_0 t}. \tag{A.16}$$

which means that we eliminate the direct dependence on the "free" Hamiltonian H_0 on the but add a time dependence.

For the case where $[H_0, V] = 0$, we have, from the equation above

$$\boxed{\tilde{H}(t) = V,} \tag{A.17}$$

which is a time-independent Hamiltonian, and means that the effective Hamiltonian will act just as the interaction Hamiltonian setting $H_0 = 0$. The assumption $[H_0, V] = 0$ is valid for almost all of our cases of study in this thesis, and represents interactions that conserve the system's internal energy.

A.4 Thermal states

Given a system with Hamiltonian H described by a density matrix ρ, we affirm that it is in a thermal state with temperature T when

$$\boxed{\rho = \sum_i \frac{e^{-\beta E_i}}{Z} |E_i\rangle \langle E_i| = \frac{e^{-\beta H}}{Z},} \tag{A.18}$$

where $\beta = 1/T$, $\{E_i\}_i$ and $\{|E_i\rangle\}_i$ are, respectively, the sets of eigenvalues and eigenvectors of H and $Z = \mathrm{Tr}\{e^{-\beta H}\}$ is the *partition function*.

This is just the quantum version of the Gibbs distribution. Where, in classical physics, the probability distribution of a system in thermal equilibrium at temperature T is only dependent on it's energy and is equal to

$$p(E_i) = \frac{e^{-\frac{1}{k_B T} E_i}}{Z}, \tag{A.19}$$

where E_i is the energy of the system, k_B is the Boltzmann constant and $Z = \sum_i e^{-\frac{1}{k_B T} E_i}$ (where the index i means "summing over all states for all possible energies E_i") is again the partition function. Finally, we just have that Eq. A.18 is

$$\rho = \sum_i p(E_i) |E_i\rangle \langle E_i| . \tag{A.20}$$

For the case of a qubit, if we are dealing, for instance, with a standard Hamiltonian

$$H = E\sigma_z, \tag{A.21}$$

xwith $E > 0$, then if $|0\rangle$ and $|1\rangle$ are the eigenvectors of σ_z (with eigenvalues -1 and 1, respectively), we shall have the same eigenvectors for H with eigenvalues $-E$ and E,

respectively. Hence, if the qubit is in a thermal state at temperature T, Eq. A.18 will result in

$$\rho = \begin{pmatrix} \frac{e^{\beta E}}{Z} & 0 \\ 0 & \frac{e^{-\beta E}}{Z} \end{pmatrix} = \begin{pmatrix} 1-p & 0 \\ 0 & p, \end{pmatrix}, \tag{A.22}$$

where $\beta = 1/T$, $Z = e^{\beta E}(1+e^{-2\beta E})$ and $p = \frac{1}{2}(1-\tanh(\beta E))$. Notice that $0 \leq p \leq 1/2$ with the bounds achieved at $\beta \to \infty$ and $\beta \to 0$, respectively.

A.5 Proof of $\rho^n_{S,\text{rest}} \to 0$ and $\rho^n_{A,\text{rest}} \to 0$

This section of the Appendix is present just for the completeness of the thesis. This was done following the results of Ref. [19].

For proving the properties above, it is sufficient to prove that ρ^n_S and ρ^n_A converge to ρ_A. The proof of these convergences can be made with the use of the Banach Theorem (see Ref. [149]). But to enunciate such theorem, we must first define what is a contractive map.

Let $\mathcal{S}$ be a space with a distance function D. A map T is called *contractive* if and only if, for any ρ and η that belong to $\mathcal{S}$, we have

$$D(T[\rho], T[\eta]) \leq kD(\rho, \eta), \text{ where } 0 \leq k < 1. \tag{A.23}$$

The **Banach Theorem** states that, if a map T is contractive, then it has a fixed point $\eta^* \in \mathcal{S}$ in which the iteraction of the map converges to it, i.e., $\lim_{N\to\infty} T^N[\rho] = \eta^*$ for any $\rho \in \mathcal{S}$.

It is important to notice that if a map is contractive and has a fixed point (of course, this will always be true by the theorem stated above), then the fixed point will be unique. The proof is very simple: let ρ and η be two fixed points of a contractive map T, then it must be true that

$$D(T[\rho], T[\eta]) \leq kD(\rho, \eta) \Rightarrow D(\rho, \eta) \leq kD(\rho, \eta),$$

and the inequality above is true for some k where $0 \leq k < 1$ if, and only if, $\rho = \eta$. Hence the Banach Theorem also implies the uniqueness of the fixed point of a contractive map.

The space $\mathcal{S}$ that we shall consider is the space of density matrices operators in the Hilbert space of the system $\mathcal{H}_S$ while we want to show that the map $\mathcal{E}$, that makes the evolution of the system in the Homogenization case of Sec. 2.3.6, is contractive and has the fixed point ρ_A.

In order to show the above facts, we first parametrize our initial system's state as

$$\rho_S^0 = \frac{1}{2}\mathbf{I} + \vec{w}\cdot\vec{\sigma}, \tag{A.24}$$

where $\mathbf{I}$ is the identity operator, $\vec{w}$ is a vector of real numbers with 3 components, with $|\vec{w}| \leq 1/2$ and $\vec{\sigma} = (\sigma_x, \sigma_y, \sigma_z)$ is the vector of Pauli matrices, it can be shown that every qubit density matrix can be parametrized in a Eq. (A.24) form (see Ref. [91]). We also parametrize the ancilla's initial state as

$$\rho_A = \frac{1}{2}\mathbf{I} + \vec{t}\cdot\vec{\sigma}. \tag{A.25}$$

These parametrization permits us to represent $\rho_S^0 = (1, w_x, w_y, w_z)$ and $\rho_A = (1, t_1, t_2, t_3)$ as vectors in the operator basis $\{\mathbf{I}/2, \sigma_x, \sigma_y, \sigma_z\}$ spanning the space of qubit density matrices.

Using this parametrizations and Eq. (2.50), we can write our map $\mathcal{E}$ as

$$\begin{aligned}\mathcal{E}[\rho_S^0] = \rho_S^1 &= \frac{1}{2}\mathbf{I} + (s^2\vec{t} + c^2\vec{w})\cdot\vec{\sigma} + ics[\vec{t}\cdot\vec{\sigma}, \vec{w}\cdot\vec{\sigma}] \\ &= \frac{1}{2}\mathbf{I} + [s^2\vec{t} + c^2\vec{w} - 2cs(\vec{t}\times\vec{w})]\cdot\vec{\sigma} = \frac{1}{2}\mathbf{I} + \vec{w}'\cdot\vec{\sigma},\end{aligned} \tag{A.26}$$

where we used that $\sigma_k\sigma_l = \delta_{kl}\mathbf{I} + i\epsilon_{jkl}\sigma_j$ (ϵ_{jkl} is the Levi-Civita symbol) in the third equality and we defined

$$w_j' = s^2 t_j + (c^2\delta_{jl} - 2cs\epsilon_{jkl}t_k)w_l.$$

Now we can write Eq. (A.26) as a transformation $\vec{w} \to \vec{w}'$ in the following way

$$\begin{pmatrix} 1 \\ w'_x \\ w'_y \\ w'_z \end{pmatrix} = \begin{pmatrix} 1 & 0 & 0 & 0 \\ s^2 t_x & c^2 & 2cst_z & -2cst_y \\ s^2 t_y & -2cst_z & c^2 & 2cst_x \\ s^2 t_z & 2cst_y & -2cst_x & c^2 \end{pmatrix} \begin{pmatrix} 1 \\ w_x \\ w_y \\ w_z \end{pmatrix}, \tag{A.27}$$

the equation above can be rewritten as $\mathcal{E}[\rho_S^0] = T\rho_S^0$, with the vector representation of ρ_S^0 and

$$T = \begin{pmatrix} 1 & \vec{0}^{\mathrm{T}} \\ s^2\vec{t} & \mathbf{T}, \end{pmatrix} \tag{A.28}$$

where $\vec{0}$ is the vector of 3 components with 0 in the entries. Finally it is straightforward to prove that $T\rho_A = \rho_A$ using Eqs. (A.27) and (A.28) and hence that ρ_A is a fixed point of $\mathcal{E}$.

Furthermore, to prove that $\mathcal{E}$ is contrative, let us define $\vec{v}$ such that $\eta = \frac{1}{2}\mathbf{I} + \vec{v}\cdot\vec{\sigma}$ is a density matrix and $\vec{r} = \vec{w} - \vec{v}$ and use the trace distance definition, so that

$$D(\rho, \eta) = \mathrm{Tr}\,|(\vec{w} - \vec{v})\cdot\vec{\sigma}| = \mathrm{Tr}\,|\vec{r}\cdot\vec{\sigma}| = 2|\vec{r}|, \tag{A.29}$$

where we used that the eigenvalues of $\vec{r}\cdot\vec{\sigma}$ are $\pm|\vec{r}|$. Similarly, we obtain that

$$D(\mathcal{E}[\rho], \mathcal{E}[\eta]) = 2|\vec{r}'|, \tag{A.30}$$

where

$$\begin{aligned} \vec{r}' &= \vec{w}' - \vec{v}' = s^2\vec{t} + \mathbf{T}\vec{w} - s^2\vec{t} - \mathbf{T}\vec{v} = \mathbf{T}(\vec{w} - \vec{v}) = \mathbf{T}\vec{r} \\ &= c^2\vec{r} - 2cs\vec{t}\times\vec{r}, \end{aligned}$$

where we used Eqs. (A.27) and (A.28) in the last equality. The equation above implies that

$$|\vec{r}'|^2 = c^4|\vec{r}|^2 + 4c^2s^2|\vec{t}\times\vec{r}|^2 = |\vec{r}|^2c^2(c^2 + 4s^2|\vec{t}|^2\sin^2\beta),$$

where in the first equality we used that $\vec{r}'$ is orthogonal to $\vec{t} \times \vec{r}$ and in the last equality we used that $|\vec{t} \times \vec{r}| = |\vec{t}||\vec{r}| \sin\beta$, for some $0 \leq \beta \leq \pi$. Now, since $|\vec{t}|^2 \leq 1/4$, we must have $c^2 + 4s^2|\vec{t}|^2 \sin^2\beta \leq c^2 + s^2 \sin^2\beta \leq 1$ since $\sin^2\beta \leq 1$. Using this in the equation above, we obtain

$$|\vec{r}'| \leq |c||\vec{r}|.$$

Finally, combining the equation above with Eqs. (A.29) and (A.30), we obtain

$$D(\mathcal{E}[\rho], \mathcal{E}[\eta]) = 2|\vec{r}'| \leq 2|c||\vec{r}| = |c|D(\rho, \eta),$$

from which we obtain that $\mathcal{E}$ is a contractive map if $|c| < 1$ and thus it converges to its fixed point ρ_A due to Banach Theorem.

Turning the attention now to the ancillae evolution, we have from Eq. 2.53 that if we want to satisfy, for any δ, the condition of Eq. (2.48), we must have a bound for the distance between the first collision and the original ancilla state $D(\rho_A^1, \rho_A)$. The condition of Eq. 2.48 implies that

$$D(\rho_A^1, \rho_A) \leq \delta. \tag{A.31}$$

Now, since ρ_A^1 depends on the initial system state ρ_S^0, we must use the value of ρ_S^0 that makes the greatest distance above. This is the case where the two states are pure and mutually orthogonal, i.e., $\vec{w} = -\vec{t}$ and $|\vec{t}| = 1/2$. Using this and Eq. (2.52) in the equation above, we obtain

$$2s^2 \operatorname{Tr}|\vec{t} \cdot \vec{\sigma}| = 2s^2 \leq \delta,$$

and this implies Eq. (2.54). And since this assures that the distance between ρ_A^n and ρ_A is smaller than δ for any $n > 1$, this completes the convergence of ρ_A^n to ρ_A.

Appendix B

Some proofs and definitions in Quantum Information

B.1 Some useful equations

Given a function that can be expanded in the series of the form

$$f(x) = \sum_{i=0}^{\infty} a_i x^i, \tag{B.1}$$

where a_i are complex numbers, and an operator A that can define $f(A)$ such that

$$f(A) = \sum_{i=0}^{\infty} a_i A^n. \tag{B.2}$$

If A can be diagonalized as

$$A = \sum_{\alpha} \lambda_\alpha \left|\lambda_\alpha\right\rangle \left\langle\lambda_\alpha\right|, \tag{B.3}$$

where $\{\lambda_\alpha\}_\alpha$ and $\{|\lambda_\alpha\rangle\}_\alpha$ are respectivley the eigenvalues and eigenvectors of A, then

$$\begin{aligned} f(A) &= \sum_{i=0}^{\infty} a_i \left(\sum_\alpha \lambda_\alpha |\lambda_\alpha\rangle \langle\lambda_\alpha| \right)^i \\ &= \sum_{i=0}^{\infty} a_i \sum_\alpha \lambda_\alpha^i |\lambda_\alpha\rangle \langle\lambda_\alpha| \\ &= \sum_\alpha \left(\sum_{i=0}^{\infty} a_i \lambda_\alpha^i \right) |\lambda_\alpha\rangle \langle\lambda_\alpha| \\ &= \sum_\alpha f(\lambda_\alpha) |\lambda_\alpha\rangle \langle\lambda_\alpha| . \end{aligned}$$

Writing succinctly,

$$\boxed{f(A) = \sum_\alpha f(\lambda_\alpha) |\lambda_\alpha\rangle \langle\lambda_\alpha| .} \tag{B.4}$$

B.2 Proof of Eq. (3.10)

Being the density matrix ρ diagonalized as in Eq. (3.8) and given that the function $x \log x$ can be Taylor expanded, we can use Eq. (B.4) to obtain

$$\rho \log \rho = \sum_i \lambda_i \log \lambda_i |\lambda_i\rangle \langle\lambda_i| , \tag{B.5}$$

and hence we arrive at

$$- \operatorname{Tr}(\rho \log \rho) = - \sum_i \lambda_i \log \lambda_i . \tag{B.6}$$

Appendix C

Some proofs and definitions in Continuous Variables

C.1 Notation for vectors and matrices of operators

Given two vector of operators $\hat{\mathbf{a}}$ and $\hat{\mathbf{b}}$, we can build an operator

$$\hat{\mathbf{a}}^{\mathrm{T}}\hat{\mathbf{b}} = \sum_j \hat{\mathbf{a}}_j \hat{\mathbf{b}}_j, \tag{C.1}$$

and matrix of operators $\hat{\mathbf{a}}\hat{\mathbf{b}}^{\mathrm{T}}$ with components

$$(\hat{\mathbf{a}}\hat{\mathbf{b}}^{\mathrm{T}})_{jk} = \hat{\mathbf{a}}_j \hat{\mathbf{b}}_k. \tag{C.2}$$

Since operators don't always commute, we have, in general $\hat{\mathbf{a}}\hat{\mathbf{a}}^{\mathrm{T}} \neq (\hat{\mathbf{a}}\hat{\mathbf{a}}^{\mathrm{T}})^{\mathrm{T}}$, because the elements inside the vectors may not commute. Therefore, we can define the following commutators and anti-commutators

$$[\hat{\mathbf{a}}, \hat{\mathbf{a}}^{\mathrm{T}}] = \hat{\mathbf{a}}\hat{\mathbf{a}}^{\mathrm{T}} - (\hat{\mathbf{a}}\hat{\mathbf{a}}^{\mathrm{T}})^{\mathrm{T}}, \tag{C.3}$$

$$\{\hat{\mathbf{a}}, \hat{\mathbf{a}}^{\mathrm{T}}\} = \hat{\mathbf{a}}\hat{\mathbf{a}}^{\mathrm{T}} + (\hat{\mathbf{a}}\hat{\mathbf{a}}^{\mathrm{T}})^{\mathrm{T}}, \tag{C.4}$$

to express such differences. Combining both equations, we obtain

$$\{\hat{\mathbf{a}}, \hat{\mathbf{a}}^{\mathrm{T}}\} + [\hat{\mathbf{a}}, \hat{\mathbf{a}}^{\mathrm{T}}] = 2\hat{\mathbf{a}}\hat{\mathbf{a}}^{\mathrm{T}}. \tag{C.5}$$

We can also write

$$[\hat{\mathbf{a}}, \hat{\mathbf{a}}^{\mathrm{T}}]_{jk} = \hat{\mathbf{a}}_j\hat{\mathbf{a}}_k - \hat{\mathbf{a}}_k\hat{\mathbf{a}}_j, \tag{C.6}$$

$$\{\hat{\mathbf{a}}, \hat{\mathbf{a}}^{\mathrm{T}}\}_{jk} = \hat{\mathbf{a}}_j\hat{\mathbf{a}}_k + \hat{\mathbf{a}}_k\hat{\mathbf{a}}_j. \tag{C.7}$$

C.2 The direct sum

Given two matrices N (with dimension $n_1 \times n_2$) and M (with dimension $m_1 \times m_2$), then the direct sum of both matrices is

$$N \oplus M = \begin{pmatrix} N & 0_{n_1\times m_2} \\ 0_{m_1\times n_2} & M, \end{pmatrix} \tag{C.8}$$

where $0_{n\times m}$ means a $n \times m$ null matrix.

The notation $\bigoplus_{n=1}^{N} A_n$ means the direct sum of the A_n matrices from 1 to N

$$\bigoplus_{n=1}^{N} A_n = A_1 \oplus A_2 \oplus \cdots \oplus A_N. \tag{C.9}$$

C.3 General Gaussian integral

For further use, here we expose the well-known generalization of the Gaussian integral. Given a positive definite $2n \times 2n$ matrix $\mathbf{A}$ and a $2n$-dimensional vector $\mathbf{b}$, we have

$$\boxed{\int_{\mathbb{R}^{2n}} d\mathbf{r}\, e^{-\mathbf{r}^\top\mathbf{A}\mathbf{r}+\mathbf{r}^\top\mathbf{b}} = \frac{\pi^n}{\sqrt{\det\mathbf{A}}} e^{\frac{1}{4}\mathbf{b}^\top\mathbf{A}^{-1}\mathbf{b}}.} \tag{C.10}$$

C.4 Proof of Eq. (4.23)

For proving this equation, we define a vector of operators $\hat{f}(\mathbf{r}) = e^{-i\mathbf{r}^{\mathrm{T}}\Omega\hat{\mathbf{r}}}\hat{\mathbf{r}}e^{i\mathbf{r}^{\mathrm{T}}\Omega\hat{\mathbf{r}}}$, from which we have $\hat{f}(0) = \hat{\mathbf{r}}$, where 0 here means a $2n$ vector of 0s. Now, making a Taylor

expansion of $\hat{f}(\mathbf{r})$ around $\mathbf{r} = 0$, we get

$$\hat{f}_k(\mathbf{r}) = \hat{f}_k(0) + \sum_j \mathbf{r}_j \frac{\partial \hat{f}_k(\mathbf{r}')}{\partial \mathbf{r}'_j}\Big|_{\mathbf{r}'=0} + \sum_{jl} \mathbf{r}_j \mathbf{r}_l \frac{\partial^2 \hat{f}_k(\mathbf{r}')}{\partial \mathbf{r}'_j \partial \mathbf{r}'_l}\Big|_{\mathbf{r}'=0} + \cdots . \tag{C.11}$$

But

$$\begin{aligned}
\frac{\partial \hat{f}_k(\mathbf{r}')}{\partial \mathbf{r}'}\Big|_{\mathbf{r}'=0} &= \frac{\partial}{\partial \mathbf{r}'} \left(e^{-i \sum_{lm} \mathbf{r}'_l \Omega_{lm} \hat{\mathbf{r}}_m} \hat{\mathbf{r}}_k e^{\sum_{st} \mathbf{r}'_s \Omega_{st} \hat{\mathbf{r}}_t} \right) \Big|_{\mathbf{r}'=0} \\
&= -i \sum_m \Omega_{jm} [\hat{\mathbf{r}}_m, \hat{\mathbf{r}}_k] \\
&= \sum_m \Omega_{jm} \Omega_{mk} \\
&= -\delta_{jk},
\end{aligned}$$

and it is easy to show that higher order derivatives are 0. Using these results in Eq. (C.11), we obtain $\hat{f}(\mathbf{r}) = \hat{\mathbf{r}} - \mathbf{r}$.

C.5 Proof of Eq. (4.31)

We have that, from the definition of $|\alpha\rangle$ (Eq. (4.30))

$$\begin{aligned}
\hat{a}_j |\alpha\rangle &= \hat{a}_j \hat{D}_\alpha |0\rangle \\
&= \alpha_j \hat{D}_\alpha |0\rangle \\
&= \alpha_j |\alpha\rangle ,
\end{aligned} \tag{C.12}$$

where in the second equality we used the following result. From Eq. (4.29), we have

$$\begin{aligned}
\hat{a}_j \hat{D}_\alpha |0\rangle &= \hat{D}_\alpha \hat{D}^\dagger_\alpha \hat{a}_j \hat{D}_\alpha |0\rangle \\
&= \hat{D}_\alpha (\hat{a}_j + \alpha_j) |0\rangle \\
&= \alpha_j \hat{D}_\alpha |0\rangle .
\end{aligned} \tag{C.13}$$

C.6 Proof of the formula of coherent state expanded in the Fock basis (Eq. (4.32))

We can assume that a coherent state can be expanded in the Fock basis as $|\alpha\rangle = \sum_{m=0}^{\infty} c_m |m\rangle$ for some coefficients c_m, then

$$\begin{aligned}
\hat{a}|\alpha\rangle &= \sum_{m=0}^{\infty} c_m \hat{a}|m\rangle \\
&= \sum_{m=0}^{\infty} c_m \sqrt{m}\,|m-1\rangle \\
&= \sum_{m=0}^{\infty} c_{m+1}\sqrt{m+1}\,|m\rangle \\
&= \alpha \sum_{m=0}^{\infty} c_m |m\rangle\,,
\end{aligned}$$

since α is the eigenvalue of $\hat{a}$ for the eigenvector $|\alpha\rangle$. From the linear independence of the kets $|m\rangle$, we must have the recurrence equation

$$c_{m+1}\sqrt{m+1} = \alpha c_m,$$

whose solution is

$$c_m = A\frac{\alpha^m}{\sqrt{m!}},$$

where A is a constant to be determined by normalization. Then

$$\begin{aligned}
\langle\alpha|\alpha\rangle &= \sum_{m=0}^{\infty} |c_m|^2 \\
&= |A|^2 \sum_{m=0}^{\infty} \frac{|\alpha|^{2m}}{m!} \\
&= |A|^2 e^{|\alpha|^2} \\
&= 1 \\
&\Longrightarrow A = e^{-|\alpha|^2/2},
\end{aligned}$$

so finally

$$|\alpha\rangle = \sum_{m=0}^{\infty} e^{-|\alpha|^2/2} \frac{\alpha^m}{\sqrt{m!}} |m\rangle . \tag{C.14}$$

C.7 Completeness relation for coherent states

Using the Fock basis decomposition (Eq. (4.32))

$$\begin{aligned}
\frac{1}{\pi}\int_{\mathbb{C}} d^2\alpha \, |\alpha\rangle\langle\alpha| &= \frac{1}{\pi}\sum_{m,n=0}^{\infty}\int_{\mathbf{C}} d^2\alpha \frac{\alpha^m \alpha^{*n}}{\sqrt{m!n!}} e^{-|\alpha|^2} |m\rangle\langle n| \\
&= \frac{1}{\pi}\sum_{m,n=0}^{\infty}\int_0^{\infty} d\rho \int_0^{2\pi} d\phi e^{i(m-n)\phi} \frac{e^{-\rho^2}\rho^{m+n+1}}{\sqrt{m!n!}} |m\rangle\langle n| \\
&= \sum_{m=0}^{\infty} 2\int_0^{\infty} d\rho \frac{e^{-\rho^2}\rho^{2m+1}}{m!} |m\rangle\langle m| \\
&= \sum_{m=0}^{\infty} |m\rangle\langle m| \\
&= \mathbf{I},
\end{aligned} \tag{C.15}$$

where in the second equality we used that $\int_0^{2\pi} e^{i(m-n)\phi} d\phi = 2\pi\delta_{mn}$ and parametrized $\alpha = \rho e^{i\phi}$ and in the last equality we used the Gamma function $\int_0^{\infty} e^{-\rho^2}\rho^{2m+1} d\rho = m!/2$.

C.8 Proof of the Fourier-Weyl relation

From the completeness relation for coherent states, we can expand any bounded operator $\hat{A}$ as

$$\hat{A} = \frac{1}{\pi^2}\int_{\mathbb{C}^2} d\alpha d\beta \, \langle\alpha|\hat{A}|\beta\rangle |\alpha\rangle\langle\beta| , \tag{C.16}$$

notice that if

$$|\alpha\rangle\langle\beta| = \frac{1}{\pi}\int_{\mathbb{C}} d^2\gamma \, \mathrm{Tr}\Big\{|\alpha\rangle\langle\beta| \hat{D}_\gamma\Big\}\hat{D}_\gamma^\dagger, \tag{C.17}$$

the proof would be complete. So we shall demonstrate Eq. (C.17), applying $\hat{D}_{-\alpha}$ from the left of Eq. (C.17) and $\hat{D}_{\beta}$ from the right, we obtain

$$\begin{aligned}
|0\rangle\langle 0| &= \frac{1}{\pi}\int_{\mathbb{C}} d^2\gamma \,\mathrm{Tr}\Big\{|\alpha\rangle\langle\beta|\,\hat{D}_{\gamma}\Big\}\hat{D}_{-\alpha}\hat{D}_{-\gamma}\hat{D}_{\beta} \\
&= \frac{1}{\pi}\int_{\mathbb{C}} d^2\gamma \,\mathrm{Tr}\{|\alpha\rangle\langle\beta-\gamma|\}e^{\frac{1}{2}(\gamma\beta^*-\gamma^*\beta)}\hat{D}_{-\alpha}\hat{D}_{-\gamma}\hat{D}_{\beta} \\
&= \frac{1}{\pi}\int_{\mathbb{C}} d^2\gamma \,\langle\beta-\gamma|\alpha\rangle\, e^{\frac{1}{2}(\gamma\beta^*-\gamma^*\beta)}\hat{D}_{-\alpha}\hat{D}_{-\gamma}\hat{D}_{\beta} \\
&= \frac{1}{\pi}\int_{\mathbb{C}} d^2\gamma e^{-\frac{1}{2}|\beta-\alpha-\gamma|^2}\hat{D}_{\beta-\alpha-\gamma} \\
&= \frac{1}{\pi}\int_{\mathbb{C}} d^2\gamma e^{-\frac{1}{2}|\gamma|^2}\hat{D}_{\gamma},
\end{aligned} \tag{C.18}$$

where in the second equality we used Eq. 4.33, in the third equality we used Eq. 4.34 and at the last equality we made a change of variables. Thus we must prove that $\frac{1}{\pi}\int_{\mathbb{C}} d^2\gamma e^{-\frac{1}{2}|\gamma|^2}\hat{D}_{\gamma} = |0\rangle\langle 0|$ in order to complete the proof. For this, notice that, applying it on a Fock basis vecor $|m\rangle$, we have

$$\begin{aligned}
\frac{1}{\pi}\int_{\mathbb{C}} d^2\gamma e^{-\frac{1}{2}|\gamma|^2}\hat{D}_{\gamma}|m\rangle &= \frac{1}{\pi}\int_{\mathbb{C}} d^2\gamma e^{-\frac{1}{2}|\gamma|^2}\hat{D}_{\gamma}\frac{\hat{a}^{\dagger m}}{\sqrt{m!}}|0\rangle \\
&= \frac{1}{\pi}\int_{\mathbb{C}} d^2\gamma e^{-\frac{1}{2}|\gamma|^2}\hat{D}_{\gamma}\frac{\hat{a}^{\dagger m}}{\sqrt{m!}}\hat{D}_{\gamma}^{\dagger}\hat{D}_{\gamma}|0\rangle \\
&= \frac{1}{\pi}\int_{\mathbb{C}} d^2\gamma e^{-\frac{1}{2}|\gamma|^2}\frac{(\hat{a}^{\dagger}-\gamma^*)^m}{\sqrt{m!}}|\gamma\rangle \\
&= \int_{\mathbb{C}}\frac{d^2\gamma}{\pi}e^{-|\gamma|^2}\frac{(\hat{a}^{\dagger}-\gamma^*)^m}{\sqrt{m!}}\sum_{n=0}^{\infty}\frac{\gamma^n}{\sqrt{n!}}|n\rangle \\
&= \sum_{n=0}^{\infty}\sum_{j=0}^{m}\int_{\mathbb{C}}\frac{d^2\gamma}{\pi}e^{-|\gamma|^2}\binom{m}{j}\frac{(-\gamma)^{*j}\gamma^n}{\sqrt{m!n!}}\hat{a}^{\dagger(m-j)}|n\rangle \\
&= \sum_{j=0}^{m}\binom{m}{j}(-1)^j|m\rangle \\
&= \delta_{m0}|0\rangle\,,
\end{aligned} \tag{C.19}$$

where in the third equality we used that $\hat{D}_{\gamma}\hat{a}^{\dagger}\hat{D}_{\gamma}^{\dagger} = \hat{a}^{\dagger}-\gamma^*$, in the forth equality we used Eq. (4.32), in the sixth equality we used $\frac{1}{\pi}\int_{\mathbb{C}} d^2\gamma e^{-|\gamma|^2}\gamma^{*j}\gamma^n = n!\delta_{jn}$ and in the last step we used the fact that $\sum_{j=0}^{m}\binom{m}{j}(-1)^j = (1-1)^m = \delta_{m0}$. Finally, we have that Eq. (C.19) implies (C.18) which is equivalent to Eq. (C.17).

C.9 Proof of Eq. (4.47)

Given the definitions of Eq. (4.46) and Eq. (4.26) and using that the one mode vector $r' = (q', p')$, we have

$$\begin{aligned} W(q,p) &= \frac{1}{\pi^2}\int_{\mathbb{R}}\int_{\mathbb{R}} dq'dp' e^{i(pq'-qp')}\chi(q',p') \\ &= \frac{1}{2\pi^2}\int_{\mathbb{R}}\int_{\mathbb{R}} dq'dp' e^{i(pq'-qp')}\int_{\mathbb{R}} dx\, \langle x|\, \hat{D}_{-\frac{r'}{2}}\rho\hat{D}_{-\frac{r'}{2}}\, |x\rangle \\ &= \frac{1}{\pi^2}\int_{\mathbb{R}}\int_{\mathbb{R}}\int_{\mathbb{R}} dq'dp'dx\; e^{ipq'}e^{ip'(x-q)}\left\langle x-\frac{q'}{2}\right|\rho\left|x+\frac{q'}{2}\right\rangle \\ &= \frac{1}{\pi}\int_{\mathbb{R}} dq'\; e^{ipq'}\left\langle q-\frac{q'}{2}\right|\rho\left|q+\frac{q'}{2}\right\rangle \\ &= \frac{2}{\pi}\int_{\mathbb{R}} dq'\; e^{ipq'}\,\langle q-q'|\,\rho\,|q+q'\rangle\,, \end{aligned} \tag{C.20}$$

where in the second equality we expanded the trace of the definition of $\chi(q', p')$ (Eq. (4.43)) in therms of a first quadrature basis $|x\rangle$, we used the cyclic property of the trace and used that $\hat{D}_{-r'} = \hat{D}_{-r'/2}\hat{D}_{-r'/2}$ and in the third equality we used that $\hat{D}_{-r'/2} = e^{-\frac{i}{2}q'\hat{p}}e^{\frac{i}{2}p'\hat{q}}e^{\frac{i}{8}q'p'}$ and thus $\hat{D}_{-r'/2}\,|x\rangle = \left|x+\frac{q'}{2}\right\rangle e^{\frac{i}{2}p'x}e^{\frac{i}{8}q'p'}$.

C.10 Proof of Eq. (4.52)

From applying the Weyl operator $\hat{D}_\alpha$ from the left of Eq. (C.18) and its conjugate transpose operator from the right of this equation, we obtain

$$|\alpha\rangle\langle\alpha| = \frac{1}{\pi}\int_{\mathbb{C}} d^2\gamma e^{-\frac{1}{2}|\gamma|^2}e^{(\alpha\gamma^*-\alpha^*\gamma)}\hat{D}_{-\gamma}, \tag{C.21}$$

where we used Eq. (4.33) so that $\hat{D}_\alpha \hat{D}_\gamma \hat{D}_{-\alpha} = e^{(\alpha\gamma^* - \alpha^*\gamma)} \hat{D}_\gamma$. Using the equation above, we obtain

$$\begin{aligned}
\int_{\mathbb{C}} d^2\alpha P(\alpha) \left|\alpha\right\rangle \left\langle\alpha\right| &= \frac{1}{\pi} \int_{\mathbb{C}} d^2\gamma e^{-\frac{1}{2}|\gamma|^2} \int_{\mathbb{C}} d^2\alpha e^{(\alpha\gamma^* - \alpha^*\gamma)} P(\alpha) \hat{D}_{-\gamma} \\
&= \frac{1}{\pi} \int_{\mathbb{C}} d^2\gamma e^{-\frac{1}{2}|\gamma|^2} \chi_1(\gamma) \hat{D}_{-\gamma} \\
&= \frac{1}{\pi} \int_{\mathbb{C}} d^2\gamma \, \chi_0(\gamma) \hat{D}_{-\gamma} \\
&= \rho, \qquad \text{(C.22)}
\end{aligned}$$

where in the second equality we used the inverse Fourier transform of $P(\alpha)$ (since $P(\alpha) = \int_{\mathbb{C}} d^2\beta e^{(\alpha\gamma^* - \alpha^*\gamma)} \chi_1(\beta)$ then it's inverse will be $\chi_1(\gamma) = \int_{\mathbb{C}} d^2\alpha e^{(\alpha\gamma^* - \alpha^*\gamma)} P(\alpha)$), in the third equality we used Eq. (4.49) to relate $\chi_1(\alpha)$ to $\chi_0(\alpha)$ and in the forth equality we used the Fourier-Weyl relation (Eq. (4.40)).

C.11 Proof of Eq. (4.54)

Using the Fourier Weyl relation, (Eq. (4.40)) we obtain

$$\begin{aligned}
\frac{1}{\pi} \left\langle\alpha\right| \rho \left|\alpha\right\rangle &= \frac{1}{\pi^2} \int_{\mathbb{C}} d^2\beta \chi_0(\beta) \left\langle\alpha\right| \hat{D}_{-\beta} \left|\alpha\right\rangle \\
&= \frac{1}{\pi^2} \int_{\mathbb{C}} d^2\beta e^{\frac{1}{2}(\alpha\beta^* - \alpha^*\beta)} \chi_0(\beta) \left\langle\alpha|\alpha - \beta\right\rangle \\
&= \frac{1}{\pi^2} \int_{\mathbb{C}} d^2\beta e^{(\alpha\beta^* - \alpha^*\beta)} \chi_0(\beta) e^{-\frac{|\beta|^2}{2}} \\
&= W_{-1}(\alpha), \qquad \text{(C.23)}
\end{aligned}$$

where in the second equality we used Eq. (4.33) to obtain $\hat{D}_{-\beta} \left|\alpha\right\rangle = \hat{D}_{\alpha-\beta} \left|0\right\rangle e^{\frac{1}{2}(\alpha\beta^* - \alpha^*\beta)} = \left|\alpha - \beta\right\rangle e^{\frac{1}{2}(\alpha\beta^* - \alpha^*\beta)}$ and in the third equality we used Eq. (4.34).

C.12 Proof of the Robertson-Schrödinger relation (Eq. (4.63))

In order to obtain the formula, first consider the following $2n \times 2n$ complex matrix

$$\tau = 2 \operatorname{Tr}\left[(\hat{\mathbf{r}} - \bar{\mathbf{r}})(\hat{\mathbf{r}} - \bar{\mathbf{r}})^\dagger \rho\right]. \tag{C.24}$$

We can show that this operator is positive semi-definite in the following way. Suppose $v \in \mathbb{C}^{2n}$, then we have

$$\begin{aligned} v^\dagger \tau v &= 2 v^\dagger \operatorname{Tr}\left[(\hat{\mathbf{r}} - \bar{\mathbf{r}})(\hat{\mathbf{r}} - \bar{\mathbf{r}})^\dagger \rho\right] v \\ &= 2 \operatorname{Tr}\left[v^\dagger (\hat{\mathbf{r}} - \bar{\mathbf{r}})(\hat{\mathbf{r}} - \bar{\mathbf{r}})^\dagger v \rho\right] \\ &= 2 \operatorname{Tr}\left[\hat{\mathcal{O}}\hat{\mathcal{O}}^\dagger \rho\right] \\ &\geq 0, \end{aligned} \tag{C.25}$$

where $\mathcal{O} = v^\dagger(\hat{\mathbf{r}} - \bar{\mathbf{r}})$. In the second equality we used Eqs. (C.1) and (C.2) which imply

$$\begin{aligned} v^\dagger \operatorname{Tr}\left[(\hat{\mathbf{r}} - \bar{\mathbf{r}})(\hat{\mathbf{r}} - \bar{\mathbf{r}})^\dagger \rho\right] v &= \sum_{jk} v_j \operatorname{Tr}\left[(\hat{\mathbf{r}} - \bar{\mathbf{r}})_j (\hat{\mathbf{r}} - \bar{\mathbf{r}})_k \rho\right] v_k \\ &= \operatorname{Tr}\left[\sum_{jk} v_j (\hat{\mathbf{r}} - \bar{\mathbf{r}})_j (\hat{\mathbf{r}} - \bar{\mathbf{r}})_k v_k \rho\right] \\ &= \operatorname{Tr}\left[v^\dagger (\hat{\mathbf{r}} - \bar{\mathbf{r}})(\hat{\mathbf{r}} - \bar{\mathbf{r}})^\dagger v \rho\right], \end{aligned}$$

and in the last step of Eq. (C.25), we used the fact that for every operator $\mathcal{O}$, $\mathcal{O}\mathcal{O}^\dagger$ is positive semidefinite and ρ is also semidefinite, hence $\mathcal{O}\mathcal{O}^\dagger\rho$ is positive semidefinite.

This concludes the proof that $\tau \geq 0$. Now, from Eq. (C.5) and from $\tau \geq 0$, we have that

$$\begin{aligned}
\tau &= 2\,\mathrm{Tr}\left[(\hat{\mathbf{r}}-\bar{\mathbf{r}})(\hat{\mathbf{r}}-\bar{\mathbf{r}})^\dagger \rho\right] \\
&= \mathrm{Tr}\left[\{(\hat{\mathbf{r}}-\bar{\mathbf{r}}),(\hat{\mathbf{r}}-\bar{\mathbf{r}})^\dagger\}\rho\right] + \mathrm{Tr}\left[[(\hat{\mathbf{r}}-\bar{\mathbf{r}}),(\bar{\mathbf{r}}-\bar{\mathbf{r}})^\dagger]\rho\right] \\
&= \mathrm{Tr}\left[\{(\hat{\mathbf{r}}-\bar{\mathbf{r}}),(\hat{\mathbf{r}}-\bar{\mathbf{r}})^\dagger\}\rho\right] + \mathrm{Tr}\left[[\hat{\mathbf{r}},\bar{\mathbf{r}}^\dagger]\rho\right] \\
&= 2\sigma + i\Omega \\
&\geq 0,
\end{aligned} \tag{C.26}$$

where in the third equality we used Eqs. (4.61) and (4.14). Finally, we obtain

$$\boxed{\sigma + \frac{i\Omega}{2} \geq 0.} \tag{C.27}$$

C.13 Density matrix and covariance matrix of free Gaussian bosonic modes

If we have a Gaussian state of N free bosonic modes, then it will have the form

$$\rho_{\text{free}} = \frac{e^{-\hat{\mathbf{r}}^\top \Lambda \hat{\mathbf{r}}}}{Z}, \tag{C.28}$$

where $\Lambda = \mathrm{diag}(\lambda_1, \lambda_2, \cdots, \lambda_N),\ \lambda_j > 0,\ \forall j$ and $Z = \mathrm{Tr}\left(e^{-\hat{\mathbf{r}}^\top \Lambda \hat{\mathbf{r}}}\right)$. Since the modes are non-interacting, we have

$$\rho_{\text{free}} = \bigotimes_{j=1}^{n} \frac{e^{-\frac{\lambda_j}{2}(\hat{q}_j^2+\hat{p}_j^2)}}{Z_j}, \tag{C.29}$$

where $Z_j = \mathrm{Tr}\left(e^{-\frac{\lambda_j}{2}(\hat{q}_j^2+\hat{p}_j^2)}\right)$. Computing explicitly and using the geometric series, we obtain

$$\begin{aligned}
Z_j &= \sum_{n_j=0}^{\infty} e^{-\lambda_j(n_j+1/2)} \\
&= \frac{e^{-\lambda_j/2}}{1-e^{-\lambda_j}}.
\end{aligned} \tag{C.30}$$

Consequently, the density matrix will be

$$\begin{aligned}\rho_{\text{free}} &= \bigotimes_{j=1}^{n} \frac{e^{-\frac{\lambda_j}{2}(\hat{q}_j^2+\hat{p}_j^2)}}{Z_j} \\ &= \bigotimes_{j=1}^{n} \sum_{n_j=0}^{\infty} \frac{e^{-\lambda_j(n_j+1/2)}}{Z_j} |n_j\rangle \langle n_j| \\ &= \bigotimes_{j=1}^{n} \left(1-e^{-\lambda_j}\right) \sum_{n_j=0}^{\infty} e^{-\lambda_j n_j} |n_j\rangle \langle n_j| \end{aligned} \tag{C.31}$$

For a mode j, we have a well-known average, called the *Bose-Einstein* distribution

$$\boxed{\bar{n}_j = \langle \hat{a}_j^\dagger \hat{a}_j \rangle = \frac{1}{e^{\lambda_j}-1}.} \tag{C.32}$$

We can rewrite the density matrix of free bosonic modes in terms of the Bose-Einstein distribution

$$\boxed{\rho_{\text{free}} = \bigotimes_{j=1}^{n} \frac{1}{1+\bar{n}_j} \sum_{n_j=0}^{\infty} \left(\frac{\bar{n}_j}{\bar{n}_j+1}\right)^{n_j} |n_j\rangle \langle n_j| .} \tag{C.33}$$

From Eq. (4.6) we have that, for a mode j,

$$\langle \hat{q}_j^2 \rangle = \langle \hat{p}_j^2 \rangle = \langle a_j^\dagger a_j \rangle + 1/2, \tag{C.34}$$

and hence, using Eq. (C.32), we have

$$\langle \hat{q}_j^2 \rangle = \langle \hat{p}_j^2 \rangle = \frac{1}{2} \coth(\lambda_j/2). \tag{C.35}$$

For this state $\langle q_j \rangle = \langle p_j \rangle = 0, \ \forall j$, so the covariance matrix will be

$$\begin{aligned}\sigma_{ij} &= \frac{1}{2} \langle \{\hat{\mathbf{r}}_i, \hat{\mathbf{r}}_j\} \rangle \\ &= \frac{1}{2} \coth(\lambda_j/2) \delta_{ij} \end{aligned} \tag{C.36}$$

which means

$$\boxed{\sigma = \frac{1}{2} \coth\left(\frac{\Lambda}{2}\right).} \tag{C.37}$$

This can also be rewritten as

$$\sigma = \bigoplus_{j=1}^{n} \nu_j \begin{pmatrix} 1 & 0 \\ 0 & 1 \end{pmatrix}, \tag{C.38}$$

where $\nu_j = \frac{1}{2}\coth\left(\frac{\lambda_j}{2}\right)$.

Notice that from Eqs. (C.34) and (C.35) we can describe the diagonal covariance matrix elements in terms of the Bose-Einstein distributions

$$\nu_j = \bar{n}_j + \frac{1}{2}. \tag{C.39}$$

Finally, we can write the density matrix in terms of the diagonal elements of the covariance matrix

$$\boxed{\rho_{\text{free}} = \bigotimes_{j=1}^{n} \frac{1}{\nu_j + 1/2} \sum_{n_j=0}^{\infty} \left(\frac{\nu_j - 1/2}{\nu_j + 1/2}\right)^{n_j} |n_j\rangle \langle n_j|.} \tag{C.40}$$

C.14 Obtaining symplectic eigenvalues

According to the Williamson's theorem (Eq. (4.83)), given a positive definite matrix M, there is a symplectic matrix S such that

$$M = SDS^{\mathrm{T}}, \tag{C.41}$$

where

$$D = D_n \otimes \mathbb{I}_2, \quad \text{with} \quad D_n = \text{diag}(d_1, d_2, \cdots, d_n), \tag{C.42}$$

with $d_j > 0,\ \forall j$.

Notice that the matrix $i\Omega M$ is hermitian, hence it can be diagonalized as

$$i\Omega M = B\Lambda B^{\dagger}, \tag{C.43}$$

where Λ is a diagonal matrix of eigenvalues and B is a unitary matrix with eigenvectors as columns. Using the properties of the symplectic matrix S and of the symplectic form Ω, we can relate Λ to the symplectic eigenvalues, this can be done as follows. From Eq.

(C.42) we obtain

$$\begin{aligned} i\Omega M &= i\Omega S D S^{\top} \\ &= i\Omega S(D_n \otimes \mathbb{I}_2)S^{\top} \\ &= iS^{-\top}(\Omega)(D_n \otimes \mathbb{I}_2)S^{\top} \\ &= iS^{-\top}(\mathbb{I}_n \otimes \Omega_1)(D_n \otimes \mathbb{I}_2)S^{\top} \\ &= iS^{-\top}(D_n \otimes \Omega_1)S^{\top} \\ &= S^{-\top}(D_n \otimes i\Omega_1)S^{\top} \end{aligned} \tag{C.44}$$

where in the third equality, we used $\Omega S = S^{-\top}\Omega$.[1]

Finally, notice that

$$i\Omega_1 = -U_2\sigma_z U_2^{\dagger}, \tag{C.45}$$

where $U_2 = \frac{1}{\sqrt{2}}\begin{pmatrix} 1 & 1 \\ i & -i, \end{pmatrix}$. The formula above can be shown by direct evaluation, and applying it in Eq. (C.44), it follows that

$$i\Omega M = S^{-\top}(\mathbb{I}_n \otimes U_2)(D_n \otimes (-\sigma_z))(\mathbb{I}_n \otimes U_2^{\dagger})S^{\top}, \tag{C.46}$$

which is in the form of Eq. (C.43). Identifying the unitary $B = S^{-\top}(\mathbb{I}_n \otimes U_2)$ and $\Lambda = D_n \otimes (-\sigma_z)$ we conclude that we can obtain the symplectic eigenvalues (the diagonal elements of D_n) by computing the eigenvalues of $i\Omega M$ and taking their absolute values (since the eigenvalues of $i\Omega M$ come in pairs of plus and minus the diagonal elements of D_n).

[1] This is a consequence of the fact that, if S is a symplectic matrix, $S^{\top}$ also is symplectic (this can be seen by taking the transpose of Eq. (4.81) and using that $\Omega^{\top} = -\Omega$). Using this fact, we have that $S^{\top}\Omega S = \Omega$ and applying $S^{-\top}$ from the left hand side, we obtain $\Omega S = S^{-\top}\Omega$.

C.15 Justifying the existence of a Hamiltonian matrix corresponding to any symplectic matrix

We want to prove that, given a matrix $S \in S_{p_{2n,\mathbb{R}}}$ with strictly positive eigenvalues, then there exist a real and symmetric matrix H such that $S = e^{\Omega H}$. Furthermore, there exists a unitary $\hat{S}$ such that

$$S\hat{\mathbf{r}} = \hat{S}^{\dagger}\hat{\mathbf{r}}\hat{S}, \tag{C.47}$$

for any $2n$ vector of canonical operators $\hat{\mathbf{r}}$.

Given $S \in S_{p_{2n,\mathbb{R}}}$ with strictly positive eigenvalues, we can define the following matrix

$$H = \Omega^{\top} \log S. \tag{C.48}$$

By construction, H has positive elements. For proving that H is symmetric, notice that

$$\begin{aligned} H^{\top} &= \log\left(S^{\top}\right)\Omega \\ &= \Omega\Omega^{\top}\log\left(S^{\top}\right)\Omega \\ &= \Omega\log\left(\Omega^{\top}S^{\top}\Omega\right) \\ &= \Omega\log\left(S^{-1}\right) \\ &= -\Omega\log\left(S\right) \\ &= \Omega^{\top}\log\left(S\right) \\ &= H, \end{aligned} \tag{C.49}$$

where repeatedly used that $-\Omega = \Omega^{\top} = \Omega^{-1}$ and in the forth equality we used the fact that $\Omega S = S^{-\top}\Omega$ (which is proved in the previous section of this Appendix) which implies $S = \Omega^{\top}S^{-\top}\Omega \Rightarrow \Omega^{\top}S^{-1}\Omega$. Since we have that H, given by Eq. (C.48), is real and symmetric, then we have $S = e^{\Omega H}$ and, by the construction of Eq. (4.70), there must be a unitary $\hat{S} = e^{-\frac{1}{2}\hat{\mathbf{r}}^{\dagger}H\hat{\mathbf{r}}}$ such that

$$S\hat{\mathbf{r}} = \hat{S}^{\dagger}\hat{\mathbf{r}}\hat{S}. \tag{C.50}$$

C.16 Proof for the parametrization of Eq. (4.82)

We can start the proof as follows. Since ρ_G is a Gaussian state, then (see Eqs. (4.57) and (4.58)) it can be described as

$$\rho_G = \frac{e^{-\frac{1}{2}(\hat{\mathbf{r}}-\bar{\mathbf{r}})^{\mathsf{T}} M (\hat{\mathbf{r}}-\bar{\mathbf{r}})}}{Z}, \tag{C.51}$$

where M is a positive definite matrix and Z is a normalization constant. From Williamson's Theorem, we can diagonalize M with the use of a symplectic matrix S. Defining a new valid vector of canonical operators $\hat{\mathbf{Y}} = S(\hat{\mathbf{r}} - \bar{\mathbf{r}})$ and using Eq. (4.83), we can rewrite the Gaussian state as

$$\rho_G = \frac{e^{-\frac{1}{2}\hat{\mathbf{Y}}^{\top} D \hat{\mathbf{Y}}}}{Z}. \tag{C.52}$$

Since D is a diagonal matrix, the state ρ_G in the equation above represents a set of free non-interacting harmonic oscillators described by the canonical operators in $\hat{\mathbf{Y}}$. The covariance matrix of non-interacting harmonic oscillators has the simple form of (see Eq. (C.37), and the whole Section for a proof)

$$\begin{aligned} \tilde{\sigma} &= \frac{1}{2}\langle \hat{\mathbf{Y}}, \hat{\mathbf{Y}}^{\top} \rangle \\ &= \frac{1}{2} \coth\left(\frac{D}{2}\right). \end{aligned} \tag{C.53}$$

Now, consider the following relations

$$\begin{aligned} \sigma &= \frac{1}{2}\langle \{ (\hat{\mathbf{r}} - \bar{\mathbf{r}}), (\hat{\mathbf{r}} - \bar{\mathbf{r}})^{\top} \} \rangle \\ &= \frac{1}{2}\langle \{ S^{-1}\hat{\mathbf{Y}}, \hat{\mathbf{Y}}^{\top} S^{-\top} \} \rangle \\ &= \frac{1}{2} S^{-1} \langle \{ \hat{\mathbf{Y}}, \hat{\mathbf{Y}}^{\top} \} \rangle S^{-\top} \\ &= S^{-1} \tilde{\sigma} S^{-\top} \\ &= \frac{1}{2} S^{-1} \coth\left(\frac{D}{2}\right) S^{-\top}. \end{aligned} \tag{C.54}$$

We can use the equation above to obtain the relation between M and σ. With the use of Eq. (C.46), we have

$$\coth\left(\frac{i\Omega M}{2}\right) = S^{-1}(\mathbb{I}_n \otimes U_2)\coth\left(\frac{D_n \otimes (-\sigma_z)}{2}\right)(\mathbb{I}_n \otimes U_2^\dagger)S, \tag{C.55}$$

where $U_2 = \begin{pmatrix} 1 & 1 \\ i & -i \end{pmatrix}$ and $D_n = \text{diag}(d_1, d_2, \cdots, d_n)$ such that $D = D_n \otimes \mathbb{I}_2$. Using the fact that $\coth(\bullet)$ is a odd function, we have that $\coth\left(\frac{D_n\otimes(-\sigma_z)}{2}\right) = \coth(D_n/2)\otimes(-\sigma_z)$, and hence

$$\begin{aligned}
\coth\left(\frac{i\Omega M}{2}\right) &= S^{-1}(\mathbb{I}_n \otimes U_2)\left(\coth(D_n/2) \otimes (-\sigma_z)\right)(\mathbb{I}_n \otimes U_2^\dagger)S \\
&= S^{-1}\coth(D_n/2) \otimes (i\Omega_1)S \\
&= S^{-1}(\coth(D_n/2) \otimes \mathbb{I}_2)(\mathbb{I}_n \otimes i\Omega_1)S \\
&= S^{-1}(\coth(D/2)i\Omega S \\
&= S^{-1}(\coth(D/2)S^{-\top}i\Omega \\
&= 2\sigma i\Omega,
\end{aligned} \tag{C.56}$$

where in the second equality we used Eq. (C.45), in the fifth equality we used that $S^{-\top}\Omega = \Omega S$ (with is proved in the previous section of this Appendix) and in the last equality we used Eq. (C.54).

Applying $i\Omega$ in both sides of Eq. (C.56), and using that $(i\Omega)^2 = \mathbb{I}$, we obtain

$$i\Omega\coth\left(\frac{i\Omega M}{2}\right)i\Omega = 2i\Omega\sigma. \tag{C.57}$$

Since $i\Omega$ is unitary, the equation above can be rewritten as

$$2i\Omega\sigma = \coth\left(\frac{Mi\Omega}{2}\right), \tag{C.58}$$

inverting this result we finally obtain

$$M = 2\text{arccoth}(2i\Omega\sigma)i\Omega. \tag{C.59}$$

C.17 Computation of quasi-probability distributions for Gaussian states

For computing the Glauber-Sudarshan P-function of a Gaussian state, we use Eq. (4.85) in Eq. (4.86) for $s = 1$ and obtain

$$\begin{aligned} P_G(\mathbf{r}) &= \frac{1}{(2\pi^2)^n} \int_{\mathbb{R}^{2n}} d\mathbf{r}' e^{-\frac{1}{2}\mathbf{r}'\Omega^\top\sigma\Omega\mathbf{r}' - i\mathbf{r}'^\top\Omega\bar{\mathbf{r}}} e^{\frac{1}{4}\mathbf{r}'^\top\mathbf{r}' + i\mathbf{r}'^\top\Omega\mathbf{r}} \\ &= \frac{1}{(2\pi^2)^n} \int_{\mathbb{R}^{2n}} d\mathbf{r}' e^{-\frac{1}{2}\mathbf{r}'\Omega^\top(\sigma - \mathbb{I}/2)\Omega\mathbf{r}' + i\mathbf{r}'^\top\Omega(\mathbf{r}-\bar{\mathbf{r}})}, \end{aligned} \tag{C.60}$$

where we reordered the terms and used that $\Omega^\top\Omega = -\Omega^2 = 1$ (Eqs. (4.11) and (4.12)) in the second equality. Now, using the Gaussian integral (Eq. (C.10)) in the equation above, we obtain

$$\begin{aligned} P_G(\mathbf{r}) &= \frac{1}{(2\pi^2)^n} \frac{\pi^n}{\sqrt{\det\left(\frac{1}{2}\Omega^\top(\sigma - \mathbb{I}/2)\Omega\right)}} e^{\frac{1}{2}(i\Omega(\mathbf{r}-\bar{\mathbf{r}}))^\top\left(\Omega^\top(\sigma-\mathbb{I}/2)\Omega\right)^{-1}(i\Omega(\mathbf{r}-\bar{\mathbf{r}}))} \\ &= \frac{1}{(2\pi)^n} \frac{1}{\sqrt{\det\left(\sigma - \mathbb{I}/2\right)}} e^{-\frac{1}{2}(\mathbf{r}-\bar{\mathbf{r}})^\top\Omega^\top\Omega^\top(\sigma-\mathbb{I}/2)^{-1}\Omega\Omega(\mathbf{r}-\bar{\mathbf{r}})} \\ &= \frac{1}{(\pi)^n} \frac{e^{-\frac{1}{2}(\mathbf{r}-\bar{\mathbf{r}})^\top(\sigma-\mathbb{I}/2)^{-1}(\mathbf{r}-\bar{\mathbf{r}})}}{\sqrt{\det\left(\sigma - \mathbb{I}/2\right)}}, \end{aligned} \tag{C.61}$$

where in the second equality we used that $\Omega^{-1} = \Omega^\top$ (Eq. (4.11)) and that $\det(A.B) = \det(A)\det(B)$ for any matrices A and B, and in the third equality we used that $\Omega\Omega = \Omega^\top\Omega^\top = -1$.Finally, we must multiply this result by $\frac{1}{2^n}$ so that this function obtain the correct normalization (Eq. (4.51)) under the space of all $\mathbf{r}$, i.e., we must have

$$\int_{\mathbb{R}^{2n}} d\mathbf{r} P_G(\mathbf{r}) = 1. \tag{C.62}$$

For the cases of the Husimi Q-function and the Wigner W-function, the proof is exactly analogous for the choice of $s = -1$ and $s = 0$, respectively.

C.18 Proof that the commutator between any second order operators is a second order operator

Given two generic second order operators $\hat{\mathcal{O}}_1 = \frac{1}{2}\sum_{jk} O_{1jk}\hat{\mathbf{r}}_j\hat{\mathbf{r}}_k + \sum_j \mu_{1j}\hat{\mathbf{r}}_j$ and $\hat{\mathcal{O}}_2 = \frac{1}{2}\sum_{jk} O_{2jk}\hat{\mathbf{r}}_j\hat{\mathbf{r}}_k + \sum_j \mu_{2j}\hat{\mathbf{r}}_j$, the commutator between them will be

$$\begin{aligned}[\mathcal{O}_1, \mathcal{O}_2] =& \frac{1}{4}\sum_{jklm} O_{1jk}O_{2lm}[\hat{r}_j\hat{r}_k, \hat{r}_l\hat{r}_m] + \frac{1}{2}\sum_{jkl} O_{1jk}\mu_{2l}[\hat{r}_j\hat{r}_k, \hat{r}_l] \\ &+ \frac{1}{2}\sum_{jlm} O_{2lm}\mu_{1j}[\hat{r}_j, \hat{r}_l\hat{r}_m] + \sum_{jm}\mu_{1j}\mu_{2m}[\hat{r}_j, \hat{r}_m]. \end{aligned} \tag{C.63}$$

In order to show that the above commutator is at most of second order, we start by noticing that

$$\begin{aligned}[\hat{r}_j\hat{r}_k, \hat{r}_l\hat{r}_m] =& \hat{r}_j[\hat{r}_k, \hat{r}_l]\hat{r}_m + [\hat{r}_j, \hat{r}_l]\hat{r}_k\hat{r}_m + \hat{r}_l\hat{r}_j[\hat{r}_k, \hat{r}_m] + \hat{r}_l[\hat{r}_j, \hat{r}_m]\hat{r}_k \\ =& i\hat{r}_j\hat{r}_m\Omega_{kl} + i\hat{r}_k\hat{r}_m\Omega_{jl} + i\hat{r}_l\hat{r}_j\Omega_{km} + i\hat{r}_l\hat{r}_k\Omega_{jm}, \end{aligned} \tag{C.64}$$

where in the first equality we used that $[AB, CD] = A[B, C]D + [A, C]BD + CA[B, D] + C[A, D]B$ an in the second equality we used Eq. (4.14). The above commutator is thus at most of second order on canonical operators, and using again Eq. (4.14) we can similarly show that $[\hat{r}_j\hat{r}_k, \hat{r}_l]$, $[\hat{r}_j, \hat{r}_l\hat{r}_m]$ and $[\hat{r}_j, \hat{r}_m]$ are all at most second order operators. Hence, we conclude that the commutator of two generic second order Hamiltonians in Eq. (C.63) is a second order operator, as we intended.

C.19 Proof of Eq. (4.124)

Analyzing a mode j, notice that

$$
\begin{aligned}
S(\rho_{\text{free}_j}) &= -\operatorname{Tr}\left[\rho_{\text{free}_j}\log\left(\rho_{\text{free}_j}\right)\right] \\
&= -\operatorname{Tr}\left[\rho_{\text{free}_j}\log\left(\frac{1}{\nu_j+1/2}\sum_{n_j=0}^{\infty}\left(\frac{\nu_j-1/2}{\nu_j+1/2}\right)^{n_j}|n_j\rangle\langle n_j|\right)\right] \\
&= -\operatorname{Tr}\left[\rho_{\text{free}_j}\log\left(\sum_{n_j=0}^{\infty}\left(\frac{\nu_j-1/2}{\nu_j+1/2}\right)^{n_j}|n_j\rangle\langle n_j|\right)\right] \\
&+\operatorname{Tr}\left[\rho_{\text{free}_j}\log\left(\nu_j+1/2\right)\right] \\
&= -\operatorname{Tr}\left[\rho_{\text{free}_j}\sum_{n_j=0}^{\infty}\log\left(\left(\frac{\nu_j-1/2}{\nu_j+1/2}\right)^{n_j}\right)|n_j\rangle\langle n_j|\right]+\log(\nu_j+1/2) \\
&= -\operatorname{Tr}\left[\rho_{\text{free}_j}\sum_{n_j=0}^{\infty}n_j\log\left(\frac{\nu_j-1/2}{\nu_j+1/2}\right)|n_j\rangle\langle n_j|\right]+\log(\nu_j+1/2) \\
&= -\log\left(\frac{\nu_j-1/2}{\nu_j+1/2}\right)\operatorname{Tr}\left[\rho_{\text{free}_j}\sum_{n_j=0}^{\infty}n_j|n_j\rangle\langle n_j|\right]+\log(\nu_j+1/2) \\
&= -\log\left(\frac{\nu_j-1/2}{\nu_j+1/2}\right)\operatorname{Tr}\left[\rho_{\text{free}_j}\hat{n}_j\right]+\log(\nu_j+1/2) \\
&= -\log\left(\frac{\nu_j-1/2}{\nu_j+1/2}\right)\bar{n}_j+\log(\nu_j+1/2) \\
&= -\log\left(\frac{\nu_j-1/2}{\nu_j+1/2}\right)(\nu_j-1/2)+\log(\nu_j+1/2) \\
&= (\nu_j+1/2)\log(\nu_j+1/2)-(\nu_j-1/2)\log(\nu_j-1/2). \qquad \text{(C.65)}
\end{aligned}
$$

The equation above, together with Eq. (4.123) justifies Eqs. (4.124) and (4.125). In the Equation above, we used that $\log\left(\sum_n(c_n)|n\rangle\langle n|\right)=\sum_n\log(c_n)|n\rangle\langle n|$ (for any positive c_n) in the forth equality, and we used Eq. (C.39) in the ninth equality.

C.20 Proof of Simon normal form statement

The statement says that any covariance matrix representing a two-mode Gaussian state can be reduced, by local single-mode sympectic transformation, to the following form

$$\sigma_S = \begin{pmatrix} a & 0 & c_+ & 0 \\ 0 & a & 0 & c_- \\ c_+ & 0 & b & 0 \\ 0 & c_- & 0 & b \end{pmatrix}, \tag{C.66}$$

with a and b positive real numbers, and c_+ and c_- real numbers satisfying the Bona-fide conditions.

For the proof, suppose that σ is a generic covariance matrix of a two-mode state. Williamson's theorem (Eq. (4.83)) states that any single-mode covariance matrix can be diagonalized by means of a single-mode symplectic transformation into $x\mathbb{I}$, where $x > 0$. Consequently, there exist symplectic transformations S_a acting in the first mode and S_b acting in the second mode, such that

$$S_b^\top S_a^\top \sigma S_a S_b = \begin{pmatrix} a\mathbb{I} & C \\ C^\top & b\mathbb{I} \end{pmatrix}, \tag{C.67}$$

where a and b are positive real numbers and C is a 2×2 real matrix. Since $a\mathbb{I}$ and $b\mathbb{I}$ are invariant under transformations which are orthogonal and symplectic, we can apply the orthogonal and symplcetic transformations needed to diagonalize the off-diagonal block-matrix C, according to the *Singular Value Decomposition* (SVD).[2]

C.21 Proof that $S(\mathcal{E}(|\alpha\rangle\langle\alpha|)) = S(\mathcal{E}(|0\rangle\langle 0|))$ for any Gaussian channel $\mathcal{E}$

The covariance matrix of any coherent state $|\alpha\rangle\langle\alpha|$ and the vacuum $|0\rangle\langle 0|$ has the same value, namely $\mathbb{I}/2$, their only difference exists in their first moments.

[2] See such version of the SVD in Chapter 5 of Ref. [14].

From the results of Section 4.7, and as it was shown in Eqs. (4.72) and (4.77), the evolution of the first moments and of the covariance matrix for a Gaussian state are decoupled during all the Stinespring dilation process. Since any quantum channel can be expressed by a Stinespring dilation, we conclude that any Gaussian channel evolution must have a decoupled behaviour between the covariance matrix and first moments. Consequently, if the input of two states with the same covariance matrix are inputs to a quantum channel, their outputs will also have the same covariance matrix.

Therefore, the outputs of $\mathcal{E}(|\alpha\rangle\langle\alpha|) = \mathcal{E}(|0\rangle|0\rangle)$ will have the same covariance matrix. Finally, since the entropy of a Gaussian state only depends on its covariance matrix (Eqs. (4.124) and (4.125)), we conclude that their entropy will be the same.

C.22 Computations to obtain Eq. (4.139)

For obtaining Eq. (4.139), we must compute $S(\rho_{AB})$, $S(\rho_B)$ and $S(\mathcal{E}(|0\rangle\langle 0|))$.

The entropies $S(\rho_{AB}) = g(\nu_-) + g(\nu_+)$ and $S(\rho_B) = g(\beta)$ are direct consequences of Eq. (4.124) and from the fact that the local covariance matrix of ρ_B is already in its diagonal form.

The entropy of $\mathcal{E}(|0\rangle\langle 0|)$ can be obtained from the fact that the covariance matrix of the vacuum is $\sigma_{\text{vac}} = \mathbb{I}/2$ and it's evolution through the phase-insensitive Gaussian channel $\mathcal{E}$ is given by Eq. (4.129). Hence, the evolved covariance matrix will be $\mathbb{I}_2(\tau + \eta)/2$, which has only the symplectic eigenvalues $(\tau + \eta)/2$, and the result follows from Eq. (4.124).

C.23 Two-mode squeezed thermal state, EPR state and friends

Here we give examples of how to construct the Simon form of the two-mode squeezed thermal state, EPR state and other kinds of locally thermal states from canonical operations acting in initial thermal states.

C.23.1 Two-mode squeezed thermal state

Given two bosonic modes A and B, the *Two-mode squeezing* operator (for further applications of the two-mode squeezing, see Refs. [55, 118, 119]) is a unitary operator defined as

$$\hat{S}_{ts}(\xi) = e^{\xi^* \hat{a}\hat{b} - \xi \hat{a}^\dagger \hat{b}^\dagger}, \tag{C.68}$$

where $\hat{a}(\hat{b})$ is the annihilator operator and $\hat{a}^\dagger(\hat{b}^\dagger)$ is the creation operator acting in the mode $A(B)$. For a real parameter r, it has the form

$$\hat{S}_{ts}(\xi)(r) = e^{r(\hat{a}\hat{b} - \hat{a}^\dagger \hat{b}^\dagger)}. \tag{C.69}$$

The Hamiltonian matrix that generates this operator is

$$H_{ts}(r) = r \begin{pmatrix} 0 & 0 & 0 & 1 \\ 0 & 0 & 1 & 0 \\ 0 & 1 & 0 & 0 \\ 1 & 0 & 0 & 0 \end{pmatrix}. \tag{C.70}$$

Therefore the correspondent symplectic matrix is

$$\begin{aligned} S_{ts}(r) &= e^{\Omega H_{ts}(r)} \\ &= \begin{pmatrix} \cosh(r) & 0 & \sinh(r) & 0 \\ 0 & \cosh(r) & 0 & -\sinh(r) \\ \sinh(r) & 0 & \cosh(r) & 0 \\ 0 & -\sinh(r) & 0 & \cosh(r) \end{pmatrix}. \end{aligned} \tag{C.71}$$

From Eq. (C.37), we have that the thermal state of two bosonic modes A and B with local Hamiltonians $H_{A(B)} = \omega \left(\hat{a}^\dagger(\hat{b}^\dagger)\hat{a}(\hat{b}) + \frac{1}{2} \right)$ is

$$\sigma_{AB}^{\text{th}} = \begin{pmatrix} \bar{n}_A + 1/2 & 0 & 0 & 0 \\ 0 & \bar{n}_A + 1/2 & 0 & 0 \\ 0 & 0 & \bar{n}_B + 1/2 & 0 \\ 0 & 0 & 0 & \bar{n}_B + 1/2 \end{pmatrix}, \tag{C.72}$$

where $\bar{n}_A + 1/2 = \frac{1}{2}\coth\left(\frac{\omega\beta_A}{2}\right)$ and $\beta_{A(B)}$ is the inverse of the temperature of $A(B)$. Hence, the *two-mode squeezed thermal state* is just the two-mode squeezed applied in this thermal state

$$\begin{aligned}\sigma_{AB}^{\text{TMST}} &= S_{ts}(r)\sigma_{AB}^{\text{th}}S_{ts}^{\top} \\ &= \begin{pmatrix} \mathbf{a} & 0 & c & 0 \\ 0 & \mathbf{a} & 0 & -c \\ c & 0 & \mathbf{b} & 0 \\ 0 & -c & 0 & \mathbf{b} \end{pmatrix},\end{aligned} \tag{C.73}$$

where $\mathbf{a} = \left(\bar{n}_A + \frac{1}{2}\right)\cosh^2(r) + \left(\bar{n}_B + \frac{1}{2}\right)\sinh^2(r)$, $\mathbf{b} = \left(\bar{n}_B + \frac{1}{2}\right)\cosh^2(r) + \left(\bar{n}_A + \frac{1}{2}\right)\sinh^2(r)$ and $c = \frac{1}{2}(1 + \bar{n}_A + \bar{n}_B)\sinh(2r)$.

C.23.2 EPR state

The EPR state is defined as the two-mode squeezed operator applied in the vacuum. The vacuum is equivalent to a thermal state at 0 temperature, thus a two-mode vacuum state has covariance matrix $\sigma_{AB}^{\text{vac}} = \frac{1}{2}\mathbb{I}_4$. Therefore, the EPR covariance matrix for a squeezing operator $\hat{S}_{ts}(r)$ is

$$\begin{aligned}\sigma_{EPR} &= \frac{1}{2}S_{ts}(r)S_{ts}^{\top}(r) \\ &= \begin{pmatrix} \beta & 0 & \sqrt{\beta^2-1} & 0 \\ 0 & \beta & 0 & -\sqrt{\beta^2-1} \\ \sqrt{\beta^2-1} & 0 & \beta & 0 \\ 0 & -\sqrt{\beta^2-1} & 0 & \beta \end{pmatrix},\end{aligned} \tag{C.74}$$

where $\beta = \frac{1}{2}\cosh(2r)$. If we change the sign of r, i.e., $r \to -r$, then the off-diagonal terms of the matrix switch sign.

Appendix D

Some proofs and definitions in Obtaining Observables Shifts Using QBNs

D.1 Proof of Eq. (7.20)

With the use of Eqs. (7.17) and (7.18) we have

$$\mathcal{P}_{\text{TPM}}(a_0, a_t) = \sum_{b_t,b,b1} \langle a_t, b_t| U(t) |a_0, b\rangle \langle a_0, b| \rho_{AB}(0) |a_0, b'\rangle \langle a_0, b'| U^\dagger(t) |a_t, b_t\rangle , \tag{D.1}$$

where we just used that $\mathbb{I}_B = \sum_b |b\rangle \langle b|$, for the basis $\{|b\rangle\}_b$ and $\{|b'\rangle\}_{b'}$ of B.

Let the characteristic function for the shift probability of Eq. (7.19) be

$$G_{\mathcal{O}_{A_{\text{TPM}}}}(k) = \int_{-\infty}^{\infty} (d\Delta a)\, e^{ik\Delta a}\, p_{\text{TPM}}(\Delta\mathcal{O}_A = \Delta a), \tag{D.2}$$

from which we have

$$G_{\mathcal{O}_{A_{\text{TPM}}}}(k) = \sum_{a_0,a_t} e^{ik(a_t-a_0)} \mathcal{P}_{\text{TPM}}(a_0, a_t). \tag{D.3}$$

Applying Eq. (D.1) in this characteristic function, we obtain

$$
\begin{aligned}
G_{\mathcal{O}_{A_{\text{TPM}}}}(k) &= \sum_{b_t,b,b',a_0,a_t} \langle b_t, a_t| U(t)e^{-ika_0} |a_0, b\rangle \langle a_0, b| \rho_{AB}(0) |a_0, b'\rangle \langle a_0, b'| U^\dagger(t)e^{ika_t} |a_t, b_t\rangle \\
&= \sum_{b_t,b,b',a_0,a_t} \langle b_t, a_t| U(t)e^{-ik\mathcal{O}_A(0)} |a_0, b\rangle \langle a_0, b| \rho_{AB}(0) |a_0, b'\rangle \langle a_0, b'| U^\dagger(t)e^{ik\mathcal{O}_A(t)} |a_t, b_t\rangle \\
&= \sum_{b_t,a_0,a_t} \langle b_t, a_t| U(t)e^{-ik\mathcal{O}_A(0)} |a_0\rangle \langle a_0| \rho_{AB}(0) |a_0\rangle \langle a_0| U^\dagger(t)e^{ik\mathcal{O}_A(t)} |a_t, b_t\rangle \\
&= \text{Tr}\left\{ U(t)e^{-ik\mathcal{O}_A(0)} \left(\sum_{a_0} |a_0\rangle \langle a_0| \rho_{AB}(0) |a_0\rangle \langle a_0| \right) U^\dagger(t)e^{ik\mathcal{O}_A(t)} \right\} \\
&= \text{Tr}\left\{ e^{-ik\mathcal{O}_A(0)} \mathcal{D}_{\mathcal{O}_A(0)}(\rho_{AB}(0)) U^\dagger(t)e^{ik\mathcal{O}_A(t)} U(t) \right\} \\
&= \text{Tr}\left\{ e^{ikU^\dagger(t)\mathcal{O}_A(t)U(t)} e^{-ik\mathcal{O}_A(0)} \mathcal{D}_{\mathcal{O}_A(0)}(\rho_{AB}(0)) \right\},
\end{aligned}
\tag{D.4}
$$

which is the desired equation, where $\mathcal{D}_{\mathcal{O}_A(0)}(\bullet) = \sum_{a_0} |a_0\rangle \langle a_0| \bullet |a_0\rangle \langle a_0|$.

D.2 Matrices for generating ensembles in Subsection 7.3.1

The matrices used to generate the different ensembles of ρ^0_{AB} with the use of Eq. (7.30) in Subsection 7.3.1 are the following

$$M_1 = \begin{pmatrix} 0 & 0 & 1 \\ 0 & -\frac{\sqrt{3}}{2} & 0 \\ \frac{\sqrt{3}}{2} & -\frac{1}{4} & 0 \\ \frac{1}{2} & \frac{\sqrt{3}}{4} & 0 \end{pmatrix}, \; M_2 = \begin{pmatrix} 0 & 1 & 0 \\ 0 & 0 & -\frac{1}{2} \\ \frac{\sqrt{3}}{2} & 0 & \frac{\sqrt{3}}{4} \\ \frac{1}{2} & 0 & -\frac{3}{4} \end{pmatrix},$$

$$M_3 = \frac{1}{\sqrt{3}} \begin{pmatrix} 0 & 1 & 1 \\ 1 & 0 & 1 \\ 1 & -1 & 0 \\ 1 & 1 & -1 \end{pmatrix}, \; M_4 = \frac{1}{\sqrt{3}} \begin{pmatrix} 0 & 1 & 1 \\ 1 & 0 & -1 \\ 1 & -1 & 1 \\ 1 & 1 & 0 \end{pmatrix},$$

$$M_5 = \begin{pmatrix} 0 & 0 & 1 \\ -\frac{1}{2} & -\frac{\sqrt{3}}{2} & 0 \\ \frac{\sqrt{3}}{4} & -\frac{1}{4} & 0 \\ -\frac{3}{4} & \frac{\sqrt{3}}{4} & 0 \end{pmatrix}, \; M_6 = \begin{pmatrix} 0 & 1 & 0 \\ 0 & 0 & 1 \\ 1 & 0 & 0 \end{pmatrix},$$

$$M_7 = \begin{pmatrix} 0 & \cos(0.1) & \sin(0.1) \\ 0 & \sin(0.1) & -\cos(0.1) \\ 1 & 0 & 0 \end{pmatrix} \text{ and } M_8 = \begin{pmatrix} 0 & \cos\left(\frac{\pi}{4}\right) & \sin\left(\frac{\pi}{4}\right) \\ 0 & \sin\left(\frac{\pi}{4}\right) & -\cos\left(\frac{\pi}{4}\right) \\ 1 & 0 & 0 \end{pmatrix}.$$

Appendix E

Some proofs and definitions in Heat Exchanged Between Bosonic Modes

E.1 The QBN generated by post-measurements

Suppose we have an observable $\mathcal{O}_C$ acting on the joint Hilbert space of A and B described in the setup of Section 7.1. Given the eigenvalues $\{|c_i\rangle\}_i$ and eigenvectors $\{|c_i\rangle\}_i$ of $\mathcal{O}_C$, we can define the projective measurement $\{M_i = |c_i\rangle\langle c_i|\}_i$. Then, if such projective measurement is made in the initial joint state $\rho_{AB}(0)$ but the outcome is not revealed, the state is uploaded to the average of all possible backactions

$$\begin{aligned}\rho'_{AB} &= \sum_i P_{c_i} \frac{M_i \rho_{AB}(0) M_i^\dagger}{P_{c_i}} \\ &= \sum_i M_i \rho_{AB}(0) M_i^\dagger \\ &= \sum_i P_{c_i} |c_i\rangle\langle c_i| , \end{aligned} \tag{E.1}$$

where $P_{c_i} = \mathrm{Tr}\left\{ M_i \rho_{AB}(0) M_i^\dagger \right\} = \langle c_i| \rho_{AB}(0) |c_i\rangle$ is the probability of the measure to have the outcome c_i. Hence, the probability distribution generated by

$$\mathcal{P}_{\mathcal{O}_C}(a_0, b_0, a_t, b_t) = \sum_i P_{c_i} |\langle a_0, b_0 | c_i\rangle|^2 |\langle a_t, b_t| U(t) |c_i\rangle|^2, \tag{E.2}$$

is withe the seed probability P_{c_i} the QBN generated by the post-measured density matrix ρ'_{AB}.

This is exactly the case of Eq. (8.13), where the seed probability P_{c_i} is the Husimi Q-function $Q(\alpha,\beta)$, representing the probability of having an outcome $(\alpha\,\beta)$ for the projeticve measurement $\{\frac{1}{\pi}M_{\alpha,\beta}\left|\alpha,\beta\right\rangle\left\langle\alpha,\beta\right|\}_{\alpha,\beta}$ and the kets $\left|c_i\right\rangle$ are coherent states $\left|\alpha,\beta\right\rangle$. Thus the matrix

$$\begin{aligned}\rho'_{AB} &= \sum_i P_{c_i}\left|c_i\right\rangle\left\langle c_i\right| \\ &= \int_{\mathbb{C}^2} d^2\alpha\, d^2\beta\, Q(\alpha,\beta)\left|\alpha,\beta\right\rangle\left\langle\alpha,\beta\right|,\end{aligned} \tag{E.3}$$

is the density matrix after an heterodyne measurement is made without the outcome being revealed. This interpretation explains the result of Eq. (8.11), i.e., $\mathcal{P}_{\mathcal{O}_C}(a_t,b_t) = \left\langle a_t,b_t\right| U(t)\rho'_{AB}U^\dagger(t)\left|a_t,b_t\right\rangle$.

E.2 Computations of Eqs. (8.16) and (8.17)

To compute $\left\langle\alpha,\beta\right| e^{-ik\omega\hat{a}^\dagger\hat{a}}\left|\alpha,\beta\right\rangle$ we first notice that $\left\langle\alpha,\beta\right| e^{-ik\omega\hat{a}^\dagger\hat{a}}\left|\alpha,\beta\right\rangle = \left\langle\alpha\right| e^{-ik\omega\hat{a}^\dagger\hat{a}}\left|\alpha\right\rangle$ since $\hat{a}^\dagger\hat{a}$ is an operator that only acts in the Hilbert space of A. Furthermore $e^{-k\omega\hat{a}^\dagger\hat{a}} = \sum_{n=0}^{\infty} e^{-ik\omega n}\left|n\right\rangle\left\langle n\right|$, where $\{\left|n\right\rangle\}_n$ is the Fock basis, then

$$\left\langle\alpha\right| e^{-ik\omega\hat{a}^\dagger\hat{a}}\left|\alpha\right\rangle = \sum_{n=0}^{\infty} e^{-ik\omega n}\left|\left\langle\alpha|n\right\rangle\right|^2. \tag{E.4}$$

From Eq. (4.32), we have

$$\begin{aligned}\left\langle\alpha\right| e^{-ik\omega\hat{a}^\dagger\hat{a}}\left|\alpha\right\rangle &= \sum_{n=0}^{\infty} e^{-ik\omega n}e^{-|\alpha|^2}\frac{|\alpha|^{2n}}{n!} \\ &= e^{-|\alpha|^2}\sum_{n=0}^{\infty}\frac{\left(|\alpha|^2e^{-ik\omega n}\right)^n}{n!} \\ &= e^{-|\alpha|^2}e^{|\alpha|^2e^{-ik\omega n}} \\ &= \exp\left\{-|\alpha|^2(1-e^{-ik\omega n})\right\},\end{aligned} \tag{E.5}$$

from which we obtain Eq. (8.16).

To compute $\langle\alpha,\beta|\, e^{-ik\omega U^\dagger(t)\hat{a}^\dagger\hat{a}U(t)}\,|\alpha,\beta\rangle$, we first call $H' = U^\dagger(t)\hat{a}^\dagger\hat{a}U(t)$. Using the BCH formula, one can show that

$$U(t)^\dagger\hat{a}U(t) = \hat{a}\cos(gt) + \hat{b}\sin(gt). \tag{E.6}$$

Using this in H', we obtain

$$\begin{aligned} H' &= U^\dagger(t)\hat{a}^\dagger U(t)U^\dagger(t)\hat{a}U(t) \\ &= \hat{a}^\dagger\hat{a}\cos^2(gt) + (\hat{a}^\dagger\hat{b} + \hat{b}^\dagger\hat{a})\cos(gt)\sin(gt) + \hat{b}^\dagger\hat{b}\sin^2(gt). \end{aligned} \tag{E.7}$$

This way, H' can be rearranged as

$$H = \vec{a}^\dagger M\vec{a}, \tag{E.8}$$

where

$$\vec{a} = \begin{pmatrix}\hat{a}\\ \hat{b}\end{pmatrix} \text{ and } M = \begin{pmatrix}\cos^2(gt) & \sin(gt)\cos(gt)\\ \sin(gt)\cos(gt) & \sin^2(gt)\end{pmatrix}. \tag{E.9}$$

Now we can diagonalize $M = S\Lambda S^\dagger$, where Λ is a diagonal matrix made of eigenvalues of M and S is an unitary matrix. With such diagonalization we can redefine the operators $\hat{a},\ \hat{a}^\dagger,\ \hat{b}$ and $\hat{b}^\dagger$ by defining $\vec{c} = S^\dagger\vec{a}$, from which we obtain $H' = \sum_j \lambda_j\hat{c}_j^\dagger c_j$, where $\{\lambda_j\}_j$ are the eigenvalues of M. Also, we can rewrite $|\vec{\alpha}\rangle = |\alpha,\beta\rangle$ and define

$$\vec{\alpha} = \begin{pmatrix}\alpha\\ \beta\end{pmatrix}$$

where α and β are the eigenvalues of $\hat{a}$ and $\hat{b}$. Consequently, the eigenvalues of the operators in $\vec{c}$ will be related to $\vec{\alpha}$ as $|\vec{\alpha}\rangle_{\hat{a}} = \left|S^\dagger\vec{\alpha}\right\rangle_{\hat{c}}$, which means that "The vectors which have eigenvalues $\vec{\alpha}$ of $\hat{a}$ have eigenvalues $S^\dagger\vec{\alpha}$ of $\hat{c}$". Using this definitions, we

have

$$\begin{aligned}\langle\alpha,\beta|\, e^{-ik\omega U^\dagger(t)\hat{a}^\dagger\hat{a}U(t)}\,|\alpha,\beta\rangle &= \langle\vec{\alpha}|_{\hat{a}}\, e^{ik\omega\vec{a}^\dagger M\vec{a}}\,|\vec{\alpha}\rangle_{\hat{a}}\\ &= \langle\vec{\alpha}|_{\hat{a}}\, e^{ik\omega\sum_j\lambda_j\hat{c}_j^\dagger\hat{c}_j}\,|\vec{\alpha}\rangle_{\hat{a}}\\ &= \left\langle S^\dagger\vec{\alpha}\right|_{\hat{c}}\, e^{ik\omega\sum_j\lambda_j\hat{c}_j^\dagger\hat{c}_j}\,\left|S^\dagger\vec{\alpha}\right\rangle_{\hat{c}},\\ &= \exp\left\{\sum_j\left(e^{ik\omega\lambda_j}-1\right)|c_j|^2\right\}\Big|_{c_j=(S^\dagger\vec{\alpha})_j},\end{aligned}$$

where in the last equality we used Eq. (E.5). Finally, if we define a diagonal matrix F such that $F_{jj}=-(e^{ik\omega\lambda_j}-1)$, we obtain

$$\begin{aligned}I_2 &= \exp\left\{-\sum_j(\vec{\alpha}^\dagger S)_jF_{jj}(S^\dagger\vec{\alpha})_j\right\}\\ &= \exp\left\{-\vec{\alpha}^\dagger SFS^\dagger\vec{\alpha}\right\}\\ &= \exp\left\{-\vec{\alpha}^\dagger S\left(1-e^{ik\omega\Lambda}\right)S^\dagger\vec{\alpha}\right\}\\ &= \exp\left\{-\vec{\alpha}^\dagger\left(1-e^{ik\omega S\Lambda S^\dagger}\right)\vec{\alpha}\right\}\\ &= \exp\left\{-\vec{\alpha}^\dagger\left(1-e^{ik\omega M}\right)\vec{\alpha}\right\},\end{aligned}$$

frim which we obtain Eq. (8.17).

E.3 Isserlis' Theorem and $\langle\mathcal{Q}_A^2\rangle$

Isserlis' Theorem states that, given a Gaussian probability distribution $p(\mathbf{r})$ for a vector of real random variables $\mathbf{r}$ with covariance matrix σ and zero average, then, for even n

$$\int_{\mathbb{R}^N}d\mathbf{r}\,p(\mathbf{r})\prod_{j=1}^n r_j=\sum_{(i_1,\cdots,i_n)}\prod_{k=1}^{n/2}\sigma_{i_{2j-1},i_{2j}},\tag{E.10}$$

where $\sum_{(i_1,\cdots,i_n)}$ represents the sum of all possible combinations $((i_1,i_2),\cdots,(i_{n-1},i_n))$ for pairs of numbers in $(1,\cdots,n)$ and r_j is an element of $\mathbf{r}$. Additionally, this integral is 0 for odd n. For instance, for a vector of random variables $\mathbf{r}=(q_A,p_A,q_B,p_B)$ with a

Gaussian probability distribution $p(\mathbf{r})$ with covariance matrix Σ and 0 average, we have

$$\begin{aligned}
&\int_{\mathbb{R}^4} d\mathbf{r}\; p(\mathbf{r}) q_A^4 = 3\Sigma_{1,1}^2, \\
&\int_{\mathbb{R}^4} d\mathbf{r}\; p(\mathbf{r}) q_A^3 p_A = 3\Sigma_{1,1}\Sigma_{1,2}, \\
&\int_{\mathbb{R}^4} d\mathbf{r}\; p(\mathbf{r}) q_A^2 p_A^2 = (\Sigma_{1,1}\Sigma_{2,2} + 2\Sigma_{1,2}^2), \\
&\int_{\mathbb{R}^4} d\mathbf{r}\; p(\mathbf{r}) q_A^2 p_A q_B = (\Sigma_{1,1}\Sigma_{2,3} + 2\Sigma_{1,2}\Sigma_{1,3}), \\
&\int_{\mathbb{R}^4} d\mathbf{r}\; p(\mathbf{r}) q_A p_A q_B p_B = (\Sigma_{1,2}\Sigma_{3,4} + \Sigma_{1,3}\Sigma_{2,4} + \Sigma_{1,4}\Sigma_{2,3}), \\
&\quad\vdots
\end{aligned} \tag{E.11}$$

A proof for this theorem can be found in Ref. [150].

The procedure used to obtain $\langle \mathcal{Q}_A^2 \rangle$ is to expand the integrating of Eq. (8.28) into a sum of polynomials of (q_A, p_A, q_B, p_B) and use the equations of (E.11) to evaluate the integral, given that $P(\mathbf{r})$ has the form of a classical Gaussian probability distribution with covariance matrix $\Sigma = \sigma_{AB} - \mathbb{I}_4/2$ and first moments 0.

E.4 Locally thermal states D-plus and D-minus

Suppose we have a bosonic system with two modes A and B initially at a EPR state with covariance matrix

$$\sigma_{EPR} = \begin{pmatrix} \beta & 0 & \sqrt{\beta^2-1} & 0 \\ 0 & \beta & 0 & -\sqrt{\beta^2-1} \\ \sqrt{\beta^2-1} & 0 & \beta & 0 \\ 0 & -\sqrt{\beta^2-1} & 0 & \beta \end{pmatrix}. \tag{E.12}$$

If we have a one-mode Gaussian quantum channel of class D, described in Subsection 4.7.6, then the map will be described by the matrices $\mathbf{T} = \sqrt{|\tau|}\sigma_z$ and $\mathbf{N} = (1+|\tau|)(\bar{n}+1)$ where $\tau < 0$ and $\bar{n} \geq 0$. If we apply this channel only in the first mode of the EPR

state, then, by Eqs. (4.112) and (4.113), the outcome will be

$$\sigma_{AB}^{D+}=\begin{pmatrix}\beta|\tau|+(1+|\tau|)(\bar{n}+1) & 0 & \sqrt{|\tau|(\beta^2-1)} & 0\\ 0 & \beta|\tau|+(1+|\tau|)(\bar{n}+1) & 0 & \sqrt{|\tau|(\beta^2-1)}\\ \sqrt{|\tau|(\beta^2-1)} & 0 & \beta & 0\\ 0 & \sqrt{|\tau|(\beta^2-1)} & 0 & \beta\end{pmatrix}. \tag{E.13}$$

We call this state the *D-plus thermal state* and for $|\tau|\geq 1$ it represents two locally thermal bosonic modes in the Simon form

$$\sigma_{AB}^{D+}=\begin{pmatrix}\mathbf{a} & 0 & c & 0\\ 0 & \mathbf{a} & 0 & c\\ c & 0 & \mathbf{b} & 0\\ 0 & c & 0 & \mathbf{b}\end{pmatrix}, \tag{E.14}$$

where $\mathbf{a}=\beta|\tau|+(1+|\tau|)(\bar{n}+1)>\mathbf{b}=\beta$ and $c=\sqrt{|\tau|(\beta^2-1)}$.

If otherwise we start with two modes in a thermal state as in Eq. (C.72) and apply the two-mode squeezing operator in the state with negative parameter $-r$ ($r>0$), we obtain

$$\begin{aligned}\sigma_{AB}^{TMST}(-r)&=S_{ts}(-r)\sigma_{AB}^{\text{th}}S_{ts}^{\top}(-r)\\ &=\begin{pmatrix}\mathbf{a} & 0 & -c & 0\\ 0 & \mathbf{a} & 0 & c\\ -c & 0 & \mathbf{b} & 0\\ 0 & c & 0 & \mathbf{b}\end{pmatrix},\end{aligned} \tag{E.15}$$

where $\mathbf{a}=\left(\bar{n}_A+\frac{1}{2}\right)\cosh^2(r)+\left(\bar{n}_B+\frac{1}{2}\right)\sinh^2(r)$, $\mathbf{b}=\left(\bar{n}_B+\frac{1}{2}\right)\cosh^2(r)+\left(\bar{n}_A+\frac{1}{2}\right)\sinh^2(r)$ and $c=\frac{1}{2}(1+\bar{n}_A+\bar{n}_B)\sinh(2r)$. Now, if we apply in the first mode the same Gaussian channel of class D, as the one defined above, we obtain the following covariance matrix

$$\sigma_{AB}^{D-}=\begin{pmatrix}\mathbf{a}' & 0 & -c' & 0\\ 0 & \mathbf{a}' & 0 & -c'\\ -c' & 0 & \mathbf{b}' & 0\\ 0 & -c' & 0 & \mathbf{b}'\end{pmatrix}, \tag{E.16}$$

where $\mathbf{a}' = \frac{1}{2}|\tau|(\bar{n}_A - \bar{n}_B + (1 + \bar{n}_A + \bar{n}_B)\cosh(2r)) + (1 + |\tau|)(\bar{n} + 1)$, $\mathbf{b}' = \frac{1}{2}(\bar{n}_B - \bar{n}_A + (1 + \bar{n}_A + \bar{n}_B)\cosh(2r))$ and $c' = \frac{1}{2}\left((1 + \bar{n}_A + \bar{n}_B)\sqrt{|\tau|}\sinh(2r)\right)$. We call this state the *D-minus thermal state*. It is not difficult to find values of $\tau,\ \bar{n},\ \bar{n}_A,\ \bar{n}_B$ and r such that $\mathbf{a}' < \mathbf{b}'$ and σ_{AB}^{D-} is a bona-fide function. For example, if we chose $\tau = 0.5,\ \bar{n} = 1.5,\ \bar{n}_A = 2,\ \bar{n}_B = 5$ and $r = 1.1$, the covariance matrix will be

$$\sigma_{AB}^{D-} = \begin{pmatrix} 12.1358 & 0 & -12.6066 & 0 \\ 0 & 12.1358 & 0 & -12.6066 \\ -12.6066 & 0 & 19.7716 & 0 \\ 0 & -12.6066 & 0 & 19.7716 \end{pmatrix}, \tag{E.17}$$

which is bona-fide.

Bibliography

[1] M. A. Nielsen and I. L. Chuang, *Quantum Computation and Quantum Information: 10th Anniversary Edition*. Cambridge University Press, 2010. DOI: 10.1017/CBO9780511976667.

[2] J. Preskill, *Course information for physics 219/computer science 219 quantum computation*.

[3] R. Horodecki, "Quantum information," *Acta Physica Polonica A*, vol. 139, no. 3, pp. 197–2018, Mar. 2021, ISSN: 0587-4246. DOI: 10.12693/aphyspola.139.197.

[4] R. S. Ingarden, "Quantum information theory," *Reports on Mathematical Physics*, vol. 10, no. 1, pp. 43–72, 1976, ISSN: 0034-4877. DOI: https://doi.org/10.1016/0034-4877(76)90005-7.

[5] I. H. Deutsch, "Harnessing the power of the second quantum revolution," *PRX Quantum*, vol. 1, p. 020 101, 2 Nov. 2020. DOI: 10.1103/PRXQuantum.1.020101.

[6] L. Jaeger, *The Second Quantum Revolution: From Entanglement to Quantum Computing and Other Super-Technologies*. Springer, 2018, ISBN: 9783319988252.

[7] T. D. Ladd, F. Jelezko, R. Laflamme, Y. Nakamura, C. Monroe, and J. L. O'Brien, "Quantum computers," *Nature*, vol. 464, no. 7285, pp. 45–53, Mar. 2010. DOI: 10.1038/nature08812.

[8] H. Wiseman and G. Milburn, *Quantum Measurement and Control*. Cambridge University Press, 2010, ISBN: 9780521804424.

[9] A. Einstein, B. Podolsky, and N. Rosen, "Can quantum-mechanical description of physical reality be considered complete?" *Phys. Rev.*, vol. 47, pp. 777–780, 10 May 1935. DOI: 10.1103/PhysRev.47.777.

[10] E. Schrödinger, "Discussion of probability relations between separated systems," *Mathematical Proceedings of the Cambridge Philosophical Society*, vol. 31, no. 4, pp. 555–563, 1935. DOI: 10.1017/S0305004100013554.

[11] N. Bohr, "Can quantum-mechanical description of physical reality be considered complete?" *Phys. Rev.*, vol. 48, pp. 696–702, 8 Oct. 1935. DOI: 10.1103/PhysRev.48.696.

[12] J. S. Bell, "On the einstein podolsky rosen paradox," *Physics Physique Fizika*, vol. 1, pp. 195–200, 3 Nov. 1964. DOI: 10.1103/PhysicsPhysiqueFizika.1.195.

[13] *Scientifc background on the nobel prize in physics 2022*, https://www.nobelprize.org/uploads/2022/10/advanced-physicsprize2022-3.pdf, Accessed: 2023-04-11.

[14] A. Serafini, *Quantum Continuous Variables: A Primer of Theoretical Methods*. CRC Press, Taylor & Francis Group, 2017, ISBN: 9781482246346.

[15] M. Wilde, *Quantum Information Theory*. Cambridge University Press, 2017, ISBN: 9781316813300.

[16] C. Weedbrook *et al.*, "Gaussian quantum information," *Reviews of Modern Physics*, vol. 84, no. 2, pp. 621–669, May 2012. DOI: 10.1103/revmodphys.84.621.

[17] J. Rau, "Relaxation phenomena in spin and harmonic oscillator systems," *Phys. Rev.*, vol. 129, pp. 1880–1888, 4 Feb. 1963. DOI: 10.1103/PhysRev.129.1880.

[18] V. Scarani, M. Ziman, P. Stelmachovic, N. Gisin, and V. Buzek, "Thermalizing quantum machines: Dissipation and entanglement," *Phys. Rev. Lett.*, vol. 88, p. 097 905, 9 Feb. 2002. DOI: 10.1103/PhysRevLett.88.097905.

[19] M. Ziman, P. Stelmachovic, V. Buzek, M. Hillery, V. Scarani, and N. Gisin, "Diluting quantum information: An analysis of information transfer in system-reservoir interactions," *Phys. Rev. A*, vol. 65, p. 042 105, 4 Mar. 2002. DOI: 10.1103/PhysRevA.65.042105.

[20] S. Campbell and B. Vacchini, *Collision models in open system dynamics: A versatile tool for deeper insights?* 2021. arXiv: 2102.05735 [quant-ph].

[21] F. Ciccarello, S. Lorenzo, V. Giovannetti, and G. M. Palma, "Quantum collision models: Open system dynamics from repeated interactions," *Physics Reports*, vol. 954, pp. 1–70, Apr. 2022. DOI: 10.1016/j.physrep.2022.01.001.

[22] J. Goold, M. Huber, A. Riera, L. del Rio, and P. Skrzypczyk, "The role of quantum information in thermodynamics:a topical review," *Journal of Physics A: Mathematical and Theoretical*, vol. 49, no. 14, p. 143 001, Feb. 2016. DOI: 10.1088/1751-8113/49/14/143001.

[23] S. Vinjanampathy and J. Anders, "Quantum thermodynamics," *Contemporary Physics*, vol. 57, no. 4, pp. 545–579, Jul. 2016. DOI: 10.1080/00107514.2016.1201896.

[24] F. Binder, L. Correa, C. Gogolin, J. Anders, and G. Adesso, *Thermodynamics in the Quantum Regime: Fundamental Aspects and New Directions*, ser. Fundamental Theories of Physics. Springer International Publishing, 2019, ISBN: 9783319990460.

[25] S. Deffner and S. Campbell, *Quantum thermodynamics: An introduction to the thermodynamics of quantum information*, 2019. DOI: 10.48550/ARXIV.1907.01596.

[26] L. Szilard, "Über die entropieverminderung in einem thermodynamischen system bei eingriffen intelligenter wesen," *Zeitschrift für Physik*, vol. 53, pp. 840–856, 1929.

[27] M. B. Plenio and V. Vitelli, "The physics of forgetting: Landauer's erasure principle and information theory," *Contemporary Physics*, vol. 42, no. 1, pp. 25–60, Jan. 2001. DOI: 10.1080/00107510010018916.

[28] C. H. Bennett, *Notes on landauer's principle, reversible computation and maxwell's demon*, 2003. arXiv: physics/0210005 [physics.class-ph].

[29] S. Bhattacharjee and A. Dutta, "Quantum thermal machines and batteries," *The European Physical Journal B*, vol. 94, no. 12, Dec. 2021. DOI: 10.1140/epjb/s10051-021-00235-3.

[30] "Quantum thermodynamics and quantum coherence engines," *TURKISH JOURNAL OF PHYSICS*, vol. 44, no. 5, Oct. 2020. DOI: 10.3906/fiz-2009-12.

[31] M. Campisi and R. Fazio, "The power of a critical heat engine," *Nature Communications*, vol. 7, no. 1, Jun. 2016. DOI: 10.1038/ncomms11895.

[32] M. P. Woods, N. H. Y. Ng, and S. Wehner, "The maximum efficiency of nano heat engines depends on more than temperature," *Quantum*, vol. 3, p. 177, Aug. 2019. DOI: 10.22331/q-2019-08-19-177.

[33] P. Talkner, E. Lutz, and P. Hänggi, "Fluctuation theorems: Work is not an observable," *Physical Review E*, vol. 75, no. 5, May 2007. DOI: 10.1103/physreve.75.050102.

[34] M. Esposito, U. Harbola, and S. Mukamel, "Nonequilibrium fluctuations, fluctuation theorems, and counting statistics in quantum systems," *Reviews of Modern Physics*, vol. 81, no. 4, pp. 1665–1702, Dec. 2009. DOI: 10.1103/revmodphys.81.1665.

[35] M. Campisi, P. Hänggi, and P. Talkner, "Colloquium: Quantum fluctuation relations: Foundations and applications," *Reviews of Modern Physics*, vol. 83, no. 3, pp. 771–791, Jul. 2011. DOI: 10.1103/revmodphys.83.771.

[36] A. E. Allahverdyan and T. M. Nieuwenhuizen, "Fluctuations of work from quantum subensembles: The case against quantum work-fluctuation theorems," *Phys. Rev. E*, vol. 71, p. 066 102, 6 Jun. 2005. DOI: 10.1103/PhysRevE.71.066102.

[37] A. Engel and R. Nolte, "Jarzynski equation for a simple quantum system: Comparing two definitions of work," *Europhysics Letters (EPL)*, vol. 79, no. 1, p. 10 003, Jun. 2007. DOI: 10.1209/0295-5075/79/10003.

[38] G. E. Crooks, "Entropy production fluctuation theorem and the nonequilibrium work relation for free energy differences," *Physical Review E*, vol. 60, no. 3, pp. 2721–2726, Sep. 1999. DOI: 10.1103/physreve.60.2721.

[39] C. Jarzynski, "Nonequilibrium equality for free energy differences," *Phys. Rev. Lett.*, vol. 78, pp. 2690–2693, 14 Apr. 1997. DOI: 10.1103/PhysRevLett.78.2690.

[40] H. Tasaki, *Jarzynski relations for quantum systems and some applications*, 2000. DOI: 10.48550/ARXIV.COND-MAT/0009244.

[41] A. E. Allahverdyan, "Nonequilibrium quantum fluctuations of work," *Physical Review E*, vol. 90, no. 3, Sep. 2014. DOI: 10.1103/physreve.90.032137.

[42] M. Lostaglio, "Quantum fluctuation theorems, contextuality, and work quasiprobabilities," *Physical Review Letters*, vol. 120, no. 4, Jan. 2018. DOI: 10.1103/physrevlett.120.040602.

[43] A. Darwiche, *Modeling and Reasoning with Bayesian Networks*. Cambridge University Press, 2009, ISBN: 9780521884389.

[44] T. Nielsen and F. JENSEN, *Bayesian Networks and Decision Graphs*, ser. Information Science and Statistics. Springer New York, 2007, ISBN: 9780387682815.

[45] R. Neapolitan and R. Neapolitan, *Learning Bayesian Networks*, ser. Artificial Intelligence. Pearson Prentice Hall, 2004, ISBN: 9780130125347.

[46] R. Neapolitan, *Probabilistic Reasoning in Expert Systems: Theory and Algorithms*. CreateSpace Independent Publishing Platform, 2012, ISBN: 9781477452547.

[47] J. Pearl, "Bayesian netwcrks: A model cf self-activated memory for evidential reasoning," in *Proceedings of the 7th conference of the Cognitive Science Society, University of California, Irvine, CA, USA*, 1985, pp. 15–17.

[48] K. Micadei, G. T. Landi, and E. Lutz, "Quantum fluctuation theorems beyond two-point measurements," *Physical Review Letters*, vol. 124, no. 9, Mar. 2020. DOI: 10.1103/physrevlett.124.090602.

[49] ——, *Extracting bayesian networks from multiple copies of a quantum system*, 2021. arXiv: 2103.14570 [quant-ph].

[50] M. H. Partovi, "Entanglement versus stosszahlansatz: Disappearance of the thermodynamic arrow in a high-correlation environment," *Physical review. E, Statistical, nonlinear, and soft matter physics*, vol. 77, p. 021 110, Mar. 2008. DOI: 10.1103/PhysRevE.77.021110.

[51] S. Jevtic, D. Jennings, and T. Rudolph, "Maximally and minimally correlated states attainable within a closed evolving system," *Physical Review Letters*, vol. 108, no. 11, Mar. 2012. DOI: 10.1103/physrevlett.108.110403.

[52] D. Jennings and T. Rudolph, "Entanglement and the thermodynamic arrow of time," *Physical Review E*, vol. 81, no. 6, Jun. 2010. DOI: 10.1103/physreve.81.061130.

[53] M. N. Bera, A. Riera, M. Lewenstein, and A. Winter, "Generalized laws of thermodynamics in the presence of correlations," *Nature Communications*, vol. 8, no. 1, Dec. 2017. DOI: 10.1038/s41467-017-02370-x.

[54] K. Micadei *et al.*, "Reversing the direction of heat flow using quantum correlations," *Nature Communications*, vol. 10, no. 1, Jun. 2019. DOI: 10.1038/s41467-019-10333-7.

[55] M. Scully and M. Zubairy, *Quantum Optics*. Cambridge University Press, 1997, ISBN: 9780521435956.

[56] R. Loudon, *The Quantum Theory of Light*. OUP Oxford, 2000, ISBN: 9780191589782.

[57] H. Breuer, P. Breuer, F. Petruccione, and S. Petruccione, *The Theory of Open Quantum Systems*. Oxford University Press, 2002, ISBN: 9780198520634.

[58] C. Gardiner, P. Zoller, and P. Zoller, *Quantum Noise: A Handbook of Markovian and Non-Markovian Quantum Stochastic Methods with Applications to Quantum Optics*, ser. Springer Series in Synergetics. Springer, 2004, ISBN: 9783540223016.

[59] D. A. Lidar, *Lecture notes on the theory of open quantum systems*, 2019. DOI: 10.48550/ARXIV.1902.00967.

[60] T. Tome and M. De Oliveira, *Dinamica Estocastica E Irreversibilidade*. EDUSP, ISBN: 9788531414800.

[61] S. Salinas, *Introducao a Fisica Estatistica Vol. 09*. EDUSP, 1997, ISBN: 9788531403866.

[62] K. Huang, *Statistical Mechanics*. Wiley, 1987, ISBN: 9780471815181.

[63] P. Strasberg, G. Schaller, T. Brandes, and M. Esposito, "Quantum and information thermodynamics: A unifying framework based on repeated interactions," *Physical Review X*, vol. 7, no. 2, Apr. 2017. DOI: 10.1103/physrevx.7.021003.

[64] H. R. Brown and W. Myrvold, *Boltzmann's h-theorem, its limitations, and the birth of (fully) statistical mechanics*, 2008. DOI: 10.48550/ARXIV.0809.1304.

[65] C. M. Caves, "Quantum mechanics of measurements distributed in time. a path-integral formulation," *Phys. Rev. D*, vol. 33, pp. 1643–1665, 6 Mar. 1986. DOI: 10.1103/PhysRevD.33.1643.

[66] ——, "Quantum mechanics of measurements distributed in time. ii. connections among formulations," *Phys. Rev. D*, vol. 35, pp. 1815–1830, 6 Mar. 1987. DOI: 10.1103/PhysRevD.35.1815.

[67] C. M. Caves and G. J. Milburn, "Quantum-mechanical model for continuous position measurements," *Phys. Rev. A*, vol. 36, pp. 5543–5555, 12 Dec. 1987. DOI: 10.1103/PhysRevA.36.5543.

[68] P. Filipowicz, J. Javanainen, and P. Meystre, "Theory of a microscopic maser," *Phys. Rev. A*, vol. 34, pp. 3077–3087, 4 Oct. 1986. DOI: 10.1103/PhysRevA.34.3077.

[69] ——, "Quantum and semiclassical steady states of a kicked cavity mode," *J. Opt. Soc. Am. B*, vol. 3, no. 6, pp. 906–910, Jun. 1986. DOI: 10.1364/JOSAB.3.000906.

[70] ——, "The microscopic maser," *Optics Communications*, vol. 58, no. 5, pp. 327–330, 1986, ISSN: 0030-4018. DOI: https://doi.org/10.1016/0030-4018(86)90237-3.

[71] M. Ziman and V. Bužek, "All (qubit) decoherences: Complete characterization and physical implementation," *Physical Review A*, vol. 72, no. 2, Aug. 2005. DOI: 10.1103/physreva.72.022110.

[72] F. Ciccarello and V. Giovannetti, "A quantum non-markovian collision model: Incoherent swap case," *Physica Scripta*, vol. T153, p. 014 010, Mar. 2013, ISSN: 1402-4896. DOI: 10.1088/0031-8949/2013/t153/014010.

[73] F. Ciccarello, G. M. Palma, and V. Giovannetti, "Collision-model-based approach to non-markovian quantum dynamics," *Physical Review A*, vol. 87, no. 4, Apr. 2013, ISSN: 1094-1622. DOI: 10.1103/physreva.87.040103.

[74] R. McCloskey and M. Paternostro, "Non-markovianity and system-environment correlations in a microscopic collision model," *Physical Review A*, vol. 89, no. 5, May 2014, ISSN: 1094-1622. DOI: 10.1103/physreva.89.052120.

[75] B. Çakmak, M. Pezzutto, M. Paternostro, and Ö. E. Müstecaplıoğlu, "Non-markovianity, coherence, and system-environment correlations in a long-range collision model," *Physical Review A*, vol. 96, no. 2, Aug. 2017, ISSN: 2469-9934. DOI: 10.1103/physreva.96.022109.

[76] S. Kretschmer, K. Luoma, and W. T. Strunz, "Collision model for non-Markovian quantum dynamics," *Physical Review A*, vol. 94, no. 1, Jul. 2016, ISSN: 2469-9934. DOI: 10.1103/physreva.94.012106.

[77] S. Campbell, F. Ciccarello, G. M. Palma, and B. Vacchini, "System-environment correlations and markovian embedding of quantum non-markovian dynamics," *Physical Review A*, vol. 98, no. 1, Jul. 2018, ISSN: 2469-9934. DOI: 10.1103/physreva.98.012142.

[78] S. Lorenzo, F. Ciccarello, and G. M. Palma, "Composite quantum collision models," *Physical Review A*, vol. 96, no. 3, Sep. 2017, ISSN: 2469-9934. DOI: 10.1103/physreva.96.032107.

[79] J. Jin and C.-s. Yu, "Non-Markovianity in the collision model with environmental block," *New Journal of Physics*, vol. 20, no. 5, p. 053 026, May 2018, ISSN: 1367-2630. DOI: 10.1088/1367-2630/aac0cb.

[80] R. R. Camasca and G. T. Landi, "Memory kernel and divisibility of gaussian collisional models," *Physical Review A*, vol. 103, no. 2, Feb. 2021, ISSN: 2469-9934. DOI: 10.1103/physreva.103.022202.

[81] T. Rybár, S. N. Filippov, M. Ziman, and V. Bužek, "Simulation of indivisible qubit channels in collision models," *Journal of Physics B: Atomic, Molecular and Optical Physics*, vol. 45, no. 15, p. 154 006, Jul. 2012. DOI: 10.1088/0953-4075/45/15/154006.

[82] N. K. Bernardes, A. R. R. Carvalho, C. H. Monken, and M. F. Santos, "Environmental correlations and markovian to non-Markovian transitions in collisional models," *Physical Review A*, vol. 90, no. 3, Sep. 2014, ISSN: 1094-1622. DOI: 10.1103/physreva.90.032111.

[83] N. K. Bernardes, A. R. R. Carvalho, C. H. Monken, and M. F. Santos, "Coarse graining a non-Markovian collisional model," *Physical Review A*, vol. 95, no. 3, Mar. 2017, ISSN: 2469-9934. DOI: 10.1103/physreva.95.032117.

[84] E. Mascarenhas and I. de Vega, "Quantum critical probing and simulation of colored quantum noise," *Physical Review A*, vol. 96, no. 6, Dec. 2017, ISSN: 2469-9934. DOI: 10.1103/physreva.96.062117.

[85] Z.-X. Man, Y.-J. Xia, and R. Lo Franco, "Temperature effects on quantum non-markovianity via collision models," *Physical Review A*, vol. 97, no. 6, Jun. 2018, ISSN: 2469-9934. DOI: 10.1103/physreva.97.062104.

[86] P. Liuzzo-Scorpo, W. Roga, L. A. M. Souza, N. K. Bernardes, and G. Adesso, "Non-markovianity hierarchy of gaussian processes and quantum amplification," *Physical Review Letters*, vol. 118, no. 5, Jan. 2017, ISSN: 1079-7114. DOI: 10.1103/physrevlett.118.050401.

[87] F. L. Rodrigues, G. D. Chiara, M. Paternostro, and G. T. Landi, "Thermodynamics of weakly coherent collisional models," *Physical Review Letters*, vol. 123, no. 14, Oct. 2019. DOI: 10.1103/physrevlett.123.140601.

[88] O. A. D. Molitor and G. T. Landi, "Stroboscopic two-stroke quantum heat engines," *Physical Review A*, vol. 102, no. 4, Oct. 2020. DOI: 10.1103/physreva.102.042217.

[89] J. v. Neumann, "Wahrscheinlichkeitstheoretischer aufbau der quantenmechanik," *Nachrichten von der Gesellschaft der Wissenschaften zu Göttingen, Mathematisch-Physikalische Klasse*, vol. 1927, pp. 245–272, 1927.

[90] K. Kraus, "General state changes in quantum theory," *Annals of Physics*, vol. 64, no. 2, pp. 311–335, 1971, ISSN: 0003-4916. DOI: https://doi.org/10.1016/0003-4916(71)90108-4.

[91] G. T. Landi, *Quantum information and quantum noise*.

[92] M. Lostaglio, "An introductory review of the resource theory approach to thermodynamics," *Reports on Progress in Physics*, vol. 82, no. 11, p. 114 001, Oct. 2019. DOI: 10.1088/1361-6633/ab46e5.

[93] N. E. Comar and G. T. Landi, "Correlations breaking homogenization," *Physical Review A*, vol. 104, no. 3, Sep. 2021. DOI: 10.1103/physreva.104.032217.

[94] F. Ciccarello, *Stochastic versus periodic quantum collision models*, 2022. DOI: 10.48550/ARXIV.2208.04353.

[95] S. Haroche and J. Raimond, *Exploring the Quantum: Atoms, Cavities, and Photons*, ser. Oxford Graduate Texts. OUP Oxford, 2013, ISBN: 9780199680313.

[96] B.-G. Englert and G. Morigi, "Five lectures on dissipative master equations," in *Coherent Evolution in Noisy Environments*, Springer Berlin Heidelberg, 2002, pp. 55–106. DOI: 10.1007/3-540-45855-7_2.

[97] H.-J. Briegel and B.-G. Englert, "Macroscopic dynamics of a maser with non-poissonian injection statistics," *Phys. Rev. A*, vol. 52, pp. 2361–2375, 3 Sep. 1995. DOI: 10.1103/PhysRevA.52.2361.

[98] S. N. Filippov, J. Piilo, S. Maniscalco, and M. Ziman, "Divisibility of quantum dynamical maps and collision models," *Physical Review A*, vol. 96, no. 3, Sep. 2017. DOI: 10.1103/physreva.96.032111.

[99] M. Cattaneo, G. D. Chiara, S. Maniscalco, R. Zambrini, and G. L. Giorgi, "Collision models can efficiently simulate any multipartite markovian quantum dynamics," *Physical Review Letters*, vol. 126, no. 13, Apr. 2021. DOI: 10.1103/physrevlett.126.130403.

[100] D. Cilluffo, A. Carollo, S. Lorenzo, J. A. Gross, G. M. Palma, and F. Ciccarello, "Collisional picture of quantum optics with giant emitters," *Physical Review Research*, vol. 2, no. 4, Oct. 2020. DOI: 10.1103/physrevresearch.2.043070.

[101] F. Ciccarello, "Collision models in quantum optics," *Quantum Measurements and Quantum Metrology*, vol. 4, Dec. 2017. DOI: 10.1515/qmetro-2017-0007.

[102] J. P. Dowling and G. J. Milburn, *Quantum technology: The second quantum revolution*, 2002. DOI: 10.48550/ARXIV.QUANT-PH/0206091.

[103] W. H. Zurek, "Decoherence, einselection, and the quantum origins of the classical," *Reviews of Modern Physics*, vol. 75, no. 3, pp. 715–775, May 2003. DOI: 10.1103/revmodphys.75.715.

[104] M. Schlosshauer, "Decoherence, the measurement problem, and interpretations of quantum mechanics," *Reviews of Modern Physics*, vol. 76, no. 4, pp. 1267–1305, Feb. 2005. DOI: 10.1103/revmodphys.76.1267.

[105] E. Jaynes and G. Bretthorst, *Probability Theory: The Logic of Science*. Cambridge University Press, 2006.

[106] C. E. Shannon, "A mathematical theory of communication," *The Bell System Technical Journal*, vol. 27, pp. 379–423, 1948.

[107] K. Modi, A. Brodutch, H. Cable, T. Paterek, and V. Vedral, "The classical-quantum boundary for correlations: Discord and related measures," *Reviews of Modern Physics*, vol. 84, no. 4, pp. 1655–1707, Nov. 2012. DOI: 10.1103/revmodphys.84.1655.

[108] R. Horodecki, P. Horodecki, M. Horodecki, and K. Horodecki, "Quantum entanglement," *Reviews of Modern Physics*, vol. 81, no. 2, pp. 865–942, Jun. 2009, ISSN: 1539-0756. DOI: 10.1103/revmodphys.81.865.

[109] L. Henderson and V. Vedral, "Classical, quantum and total correlations," *Journal of Physics A: Mathematical and General*, vol. 34, no. 35, pp. 6899–6905, Aug. 2001. DOI: 10.1088/0305-4470/34/35/315.

[110] W. Zurek, "Einselection and decoherence from an information theory perspective," *Annalen der Physik*, vol. 512, no. 11-12, pp. 855–864, Nov. 2000. DOI: 10.1002/andp.200051211-1204.

[111] H. Ollivier and W. H. Zurek, "Quantum discord: A measure of the quantumness of correlations," *Physical Review Letters*, vol. 88, no. 1, Dec. 2001. DOI: 10.1103/physrevlett.88.017901.

[112] K. Micadei *et al.*, "Experimental validation of fully quantum fluctuation theorems using dynamic bayesian networks," *Physical Review Letters*, vol. 127, no. 18, Oct. 2021. DOI: 10.1103/physrevlett.127.180603.

[113] K. Micadei, G. T. Landi, and E. Lutz, *Extracting bayesian networks from multiple copies of a quantum system*, 2021. DOI: 10.48550/ARXIV.2103.14570.

[114] P. Kaye, P. Mosca, I. Kaye, R. Laflamme, M. Mosca, and I. Mosca, *An Introduction to Quantum Computing*, ser. An Introduction to Quantum Computing. OUP Oxford, 2007, ISBN: 9780198570004.

[115] M. Gu, C. Weedbrook, N. C. Menicucci, T. C. Ralph, and P. van Loock, "Quantum computing with continuous-variable clusters," *Physical Review A*, vol. 79, no. 6, Jun. 2009, ISSN: 1094-1622. DOI: 10.1103/physreva.79.062318.

[116] A. Altland and B. Simons, *Condensed Matter Field Theory*, ser. Cambridge books online. Cambridge University Press, 2010, ISBN: 9780521769754.

[117] R. Shankar, *Quantum Field Theory and Condensed Matter: An Introduction*, ser. Cambridge monographs on mathematical physics. Cambridge University Press, 2017, ISBN: 9781108363464.

[118] P. Meystre and M. Sargent, *Elements of Quantum Optics*, ser. SpringerLink: Springer e-Books. Springer Berlin Heidelberg, 2007, ISBN: 9783540742111.

[119] D. Walls and G. Milburn, *Quantum Optics*. Springer Berlin Heidelberg, 2010, ISBN: 9783642066764.

[120] K. E. Cahill and R. J. Glauber, "Density operators and quasiprobability distributions," *Phys. Rev.*, vol. 177, pp. 1882–1902, 5 Jan. 1969. DOI: 10.1103/PhysRev.177.1882.

[121] K. Ikramov, "On the symplectic eigenvalues of positive definite matrices," *Moscow University Computational Mathematics and Cybernetics*, vol. 42, pp. 1–4, Jan. 2018. DOI: 10.3103/S0278641918010041.

[122] F. Nicacio, "Williamson theorem in classical, quantum, and statistical physics," *American Journal of Physics*, vol. 89, no. 12, pp. 1139–1151, Dec. 2021. DOI: 10.1119/10.0005944.

[123] R. Bhatia and T. Jain, "On symplectic eigenvalues of positive definite matrices," *Journal of Mathematical Physics*, vol. 56, no. 11, p. 112 201, Nov. 2015. DOI: 10.1063/1.4935852.

[124] V. Arnold, K. Vogtmann, and A. Weinstein, *Mathematical Methods of Classical Mechanics*, ser. Graduate Texts in Mathematics. Springer New York, 2013, ISBN: 9781475716931.

[125] M. Wilde, *Gaussian quantum information—phys 7895*.

[126] A. Holevo, "One-mode quantum gaussian channels: Structure and quantum capacity," *Problems of Information Transmission*, vol. 43, pp. 1–11, Mar. 2007. DOI: 10.1134/S0032946007010012.

[127] G. Adesso, S. Ragy, and A. R. Lee, "Continuous variable quantum information: Gaussian states and beyond," *Open Systems &amp mathsemicolon Information Dynamics*, vol. 21, no. 01n02, p. 1 440 001, Mar. 2014. DOI: 10.1142/s1230161214400010.

[128] S. Pirandola, G. Spedalieri, S. L. Braunstein, N. J. Cerf, and S. Lloyd, "Optimality of gaussian discord," *Physical Review Letters*, vol. 113, no. 14, Oct. 2014. DOI: 10.1103/physrevlett.113.140405.

[129] A. Mari, V. Giovannetti, and A. S. Holevo, "Quantum state majorization at the output of bosonic gaussian channels," *Nature Communications*, vol. 5, no. 1, May 2014. DOI: 10.1038/ncomms4826.

[130] V. Giovannetti, R. Garcia-Patron, N. J. Cerf, and A. S. Holevo, "Ultimate classical communication rates of quantum optical channels," *Nature Photonics*, vol. 8, no. 10, pp. 796–800, Sep. 2014. DOI: 10.1038/nphoton.2014.216.

[131] G. Pantaleoni, B. Q. Baragiola, and N. C. Menicucci, *Subsystem analysis of continuous-variable resource states*, 2021. arXiv: 2102.10500 [quant-ph].

[132] M. Hein, J. Eisert, and H. J. Briegel, "Multiparty entanglement in graph states," *Phys. Rev. A*, vol. 69, p. 062 311, 6 Jun. 2004. DOI: 10.1103/PhysRevA.69.062311.

[133] L. Aolita, A. J. Roncaglia, A. Ferraro, and A. Acín, "Gapped Two-Body hamiltonian for Continuous-Variable quantum computation," *Physical Review Letters*, vol. 106, no. 9, Feb. 2011, ISSN: 1079-7114. DOI: 10.1103/physrevlett.106.090501.

[134] N. C. Menicucci, S. T. Flammia, and P. van Loock, "Graphical calculus for gaussian pure states," *Physical Review A*, vol. 83, no. 4, Apr. 2011, ISSN: 1094-1622. DOI: 10.1103/physreva.83.042335.

[135] O. Pfister, "Continuous-variable quantum computing in the quantum optical frequency comb," *Journal of Physics B: Atomic, Molecular and Optical Physics*, vol. 53, no. 1, p. 012 001, Nov. 2019. DOI: 10.1088/1361-6455/ab526f.

[136] R. M. Gray, *Toeplitz and circulant matrices: A review*.

[137] B. Dakić, V. Vedral, and Č. Brukner, "Necessary and sufficient condition for nonzero quantum discord," *Physical Review Letters*, vol. 105, no. 19, Nov. 2010. DOI: 10.1103/physrevlett.105.190502.

[138] D. Girolami and G. Adesso, "Observable measure of bipartite quantum correlations," *Physical Review Letters*, vol. 108, no. 15, Apr. 2012. DOI: 10.1103/physrevlett.108.150403.

[139] L. P. Hughston, R. Jozsa, and W. K. Wootters, "A complete classification of quantum ensembles having a given density matrix," *Physics Letters A*, vol. 183, no. 1, pp. 14–18, 1993, ISSN: 0375-9601. DOI: https://doi.org/10.1016/0375-9601(93)90880-9.

[140] P. van Loock, C. Weedbrook, and M. Gu, "Building gaussian cluster states by linear optics," *Physical Review A*, vol. 76, no. 3, Sep. 2007. DOI: 10.1103/physreva.76.032321.

[141] S. L. Braunstein, "Squeezing as an irreducible resource," *Physical Review A*, vol. 71, no. 5, May 2005. DOI: 10.1103/physreva.71.055801.

[142] N. C. Menicucci, S. T. Flammia, H. Zaidi, and O. Pfister, "Ultracompact generation of continuous-variable cluster states," *Phys. Rev. A*, vol. 76, p. 010 302, 1 Jul. 2007. DOI: 10.1103/PhysRevA.76.010302.

[143] A. J. Daley, "Quantum trajectories and open many-body quantum systems," *Advances in Physics*, vol. 63, no. 2, pp. 77–149, Mar. 2014. DOI: 10.1080/00018732.2014.933502.

[144] D. Girolami, T. Tufarelli, and C. E. Susa, "Quantifying genuine multipartite correlations and their pattern complexity," *Physical Review Letters*, vol. 119, no. 14, Oct. 2017. DOI: 10.1103/physrevlett.119.140505.

[145] T. Theurer, N. Killoran, D. Egloff, and M. Plenio, "Resource theory of superposition," *Physical Review Letters*, vol. 119, no. 23, Dec. 2017. DOI: 10.1103/physrevlett.119.230401.

[146] K. A. Kirkpatrick, *The schrodinger-hjw theorem*, 2005. arXiv: quant-ph/0305068 [quant-ph].

[147] A. Levy and M. Lostaglio, "Quasiprobability distribution for heat fluctuations in the quantum regime," *PRX Quantum*, vol. 1, no. 1, Sep. 2020. DOI: 10.1103/prxquantum.1.010309.

[148] P. P. Hofer, "Quasi-probability distributions for observables in dynamic systems," *Quantum*, vol. 1, p. 32, Oct. 2017. DOI: 10.22331/q-2017-10-12-32.

[149] M. Reed, B. Simon, A. P. (Londyn), and A. P. (Londyn)., *I: Functional Analysis*, ser. Methods of Modern Mathematical Physics. Elsevier Science, 1980, ISBN: 9780125850506.

[150] T. Alberts and D. Khoshnevisan, *Calculus on gauss space: An introduction to gaussian analysis*.